

GENERATION OF α -EPCR MONOCLONAL
ANTIBODIES AND THEIR USE IN THE
DEVELOPMENT OF AN ANTIBODY-BASED
TARGETING THERAPY OF INVASIVE PROSTATE
CANCER

ANNA DI BIASE

A Thesis submitted in Partial Fulfilment of the
Requirements of Nottingham Trent University for the
degree of Doctor of Philosophy.

September 2020



This project, as part of the Immutrain program, has received funding from the European Union's Horizon 2020 research and innovation programme under the Marie Skłodowska - Curie grant agreement No 641549.

Copyright Statement

This work is the intellectual property of the author. You may copy up to 5% of the work for private study, or personal, non-commercial research. Any re-use of the information contained within this document should be fully referenced, quoting the author, title, university, degree level and pagination. Queries or requests for any other use, or if a more substantial copy is required, should be directed in the owner(s) of the Intellectual Property Rights.

Acknowledgements

Four years is a long time, hence why I have many people to thank!

First, I would like to thank my Director of Studies Dr Tarik Regad for giving me the opportunity to work on this exciting project and for guiding me through my PhD journey. My journey has taught me how important it is for a good scientist to be a trustworthy, competent, and altruistic. I would also like to express my deep gratitude to my second Director of Studies Dr David Boocock and my supervisors Prof Graham Pockley and Dr Jay Vadakekolathu who all very patiently supported, motivated, and inspired me during the writing of my thesis. I consider myself extremely lucky to have had such an amazing team. In such a crucial moment, you turned what I was expecting to be a very challenging task into an enjoyable scientific adventure. Special thanks to Jay for his support from day one, I think you are the colleague that everyone hopes to have on their side! My work experience at the van Geest has been priceless and this is thanks to all the amazing people who make this research centre a place of scientific relevance. Thanks to Anne and Steve, the angels of the van Geest; thanks to Murrium who has always been there in the worst moments with an exceptional kindness. Thanks to Andy and his unit, working with you has been a pleasure! Thanks to my "lab buddies" in a pretty random order Luisa, Josh, Marco, Abdullah, Rukaia, Shaymaa, Gemma, Jenny, Mellissa, Arif, Divya, Joseph, Grace, Graham, Arish, Simon, Magda, Pauline, Sarra, Elena, Devika, Carmela. Sharing these last four years with you has been amazing, I will miss you all.

I would like to thank the EU for funding my project through the Marie-Curie bursary. Being part of the Immutrain program, I had the opportunity to visit many places in Europe, meet incredible scientists and developing key skills and connections important for my professional development. I would like to thank all the ESRs who shared with me this adventure, as well as the PIs and Simone who made this possible. My special thanks go to Prof Hans-Martin Jäck and the people of his team in Erlangen, specially Edith and Wolfgang whose help and support was invaluable during the months I spent in Germany.

During the years I spent in Naples, I met amazing people who own a special piece of my heart. Massimo, Maria and their family, in the widest possible sense, are some of those people. I will never end thanking them for all they did and still do for me. Thanks to Vincenzo

who gave me the opportunity to get thus far in my career, I will always be grateful for what you did for me and I wish to say how much I admire you for your human altruism and scientific competence. Thanks to Sabrina and Irene for all the endless chats, tears and laughs.

I like to think that I have a piece of home in every place I have been and established important relationships. I can tell that Nottingham is now my main home because of course of all the people that in the last few years have become family to me. Being an expat is not an easy thing, but the community that it forms is an important hybrid between friendship and family. This is why I must thank all the people that made me feel at home from the day I moved here: Stefano, Anahita, Pericle, Luigi, Brunetta, Tatiana, Marcolino, Nicobao, Dena.

This last year has been peculiar and at the very least and has revealed many surprises, one of which was meeting one of the loveliest and kindest people I have ever met, Adam. Finding you has been unexpected, and you manage to surprise me day after day (and, I tell you, I do not get surprised that easily lately). Through you I met your beautiful family, who welcomed me in the middle of a pandemic. When my family could not be next to me and look after me, your parents did.

Last, but not least, the biggest thanks are for my family. I would not be who I am (proud to be) now if it was not for you and your unconditional and loving support, dearest dad, mum, brother, sister, grandparents, and Andrea.

You all taught me something, and this represents the most valuable belonging I will always carry with me.

Grazie di tutto.

Table of Contents

Abbreviations.....	1
List of Figures.....	4
List of Tables.....	6
Abstract.....	8
1. Introduction.....	9
1.1 Cancer	9
1.2 Cancer Cell-Signatures.....	11
1.2.1 Selective growth and proliferative advantage.....	12
1.2.1.1 Altered stress response favouring overall survival.....	13
1.2.1.2 Vascularisation	14
1.2.1.3 Invasion and metastasis	15
1.2.1.4 Metabolic rearrangement	15
1.2.1.5 The Tumour Microenvironment (TME)	16
1.3 Metastasis	19
1.3.1 Local invasion	20
1.3.2 Hematogenous/lymphatic intravasation.....	21
1.3.3 Navigating in a new environment: survival in the circulation	21
1.3.4 Homing to a distant body district: tissue tropism and extravasation.....	22
1.3.5 Metastatic colonization	22
1.4 Epithelial-to-Mesenchymal Transition (EMT)	24
1.4.1 EMT program.....	24
1.4.2 EMT in cancer and PCa	25
1.4.3 EMT and cancer cell ‘stemness’.....	27
1.4.4 EMT-inducing transcription factor families	27
1.4.5 EMT markers.....	28
1.5 Prostate Cancer	31
1.5.1 Characterisation	31
1.5.2 Diagnostic approaches	32
1.5.3 Current treatment for local and metastatic PCa	35
1.5.4 Prostate cancer <i>in vitro</i> models.....	37
1.6 Cancer Immunotherapy	38
1.6.1 Immune surveillance	38
1.6.2 Immunotherapeutic approaches, an overview	41
1.6.2.1 Immune checkpoint blockade	41
1.6.2.2 Cytokine therapy	45
1.6.2.3 Vaccine-based therapy.....	45
1.6.2.4 Adoptive T-cell transfer.....	46
1.7 Therapeutic Antibodies.....	50
1.7.1 Immunoglobulin structure.....	50
1.7.2 Mechanisms of action of mAbs	54
1.7.3 Full monoclonal antibodies and antibody fragments	57
1.7.4 Bispecific and trispecific antibodies.....	61
1.8 EPCR as A Novel Marker for Aggressive PCa and Its Use in Therapy Design.....	63
1.9 Aims and Objectives	63

2. Identification and Characterisation of EPCR as A Potential Target for Immunotherapy of Aggressive Prostate Cancer.....	64
2.1 Introduction.....	64
2.2 Materials and Methods.....	68
2.2.1 Materials.....	68
2.2.1.1 Reagents.....	68
2.2.1.2 Equipment.....	69
2.2.1.3 Cell line growth media.....	71
2.2.1.4 Buffers and gels.....	71
2.2.2 Methods	73
2.2.2.1 Routine cell culture	73
2.2.2.2 Mass spectrometry analysis of differentially expressed proteins	74
2.2.2.3 Expression of endogenous PROCR mRNA in normal tissues: Real-time quantitative PCR (qRT-PCR)	76
2.2.2.4 Expression of endogenous EPCR protein in normal tissues: Western Blot.....	78
2.2.2.5 Cell surface expression of endogenous EPCR protein in normal tissues: Flow Cytometry	81
2.2.2.6 Immunohistochemistry staining of Tissue Microarrays (TMAs)	83
2.3 Results.....	85
2.3.1 Identification of the target: the human EPCR.....	85
2.3.2 Differential expression of EPCR in benign and prostate cancer cells.....	93
2.3.3 Evaluation of EPCR as a novel PCa biomarker.....	97
2.4 Discussion	99
3. Investigating the Role of EPCR in Prostate Cancer Progression.....	102
3.1 Introduction.....	102
3.2 Materials and Methods.....	103
3.2.1 Materials.....	103
3.2.1.1 Reagents.....	103
3.2.1.2 Equipment.....	104
3.2.1.3 Cell line growth media.....	106
3.2.1.4 Buffers and gels.....	106
3.2.2 Methods	108
3.2.2.1 Routine cell culture	108
3.2.2.2 Silencing of EPCR in DU145 and PC3 cells.....	109
3.2.2.3 Assessment of silencing of EPCR in DU145 and PC3 cells.....	112
3.2.2.4 Effects of EPCR silencing on cell proliferation and clonogenicity	113
3.2.2.5 Effects of EPCR silencing on cell migration and invasion.....	114
3.2.2.6 Effects of EPCR silencing on EMT and cancer progression	115
3.3 Results.....	118
3.3.1 Assessment of effective EPCR silencing in DU145 and PC3 cells	118
3.3.2 Effects of EPCR silencing on cell proliferation and clonogenicity.....	123
3.3.3 Effects of EPCR silencing on cell migration and invasion	126
3.3.4 Effects of EPCR silencing on EMT and cancer progression.....	127
3.3.4.1 EMT markers expression modulation upon EPCR silencing	127
3.3.4.2 Profile changes in mRNA expression after EPCR knock down.....	130
3.3.4.3 Analysis of the effect of EPCR silencing on cellular protein expression in DU145 cells	133
3.4 Discussion	141
4. Generation, Characterisation, and Validation of Monoclonal Antibodies Targeting EPCR.....	146
4.1 Introduction.....	146

4.2 Materials and Methods.....	152
4.2.1 Materials.....	152
4.2.1.1 Reagents.....	152
4.2.1.2 Equipment.....	153
4.2.1.3 Cell line growth media.....	154
4.2.1.4 Buffers and gels	155
4.2.2 Methods	158
4.2.2.1 Routine cell culture	158
4.2.2.2 Generation of mouse mAbs against human EPCR.....	159
4.2.2.3 Characterisation and validation of newly generated mouse mAbs against human EPCR	167
4.3 Results.....	179
4.3.1 Generation and selection of hybridoma clones producing specific mAbs against human EPCR ..	179
4.3.1.1 Mice immunisation with target antigen.....	179
4.3.1.2 Cell fusion, selection and primary screening.....	184
4.3.2 Sequencing of newly generated anti-human EPCR mAbs.....	188
4.3.3 Validation of purified anti-human EPCR mAbs	190
4.3.2.1 Purification of mAbs from hybridoma cell culture supernatants	190
4.3.3.2 Application of purified mAbs in Western blot.....	191
4.3.3.3 Application of purified mAbs in flow cytometry.....	192
4.3.3.4 Application of purified mAbs in immunofluorescence	195
4.2.3.4 Application of purified mAbs in ELISA	195
4.3.2.5 Mapping of epitope recognised by purified mAbs on the target antigen	196
4.4 Discussion	203
5. Anti-EPCR mAb Subtype Switching and Testing Its Therapeutic Utility Using Targeting Experiments	209
5.1 Introduction.....	209
5.2 Materials and Methods.....	213
5.2.1 Materials.....	213
5.2.1.1 Reagents.....	213
5.2.1.2 Equipment.....	214
5.2.1.3 Cell line growth media.....	215
5.2.1.4 Buffers and gels	215
5.2.2 Methods	216
5.2.2.1 Routine cell culture	216
5.2.2.2 Anti-human EPCR mAbs subtype switch	217
5.2.2.3 ADCC assay	217
5.2.2.4 Administration of anti-human EPCR antibodies to CB17/SCID mice.....	221
5.2.2.5 Generation of DU145-Luc2 cells expressing Luciferase Reporter Gene	223
5.2.2.6 DU145-Luc2 tumour growth in CB17/SCID mouse model.....	226
5.2.2.7 Tumour growth and antibody administration in CB17/SCID mouse model	226
5.3 Results.....	229
5.3.1 Antibody subtype switch from IgG1 to IgG2b.....	229
5.3.2 Application of generated mAbs for <i>in vitro</i> tumour targeting: ADCC	229
5.3.3 Antibody persistence <i>in vivo</i> in CB17/SCID mouse model	232
5.3.4 DU145-Luc2 tumour growth in CB17/SCID mouse model	234
5.3.5 Tumour growth and antibody administration in CB17/SCID mouse model	236
5.3.6 Anti-human EPCR JvGCRC-H61.3 mAbs patenting and commercialisation	240
5.4 Discussion	241
6. Summary of Discussion.....	246
Bibliography	252

Abbreviations

α2M	Alpha-2-Macroglobulin
ACT	Adoptive T-Cell Transfer
ACT	Alpha-1-Antichymotrypsin
ADC	Antibody-Drug Conjugates
ADCC	Antibody-Dependent Cellular Cytotoxicity
ADCP	Antibody-Dependent Cellular Phagocytosis
ADT	Androgen Deprivation Therapy
AM	Affinity Maturation
aPC	Activated Protein C
APC	Antigen Presenting Cell
AR	Androgen Receptor
AWE	Alive Without Events
BM	Basal Membrane
BME	Basal Membrane Extract
Breg	Regulatory B Cell
BY	Benjamini Yekutieli
CAF	Cancer Associated Fibroblast
CAR	Chimeric Antigen Receptor
CDC	Complement-Dependent Cytotoxicity
CDR	Complementary-Determining Region
CDX	Cell Line-Derived Xenograft
cPML	Cytoplasmic Promyelocytic Leukaemia
cPSA	Complexed PSA
CSC	Cancer Stem Cell
CTC	Circulating Tumour Cell
CTLA-4	Cytotoxic T-Lymphocyte-Associated Protein 4
ECM	Extra Cellular Matrix
EMP	Epithelial-Mesenchymal Plasticity
EMT	Epithelial to Mesenchymal Transition
EMT-TFs	Emt-Associated Transcription Factors
EndMT	Endothelial-Mesenchymal Transition
Fab	Fragment Antigen Binding
FcγR	Fcγ Receptor
FCM	Flow Cytometry
FCS	Fetal Calf Serum
FDA	Food and Drug Administration
FDR	False Discovery Rate
FGFR	Fibroblast Growth Factor Receptor
FOV	Field of View
fPSA	Free PSA
GEMM	Genetically Engineered Mouse Model
GF	Growth Factor
GLUT	Glucose Transporter
GM-CSF	Granulocyte Macrophage Colony-Stimulating Factor
HC	Heavy Chain
HIF	Hypoxia-Inducible Transcription Factor

HLA	Human Leukocyte Antigen
HRPC	Hormone-Relapsed Prostate Cancer
HSPC	Hormone Sensitive Prostate Cancer
IDA	Information Dependent Acquisition
IFN	Interferon
IgG	Immunoglobulin G
IL	Interleukin
ITAM	Immunoreceptor Tyrosine-Based Activation Motif
KIR	Killer Cell Ig-Like Receptors
LC	Light Chain
LOX	Lysyl Oxidase
mAbs	Monoclonal Antibodies
MAC	Membrane Attack Complex
MaSCs	Multipotent Mammary Stem Cells
MHC	Major Histocompatibility Complex
MMPs	Metalloproteinases
MoA	Mechanisms of Action
MPM	Malignant Pleural Mesothelioma
MS	Mass Spectrometry
NFAT	Nuclear Factor of Activated T Cells
NHL	Non-Hodgkin Lymphoma
NK	Natural Killer
NOD/SCID	Non-Obese Diabetic/Severe Combined Immunodeficiency
OS	Overall Survival
PAP	Prostatic Acid Phosphatase
PARP	Poly(Adenosine Diphosphate-Ribose) Polymerase
PC	Protein C
Pca	Prostate Cancer
PD-1	Programmed Death 1
PD-L1	Programmed Death Ligand 1
PD-L2	Programmed Death Ligand 2
PDX	Patient-Derived Xenograft
PEG	Polyethylene Glycol
PET	Polyethylene Terephthalate
PIN	Prostatic Intraepithelial Neoplasia
PSA	Prostate Specific Antigen
PsMab	Polispecific Monoclonal Antibodies
QC	Quality Control
Rb	Retinoblastoma
RIPA	Radioimmunoprecipitation Assay
RIT	Radioimmunotherapy
RT	Room Temperature
scFv	Single-Chain Variable Fragment
sdAb	Single-Domain Antibody
shRNA	Short Hairpin RNA
SHM	Somatic hypermutations
SLAMF7	Signalling Lymphocytic Activation Molecule Family Member 7
SN	Supernatant
SWATH	Sequential Window Acquisition of All Theoretical Fragment Ion Spectra
TAA	Tumour Associated Antigen
TCR	T-Cell Receptor

TEAB	Tetraethylammonium Bromide
TF	Transcription Factor
TGF-β	Transforming Growth Factor-B
TIB	Tumour Infiltrating B Cell
TIC	Tumour-Initiating Cell
TIL	Tumour Infiltrating Lymphocyte
TMA	Tumour Microenvironment
TNF	Tumour Necrosis Factors
tPSA	Total PSA
Treg	Regulatory T Cell
VEGF	Vascular Endothelial Growth Factor
WHO	World Health Organisation
WT	Wild Type

List of Figures

Figure 1.1 – Top cancer incidence per country.....	10
Figure 1.2 – The 20 most common cancers, UK, 2017	10
Figure 1.3 – Cancer signatures at a glance.....	11
Figure 1.4 – Tumour microenvironment complexity.....	16
Figure 1.5 – Stages of metastatic progression.....	19
Figure 1.6 – Normal and cancer prostate cells	32
Figure 1.7 – Gleason’s pattern standard drawing.....	35
Figure 1.8 – The Cancer-Immunity Cycle.....	38
Figure 1.9 – Antigen presentation and T-cell activation.....	39
Figure 1.10 – Immune Escape Mechanisms	40
Figure 1.11 – CTLA-4 and PD-1 checkpoints.....	41
Figure 1.12 – Currently available adoptive T-cell transfer (ACT) approaches	46
Figure 1.13 – Structure of different CAR molecules showing their evolution across the five generations.....	48
Figure 1.14 – Human immunoglobulins classification	51
Figure 1.15 – Immunoglobulin structure and classification of therapeutic monoclonal antibodies (mAbs)	52
Figure 1.16 – Mechanisms of action of functional mAbs	55
Figure 1.17 – Functional fragments of mAbs used for cancer treatment.....	60
Figure 2.1 – PMLI mutant constructs	66
Figure 2.2 – Primer optimisation for Real-time quantitative PCR (qRT-PCR).....	77
Figure 2.3 – Gating scheme for flow cytometric analysis.	83
Figure 2.4 – Schematic representation of the process for the identification of target and results.....	86
Figure 2.5 – Representation of the human EPCR protein.....	91
Figure 2.6 – EPCR protein expression in normal tissues and cancer biopsies	92
Figure 2.7 – Relative PROCR mRNA expression levels in normal and PCa cell lines.....	93
Figure 2.8 – Relative EPCR protein expression levels in normal and PCa cell lines.....	94
Figure 2.9 – Cell surface expression of EPCR.....	96
Figure 2.10 – Immunohistochemistry analysis of EPCR expression in prostate cancer biopsies	98
Figure 2.11 – Ligands of EPCR and related signalling responses	100
Figure 3.1 – Workflow for the generation of stable knockdowns for EPCR.....	109
Figure 3.2 – Schematic guide for selection antibiotic optimal concentration	110
Figure 3.3 – Expression of EPCR mRNA in DU145 and PC3 cells following silencing knockdowns with EPCR shRNAs.....	119
Figure 3.4 – Expression of EPCR in DU145 and PC3 cells following knockdowns with EPCR shRNAs	120
Figure 3.5 – Micrographs showing wild type and EPCR knock down populations of DU145 and PC3 cells	121
Figure 3.6 – Expression of EPCR in DU145 and PC3 cells following knockdowns with EPCR shRNAs.....	122
Figure 3.7 – Proliferation growth curve in DU145 and PC3 cells following knockdowns with EPCR shRNAs.....	124
Figure 3.8 – Colony formation assay	125
Figure 3.9 – Cell migration and invasion assays.....	126

Figure 3.10 – Western blot of EMT markers in DU145 cells.....	128
Figure 3.11 – Western blot of EMT markers in PC3 cells	129
Figure 3.12 – Profile changes in mRNA expression after EPCR knock down with shRNA4 in DU145 cells.....	131
Figure 3.13 – Heatmap showing the top 100 significantly modulated proteins in shRNA4 vs. control DU145 cells.....	136
Figure 3.14 – Genome-wide overview of the Reactome pathway analysis.....	138
Figure 4.1 – Overview of the mAbs generation process.....	147
Figure 4.2 – Human EPCR protein	149
Figure 4.3 – HAT selection for hybridomas	150
Figure 4.4 – Indirect ELISA for specific anti-EPCR IgG detection in purified antibodies ...	160
Figure 4.5 – Sandwich ELISA for IgG detection in hybridoma CSNs.....	164
Figure 4.6 – Hybridoma sequencing approach developed by Absolute Antibody.....	167
Figure 4.7 – Antibody purification steps overview	168
Figure 4.8 – Antibody titre in sera isolated from immunised mice	180
Figure 4.9 – Full panel of control tests on 38 B9 and NIH 3T3 cells	182
Figure 4.10 – Full panel of sera tests on 38 B9 and NIH-3T3 cells	183
Figure 4.11 – Hybridoma cell cultures.....	184
Figure 4.12 – Screening of hybridoma CSNs with ELISA	185
Figure 4.13 – Flow cytometry analysis of anti-human EPCR specific subclones.....	187
Figure 4.14 – SDS-PAGE of purified anti-EPCR mAbs	191
Figure 4.15 – Validation of purified antibodies against human EPCR in Western blotting	192
Figure 4.16 – Antibody Titration for Flow Cytometry Analysis	192
Figure 4.17 – Validation of purified antibodies against human EPCR in Flow Cytometry analysis.....	194
Figure 4.18 – Validation of purified antibodies against human EPCR in Immunofluorescence.....	195
Figure 4.19 – Validation of purified antibodies against human EPCR in ELISA	196
Figure 4.20 – Epitope mapping of Sigma anti-EPCR mAb.	198
Figure 4.21 – Epitope mapping of JvGCRC-H61.3 anti-EPCR mAb	199
Figure 4.22 – Epitope mapping of JvGCRC-H589.9 anti-EPCR mAb	200
Figure 4.23 – Epitope mapping of JvGCRC-H599.5 anti-EPCR mAb	201
Figure 4.24 – Epitope mapping of JvGCRC-H754.6 anti-EPCR mAb	202
Figure 5.1 – Representation of the mFc _y RIV ADCC Reporter Bioassay	218
Figure 5.2 – Antibody serial dilutions.....	220
Figure 5.3 – 24 well plate map used for selection of antibiotic optimal concentration....	223
Figure 5.4 – Vector map of pBudCE4.1/Luc2 plasmid.....	224
Figure 5.5 – Assessment of the ability of anti-EPCR mAbs to mediate effector cell activation.	230
Figure 5.6 – Antibody persistence in serum from mice.....	233
Figure 5.7 – DU145-Luc2 optimisation	234
Figure 5.8 – <i>In vivo</i> DU145-Luc2-derived tumour growth rate study.....	235
Figure 5.9 – Antibody persistence in sera from mice.....	237
Figure 5.10 – <i>In vivo</i> assessment of the effects of the treatment with JvGCRC61.3 and JvGCRC599.5 mAbs against human EPCR on tumour growth.....	238
Figure 5.11 – <i>Ex vivo</i> assessment of the effects of the treatment with JvGCRC61.3 and JvGCRC599.5 mAbs against human EPCR on tumour growth.....	239

List of Tables

Table 1.1 – TNM staging system for PCa.....	34
Table 1.2 – FDA-approved immune checkpoint inhibitors	42
Table 1.3 – Localisation of the major IgG Fc-receptors (Fc _Y Rs) in human.....	53
Table 1.4 – Mechanism of action (MoA) of the principal antibody-based drugs used in cancer treatment	59
Table 2.1 – Current FDA approved therapies for mHRPC	65
Table 2.2 – cDNA master mix	76
Table 2.3 – <i>PROC</i> R primers specifications	77
Table 2.4 – Real-time quantitative PCR (qRT-PCR) master mix	78
Table 2.5 – PCR conditions	78
Table 2.6 – BSA standard curve	79
Table 2.7 – Antibodies and dilutions used in Western blot analysis.....	81
Table 2.8 – Primary and secondary antibodies used for flow cytometry analyses.....	82
Table 2.9 – Proteins differentially expressed in DU145 PMLΔNES vs PMLΔNLS.....	87
Table 2.10 – Final candidate target selection process	89
Table 3.1 – Specification of the MISSION® shRNA clones used to perform gene silencing in target cells	112
Table 3.2 – List of the antibodies used in Western Blot analysis.....	113
Table 3.3 – List of the antibodies used in Western Blot analysis for EMT markers.....	115
Table 3.4 – NanoString probe hybridisation master mix.....	116
Table 3.5 – PanCancer Progression Panel pathways	130
Table 3.6 – Top 20 significant p-value genes.....	132
Table 3.7 – The list of proteins differentially expressed in whole cell lysate from DU145 EPCR knockdown (EPCR shRNA4) vs. DU145 control (Empty vector) cell populations	133
Table 3.8 – Pathways regulated by proteins differentially expressed in EPCR knockdown (shRNA4) vs. control (Empty vector) cell populations	139
Table 4.1 – Panel of immunisation steps	159
Table 4.2 – Secondary antibody used for ELISA analysis.....	161
Table 4.3 – Primary and secondary monoclonal antibodies used for flow cytometry analyses	162
Table 4.4 – Parameters setting for fusion ECFG21 Super Electro Cell Fusion Generator ...	163
Table 4.5 – Antigen, primary and secondary monoclonal antibodies used for ELISA analysis	165
Table 4.6 – Primary and secondary monoclonal antibodies used for flow cytometry analyses	166
Table 4.7 – Generation of protein standards	170
Table 4.8 – Antibodies and dilutions used in Western Blot analysis.....	171
Table 4.9 – Primary and secondary monoclonal antibodies used for flow cytometry.....	173
Table 4.10 – Primary and secondary monoclonal antibodies used for Immunofluorescence	174
Table 4.11 – Primary and secondary monoclonal antibodies used for ELISA analysis	176
Table 4.12 – Library of Overlapping Peptides of EPCR Generated for Epitope Mapping of Purified Antibodies	177

Table 4.13 – Antigen, primary and secondary monoclonal antibodies used for ELISA analysis	178
Table 4.14 – Sequencing of anti-EPCR hybridomas	189
Table 4.15 – Summary of the suitability of purified mAbs for different applications.....	205
Table 4.16 – Epitope mapping and ligand binding residues comparison.....	207
Table 5.1 – Effector cells and activating Fc γ Receptors Involved in ADCC.....	209
Table 5.2 – Target cells and antibodies tested in the ADCC bioassay	218
Table 5.3 – Antibody persistence in mouse serum, study design	221
Table 5.4 – Secondary antibody used for ELISA analysis.....	222
Table 5.5 – Cell dilutions for Luciferase activity assay	225
Table 5.6 – Primary and secondary monoclonal antibodies used for flow cytometry.....	226
Table 5.7 – DU145-Luc2 tumour growth in CB17/SCID mouse model dose group panel..	226
Table 5.8 – Tumour growth and antibody administration in CB17/SCID mouse model dose groups panel.....	227
Table 5.9 – Mice immunisation with anti-EPCR mAbs dose groups panel	228
Table 5.10 – Antibody subtype switch	229
Table 5.11 – Half maximal effective concentration (EC ₅₀) and maximum fold induction...	231

Abstract

Background: Despite androgen deprivation treatment, hormone-relapsed prostate cancer (HRPC) typically progresses to metastasis - metastatic prostate cancer remains incurable and there is a clear unmet clinical need to identify new therapeutic approaches. A previous study carried out by our team demonstrated that the expression of the human Endothelial Protein C Receptor (EPCR, CD201) in prostate cancer cells *in vitro* is associated with Epithelial to Mesenchymal Transition (EMT), a key element of the metastatic pathway.

Hypothesis: That targeting of prostate cancer cells expressing EPCR using a monoclonal antibody (mAb) has therapeutic potential against aggressive, metastatic prostate cancer.

Aims of the Study: To develop mAbs against the human EPCR and evaluate their therapeutic potential by assessing their capacity to target and kill invasive prostate cancer cells *in vitro* and *in vivo*.

Experimental Approach: Functional analysis of prostate cancer cell lines expressing a construct for knock down of EPCR were performed in order to validate EPCR as a valid target for immunotherapeutic treatment of aggressive prostate cancer. Four murine mAbs against EPCR were generated, the hybridomas sequenced and recombinant mAbs produced. The specificity of the purified mAbs was confirmed using flow cytometry, immunofluorescence, ELISA and immunoblotting assays. An *in vitro* antibody-dependent cell-mediated cytotoxicity (ADCC) reporter assay demonstrated the ability of the recombinant mAbs to mediate ADCC against human prostate cancer cell lines (DU145, PC3). These results were further investigated *in vivo* using a CB17/SCID mouse xenograft tumour model. Recombinant mAbs did not produce any significant effect on tumour growth rate or metastasis formation *in vivo*.

Summary and Impact: We have generated a new panel of mAbs against EPCR/CD201 which have the potential to form the basis of new therapeutic approaches for treating aggressive, metastatic prostate cancer based on the triggering of ADCC or the delivery of Antibody-Drug Conjugates (ADCs). This project also opens the way to the development of therapies based on EPCR chimeric antigen receptor (CAR) T cells and bispecific antibodies.

1. Introduction

1.1 Cancer

In 1775 Sir Percival Pott, a British surgeon, carried out a study on the epidemiology of scrotal cancer in which for the first time a potential carcinogenic was identified and the theory of cancer development even years after exposition demonstrated. That was the first research about causes related to cancer and potential prevention. Since then, many revolutionary advances have been made in cancer understanding, prevention and treatment. The biggest challenge that modern medicine is facing in cancer treatment is to understand the molecular and cellular mechanisms that allow its development and evolution to develop more effective treatments.

The term "cancer" defines a condition in which abnormal cells go through uncontrolled growth and eventually generate metastases that invade organs impairing their function thus leading to death. More precisely, "cancer" – according to the American Cancer Society - refers to over 100 different diseases, depending on the target organ and its cellular heterogeneity. Several genetic, lifestyle and environmental factors can increase the risk of developing cancer in humans. Monitoring such factors can help identify predisposition of an individual to a specific cancer type, thus providing a powerful tool for prevention of malignancies. Indeed, extensive screening programs led to the detection of early signs of cancer, improving the prognosis of patients due to prompt and targeted treatment interventions.

Cancer numbers are high worldwide and, according to World Health Organisation (WHO <https://www.who.int/cancer>), there were 17 million new cancer cases in the world in 2018, with the most common - lung, female breast, prostate and bowel cancers - accounting for more than 43% of the total (Figure 1.1). Projections about the incidence of cancer say that by 2040 the rates will increase up to 61.7% of the cases registered in 2018 worldwide (International Agency for Research on Cancer 2018).

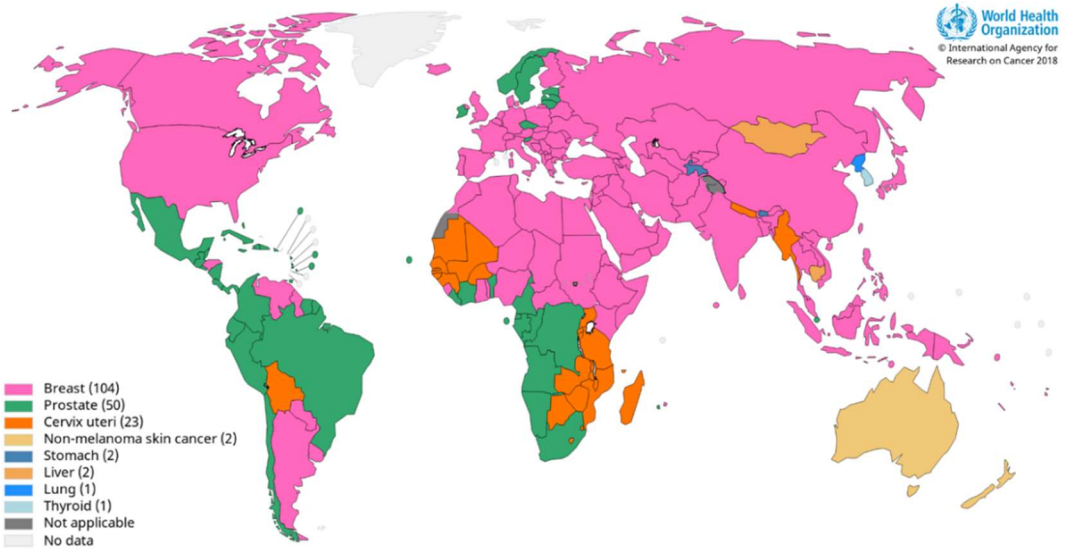


Figure 1.1 - Top cancer incidence per country. The map represents the estimated age-standardized incidence rates (World) in 2018, considering both sexes and all ages. (Data source: GLOBOCAN 2018, Graph production: IARC, <http://gco.iarc.fr/today/home> - WHO)

In the UK, there are on average 367,000 new cancer cases each year. Men are affected more than women and there is a higher incidence in people aged 85 to 89 (data collected over 2015-2017). Cancer accounts for 165,000 deaths in the UK every year (2015-2017), more than 28% of the total deaths. The most commonly diagnosed cancers in the UK affect breast, prostate, lung and bowel, accounting together for 53% of all new cancer cases in 2017 (Figure 1.2). (Cancer Research UK <http://www.cancerresearchuk.org>).

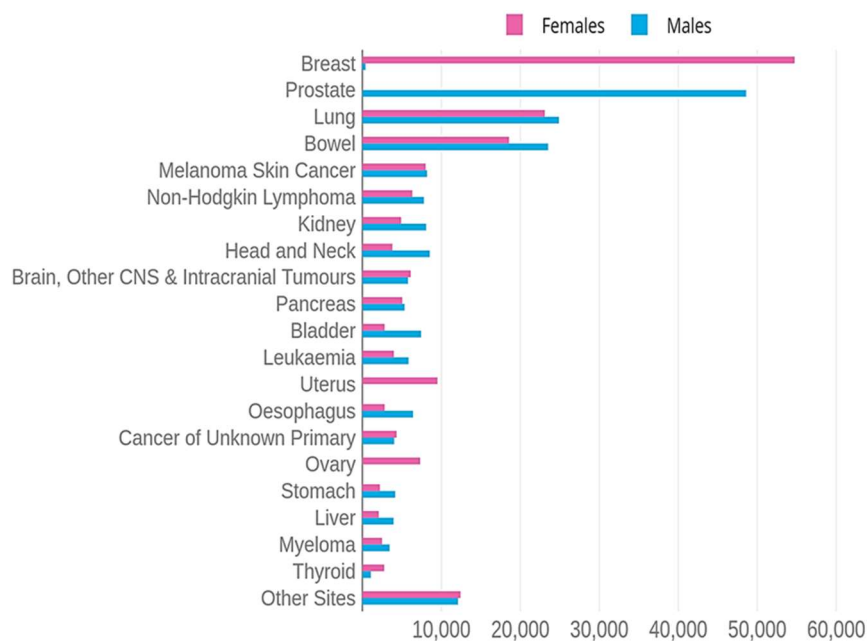


Figure 1.2 - The 20 most common cancers, UK, 2017. The graph represents numbers of cases per site of primary cancer divided by gender.

1.2 Cancer Cell-Signatures

Hanahan and Weinberg published two inspiring reviews on what they called the "Hallmarks of Cancer". In the first review (Hanahan, Weinberg 2000), cancer-specific features were organised into six main biological capabilities that normal cells gain during their transformation into malignant cells, and these were subsequently updated to eight in the second review (Hanahan, Weinberg 2011). Such features were identified as (i) sustaining proliferative signalling, (ii) evading growth suppressors, (iii) resisting cell death, (iv) enabling replicative immortality, (v) inducing angiogenesis, (vi) activating invasion and metastasis, (vii) reprogramming of energy metabolism and (viii) evading immune destruction. The first critique to such a classification came by Lazebnik, who argued that all the hallmarks, except the invasion/metastasis formation ability, apply to both benign and malignant neoplasia, whereas cancer univocally refers to the malignant diseases (Lazebnik 2010). In 2017, Fouad and Aanei revised the Hallmark theory, suggesting a more comprehensive, tissue-integrated rather than cell-focused, point of view (Figure 1.3). Recently, these cancer signatures have been suggested to be shared by the wound healing process (MacCarthy-Morrogh, Martin 2020).

In their review, Fouad and Aanei defined cancer hallmarks as being specific features acquired by normal cells during their life and that confer evolutionary advantages that can allow cell transformation and malignant progression at the expense of surrounding tissue (Fouad, Aanei 2017).

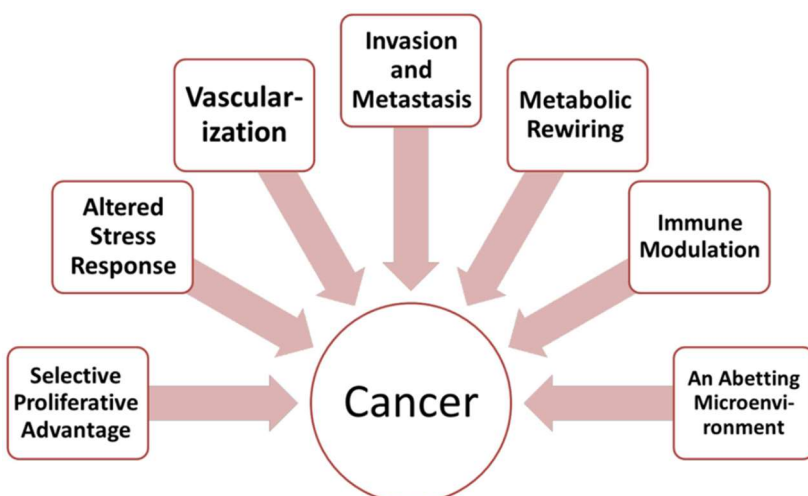


Figure 1.3 - Cancer signatures at a glance. Cancer Hallmarks were organised for the first time by Hanahan and Weinberg, here shown as revisited in the *Revisiting the Hallmarks of Cancer* (Adapted from Fouad, Aanei 2017)

1.2.1 Selective growth and proliferative advantage

Tissue homeostasis is essential for the correct functioning of organs and related physiologic systems. Such organisation is maintained by a finely tuned network of genes involved in the maintenance of a correct cell cycle regulation that prevents uncontrolled cell proliferation, such as deregulation caused by gene mutations that cause the disruption of the normal tissue organisation. Cancer cells often carry passenger and driver mutations within their genome, with the latter alone being responsible for oncogenesis, conferring enhanced growth advantage to transforming cells and "driving" clonal expansion of malignant cells (Stratton, Campbell et al. 2009). The amplification of mutated clones enables the oncogenic mutations to be permanently fixed in their genome, thus permitting the accumulation of further mutations in what is considered the multi-step process underlying cancer progression. The main regulatory genes responsible for correct cell cycle progression are retinoblastoma (Rb) and p53. Rb is responsible for the cellular genomic stability, and is a key regulator of cell metabolism, senescence, and apoptosis (Indovina, Marcelli et al. 2013). Alongside Rb, p53 - also known as the "Guardian of the Genome" -, is a tumour suppressor that has been found to be mutated in over 50% of sequenced tumours (Stracquadanio, Wang et al. 2016). In physiological conditions, p53 becomes activated in response to DNA damage, such as double-strand breaks, which stops cell cycle progression to allow the repair mechanisms to act. When the damage is not fixable, p53 activates cell-death pathways.

Alterations in growth factor (GF) signalling pathways can enhance the uncontrolled growth of normal cells, which promotes their escape from the mechanisms that maintain tissue homeostasis. Mutations affecting both growth-promoting and growth-inhibiting factors, boosting or impairing their expression respectively, leads to the increased proliferative ability of transforming cells (Witsch, Sela et al. 2010). Transforming growth factor- β (TGF- β) can trigger cancer progression by promoting the acquisition of cancer stem cell (CSC)-like properties and cell de-differentiation in transforming cells (Katsuno, Lamouille et al. 2013). Interestingly, TGF- β is also involved in immune suppression (Yoshimura, Muto 2011). Alterations can affect GF signalling pathways at several levels. Amplification of receptor genes, constitutive ligand-independent receptor activation, and mutations impairing genes of other proteins involved in the signal transduction, can all converge to result in aberrant cell proliferation. One protein of which mutations are found in 25% of cancers is the RAS family of oncogenes (Hobbs, Der et al. 2016). Abnormal RAS activity can also lead to the suppression of apoptosis and immune escape (Simanshu, Nissley et al. 2017, Pylayeva-

Gupta, Grabocka et al. 2011). Moreover, many cancer cells acquire the ability to secrete GFs that can activate growth pathways in an autocrine fashion (Witsch, Sela et al. 2010).

1.2.1.1 Altered stress response favouring overall survival

Stress conditions can generate damage in the cellular genome and to varying degrees (Chircop, Speidel 2014). During physiological responses to any source of stress, normal cells activate specific systems to minimise damage or, if the damage cannot be fixed, to activate senescence, permanent cell cycle arrest, programmed death or apoptosis. Failures of the DNA repair system intuitively allow the establishment of new somatic mutations in transforming cells. The upregulation of the same systems has been reported to increase therapeutic resistance, as they can fix genomic breaks introduced by therapeutic agents, thereby contributing to tumour relapse after treatment (Srivastava, Raghavan 2015).

High levels of molecular stress can generate dangerous amounts of abnormal proteins/organelles that can be responsible for abnormal cellular activities. Cells can use *autophagy* as a protective mechanism through which they remove the unwanted damaged structures. Similar to what happens during DNA repair-mediated therapeutic resistance, upregulated autophagy in treated cancer cells can help them neutralise the cellular damage caused by the therapy. Indeed, increased autophagy levels have been linked to cancer survival and progression due to its role in immune escape and cancer progression via tumour microenvironment remodelling (Yun, Lee 2018).

Cells have a physiological replicative potential, which is defined by telomere length. With each division, telomeres shorten and when they become excessively short, the cells irreversibly exit the cell cycle and enter *senescence*. Telomerase is an enzyme that can restore telomeres and is upregulated in 85-90% of cancers (Shay 2016).

As an extreme reaction to stress damage and to maintain tissue homeostasis, cells can activate *apoptosis*, a controlled suicidal pathway that revolves on the activity of caspases. By avoiding apoptosis, cancer cells can gain resistance to apoptotic agents and uncontrollably proliferate (Hassan, Watari et al. 2014).

1.2.1.2 Vascularisation

Without a dedicated network of blood that provides nutrient supply, tumour growth is limited to 2-3 mm³ (Folkman 1971). While cancer cells are proliferating, the environment within the neoplastic lesion is poorly supplied which results in shortage of nutrients and oxygen, and accumulation of waste metabolites leading to hypoxia and a drastic decrease in pH (Erler, Bennewith et al. 2009). Hypoxia is characterised by the increase in the expression of the hypoxia-inducible transcription factor-1α (HIF-1α), the expression of which correlates with poor clinical prognosis in several cancers (Jing, Yang et al. 2019). HIF-1α activity, in combination with GF signalling, leads to the induction of metalloproteases (MMPs) and a large number of pro-angiogenic factors, especially the vascular endothelial growth factor (VEGF) (Lv, Li et al. 2017). Although pro-angiogenic and anti-angiogenic factors activities are maintained in a balanced state, when the expression of pro-angiogenic factors overcomes that of the anti-angiogenic factors, an angiogenic switch occurs, in which VEGF acts as a master trigger and regulator of vasculature formation (Baeriswyl, Christofori 2009). The main mechanism implied in tumour vascularisation is sprouting angiogenesis, in which tumour cells induce the formation of new vascular vessels from pre-existing capillaries. Such a mechanism is regulated by VEGF, which blocks Notch signalling in some of the endothelial cells that form the inner layer of capillaries. The cells in which Notch is deactivated, the so-called "tip cells", start to loosen their connections with the basement membrane and supportive pericytes, thus entering the EMT. Consequently, they release proteases that enable ECM degradation and start a polarised migration towards the tumour, following the VEGF gradient (Gerhardt, Golding et al. 2003). Fibroblast growth factor-2 (FGF-2) is also involved in tumour-associated neo-angiogenesis. Activation of the FGF-2 pathway in tumours has been linked to the acquired resistance to anti-angiogenic therapy targeting VEGF (Ichikawa, Watanabe Miyano et al. 2020). Alongside VEGF and FGF-2, platelet-derived growth factor (PDGF) induces tumour growth and angiogenesis. Although all the members of the PDGF family are known for their role in cancer progression, PDGF-B is the most characterised factor in the family (Lugano, Ramachandran et al. 2020). Remodelling of the tumour microenvironment through secretion of metalloproteases is a relevant factor in inducing angiogenesis. Indeed, MMP-2 and MMP-9 released in the neoplastic environment can activate latent forms of TGF-β, which act as an important regulator of neoangiogenesis (Yu, Stamenkovic 2000). Hypoxic tumours have been reported to be resistant to radiotherapy (Graham, Unger 2018).

1.2.1.3 Invasion and metastasis

Probably the characteristic that best defines a malignancy is the ability of cancer cells to invade surrounding tissues and metastasise to distant sites. Metastases are highly correlated with cancer death. For instance, in prostate cancer, deaths due to metastatic malignancies are 50.5% of the total (Dillekås, Rogers et al. 2019). Formation of metastases will be discussed in more detail within the forthcoming sections.

1.2.1.4 Metabolic rearrangement

Malignant cells utilise altered metabolic pathways that are necessary to sustain high cell growth rates and improve survival under metabolic stress, due to adverse environment conditions (tumour microenvironment, blood circulation, distal sites). Although tumour cells require higher levels of nutrients, they face a hostile microenvironment which is characterised by incomplete vasculature and high cellular density that drives nutrient shortage. As such, malignant cells go through a metabolic adaptation in order to sustain their growth.

The metabolism of cancer cells preferentially employs aerobic glycolysis over oxidative phosphorylation to fulfil their needs for rapid ATP production, a cellular process that was discovered by Otto Warburg and named after him as the 'Warburg Effect' (Warburg, Wind et al. 1927). Aerobic glycolysis requires high levels of *glucose* that is eventually fermented into lactate that contributes to the acidification of the tumour microenvironment (TME). Interestingly, the acidic microenvironment has been shown to promote tumour growth and progression (Estrella, Chen et al. 2013). Many cancers are characterised by upregulated expression of glucose transporter (GLUT) proteins (Ancey, Contat et al. 2018), the upregulation of which is driven by HIF-1 α . Interestingly, cancer cells also require intense mitochondrial metabolism in addition to glycolysis for their ATP production. Such a process is highly advantageous in a microenvironment with poor glucose availability (Reid, Sanderson et al. 2020). The higher metabolic demand in dividing cancer cells is met by increasing the supply of amino acids. Glutamine metabolism is one of the most studied (De Berardinis, Mancuso et al. 2007). Glutamine serves as a source of both carbon and nitrogen – needed to synthesise nucleic acid – which therefore establishes a 'glutamine addiction' state in cancer cells (Eagle 1955). In response to the increased growth rate, neoplastic cells require more lipids, resulting in increased lipid metabolism with high *de novo* fatty acid synthesis (Munir, Lisec et al. 2019).

1.2.1.5 The Tumour Microenvironment (TME)

Alone, tumour cells are not able to sustain their growth without organising their supportive niche. The ensemble of malignant cells with surrounding tumour stromal cells (like stromal fibroblasts, endothelial cells, and cells of the immune system) and acellular components (such as collagen and fibronectin among other extracellular matrix factors) is referred to as TME (Figure 1.4) (Baghban, Roshangar et al. 2020).

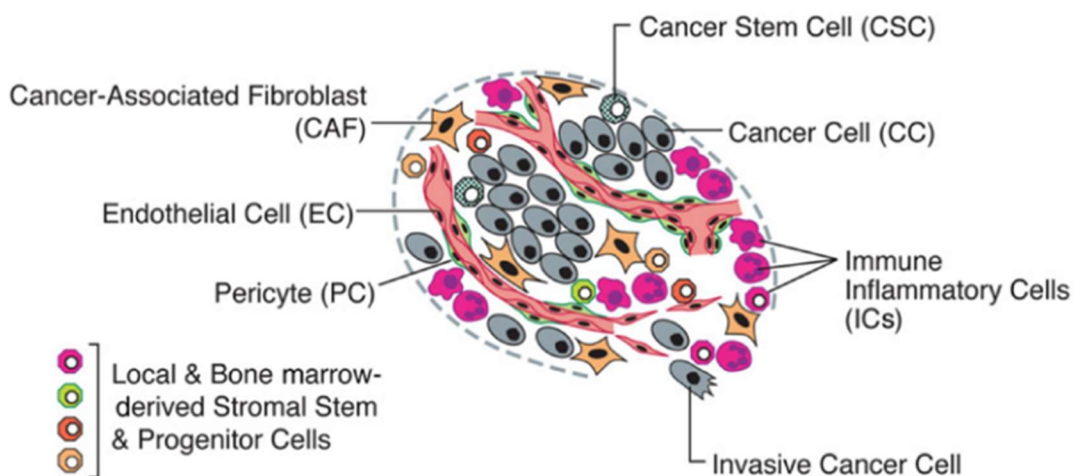


Figure 1.4 - Tumour microenvironment complexity. Other than cancer cells, the TMA landscape in solid tumours also consists of distinct immune cells. (Adapted from Hanahan, Weinberg 2011)

The TME plays a pivotal role in many aspects of the cancer progression, such as metabolism, growth, and metastasis formation thanks to the support provided to cancer cells by each component. In order for a tumour to be established efficiently in primary and secondary sites, the development of a dynamic and effective cross talk amongst the several cells in the complex TME is fundamental. Such exchange of information within the TME is guaranteed not only by direct cell contact, but also by a fine tuned network of cytokines, growth factors, inflammatory mediators, exosomes, and cell-free DNA released by both malignant and normal cells (Baghban et al. 2020). Recently, the TMA and its mechanisms are captivating great attention since disrupting those interactions that promote tumour progression have applications in cancer treatment. Below follows a concise summary of the cell populations that constitute the TMA.

- *Cancer-Associated Fibroblasts* (CAFs) are myofibroblasts that can differentiate from resident precursors (such as endothelial cells, myoepithelial cells, and mesenchymal stem cells). They are abundant in TME of several tumour types (Balkwill, Capasso et al. 2012) and play a critical role in various aspects of tumorigenesis by exerting both pro and anti-

tumour activities (Sugimoto, Mundel et al. 2006). CAFs are involved in the remodelling of the extracellular matrix (ECM), which induces recruitment of immunosuppressive cells to the TME eliciting immunosuppression of cancer cells (Monteran, Erez 2019). CAFs secrete growth factors such as VEGFA and PDGRF, which can promote inflammation and angiogenesis (Werb, Lu 2015), and EGF and FGF factors that have a mitogenic effect on cancer cells (Balkwill et al. 2012). Moreover, induction of EMT in cancer cells has been reported to be initiated by TGF- β secretion from CAFs (Erdogan, Webb 2017). Cell metabolism and proliferation has been reported to be positively affected by CAF activity in colorectal (Zhou, Xu et al. 2017) and ovarian cancer (Curtis, Kenny et al. 2019). Furthermore, in response to TGF- β and interleukin 1 (IL1) stimulation, CAFs have been shown to develop two distinct subtypes, respectively inflammatory and myofibroblastic (Biffi, Oni et al. 2019), which highlights how multifaceted their contribution to the TME design can be.

- *Tumour Endothelial Cells* (TECs) can be the product of cancer cells differentiation and can induce cancer progression and metastasis (Dudley 2012). TECs are required during angiogenesis in TME and together with *pericytes* are the basic units of the new vasculature associated to the tumour (Barbato, Bocchetti et al. 2019). As TECs show altered morphology, they contribute to hypoxia and acidosis in the TME by generating abnormal blood vessels (Jain 2005).
- *Circulating Tumour Cells* (CTCs) represent a very important subpopulation in the TME. Due to their ability to enter the blood stream, either passively or actively invading the vasculature, CTCs are regarded to be responsible for tumour metastasis, drug resistance and cancer relapse (Micalizzi, Maheswaran et al. 2017). Although CTCs presence in blood is very low (1-10 cells per 10 mL of blood), their detection and analysis are possible via simple non-invasive liquid biopsy and is currently used to assess the efficacy of cancer therapy. Moreover, increased numbers of CTCs correlate with poor prognosis (Kim, Yoo et al. 2018).
- *Tumour Infiltrating Lymphocytes* (TILs) in the TME promote progression in several cancers (Antohe, Nedelcu et al. 2019; Badalamenti, Fanale et al. 2019). Elucidating the context of the TILs in solid tumours is fundamental to predicting the clinical outcome and designing the most appropriate therapy in patients with cancer (Plesca, Tunger et al.

2020). Inflamed tumours are referred to as 'hot' and are characterised by significant T cell infiltration (Zhang, Endres et al. 2019), which are considered the major actors in anti-tumour immunity. Indeed, high numbers of CD8⁺ T cells is associated with good prognosis as they are a sign of ongoing immune surveillance, whereas infiltration of T regulatory cells (Tregs) is associated with tumour promotion due to their immunosuppressive effect. Recently, more focus has gone into tumour-infiltrating B cells (TIBs) since their activity has been reported to modulate TME and be associated with more favourable prognosis. Interestingly, regulatory B cells (Bregs) are also responsible for immunosuppression in the context of TME, where they indirectly modulate CD4⁺ T cells, Tregs and Natural Killer (NK) cells (Guo, Cui 2019). NK cells are effector cells of the immune system that are emerging as a promising approach for cancer therapy, although their ability to infiltrate solid tumours, where they can be recruited via chemokines such as CXCL9/10/11 (Susek, Karvouni et al. 2018), is significantly low (Nayyar, Chu et al. 2019).

- *Tumour-Associated Macrophages* (TAMs). Macrophages are naturally involved in innate and adaptive immunity, but can be recruited to the TME during local anoxia and inflammation through factors secreted by tumour cells, such as chemokines and cytokines, becoming plastic TAMs with tumour-promoting and immune evasion and suppression activity (Zhou, Tang et al. 2020). TAMs have been shown to exert their pro-tumour effects through secretion of chemokines and cytokines that are ultimately promoting EMT and stemness in cancer cells (Chen, Tan et al. 2018). Moreover, TAMs can also promote tumour immune escape by expressing PD-1 (Gordon, Maute et al. 2017). Contrarily, TAMs appear to have also an antitumour effect since they have been reported to inhibit TGF- β 1-induced EMT and impair tumour invasion in lung cancer (Kim, Ahn et al. 2019).
- *Dendritic Cells* (DCs) are heterogeneous population of antigen presenting cells (APCs), with multiple subsets of cells with differential roles during cancer pathogenesis. DCs are crucial during the immune response for their role in T cell activation and differentiation, and modulation of Bregs and NK cells (Tran Janco, Lamichhane et al. 2015). DCs exert an immunosuppressive activity in TME by inducing T cell tolerance. Currently, tumour-associated DCs activities are of great interest for the response to checkpoint blockade immunotherapy (Wylie, Macri et al. 2019).

1.3 Metastasis

As more than 90% of cancer-associated mortality is due to metastasis (Gupta, Massague 2006), understanding the mechanisms underlying this process is key in developing successful therapies. The first hypothesis on how cancer progresses through metastases was formulated by Stephen Paget in 1889 (Paget 1889) and then revived in 1980 by Ian Hart and Isaiah Fidler (Hart, Fidler 1980). According to the 'Seed and Soil' hypothesis which is based on clinical observations and analysis of case histories of several cancers, for a primary tumour to develop secondary tumours in distant sites it takes not only the ability of reaching a different tissue, but also the sustained growth of the cancerous cells in such tissue.

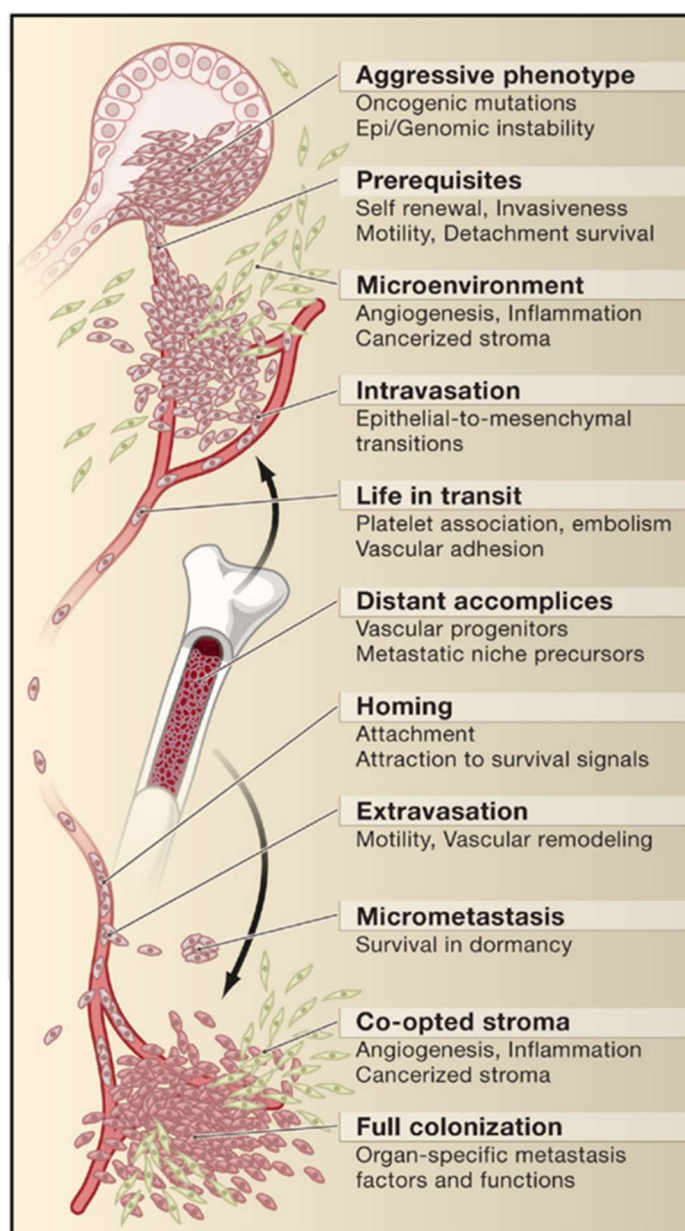


Figure 1.5 - Stages of metastatic progression. The process of metastasis formation consists of subsequent events involving transforming cancerous cells from the primary tumour that can then reach distant sites and there proliferate (Adapted from Gupta and Massagué, 2006).

For a secondary tumour to grow in a different part of the body it takes several events (Figure 1.5) that together are referred to as the *invasion-metastasis cascade* and which is directed by finely regulated molecular pathways (Valastyan, Weinberg 2011). Nevertheless, this process is highly inefficient, with less than 0.01% of the CTCs ultimately giving rise to metastasis (Chambers, Groom et al. 2002). Indeed, most of the CTCs are unable to go beyond the intravasation step.

1.3.1 Local invasion

Some of the cells within a primary solid tumour can acquire, at a certain point of their evolution, aggressive features that enable them to enter the first step for metastasis formation. By disrupting the components of the basal membrane (BM), cancer cells can enter the stroma.

The invasion of the stroma can take place either as a “collective” action by a cluster of metastatic cells or as a “single” event (Friedl, Gilmour 2009). Before single cells can start the invasive process, they need to detach from the neighbouring epithelial cells. The process that enables cell detachment is called epithelial-to-mesenchymal transition (EMT). Once they start acquiring a mesenchymal phenotype, they also acquire the ability to secrete metalloproteinases (MMPs), via which the ECM is degraded. Moreover, during the proteolysis of the ECM, many growth factors that promote cell proliferation are released (Kessenbrock, Plaks et al. 2010). Invading cells gain access to the active stroma via the BM. There, they interact with fibroblasts, as well as epithelial and mesenchymal-stem cells, and macrophages and other immune cells (Joyce, Pollard 2009). In the context of the TME, all these cell types have a promoting effect on the cancer cells. Zhu and his colleagues showed that in prostate cancer (PCa), the inflammatory cytokine IL-1 β that is produced by macrophages in the surrounding stroma can convert the androgen-receptor modulators from inhibitory to stimulatory (Zhu, Baek et al. 2006; Mantovani, Allavena et al. 2008). The establishment of an inflammatory environment facilitates the demolition of the tissues surrounding the primary tumour (Mantovani et al. 2008). TAMs have been demonstrated to be major producers of proteases in the TME (Joyce, Pollard 2009).

1.3.2 Hematogenous/lymphatic intravasation

The main route used by invasive cells to disperse through the body is the hematogenous circulation, rather than the lymphatic (Gupta, Massague 2006). The passage through the lymphatic vessels appears to be more of a passive process due to the structure of their walls, which are formed by endothelial cells resting on a discontinuous BM that allows a certain degree of leakiness. To enter the blood stream instead, cancer cells must pass through the pericytes and endothelial cells that constitute the walls of the microvessels, thereby disrupting the cell-cell connections. This is greatly facilitated by the formation of new blood vessels during neoangiogenesis, a process that is guided by carcinoma cells, primarily by the secretion of vascular endothelial growth factors (VEGFs). Blood vessels associated with the tumour are typically more tortuous and prone to leakiness due to their continuous rearranging (Carmeliet, Jain 2011), which makes them weaker and easier to break through.

1.3.3 Navigating in a new environment: survival in the circulation

Once tumour cells enter the circulation, they become CTCs, an intermediate state between primary and metastatic cancer cells. Surviving in the hematogenous environment is extremely challenging for CTCs. Cell connection to the ECM, mediated by integrins, is vital to epithelial cells, which explains why CTCs, which have lost their connections with other cells, can undergo *anoikis* while travelling through the blood stream (see section 1.4.3). The diameter of cancer cells (20–30 μm) is larger than that of the smallest capillaries (8 μm) which leads to the arrest of CTCs. Tumour cells in the blood stream can be damaged by its hemodynamic shear forces (Valastyan, Weinberg 2011). As an additional challenge, CTCs must avoid the immune surveillance by NK cells (Joyce, Pollard 2009). Interestingly, CTCs have been reported to be able to shield themselves from the effector cells of the immune system using platelets (Wang, Zhang et al. 2018), in that platelet-derived growth factor (PDGF) impairs immune surveillance by downregulating activating immune receptors on NK cells (Mitrugno, Moran et al. 2015). Tumour cell-associated tissue factor (TF) expression is linked to cancer progression (Palumbo, Degen 2007). TF is a membrane receptor for Factors VIIa and X and it is able to initiate blood coagulation. It has been shown to be involved in metastasis formation by triggering the formation of local thrombin-mediated microthrombi, in which platelet aggregates protect CTCs from the cytolytic activity of NK cells (Joyce, Pollard 2009). Furthermore, TF-mediated thrombin generation activates several

procoagulant molecules, such as protease activated receptors (PARs), fibrinogen and Protein C, all of which support the metastatic process (Palumbo, Degen 2007).

1.3.4 Homing to a distant body district: tissue tropism and extravasation

CTCs can theoretically end their journey when reaching any distant organ or tissue in the body through the blood stream. The first element that can determine the final destination of CTCs is the size of the blood vessels they are travelling through. As indicated above, restrictions in the diameter of the vasculature can trap CTCs. The most mentioned example is the massive trapping of colorectal cancer cells in the liver, as a consequence of the connection via the portal vein (Gupta, Massague 2006). Several studies have shown that certain tumours tend to form secondary foci in recurring specific organs (Fidler 2003). Lung tumours metastasise to liver, brain and bone, whereas breast cancer metastasises to the lung, bone, liver and brain and PCa metastases occur mainly in bone (Joyce, Pollard 2009). Such phenomena are explained by the tropism of metastases for specific tissues and are determined by the chemotaxis that chemokines generate in the target tissue and its attraction of CTCs expressing cognate chemokine receptors.

Once CTCs reach the ultimate stop of their journey, they can start to proliferate in the lumen of the vessel in which they have localised, before outgrowing into the parenchyma of the surrounding tissue (Al-Mehdi, Tozawa et al. 2000). Alternatively, they can pass through the wall of the vessel and immediately move into the parenchyma prior to proliferating again, in what is called the extravasation process. The structure of the vasculature in normal tissues represents an obstacle for tumour cells which is more difficult to overcome than the leaky structure of the neovasculature, via which the tumour in the primary site is fed. Barriers such as the hematoencephalic (blood-brain) or lung, represent a hermetic limit to the extravasation, whereas bone and liver tissues are much easier to penetrate because of the fenestrations in their vasculature (Valastyan, Weinberg 2011).

1.3.5 Metastatic colonization

In the new parenchyma at distal sites, metastatic cells face a different environment. Survival in such a foreign microenvironment can be challenging, as the extravasated cells are not yet adapted to it. Psaila and Lyden proposed that the organisation of a pre-metastatic niche at

distant sites is key for the establishment of a secondary tumour (Psaila, Lyden 2009). Formation of a hospitable pre-metastatic niche has been shown to be enhanced by cancer cells from the primary tumour (Doglioni, Parik et al. 2019). According to Erler's model, carcinoma cells secrete factors – such as lysyl oxidase (LOX) – (Erler et al. 2009) that act as systemic signals, inducing the production of fibronectin in the receiving tissues, making them a more permissive environment, as well as through the recruitment of hematopoietic progenitor cells responsible for the modification of the ECM (Valastyan, Weinberg 2011).

Extravasated cells can survive as dormant micrometastases for a long time, in which the net growth due to cell proliferation is counterbalanced by the rate of apoptosis. To evade dormancy, the disseminated cells must activate genes that can support their growth pathways and at the same time help them modify their new microenvironment. Furthermore, effective metastatic cells have been proposed to possess a high self-renewal potential that enables them to colonise secondary sites: such cells, considered to be the ones that can give rise to a macro metastasis, are called tumour-initiating cells (TICs) (Qureshi-Baig, Ullmann et al. 2017). Interestingly, some EMT-promoting transcription factors, such as Snail, Twist and ZEB-1, are responsible for the transition of the disseminated cells into the TIC state (Valastyan, Weinberg 2011), as they also confer self-renewal features to them (Thiery, Acloque et al. 2009).

1.4 Epithelial-to-Mesenchymal Transition (EMT)

1.4.1 EMT Program

Epithelial cells are characterised by tight intercellular junctions via which they are connected to each other to form single or multiple layers of cells. They present an apical-basal polarity with the basal part of the cell grounded on the so-called basement membrane and the apical part typically opening into a lumen (i.e. blood vessels and organ ducts) (Alberts, Johnson et al. 2002). On the other hand, mesenchymal cells are loosely organised cells and, being immersed in the ECM, can actively respond to chemotaxis signals and move in three-dimensions (Spees, Lee et al. 2016). Fibroblasts are mesenchymal-like cells present in many tissues, in which they are involved in repair processes (Kalluri, Zeisberg 2006).

Physiologically, epithelial to mesenchymal transition (EMT) occurs during embryogenesis for embryonic stem cell differentiation and induced pluripotency (*type 1* EMT), in adult life during physiological wound healing and organ fibrosis (*type 2* EMT). EMT is also involved in cancer progression (*type 3* EMT) (Kalluri, Weinberg 2009). This process was first described during the 1980s by Hay and Greenburg who - with their pioneering work on epithelial cells from embryonic and adult anterior lens suspended in a collagen matrix - characterised EMT as a distinct cellular program (Greenburg, Hay 1982). This opened a wider perspective on cell plasticity, leading the scientists to reconsider the concept of cell fate determination.

During EMT, cells undergo several reversible morphological and genetic changes that enable them to lose the epithelial features, becoming less differentiated, and switch to a more mesenchymal-like phenotype. Such rearrangements encompass the loss of cell-to-cell junctions and apical-basal polarity, reorganisation of the cytoskeleton with subsequent acquisition of an elongated shape and increased motility and degradation of the ECM by production of metalloproteases.

The loss of apical-basal polarity in cells is achieved by the removal of proteins, such as Crumbs and those forming the Par complex from the intercellular tight junctions (Whiteman, Liu et al. 2008). To be able to disseminate to different sites, EMT cells that have disconnected from the neighbouring epithelial cells must then pass through the BM. To do so, it is essential that EMT cells activate metalloproteases with which to degrade the BM.

Furthermore, to ensure the movement of the cells, the cytoskeleton has to undergo conformational changes that, for instance, in mammary epithelial cells occurs through the action of the small GTP-binding protein Rac1p (Nelson, Khauv et al. 2008).

Interestingly, EMT is not a one-way process. Mesenchymal to epithelial transition (MET) is the reverse process of EMT, by which metastatic cells can reactivate epithelial features, such as the expression of E-cadherin. The hypothesis of MET was introduced based on the observation that cells from the metastatic lesions and those from primary tumours share similar epithelial morphology (Yao, Dai et al. 2011).

The terms EMT and MET are to be considered only referred to changes in shape and cell-cell/cell-matrix adhesion and not to a cell fate specification. Indeed, the EMT process can be partial, in response to environmental factors and depending on the tissue and signalling context, thereby confirming the cell plasticity in disseminating tumour cells (Saitoh 2018). Interestingly, during complete transition, EMT cells can still express differential sets of either epithelial or mesenchymal markers (Jolly, Mani et al. 2018).

Similarly, a mesenchymal transition in endothelial cells (EndMT) has been documented to be involved in tumour progression (Platel, Faure et al. 2019). Zeisberg and colleagues have provided evidence that endothelial cells contribute to up to 40% of the pool of CAFs in models of pancreatic cancer and melanomas (Zeisberg, Potenta et al. 2007). The hypothesis of EndMT having a role in cancer cell extravasation via TGF- β 1 signalling has been confirmed by Krizbai in brain and melanoma tumours (Krizbai, Gasparics et al. 2015).

EMT and EndMT are collectively referred to as epithelial-mesenchymal plasticity (EMP)

1.4.2 EMT in cancer and PCa

Cells that undergo the EMT process present an ability to migrate far from the original site in the body towards different compartments, in which they can form micrometastases. As previously discussed, intravasation and extravasation are key events in this metastatic process. Invasion, migration, and survival in secondary sites are critical for PCa progression too.

To spread from the primary tumour site, invasive cells need to become independent from the surrounding cells in the epithelium by losing mutual cell-cell junctions. They then need

to make their way to the blood stream through the intravasation process. At this point, migrating cells are able to move through the blood stream as circulating tumour cells (CTCs) (Jie, Zhang et al. 2017). This event is possible because cells that undergo EMT produce metalloproteases with which the ECM is degraded. Interestingly, the invasive cells can survive in the blood stream by avoiding *anoikis* death (Frisch, Screamton 2001). When epithelial cells, being anchorage-dependent cells, either detach from the extra cellular matrix (ECM) or are connected to the wrong cell type, they normally go through a specific programmed cell death pattern which is called *anoikis* (that means "*homelessness*" in Greek). This death program is mediated by integrins, cell surface receptors that bind to specific ECM components. During cancer progression, the resistance to *anoikis* can be due to a switch in the integrins, modulation of the metabolism, constitutive activation of anti-apoptotic signalling and EMT (Paoli et al. 2013). EMT is connected to *anoikis* resistance through EMT-promoting proteins (Kim et al. 2012). Indeed, *anoikis* resistance is promoted by N-cadherin expression and E-cadherin reduction as well as by the increase of Twist expression, which mediates the loss of E-cadherin.

Dysregulation of the AR signalling in has been reported as a factor promoting EMT and therapy resistance in studies on advanced PCa (Miao et al. 2017). Studies by Stylianou on PCa patient samples revealed that transcriptional events underlying EMP are a signature of the metastatic phenotype rather than the primary or benign form of PCa (Stylianou, Lehman et al. 2019).

Amongst the several growth factors and cytokines that play important roles in sustaining EMT during cancer progression, TGF- β signalling is involved in cell proliferation and migration, thus representing an important factor during cancer progression. More specifically, TGF- β signalling has a tumour suppressive effect – causing cell cycle arrest and apoptosis – during the early stages of tumour development, whereas in later stages it acts as a tumour promotor inducing EMT in malignant cells (David, Massagué 2018). TGF- β has been demonstrated to have angiogenic and tumorigenic activity in prostate cancer by inducing EMT via activation of Smad-dependent and -independent downstream signaling pathways (Matuszak, Kyprianou 2011). Another key role of TGF- β during prostate cancer advancement is its suppressive activity of tumour immune surveillance by inhibiting T-cell proliferation (Batlle, Massagué 2019). Interestingly, patients with advanced prostate cancer show increased expression of TGF- β and higher levels of TGF- β in the serum (Wu et al. 2015).

1.4.3 EMT and cancer cell ‘stemness’

Cancer stem cells (CSCs) represent an important and dangerous subset of cells within a tumour. They have the ability to initiate a tumour as their two main features are self-renewal and potential to differentiate (Schoenhals, Kassambara et al. 2009).

Studies in which EMT was experimentally activated unexpectedly unveiled a strong connection between a role for EMT during invasion-metastasis cascade and the cancer stem cell phenotype. Mani et al. showed that inducing EMT via constitutive expression of either Snail or Twist1 in immortalised human mammary epithelial cells eventually led these cells to acquire stem-like properties (increased CD44 and reduced CD24 expression, increased ability to form tumorspheres) (Mani, Guo et al. 2008; Morel, Lièvre et al. 2008). This finding would then explain how the disseminating EMT cells moving from a primary tumour can eventually generate macroscopic metastases out of micrometastasis, even though they initially lacked self-renewal capability. However, conditionally deleting Twist1 in an experimental skin tumour model suggested that EMT and stemness in tumours can be regulated by distinct mechanisms (Beck, Lapouge et al. 2015). Studies in animal models showed that the expression of Zeb proteins correlated with increased self-renewal features (Wellner, Schubert et al. 2009). Furthermore, Yang et al. showed that Twist, in mutual cooperation with proteins from the polycomb-group responsible for self-renewal, can repress E-cadherin and promote tumour initiation in patients with head and neck cancer (Yang, Hsu et al. 2010). Taken together, this evidence suggests a link between EMT and therapy-resistance, via the ability of EMT-TFs to promote and maintain stemness in cancer cells and sustain tumour initiation – for example in glioblastoma and pancreatic cancer (Siebzehnrabl, Silver et al. 2013; Zheng, Carstens et al. 2015).

1.4.4 EMT-inducing transcription factor families

Amongst the inducers of EMT are TGF- β , Wnt, Notch, Hedgehog signalling pathways (Liu, Yun et al. 2015) and growth factor receptor tyrosine kinases. These pathways directly cross regulate three main families of protein: Snail, Twist and ZEB. Members of these families either directly or indirectly regulate the expression of downstream target genes, such as E-cadherin, vimentin, N-cadherin and fibronectin, which are the main EMT markers (Goossens, Vandamme et al. 2017). Indeed, behind the drastic changes that happen in cells during the transitions from one state to the other, lies a very fine-tuned network of EMT-associated

transcription factors (EMT-TFs). These will be discussed in the next section (1.4.5) since they are considered valid EMT biomarkers.

Important regulators in protein expression are microRNAs, short non-coding RNAs that act specifically through mRNA binding, resulting in their destabilisation and subsequent translational repression. The main miRNA family involved in EMT regulation is miR200 (Mongroo, Rustgi 2010). A double-negative feedback between ZEB1/2 proteins and miR200 has been reported. Indeed, miR200 binding to ZEB1 and ZEB2 downregulates their expression and determines the epithelial phenotype (Park, Gaur et al. 2008), whereas the two proteins, on the other hand, exert a negative regulation on the miR200 molecule (Brabertz, Brabertz 2010).

1.4.5 EMT markers

Several biomarkers have been linked to the three types of EMT. EMT markers can be either acquired or attenuated during the process, the most common are presented below.

Cadherins are calcium-dependent transmembrane proteins that translate the signals coming from cell-cell interaction: type I cadherins are E-cadherin, N-cadherin and P-cadherin. The transmission of adherence (cell-cell or cell-BM) signals occurs through catenins, proteins coating the inner layer of the cell membrane, namely α -catenin, β -catenin, and γ -catenin (plakogobin). Alterations in the adhesion between cells in an epithelial compartment, with a consequent loss of apico-basal polarisation in cells, correlate with an invasive cancer behaviour (Christofori 2003). E-cadherin and N-cadherin are key regulators of the tumorigenic process driven by EMT (Yu, Yang et al. 2019) and both proteins are markers of the EMT process, although they show opposite patterns of expression. Such an alternation in the expression of E-cadherin and N-cadherin is referred to as "cadherin-switch" and it typically occurs in invasive cells (Loh, Chai et al. 2019). Whereas E-cadherin is normally expressed in epithelial cells, N-cadherin expression is constitutively higher in mesenchymal and neural cells. E-cadherin is regarded as a tumour and invasion suppressor due to its activity in stabilising the epithelial phenotype and polarisation in epithelial cells. On the other hand, N-cadherin expression increases cell motility and migration by stimulating the MAPK/ERK pathway via interaction with FGFR (Nguyen, Mège 2016). E-cadherin sequesters β -catenin to the membrane, thereby making it unavailable to activate Wnt signalling. The stimulation of cadherin signalling activates the downstream Wnt/ β -catenin

pathway, which can also be activated by BMP4 (Stemmler 2008), and is a major pro-tumorigenic pathway (Polakis 2012), encoding tumour invasion and metastasis-promoting molecules such as MMPs and CD44 (Mrozik, Blaschuk et al. 2018).

Vimentin is a class III intermediate filament that is expressed in a variety of cells and is used to identify EMT due to the correlation of its expression with invasive and metastatic cancer cells. However, the use of vimentin as a marker for EMT is controversial since epithelial cells can express such marker as a response to various stimuli (Zeisberg, Neilson 2009). Vimentin mediates cytoskeletal rearrangement and increase of focal adhesion generation in cells during the mesenchymal transition and migration (Liu, Lin et al. 2015). Furthermore, vimentin upregulation is a downstream component in the Slug-induced EMT (Vuoriluoto, Haugen et al. 2011).

β -catenin has a dual role in EMT. β -catenin is associated to cell membrane where it connects cadherins to the cytoskeleton in epithelial cells and non-invasive tumours (Zeisberg, Neilson 2009). Conversely, cytoplasmic and nuclear localisation of β -catenin is associated with activated EMT since it acts as a cotranscriptional activator of Snai1 (Yook, Li et al. 2006).

Snail (*Snai1*) and **Slug** (*Snai2*) are hallmarks of metastatic cancers belonging to the Snail family of transcription factors. They have been demonstrated to promote tumour growth and metastasis in several cancers (Jin, Yu et al. 2010; Olmeda, Montes et al. 2008; Li, Chen et al. 2019). The activation of Snail proteins leads to the repression of E-cadherin, claudin and occludin expression by binding to E-box consensus sequences in the promoters of their target genes. The regulation of Snail factors occurs through phosphorylation by PAK and GSK3 β (Liu, Chen et al. 2014), and the protein stabilisation is promoted by NF κ B during inflammation-induced cell migration and invasion (Wu, Deng et al. 2009). Furthermore, Snail is responsible for the activation of MMP2, MMP3, and MMP9, metalloproteases that are important during the matrix degradation process (Miyoshi, Kitajima et al. 2004). On the other hand, MMP3 concurs in starting EMT by inducing Snai1 expression through the increased intracellular levels of reactive oxygen species (Radisky, Levy et al. 2005). Moreover, Snail can repress the expression of genes encoding for proteins involved in defining the apico-basal polarisation, such as *Crumbs* and *Disc large*. Snai1 can also positively interact

with β -catenin by regulating its transcriptional activity during the EMT process (Whiteman et al. 2008).

Twist is a family of basic-helix-loop-helix proteins. In a murine model of breast cancer, Twist-induced expression correlates with loss of E-cadherin and increased expression of vimentin, N-cadherin and fibronectin, all of which are fibroblast markers (Yang, Mani et al. 2004). A study in luminal breast cancer cells shows the active role of Twist in promoting cell migration and invasion, and expansion of the stem cell population (Wang, Liu et al. 2016). Furthermore, Wnt1 signalling has been reported to upregulate Twist, thus inhibiting mouse mammary cell differentiation, contributing to mammary tumorigenesis (Howe, Watanabe et al. 2003). Interestingly, Twist is responsible for the upregulation of stemness markers such as *Nanog*, *Oct4* and *Sox2* via *Bmi1* direct regulation (Yang, Hsu et al. 2010).

ZEB (Zinc finger E-box Binding homeobox) transcription factor protein family can repress E-cadherin expression by binding to its promoter. Either ZEB1 or ZEB2 proteins have been mostly studied individually in different cancers, such as colorectal, ovarian, gastric, and pancreatic (Peinado, Olmeda et al. 2007).

ZO1 (Zonula Occludens 1) is a membrane phosphoprotein associated with tight junctions of epithelial and endothelial cells, where its role is to connect the cytoskeleton to the tight junctions, whereas during EMT it translocates to the nucleus. ZO1 expression is considered a signature of EMT in colorectal and bile duct cancers (Scanlon, Van Tubergen et al. 2013).

1.5 Prostate Cancer

1.5.1 Characterisation

Prostate cancer (PCa) is the primary cause of death in the male population worldwide. In the UK alone, it is responsible for 47,700 new cases and 11,700 deaths every year (Prostate cancer UK). The incidence of PCa is related to age, environment, diet, family history and ethnicity. For instance, the USA, Canada, Sweden, Australia, and France show the highest rate of incidence, whereas Europe has a medium rate, and Asian countries the lowest. Differences in the incidence between countries can be due to the coverage and method of screening, typically assessing the levels of Prostate Specific Antigen (PSA) in patient's blood (Schaid 2004).

The clinical course of PCa is highly heterogeneous, ranging from indolent to aggressive and rapidly metastasising forms (Tolkach, Kristiansen 2018). The development of PCa is a multistep process, in which the first is the formation of a prostatic intraepithelial neoplasia (PIN). Such neoplasia can evolve into a localised and then even advanced adenocarcinoma which, if invasion of the local tissues happens, can lead to metastases (Wang, Zhao et al. 2018). Metastases starting from the primary tumour invade primarily adjacent lymph nodes and bones, but can colonise liver, lungs, and brain (Datta et al. 2010). Most of the PCa cases are slow-growing forms, with the prevalence of metastatic disease being ~10-15% of the total. Overall survival rate for patients with localised PCa is high (~100% at 5 years) but is dramatically lower for patients with metastatic disease (~30% at 5 years – Damodaran, Kyriakopoulos et al. 2017).

Based on the type of cells from which a tumour starts, different kinds of PCa can be distinguished. The most common is the acinar adenocarcinoma, which originates from the gland cells (Figure 1.6). At the present, it is still to be clarified whether the nature of the tissue of origin of PCa can be considered a reliable prognostic signature or not. Indeed, tumours originated from either a luminal or basal lineage seem to correlate with a poorer prognosis, when compared to each other.

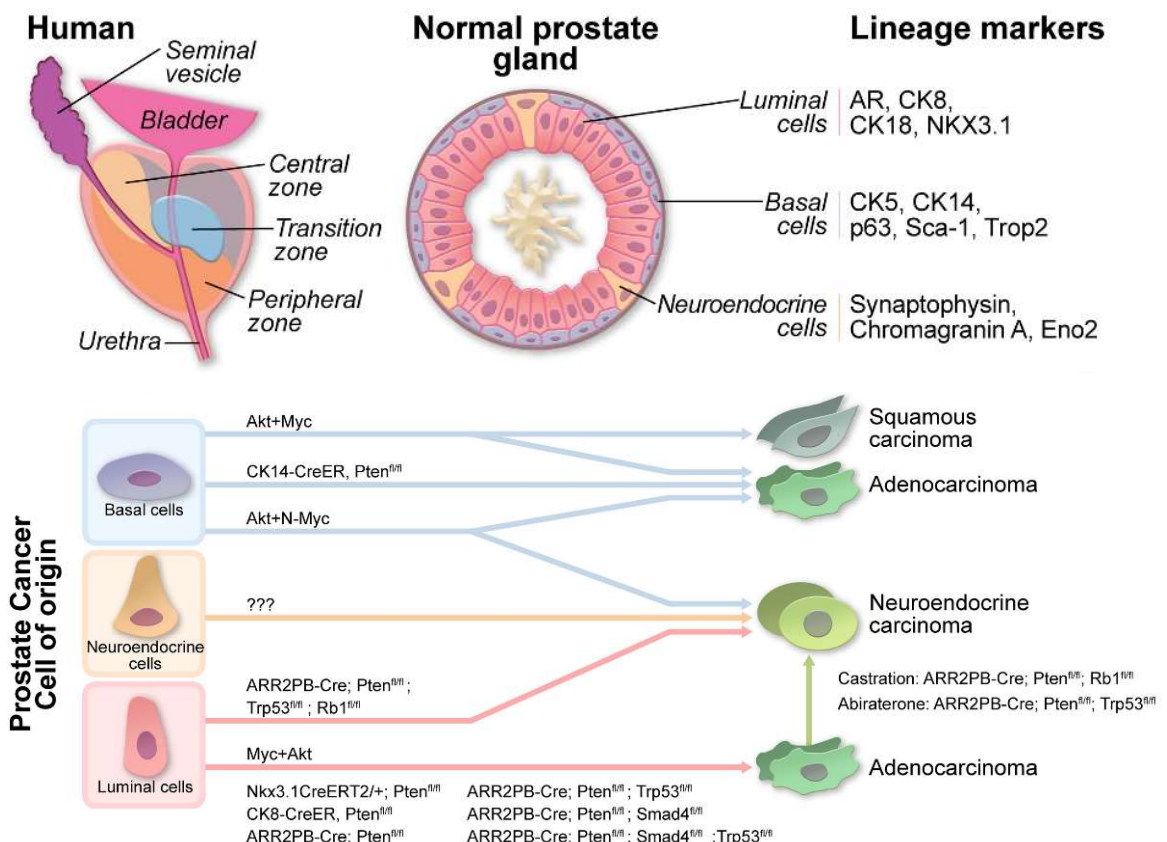


Figure 1.6 – Normal and cancer prostate cells. Schematic anatomy of human prostate and showing the three cell types – luminal, basal and neuroendocrine - that compose the prostate gland (top panel). PCa originates from basal and luminal cells. It is not known yet whether it can also originate from neuroendocrine cells. Genes that are involved in neoplastic formation are listed along the arrows (bottom panel). (Adapted from Wang et al. 2018)

It is extremely important to make the right diagnosis since it can lead to the best treatment for each patient, thus limiting unwanted and unnecessary impacts on the quality of life of patients.

1.5.2 Diagnostic approaches

Prostate Specific Antigen (PSA) levels

Prostate Specific Antigen (PSA) is a serine protease glycoprotein that can be expressed by either normal or malignant prostate cells. PSA is normally secreted as proPSA into the prostate glands lumen, where it becomes active PSA. Active PSA then undergoes proteolysis thus generating inactive PSA, which can then enter the blood stream as free PSA (fPSA). However, active PSA can directly enter the circulation and bind to alpha-1-antichymotrypsin (ACT) and alpha-2-macroglobulin (α 2M), generating complexed PSA (cPSA) (Dasgupta, Wahed 2014). A normal total PSA (tPSA) in serum level is < 4 ng/mL, although different thresholds can be adopted. With normal levels of PSA in serum, the assessment of the ratio fPSA/cPSA or fPSA/tPSA can increase sensitivity of cancer detection. In patients with altered

total (tPSA) levels (between 4.1 and 10 ng/mL), the ratio fPSA/cPSA or fPSA/tPSA is used to discriminate between benign and malignant hyperplasia, thereby improving the specificity of the test. Thus, PSA-based screening is an extremely controversial topic. Tests based on PSA levels in blood are not reliable as they can give a high percentage of false positive results, with 17.8% cases observed in Europe (Kilpeläinen, Tammela et al. 2011). Furthermore, up to 15% of men with PCa have also normal PSA values, which represents a false negative result. Although in the UK there is no screening policy for PCa, scientists at the Universities of Bristol and Oxford conducted a trial to further investigate the effective reliability of the PSA screening (Martin, Donovan et al. 2018). The CAP (Cluster Randomized Trial of PSA Testing for PCa) randomised clinical trial aimed to clarify the actual ratio between benefits of the screening and the harm caused by over detection and consequent overtreatment. Indeed, it has been found that cases of overdiagnosis are between 20 and 50%. The study showed that a single PSA screening intervention (compared to a standard practice in patients without screening), made no significant difference in PCa mortality over a 10 years-long follow-up. On the other hand, the single PSA screening increased the detection of low-risk PCa cases (Martin et al. 2018).

However, contradictory results were provided by the European Randomized Study of Screening for PCa (ERSPC), launched in 1993. The ERSPC was the world's largest randomised controlled trial evaluating the effect of PSA screening on PCa mortality. The study involved men aged between 50 and 69. The 16-year follow-up recently published showed significant reduction of PCa mortality due to PSA screening (Hugosson, Roobol et al. 2019).

Histopathological scores

By staging a tumour, the therapist will know its size and if it has spread to other areas of the body. The most widely used system to score tumours is the TNM. It refers to the size of the tumour (T), whether it has spread to lymph nodes or not (N) and if metastases have occurred anywhere in the body (M, Table 1.1).

Table 1.1 - TNM staging system for PCa. The TNM (Tumour, Node, Metastasis) system is used by clinicians to describe the stage of PCa in patients, together with the PSA levels and the Gleason score. (Adapted from Prostate Conditions Education Council)

CLASSIFICATION	DEFINITION
TUMOR	
Tx	Tumor cannot be evaluated (due to lack of information)
T0	No evidence of a primary tumor
T1*	Tumor was not detected during a digital rectal exam (DRE) and cannot be seen on imaging studies (tumor may be discovered during surgery for a reason other cancer)*
T2 T2a T2b T2c	Tumor can be detected during a DRE but is present in the prostate only Tumor is in half or less than one side (lobe) of the prostate Tumor is in more than half of one prostate lobe, but has not yet invaded the other lobe Tumor is in both prostate lobes
T3 T3a T3b	Tumor extends outside of the prostate Tumor extends outside the prostate on one or both sides Tumor has spread to the seminal vesicles (the glands on each side of the bladder)
T4	Tumor has spread to tissues near the prostate other than the seminal vesicles, such as the bladder or wall of the pelvis
Nearby (regional) lymph nodes (N)	
Nx	Nearby lymph nodes are not evaluated
N0	No cancer cells are found in nearby lymph nodes
N1	Cancer cells are found in nearby lymph nodes
Distant Metastasis (M)	
M0 M1 M1a M1b M1c	Cancer has not spread beyond the prostate Cancer has spread beyond the prostate Cancer has spread to distant lymph nodes Cancer has spread to bone Cancer has spread to another organ or site, with or without bone disease

PCa aggressiveness can also be graded using the Gleason system (Gleason, Mellinger 1974), which is based on histological analysis of biopsy tissues (Figure 1.7). Since each tumour is made of different areas of cells with different grade, each patient gets a double scoring, relative to the two most represented areas and that provides the overall grade, with values that range from 6 to 10. The higher the score, the more aggressive is the tumour.

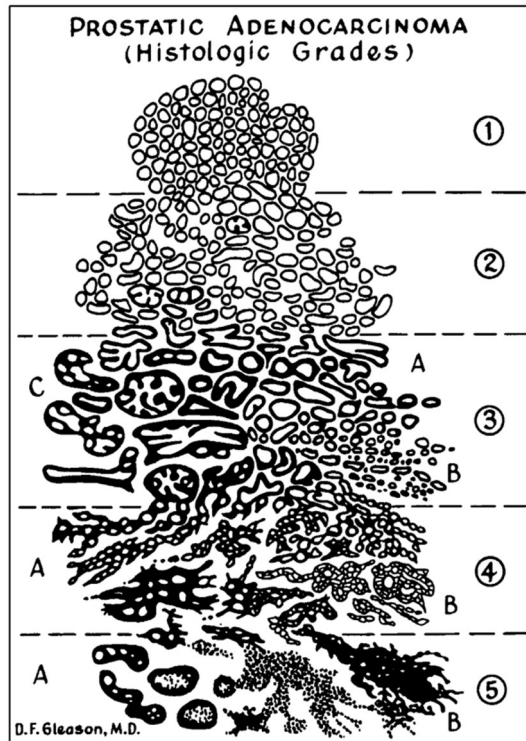


Figure 1.7 – Gleason’s pattern standard drawing. This system relies on the analysis of histologic prostate samples from patients. The total scoring of the PCa grade is given according to the histomorphological appearance of the tissue analysed. (Adapted from Humphrey, 2004)

Imaging diagnosis

Imaging is currently one of the mainstream approaches for PCa diagnosis, staging, and surveillance. Such methodologies include multiparametric ultrasound (mpUS), multiparametric magnetic resonance imaging (mpMRI), and positron emission tomography (PET). US and MRI imaging are used in wider capacity for PCa detection, whereas PET imaging finds better application for cancer staging and surveillance. US is used to image alterations in the anatomy as well as the local vascularity of prostate as an indication of angiogenesis in a developing tumour. Interestingly, MRI has gained relevance in the last few years since its use demonstrated to prevent under-detection of aggressive PCa and over-detection of indolent cancer. As previously mentioned, PET is mostly used for relapse and metastasis surveillance. PET makes use of radiolabelled tracers which uptake happens in hot spots. (Sarkar, Das 2016)

1.5.3 Current treatment for local and metastatic PCa

A main characteristic of PCa is its responsiveness to androgen hormones. Testosterone and dihydrotestosterone are the key androgen hormones in the signalling axis that plays a pivotal role in PCa pathogenesis (Fujita, Nonomura 2019). The androgen receptor (AR) is a

steroid receptor transcriptional factor for androgens. Huggins and Hodges showed that castration in PCa patients led to tumour regression (Huggins, Hodges 1941). Indeed, androgen deprivation therapy (ADT) is currently performed as surgical or medical castration to treat hormone sensitive PCa (HSPC). Surgical castration as radical prostatectomy is applied to drastically reduce the levels of testosterone to < 50 ng/dl, whereas medical castration uses chemical agents that interfere with and block the androgen pathway (Perlmutter, Lepor 2007). Abiraterone acetate (zytiga) was approved by the FDA in 2011 for PCa treatment as hormonal therapy with prednisone, which showed a significant increase in overall survival (OS) when administered in combination with ADT (Barata, Sartor 2019). Enzalutamide (xtandi), a second-generation antiandrogen used for PCa hormonal therapy, acts as an androgen receptor (AR) inhibitor by blocking the androgen binding to the AR and the nuclear translocation of activated AR (Scott 2018). Effects of such treatments are currently being investigated during the phase 3 STAMPEDE (Systemic Therapy in Advancing or Metastatic Prostate Cancer: Evaluation of Drug Efficacy) study in 1800 patients (Sydes, Spears et al. 2018).

Resistance to ADT is a consequence of the alteration in AR expression and function (Feldman and Feldman, 2001; Chen et al., 2004; reviewed in Debes and Tindall, 2004), which makes the growth of prostate cells independent of androgen regulation. When PCa becomes resistant to hormonal therapy it is referred to as Hormone-Relapsed Prostate Cancer (HRPC). HRPC does not respond to ADT and typically metastasises with a lethal outcome (Quinn, Shore et al. 2015). Indications of castration-resistant PCa are increases in PSA level or the progression of metastasis. In 2004, the American Food and Drug Administration (FDA)-approved docetaxel (taxotere) therapy was shown to significantly increase survival in metastatic HRPC (mHRPC) patients (Petrylak, Tangen et al. 2004, Tannock, de Wit et al. 2004). The TOPARP phase 2 trial on Poly(adenosine diphosphate-ribose) polymerase (PARP) demonstrated that PARP inhibition with olaparib (lynparza) led to good response in patients with mHRPC (Mateo, Carreira et al. 2015). In 2013, the FDA approved the use of radium-223 dichloride (xofigo) for the treatment of bone metastases in HRPC patients (Wilson, Parker 2016). Sipuleucel-T, a cell-based immune therapy, was the first immune therapeutic treatment for minimally symptomatic metastatic HRPC and to date is the only immune therapy approved by the FDA (Schepisi, Farolfi et al. 2017). Sipuleucel-T has been shown to slightly improve OS (about 4 months) in three double-blind randomized phase III clinical trials (Small, Schellhammer et al. 2006, Higano, Burch et al. October 2005). Only recently, a

promising clinical trial for a new immune-based therapeutic approach to mHRPC using monoclonal antibodies started (Antonarakis, Piulats et al. 2020). Indeed, the phase II KEYNOTE-199 study conducted in 2019 on the monotherapeutic use of the immune checkpoint inhibitor pembrolizumab (Keytruda™) in 285 mHRPC patients showed antitumour activity and encouraging OS estimates, with 1 in 20 men gaining up to two years of life. The efficacy of another immune checkpoint inhibitor (ipilimumab, Yervoy™) for treating mHRPC has also been evaluated, however the phase 3 RCT trial demonstrated no significant impact on OS (Kwon, Drake et al. 2014; Fizazi, Drake et al. 2020).

Although the different therapeutic approaches to metastatic PCa have demonstrated significant improvements in OS, this disease remains incurable. Immunotherapy represents the only chance of treating metastatic HRPC. Currently therapies combining different immunotherapy approaches or immunotherapy and conventional treatments are under study for their effects on metastatic HRPC (Silvestri, Tortorella et al. 2019). Notably, PCa is very suitable for immunotherapy as it presents several tumour associated antigens (TAAs), such as prostate specific antigen (PSA), prostate acid phosphatase (PAP) and prostate-specific membrane antigen (PSMA) (Maia, Hansen 2017), whose immunogenicity has been demonstrated to induce significant clinical response in patients (Fernandez-Garcia, Vera-Badillo et al. 2015).

1.5.4 Prostate cancer *in vitro* models

In order to better understand the molecular mechanisms that characterise PCa pathogenesis, prostate-derived cell lines are used as *in vitro* models, such as the benign prostate epithelium PNT2 (immortalized with SV40), the androgen-independent DU145 (prostate carcinoma, derived from brain metastasis) and PC3 (prostate adenocarcinoma, derived from bone metastasis), and the androgen-dependent LNCaP (prostate carcinoma, derived from left supraclavicular lymph node metastasis). It is important to note that DU145 cells have been reported to show a similar behaviour to PCa tissues where the antiproliferative effect of TGF- β is impaired due to reduced expression of TGF- β II receptors (Blanchère, Saunier et al. 2002). As mentioned in section 1.4.2, alterations in TGF- β pathway underlie the EMT process. Such evidence further support the existence of a link between cancer progression as represented in the *in vitro* models used for advanced PCa and EMT.

1.6 Cancer Immunotherapy

The Editors of *Science* named Cancer Immunotherapy as the “Breakthrough of the Year” in 2013 (Couzin-Frankel 2013). The principle underlying immunotherapy is to harness the patient’s immune system to target and destroy tumours.

1.6.1 Immune surveillance

Advances in understanding the mechanisms underlying immune responses, especially those mediated by T-cells, have made it possible to establish immunotherapy as a modern pillar in cancer treatment. The key principle in the immune response to cancer is ‘immune surveillance’. The immunosurveillance hypothesis was postulated for the first time by Burnet during the second half of the 20th century (Burnet 1970), and was based on Lawrence Thomas’ studies on the immune response to malignant cells. According to this hypothesis, the immune system can identify specific antigens on transforming cells, thus controlling their growth or killing them (Ribatti 2017). The activity of the immune system against a developing tumour is cyclic (Figure 1.8).

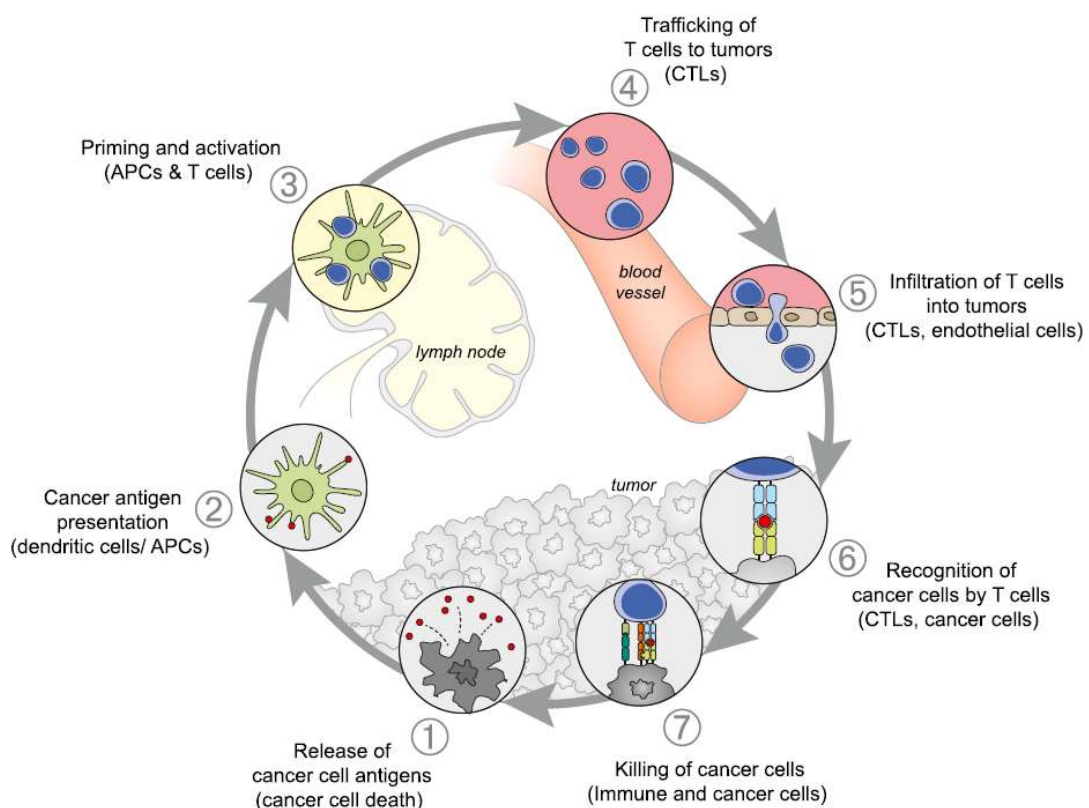


Figure 1.8 – The Cancer-Immunity Cycle. Immunity to cancer is a multi-step process and can be self-propagating. It usually starts with the release of antigens from cancer cells that are presented to T-cells, leading to the killing of the cancer cells that express the recognised antigens. (Adapted from Chen and Mellman, 2013)

The first step of the immune reaction sees dendritic cells (DCs) as main characters that recognise tumour-associated antigens and neo-antigens (a newly generated antigen resulting from a mutation within the tumour), both of which appear 'new' to the immune system. DCs capture and process antigens as peptides derived from tumour cells, which are then loaded on MHC Class I and II molecules. Processed peptides from these tumour-associated antigens are then presented to appropriately specific CD4⁺ and CD8⁺ T-cell populations via their TCRs (T-cell Receptors) (Figure 1.9). However, in order for T-cells to be activated, the stimulation of TCRs only is not enough and a second activator signal is required, i.e. binding of B7 molecules (CD80/86) on the APC to CD28 on the T-cells (Sharma, Campbell et al. 2019). Once activated, T-cells migrate in the tumours where they exert their cytotoxic activity on the tumour cells expressing the relevant antigen. Target cell lysis generates the release of more antigen molecules that can further propagate the immune response (Chen, Mellman 2013).

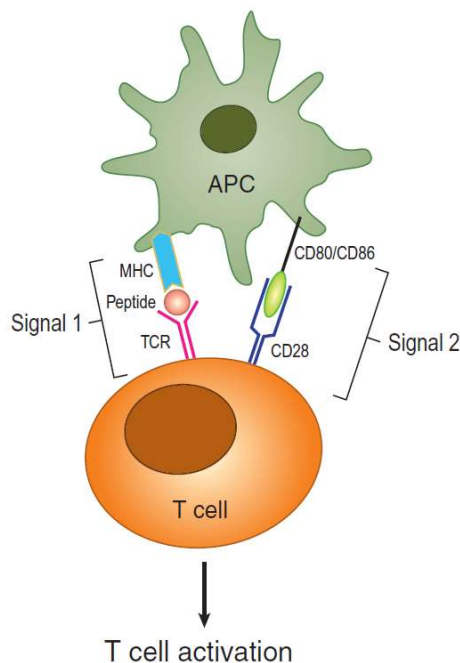


Figure 1.9 – Antigen presentation and T-cell activation. T-cells are activated in response to two different signals on TCRs and CD28 receptors. The stimulation of both signals simultaneously is required for the activation of T-cells. The molecules recognised by the receptors on the T-cells are presented by antigen presenting cells (APCs). (Adapted from Sharma et al., 2019)

Such immune responses can exert a selective pressure on the tumour population, saving the cancer clones with either lower antigenicity or immunogenicity, or both, allowing their proliferation and promoting tumour outgrowth in what is called the cancer immunoediting process. Three phases have been identified in such process, together referred to as the *Three E's* (Dunn, Old et al. 2004). During the first phase, the *Elimination*, both adaptive and innate

immunity detect and identify cancer cells (Schreiber, Old et al. 2011). However, some cancer cells can evade the immune system control and enter the *Equilibrium* phase, in which they remain quiescent and safe from the cytotoxic activity of T-cells. Cancer cells can remain in the equilibrium phase for an indeterminate period (Schreiber et al. 2011). Nevertheless, the immune system continues to interact with the cancer cells. This can promote the selective growth of less immunogenic cells that can elude immune control and lead to the *Escape* phase (Sharma et al. 2019). Tumour cells can escape the immune system through several mechanisms (Figure 1.9). First, they can lose expression of the relevant antigen(s), thus becoming invisible to the immunity check. Some tumour cells activate antiapoptotic strategies that promote their resistance to the cytotoxic activity of immune effectors. However, the establishment of an immunosuppressive TME, by recruiting immunosuppressive cells that can downregulate the activity of infiltrating T-cells, can be another way for tumours to escape immunosurveillance (Dunn et al. 2004). For that to happen, a local immune privilege status is enough. The development of a subsequent generalised suppression can lead to the ablation of the immunological control outside the primary tumour site, thereby also facilitating the formation of metastases (Valastyan, Weinberg 2011).

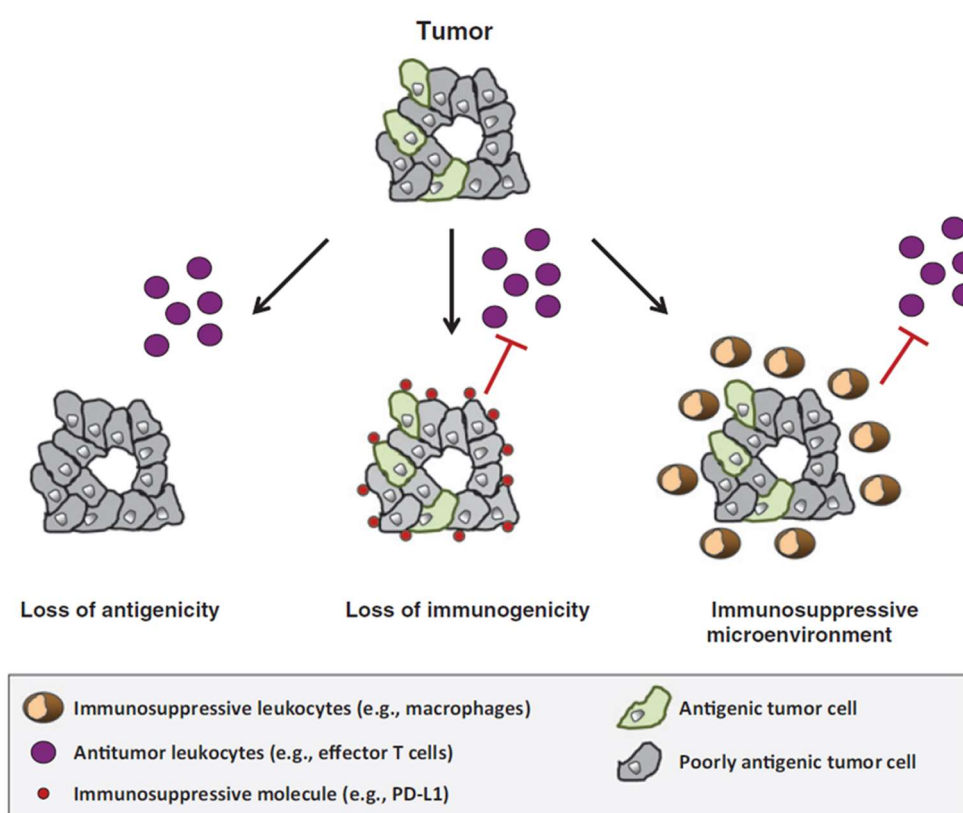


Figure 1.10 – Immune Escape Mechanisms. Immune-elimination evasion is the process that takes place in clinically apparent tumours. Neoplastic cells can avoid the immune system control losing either their antigenicity or their immunogenicity and creating a microenvironment hostile to the immune cells. (Adapted from Beatty, Gladney 2015)

Local chronic inflammation is another key factor in tumour development and growth (Mellor, Munn 2008), preceding 15-20% of all cancer cases (Mantovani et al. 2008). Upregulated inflammatory mediators and the presence of tumour-promoting immune cells (i.e. monocytes, macrophages, innate lymphoid cells and neutrophils) are hallmarks of a cancer-promoting inflammation (Greten, Grivennikov 2019).

1.6.2 Immunotherapeutic approaches, an overview

1.6.2.1 Immune checkpoint blockade

Immune checkpoints are membrane ligand/receptor systems acting as modulators of the natural response of the body's immune system that prevent damage to normal tissues and cells. Cancer cells can develop the ability to circumvent such important mechanisms, exerting a negative modulation on T-cells, which eventually helps them to avoid the immune system effectors check (Beatty, Gladney 2015).

Figure 1.10 shows the CTLA-4 and PD-1 immune checkpoint systems that are discussed in this section. For their pioneering work that led to the establishment of the checkpoint blockade therapy against CTLA-4 and PD-1 respectively (Figure 1.15), James Allison and Tasuku Honjo were honoured with the Physiology or Medicine Nobel Prize in 2018 (Guo 2018).

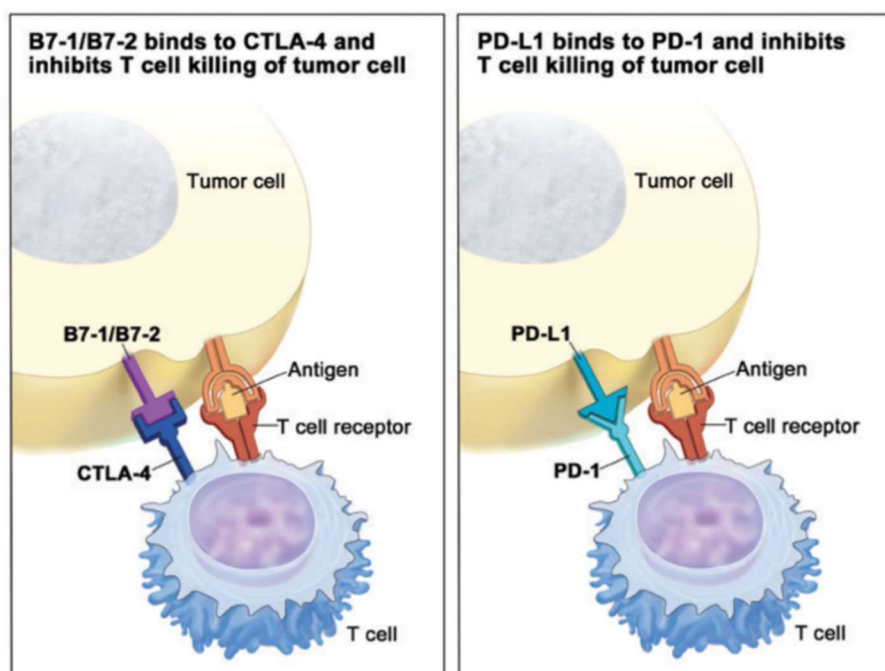


Figure 1.11 – CTLA-4 and PD-1 checkpoints. The interaction of CTLA-4 and PD-1 with their specific ligands limits T-cell activation. These two systems pathways are activated in the early and later stages, respectively, of the immune response. (Adapted from Eno, 2017)

Table 1.2 shows the immune checkpoint therapies that have been approved so far by the FDA for the treatment of several tumours.

Table 1.2 – FDA-approved immune checkpoint inhibitors. Immune checkpoint blockade therapies currently approved by the FDA. Adapted from (Wei, Duffy et al. 2018).

Therapeutic agent	Tumour type	FDA approval year
Ipilimumab	Melanoma	2011
Nivolumab	Melanoma	2014
Pembrolizumab	Melanoma	2014
Nivolumab	Non-small cell lung cancer	2015
Pembrolizumab	Non-small cell lung cancer	2015
Ipilimumab + nivolumab	Melanoma (BRAF wild type)	2015
Ipilimumab	Melanoma (adjuvant)	2015
Nivolumab	Renal cell carcinoma	2015
Nivolumab	Hodgkin lymphoma	2016
Atezolizumab	Urothelial carcinoma	2016
Nivolumab	Head and neck squamous cell carcinoma	2016
Pembrolizumab	Head and neck squamous cell carcinoma	2016
Ipilimumab + nivolumab	Melanoma (any BRAF status)	2016
Atezolizumab	Non-small cell lung cancer	2016
Pembrolizumab	Hodgkin lymphoma	2017
Avelumab	Merkel cell carcinoma	2017
Avelumab	Urothelial carcinoma	2017
Durvalumab	Urothelial carcinoma	2017
Nivolumab	Urothelial carcinoma	2017
Pembrolizumab	Urothelial carcinoma	2017
Pembrolizumab	MSI-high or MMR-deficient solid tumours of any histology	2017
Nivolumab	MSI-high, MMR-deficient metastatic colorectal cancer	2017
Ipilimumab	Pediatric melanoma	2017
Nivolumab	Hepatocellular carcinoma	2017
Pembrolizumab	Gastric and gastroesophageal carcinoma	2017
Durvalumab	Non-small cell lung cancer	2018
Ipilimumab + nivolumab	Renal cell carcinoma	2018
Cemiplimab	Squamous cell skin cancer	2018

CTLA-4 (cytotoxic T-lymphocyte-associated protein 4), a receptor constitutively expressed on regulatory T-cells and upregulated in active T-cells, mediates immunosuppression by binding to CD80/86 on APCs and competing with CD28 on active T-cells (Walunas, Lenschow et al. 1994). Moreover, CTLA-4 expression in Tregs is fundamental to their activity in preventing T-cell aberrant activation during T-cell homeostasis and tolerance to self (Jain, Nguyen et al. 2010).

Ipilimumab (Yervoy) is an anti CTLA-4 monoclonal antibody approved for the treatment of metastatic melanoma by the FDA in 2011, based on the demonstration of effective antitumor immune responses with significant OS increase in a phase III clinical trial (Hodi, O'Day et al. 2010). Interestingly, ipilimumab has been reported to induce expansion of pre-existing T-cells directed against a tumour-specific neo-antigen in a responding patient with melanoma (van Rooij, van Buuren et al. 2013). A study on CTLA-4 blockade in murine cancer models has shown that CTLA-4 therapy also leads to depletion of Treg populations, thus attenuating T-cell inactivation (Wei et al. 2018). Phase I and II trials demonstrated that ipilimumab was able to induce tumour regression in melanoma, and ovarian cancer patients (Sharma, Allison 2015). Such evidence has also been recently reported in a murine sarcoma model, where CTLA-4 blockade determined the expansion of a neo-antigen specific CD8⁺ T-cell population (Fehlings, Simoni et al. 2017). Another mechanism of action reported for ipilimumab is ADCC of Tregs *ex vivo* (Romano, Kusio-Kobialka et al. 2015), suggesting a contribution of Fc-mediated function to the activity of ipilimumab. Nevertheless, no OS improvement was observed in a double-blind phase III trial for ipilimumab treatment of mHRPC. However, a case report of two patients within two large phase III trials shows improvement of progression-free survival, suggesting clinical activity in a small subset of patients (Cabel, Loir et al. 2017).

Programmed death 1 (PD-1) is a surface receptor expressed in activated T-cells, B-cells, DCs and natural killer (NK) cells which maintains peripheral tolerance and dampens T-cell activation. Unlike CTLA-4, PD-1 directly interferes with the activating TCR signalling in T-cells by interacting with its two ligands PD-L1 and PD-L2 (Iwai, Ishida et al. 2002). Such ligands are also expressed by tumour cells that can in this way directly inactivate T-cells (Zitvogel, Kroemer 2012, Kleffel, Posch et al. 2015). Moreover, studies have linked PD-L1 expression in TAMs with the active clearance of T-cells from the TME (Kortlever, Sodir et al. 2017). PD-1 blockade acts on exhausted CD8⁺ T-cells increasing their activity, although CD4⁺

are required for the process to be effective. Nivolumab and pembrolizumab (Opdivo) are both blocking IgG4 against PD-1, which means that their activity is mainly blockage/neutralisation rather than Fc-mediated effector. Nivolumab has been reported to enhance neo-antigen specific T-cell responses in lung cancer cells (Forde, Chafft et al. 2018).

The current model for checkpoint blockade mechanisms considers that CTLA-4 blockade mainly occurs in draining lymph nodes of tumours where T-cells are primed, whereas PD-1 blockade primarily occurs in inflamed tumours (Wei et al. 2018). Due to their extrinsic effect on T-cell regulation, checkpoint blockade can revert the dysfunctional state in exhausted T-cells (Zhang, Liu et al. 2020). Despite the promising response obtained with ipilimumab, the immune checkpoint therapy also presents some relevant challenges. For instance, tumours with low mutational burden might present a lower responsiveness to the checkpoint blockade due to their low immunogenicity. Furthermore, it has been reported that for the first effect of ipilimumab to manifest might take several months (Mellman, Coukos et al. 2011). Combining PD-1 and CTLA-4 blockade appears to deliver greater efficacy than respective monotherapies in B16 melanoma preclinical tumour models (Wolchok, Kluger et al. 2013). The order of treatment also appears to be important, as a phase II study conducted in patients with advanced melanoma has shown that sequential administration of nivolumab followed by ipilimumab delivers greater therapeutic responses than the reverse (Weber, Gibney et al. 2016).

In the last few years, checkpoint inhibitor monotherapy has also been tested in PCa. The first study using CTLA-4 blocking in TRAMP murine model showed a significant reduction of metastatic relapse (Kwon, Foster et al. 1999). The effects of ipilimumab in mCRPC patients, both previously treated and not treated with chemotherapy, were evaluated in a phase III trial, which reported no significant OS benefit (Kwon et al. 2014). Interestingly, the Keynote 199 phase II trial, the largest study to consider the effect of PD-1 blockage in PCa, showed that although treatment of mCRPC with Pembrolizumab yielded few responses, they are durable (Antonarakis et al. 2020). Combination of ipilimumab and nivolumab for the treatment of mCRPC is currently being evaluated in the Checkmate 650 phase II clinical trial (Sharma, Pachynski et al. 2019).

1.6.2.2 Cytokine therapy

Cytokines are small proteins that are involved in cell signalling, by acting as immunomodulating agents, and that are secreted by a broad range of immune cells. This category of peptides includes chemokines, interleukins, interferons (IFNs), lymphokines and tumour necrosis factors (TNFs). The use of cytokines in cancer therapy has mainly been associated with IL-2 and IFN- α treatments of patients with melanoma and renal cell carcinomas (Floros, Tarhini 2015). However, the use of high-dose cytokines in clinical practice decreased with time. This is because cytokines can only augment a pre-existing immune response in a non-specific fashion and the use of high doses is associated with a number of toxic side-effects (Lee, Margolin 2011). Moreover, stimulation with cytokine, such as IL-2, can induce undesirable immune checkpoint mechanisms.

1.6.2.3 Vaccine-based therapy

Anti-cancer vaccines can be divided into preventive and therapeutic. Preventive vaccines are directed against infectious agents, responsible for the development of a cancer, such as some HPV strains that are accountable for head-neck and cervical cancers. The main categories comprise cell vaccines, protein/peptide vaccines and genetic (DNA, RNA and viral) vaccines. The translation of the effects of anti-cancer vaccination into the clinics has been challenging for many years (Guo, Manjili et al. 2013). Cancer vaccines face significant challenges from the immunosuppressive nature of the TME.

In order to improve the efficacy of vaccines, stimulants such as interleukin-2 (IL-2) are co-administrated (Topalian, Weiner et al. 2011). Sipuleucel-T has been the first therapeutic cell vaccine approved by the FDA in 2010 for the treatment of asymptomatic metastatic hormone-relapsed PCa (mHRPC), based on the outcomes of three randomised clinical trials (Longo 2010). The antigen used is a recombinant protein obtained fusing the prostatic acid phosphatase (PAP), expressed by the prostate adenocarcinoma cells, and the granulocyte macrophage colony-stimulating factor (GM-CSF) which are used to activate ex vivo generated DCs from the patient. The therapy has been shown to be well tolerated by the patients, with a significant 4.1-month improvement in the overall survival (Graff, Chamberlain 2014).

PSA-TRICOM (Prostvac) is a peptide-based vaccine using a recombinant vector with PSA, ICAM, B7.1, and LFA3 to challenge DCs and trigger the immune reaction directed against

PCa cells (Yeku, Slovin 2016). A novel peptide-based vaccine approach for PCa which is based on PAP as antigen has shown promising results in a pre-clinical murine model (Saif, Vadakekolathu et al. 2014).

1.6.2.4 Adoptive T-cell transfer

Adoptive T-cell transfer (ACT) refers to the transfusion of patients with lymphocytes having enhanced effector functions. Such a strategy provides a revolutionary tool for overcoming critical obstacles imposed by intrinsic characteristics of most conventional tumour treatments. ACT has been shown to be able to overcome poor antigenicity of cancers as well as the effects of an immune suppressive TME on lymphocytes. Clinical studies have reported ACT to achieve tumour regression (Yee 2014) and improved survival in cancer patients with blood cancers (Sharma et al. 2019). However, clinical success of ACT has only been achieved in melanoma and blood cancers that account for 6% of all cancer-related deaths, whereas similar results have not been obtained yet in solid tumours (Rosenberg, Yang et al. 2011). There are currently three different ACT approaches (Figure 1.12).

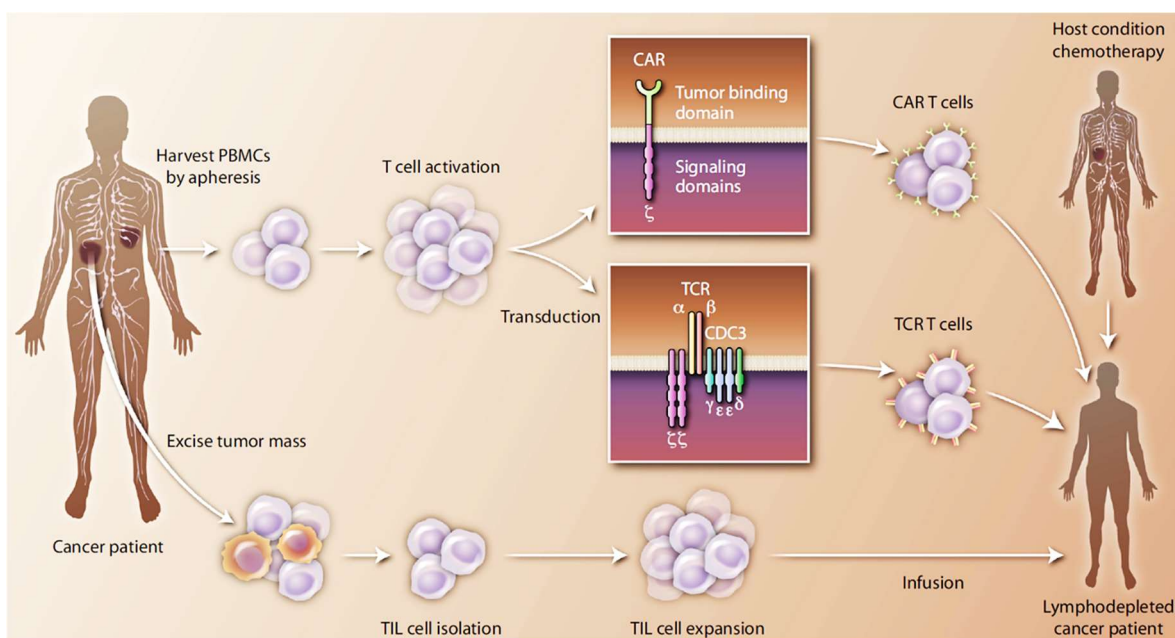


Figure 1.12 – Currently available adoptive T-Cell Transfer (ACT) approaches. Adoptive T-cell transfer (ACT) therapy is a personalised treatment for cancer patients based on the use and manipulation of either autologous or donors' lymphocytes. Tumour infiltrating lymphocytes (TILs) are isolated from the tumour mass and expanded *ex vivo* before being reinfused into the patient. A different approach to ACT involves the use of genetically engineered T-cells that can be transduced either with T-cell receptors (TCRs) or chimeric antigen receptors (CARs) targeting a desired antigen. (Adapted from June, Riddell et al. 2015)

The first approach uses autologous antigen-specific *tumour-infiltrating lymphocytes (TILs)*, CD4⁺ and CD8⁺ T-cells, isolated from the patient's excised tumour, clonally expanded *ex*

vivo by culturing them with IL-2, and finally reinfused into the patient (Rosenberg, Restifo 2015). Recent findings show that ACT of NF-κB p50 immature myeloid cells can decrease tumour growth in murine models of PCa by increasing the activation of CD8⁺ T-cells (Suresh, Barakat et al. 2020).

Another approach to overcome the immune tolerance that can occur with TILs is based on the genetic engineering of T-cells with chimeric antigen receptors (CARs). CARs have been developed to promote and propagate activation of the lytic function in genetically engineered T-cells, directing them towards selected antigens. In contrast to normal TCRs, CARs do not need processed antigens presentation to be activated as they directly bind to the antigen in its native conformation, as expressed on the target cells and in the context of any HLA type.

The modular structure of a CAR construct comprises the following components:

- *Extracellular antigen recognition zone*, in which a single-chain variable fragment (scFv) helps identify tumour-specific antigens
- *Immunoglobulin (Ig)-like domain hinge*, that separates the binding domain from the transmembrane units, providing more stability and flexibility to the construct
- *Transmembrane domain*, formed by a hydrophobic α helix which secures the CAR to the T-cell membrane
- *Intracellular module* consisting of the costimulatory signalling domains, usually endodomains derived from molecules of the CD28 and 4-1BB families, which increase T cell activation, proliferation and cytolysis (Guedan, Calderon et al. 2019). The structural composition of the endodomain has been upgraded through five generations so far as illustrated in Figure 1.13.

The first-generation CARs are characterised by a single CD3ξ unit, containing three immunoreceptor tyrosine-based activation motifs (ITAMs) in their endodomain. In order to overcome the limited cytotoxicity and proliferation conferred to the T-cells, the second-generation CARs were improved by adding portions of CD28 or CD137 as costimulatory domains. An additional costimulatory domain such as CD134 or CD137 was added to the third-generation CARs. The fourth-generation CARs are also referred to as TRUCKs (T cells redirected for universal cytokine-mediated killing) due to the presence of interleukin 12 (IL-12) inducer that induces IL-12 expression upon CAR activation. Fifth-generation CARs are

currently being tested. In addition to the CD3ξ and CD28 domains, the intracellular module comprises a truncated cytoplasmic IL-2 receptor form with the binding site for STAT3. Thus, CAR stimulation also leads to activation of cytokine signalling required to full T-cell activation and proliferation (Tokarew, Ogonek et al. 2019).

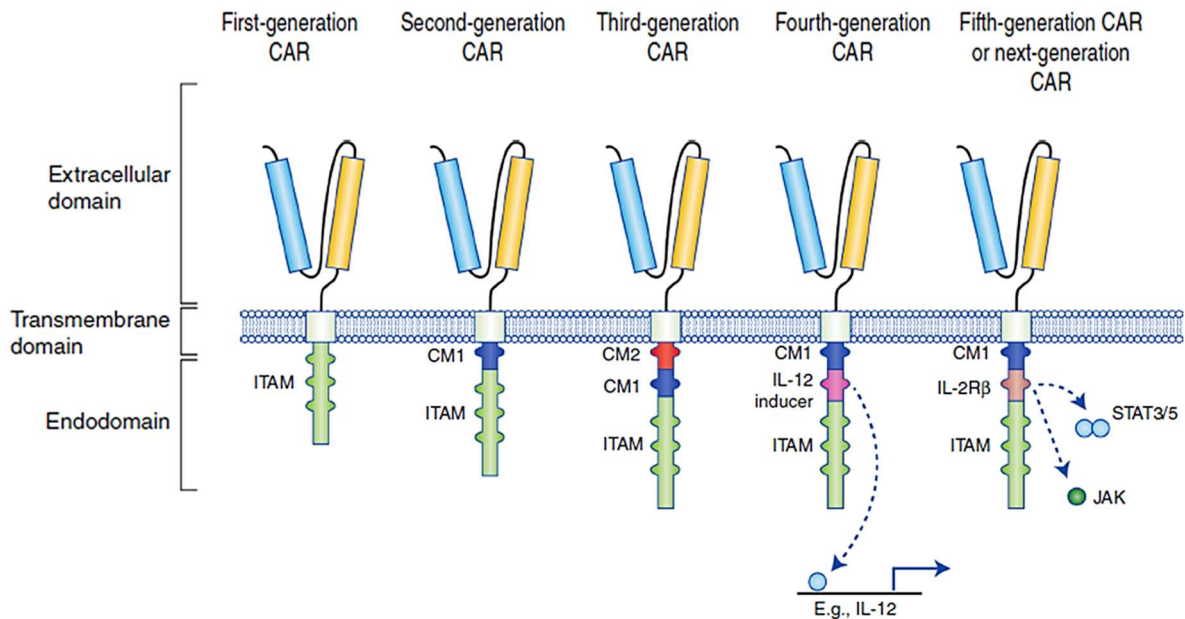


Figure 1.13 – Structure of different CAR molecules showing their evolution across the five generations.
The picture shows the structural modules added to the endodomain of CARs that characterise each generation. The endodomain of first-generation CARs only contain the ITAM motifs. In the second-generation CARs one co-stimulatory molecule (CM) was added, while in third-generation CARs a second CM was added. Fourth-generation CARs (also called TRUCKs) are based on second-generation, with the addition of a chemokine inducer. Fifth-generation CARs are also based on second-generation CARs and are improved with intracellular domains of cytokine receptors. (Adapted from Tokarew et al. 2019)

The first excellent results with CAR-armed T-cells were obtained in studies on haematological tumours that showed significant response rates and durable remission (Porter, Hwang et al. 2015). In 2017 the FDA approved two CAR T-cell therapies targeting CD19 for personalised treatment of refractory or relapse blood cancers. Tisagenlecleucel (Kymriah™) is used to treat acute lymphoblastic leukaemia and large B cell lymphoma (Maude, Laetsch et al. 2018), whereas axicabtagene ciloleucel (Yescarta™) is used in patients with large B cell lymphoma (Neelapu, Locke et al. 2017). Both therapies showed a lifesaving potential, with extremely high overall response rates in the short term. Unfortunately, cancer relapsed few months after either treatment in a significant number of patients and none of the patients involved in the trials was followed up for a long-term evaluation of the effects of the therapy (Zheng, Kros et al. 2018). Moreover, such therapies can induce severe health complications, such as cytokine-release syndrome and neurotoxicity. CD19 targeting can also induce B-cell aplasia as on-target off-tumour toxicity due to the endogenous

expression of the target on B-cells cell-surface (Sadelain 2017). Furthermore, clinical cardiotoxicity has been reported as a consequence of the lymphodepletion chemotherapy administrated before the CAR T-cell treatment to enhance its effects (Zheng, Li et al. 2018).

Two phase I clinical trials for CAR-T cell therapy for PCa are currently ongoing. The NCT01140373 and NCT03089203 studies are testing CAR-T cells directed against PSMA in mHRPC patients (Kloss, Lee et al. 2018). Particularly, the NCT03089203 trial aims to assess safety and feasibility of TGF- β resistant T cells (CART-PSMA-TGF β RDN cells), retrovirally transduced with a dominant negative TGF- β type II gene which blocks TGF- β inhibitory signalling in CAR-T cells. Indeed, the expression of such receptor has been reported to induce lymphoproliferative disorder in transgenic mice and increase antitumour immunity and trigger autoimmunity. Moreover, transduced cells also expressed HSV1 thymidine kinase in order to enable ganciclovir cell killing mechanism if needed in case of uncontrolled cell proliferation (Schepisi, Cursano et al. 2019). Recently, additional application of CARs involving NK cells has been developed. CAR-engineered NK cells provide interesting advantages compared to CAR-T cells, such as increased safety and reduced cytokine release syndrome, improved activation of cytotoxic activity, and more standardisable production for broader application across different patients (Xie, Dong et al. 2020).

Another approach is based on T-cells isolated from peripheral blood engineered to express cancer antigen-specific TCRs α and β chain heterodimers that can recognise the target antigens expressed on cancer. In association with the TCR there is the CD3 complex, which contains 10 ITAMs that are required for T-cell activation. Due to the interaction of the TCRs with the MHC, TCRs-armed T-cells can be used to target also intracellular proteins. Such approach has provided more promising results compared to CAR-modified T-cells in solid tumours. Indeed, TCR T-cells showed to penetrate tumours more efficiently than CAR T-cells. Moreover, TCRs showed higher sensitivity and reduced amount of cytokine release compared to CARs (Harris, Hager et al. 2018).

Despite unexpected and sometimes fatal toxicity observed during the initial clinical trials for TCR treatment of solid tumours, currently ongoing TCR clinical trials are showing more acceptable toxicity (Garber 2018).

1.7 Therapeutic Antibodies

The first mAb for clinical use in human was approved by the FDA in 1986. Muromonab (Orthoclone OKT3™) is a mouse mAb targeting CD3 on T-cells and was initially used to reduce acute organ transplant rejection (Todd, Brogden 1989). Then, in 1997, the FDA approved the use of rituximab (a CD20 antibody for treating B-cell cancers), the first mAb used for cancer therapy, for the treatment of Non-Hodgkin's lymphoma (Pierpont, Limper et al. 2018). Sales of mAbs generate huge incomes within the pharmaceutical market that score over US\$60 billion per year. Due to their modular structure, with each domain involved in a specific function, modified mAbs are currently investigated in a variety of therapeutic and diagnostic applications.

1.7.1 Immunoglobulin structure

Immunoglobulins, also referred to as antibodies, are large multimeric proteins (146-160 kDa for 10 nm length) that mediate the cellular and humoral reactions of the immune system against antigens. Monoclonal antibodies (mAbs) are produced by clones from a terminally differentiated single parent B-cells and can be expressed as a membrane bound form on B-cells and secreted by plasma cells. There are five different antibody classes in humans: IgA, IgD, IgE, IgG, and IgM, with IgA and IgG further divided in different subclasses, two and four respectively. All five immunoglobulin isotypes share the heterodimeric molecular structure; although IgD, IgE, and IgG are found as monomers while IgA molecules are organised in dimers and IgM ones in pentamers (Figure 1.14).

Isotypes	IgA	IgD	IgE	IgG	IgM
Subclass	IgA1 IgA2			IgG1 IgG2 IgG3 IgG4	
Allotypes	IgA2m		IgEm	IgG1m IgG3m IgG2m	
Heavy chain	α	δ	ϵ	γ	μ
Light chain	κ or λ	κ or λ	κ or λ	κ or λ	κ or λ
Structure	 Dimer	 Monomer	 Monomer	 Monomer	 Pentamer
In serum	13%	< 1%	< 1%	80%	6%

Figure 1.14 – Human immunoglobulins classification. The picture presents the five human immunoglobulin isotypes and relative subclasses, allotypes, and schematic structure. In addition, their relative abundance in serum is expressed as percentage of the total immunoglobulins.

Amongst the five different immunoglobulin isotypes, most of the mAbs approved for disease therapy are of the immunoglobulin G (IgG) isotype. The immunoglobulin molecule (Figure 1.15-A) is a homodimer consisting of two heterodimers formed by one light chain (LC – 25 kDa) and one heavy chain (HC – 50 kDa).

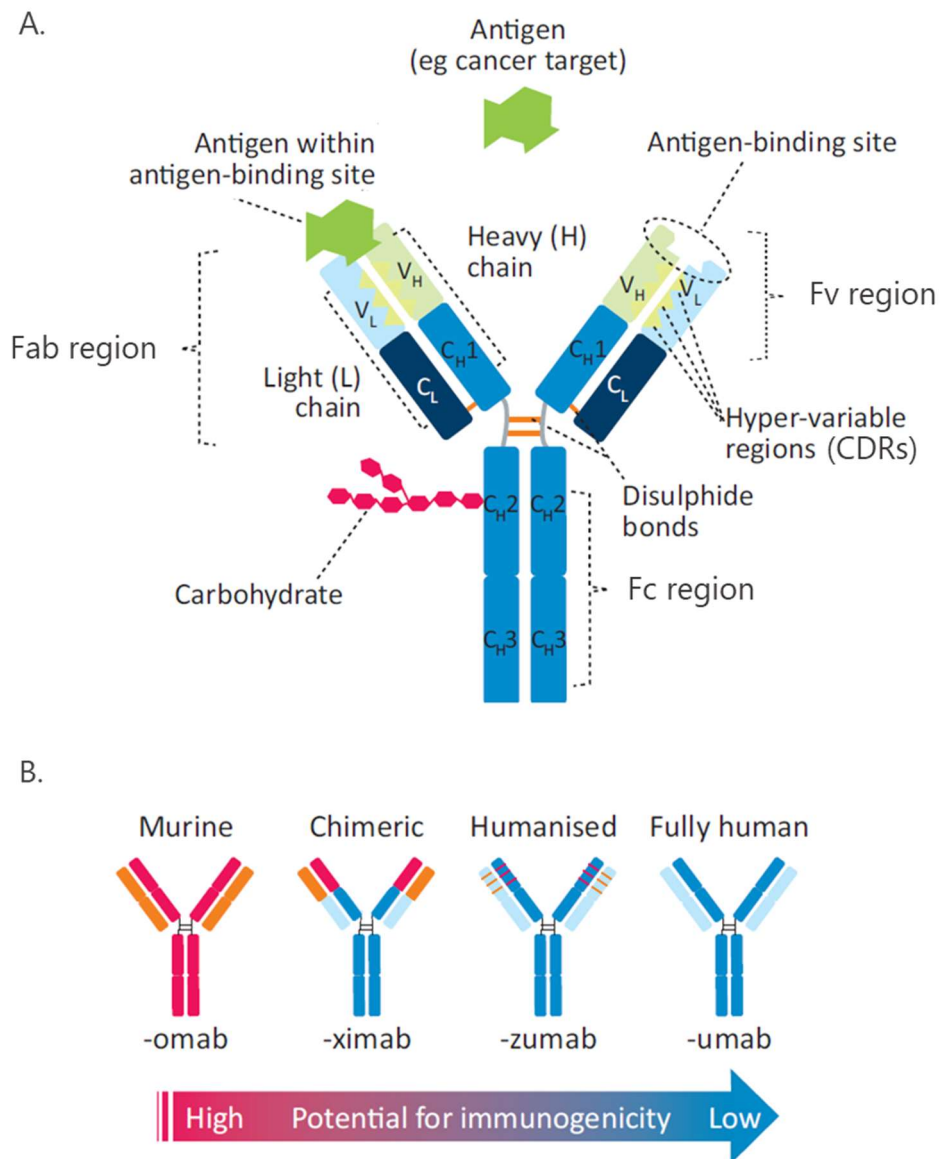


Figure 1.15 – Immunoglobulin structure and classification of therapeutic monoclonal antibodies (mAbs). (A.) Structure of mAbs molecule. The different regions of the antibody molecule are represented as: variable fragment (Fv), antibody-binding fragment (Fab), fragment crystallisable (Fc) variable heavy chain (VH), variable light chain (VL), constant heavy chain (CH), constant light chain (CL), complementarity determining regions (CDRs). (B.) Genetically engineered mAbs present different ratios of mouse:human sequence in their structure, the picture shows the suffixes used to design mAbs accordingly. Higher content of murine sequence can have higher immunogenic effect when used in human compared to human sequences. (Adapted and modified from Shepard, Phillips et al. 2017)

Disulphide bonds link the subunits of the molecule to each other. Immunoglobulins are characterised by unusual solubility and stability that confer to this class of proteins longer plasma residency. Both light and heavy chains contain variable regions (approximately 110 amino acids long), respectively VL and VH, together representing the antigen-binding site (Fv: variable fragment), one for each arm. Each variable domain is characterised by three short hypervariable amino acid sequences called complementarity determining regions (CDRs: CDR1, CDR2, and CDR3), which are responsible for antigen binding (Fab: antigen-binding Fragment) (An 2010). Antibody diversity is ensured by the random recombination

of variable (V), diversity (D), and joining (J) segments on the immunoglobulin gene. CDRs are subject to high rates of sequence variation, with CDR3 regions presenting the highest variability. CDR3 in light chains can be distinguished as either kappa (κ) or lambda (λ), presenting different physiochemical properties and thus different functions and specificity in binding to the antigen. The two classes show significantly different secondary structures, with λ chains being more hydrophobic. In human peripheral blood the ratio κ/λ is 1.5-2, value that can be altered in certain diseases such as hairy cell leukaemia and chronic HIV infection (Townsend, Laffy et al. 2016).

At the other end of the constant region of the antibody molecule, the 'stalk', resides the fragment crystallisable region (Fc region), connected to the Fab region by a flexible hinge. The Fc region is of paramount importance for the activity of the antibody and its serum half-life, which for mAbs is normally 2 to 4 weeks in blood circulation. Plasma availability of antibodies is prolonged by a pH-dependent intracellular trafficking and recycling process taking place in cells upon binding of the Fc region to the Fc γ Rs. There are six different Fc γ Rs in their cellular distribution, of which the best characterised are showed in Table 1.3. Fc γ RIIb is the only receptor with inhibitory activity.

Table 1.3 – Localisation of the major IgG Fc-receptors (Fc γ Rs) in human. This table shows localisation of the Fc γ Rs on immune cells. * = inhibitory receptor; (i): inducible; (s): expressed only in a subset population. (Stewart, Hammond et al. 2014)

Cell type	Fc γ RI	Fc γ RIIa	Fc γ RIIb*	Fc γ RIIIa
B cells			+	
DCs	+	+	+	
NK cells				+
Monocytes/Macrophages	+	+	+(s)	+
Neutrophils	+(i)	+	+(s)	

The first mAbs generated were murine proteins and showed poor pharmacokinetics. They are not suitable for long-term treatment of humans due to their immunogenicity. Such limitations were overcome by engineering antibodies to replace murine sequences with human ones. Based on the ratio between murine and human sequence in a mAb, four classifications of mAbs can be distinguished that are identified by specific suffixes as shown in Figure 1.15-B. Chimeric mAbs are characterised by a murine variable region joined to human constant regions (66% of the whole molecule), generated using recombinant DNA

techniques (Morrison, Johnson et al. 1984). In the humanised mAbs, 97% of the molecule is human, since only the hypervariable peptide binding loops are still murine (Jones, Dear et al. 1986). Therapeutic mAbs have found extensive application for the treatment of different types of diseases. The first mAb approved by the FDA was the anti-CD41 abciximab (ReoPro) in 1994 for hemostasis, while the anti-CD25 Daclizumab (Zenapax) was the first humanised mAb approved in 1997 for kidney transplant rejection. More recently, fully human antibodies have been generated using technologies such as *in vitro* phage display and transgenic mice (Röthlisberger, Honegger et al. 2005). The first fully human therapeutic mAbs approved from FDA in 2002 was the anti-TNF α adalimumab (Humira). The following sections will focus predominantly on mAbs and their derivatives used for cancer treatment.

1.7.2 Mechanisms of action of mAbs

Antibodies are extremely fascinating and versatile molecules. Most of their appeal comes from the variety of processes that they mediate. mAbs can exert their therapeutic functions through different mechanisms of action (MoA – Figure 1.16), which are determined by the combination of a variety of factors, such as the type of antigen targeted, the immunoglobulin subclass, and the receptors involved in binding the Fc region. Contrarily, IgG2 and IgG4 are preferred for the design of the so-called benign blocking therapies, due to their weaker ability to trigger Fc-mediated effector functions. Interestingly, IgG3 shows the higher binding affinity for most of the Fc γ Rs, but presents higher instability and immunogenicity compared to IgG1.

The preferential route of administration for therapeutic mAbs are intravenous or subcutaneous, whereas oral administration is not applied due to the degradation that mAbs undergo to in the digestive tract. Importantly, therapeutic mAbs do not pass the intact blood-brain barrier in sufficient amounts. mAbs can exert their therapeutic effect either as "naked" molecules or as conjugates with other drugs or radioactive material (Suzuki, Kato et al. 2015).

Nowadays, modifications of mAbs are relatively easy to perform, thus enabling the generation of molecules that exert the desired effect tailored according to each disease. For this reason, great effort has been put into engineering the variable regions of mAbs (as in the development of mAbs fragments) and Fc functions (to increase/mute effector functions). Such objectives can be achieved by inducing point mutations in the Fc regions as well as

multimerising IgG molecules or exchanging Fc domains across immunoglobulin isotypes (Saunders 2019). Moreover, since glycosylation of the mAbs affects their binding to the receptors, glyco-engineering strategies have been developed. Indeed, low or no fucosylation of the Fc region increases the binding avidity to the Fc_YRIIIa enhancing ADCC function (Strohl 2018).

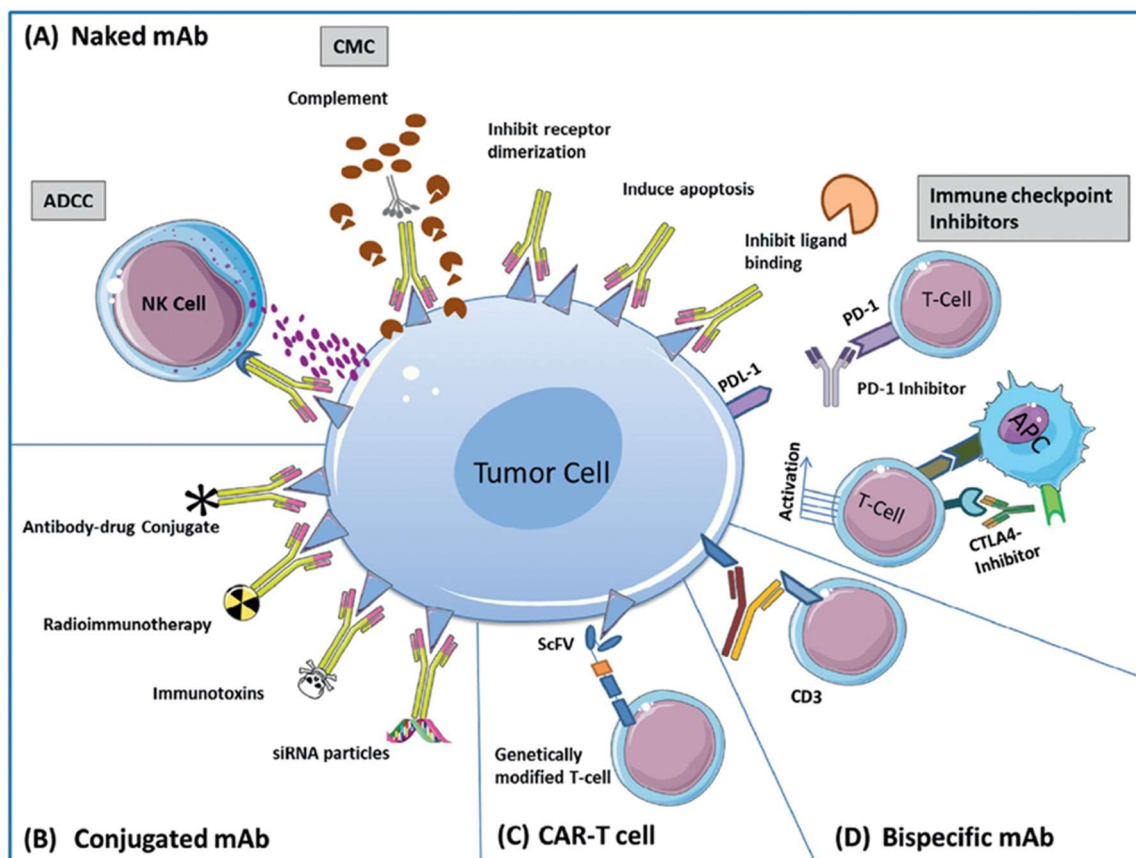


Figure 1.16 – Mechanisms of action of functional mAbs. mAbs can exert their functions either as unconjugated antibodies (blocking, signalling, CDC, ADCC) or conjugated antibodies (drug delivery). (Adapted from Charmsaz, Scott et al. 2017)

Disruption of ligand-receptor interaction. Antibodies binding to a ligand or surface receptor act as either blocking or neutralising agents. The blocking activity of a therapeutic antibody on its target directly interferes with its cellular function, such as cell adhesion or receptor-ligand binding. A neutralizing antibody binds its target and inhibits cell proliferation, adhesion, migration and activates pro-apoptotic pathways. Blocking and neutralising antibodies do not require the Fc region to achieve the desired biological effect. Thus, antibody fragments as well as different immunoglobulin isotypes can be used. Nowadays, the range of ligands targeted for antibody-based blockade comprises growth factors, cytokines, and viral and bacterial targets. A great example of mAbs exerting such activity

are the ones used in the checkpoint blockade therapy, of which ipilimumab, nivolumab and pembrolizumab are examples, as already discussed previously in section 1.6.2.1

Cytotoxicity. Effector cells of the immune system such as NK cells and macrophages can interact with the Fc region through dedicated receptors (Fc γ Rs) expressed on their surface. Binding with sufficient avidity between the Fc region and its receptor leads to recruitment and activation of the effector cells that result in antibody-dependent cell-mediated cytotoxicity (ADCC) and antibody-dependent cell-mediated phagocytosis (ADCP) (Hubert, Amigorena 2012).

Binding of the effector cell Fc γ RIIIA (CD16A) receptor to the Fc region of the IgG1 molecule in the human is essential to mediate ADCC. The main effector cell types involved in ADCC are NK cells, the activation of which results from a fine regulation of inhibitory and stimulating cell surface receptors (Ochoa, Minute et al. 2017). Activation of ADCC induces the secretion of pro-inflammatory cytokines such as IFN γ and the release of cytotoxic molecules such as perforin and granzyme. Such MoA is a significant component in the therapeutic effects of rituximab (CD20) and trastuzumab (HER2) mAbs.

Tumour cells opsonised with mAbs can also trigger the antibody-dependent cellular phagocytosis (ADCP), during which receptors for the Fc region of the antibody on phagocytic cells such as macrophages can activate the phagocytic pathway (Weiskopf, Weissman 2015). Following macrophage activation, the opsonised target cell is taken up into a phagosome that ultimately fuses with the lysosome leading to the target cell lysis (Kamen, Myneni et al. 2019). Trastuzumab has been demonstrated to mediate ADCP in *in vitro* and *in vivo* breast cancer models (Shi, Fan et al. 2015).

Moreover, the Fc region can bind to the serum complement molecule (C1q) triggering the complement-dependent cytotoxicity (CDC) canonical pathway, which ends in cell opsonisation that induces phagocytosis and cytotoxic killing. Furthermore, cleavage of C3 during CDC also induces the deposition of the membrane attack complex (MAC) that produces pores and lysis in the target cells. Thus, during CDC target cells are lysed without the intervention of effector cells (Rogers, Veeramani et al. 2014). IgG1 and IgG3 have high efficacy in mediating CDC. Complement depletion has been observed in chronic lymphocytic leukaemia patients after administration of rituximab, suggesting the activation

of CDC (Kennedy, Beum et al. 2004). Likewise, treatment of HER2-positive cancer cells with trastuzumab and petruzumab together shows increased tumour cell killing due to the CDC activity mediated by trastuzumab (Mamidi, Cinci et al. 2013). Although the intensity of CDC induced directly correlates with the amount of antigen expressed on the cell target, the same is not true for ADCC (Rogers, Veeramani et al. 2014). Interestingly, CDC was reported to be more efficient in the circulation, while ADCC has higher activity in tissues and TME.

Targeting. mAbs can be used as *targeted delivery agents* to deliver other treatments like radiotherapy and chemotherapy (Vankemmelbeke, Durrant 2016). Such a specific targeted systems helps to minimise the side-effects of the therapy on healthy cells. Radioimmunotherapy (RIT) refers to treatments in which mAbs are radiolabelled, while *antibody-drug conjugates* (ADC) are mAbs coupled to chemotherapeutic drugs. Such MoA relies on the internalisation of the ADC upon binding to the target. Designing such therapeutics is not easy task. Indeed, the concept is based on targeting cells expressing specific TAAs with a drug that is conjugate to the mAb through a strong enough linker to be stable in the blood circulation yet easy to be cleave once in the final target, and of course a potent cytotoxic conjugate (Chau, Steeg et al. 2019). Once the ADC reaches the lysosomal compartment, the cytotoxic payload is released and can exert its targeted activity. ADCs can carry cytotoxic drugs that either target DNA (i.e. gemtuzumab ozogamicin or inotuzumab ozogamicin) or act as tubulin inhibitors (such as brentuximab vedotin, glembatumumab vedotin, and depatuxizumab mafodotin), thus causing cell cycle arrest. However, as target cells die, the release of still active drug can cause cytotoxicity in adjacent cells too.

At the present, nine ADCs have been approved, one of which (gemtuzumab ozogamicin) was then removed from the market (Joubert et al. 2020). Brentuximab vedotin was approved for treatment of relapsed CD30-positive Hodgkin lymphoma patients. Two phase II trials showed favourable response rates and durations compared to the observed toxicities (De Claro, McGinn et al. 2012).

1.7.3 Full monoclonal antibodies and antibody fragments

The development of hybridoma technology (Köhler, Milstein 1975) and the phage/yeast or ribosome display technology (Lilian 2018) led to the large-scale production of mouse monoclonal antibodies (mAbs) that have provided a basis to a number of cancer therapeutic approaches. Since they first appeared on the laboratory benches worldwide, applications

that rely on mAbs have multiplied and the technology has further improved, as it is demonstrated by the generation of chimeric antigen receptors (CARs) and bispecific antibodies. At the present mAb-based therapies are used for the treatment of over 30 neoplastic, inflammatory, and infectious diseases (Shepard et al. 2017), some of which are shown in Table 1.4.

Since 2008, 48 US FDA-approved mAbs have reached the market. The first therapeutic mAb approved by the FDA against B-cell non-Hodgkin lymphoma was rituximab, a chimeric antibody targeting the CD20 protein, expressed on the surface of B-cells. A similar example of therapeutic mAbs is provided by trastuzumab (Herceptin), directed against the human EGFR-2 (HER-2), a protein which is over-expressed in 20-30% of breast cancers. Trastuzumab is a humanised IgG1 mAbs with 95% of its sequence human, while the remaining 5% mouse (Figure 1.13). Due to its subclass, trastuzumab exerts dual MoA since it accelerates the internalisation of HER2 with a strong anti-proliferative effect, prevents the receptor dimerization, as well as mediating an ADCC function. Despite its therapeutic effects, many metastatic breast cancers with HER2 amplification show resistance to trastuzumab monotherapy (Gajria, Chandarlapaty 2011). Mechanisms that can lead to resistance are: (i) escape from ADCC due to the presence of polymorphisms in the Fc γ receptors in breast cancer patients; (ii) expression of redundant ligands and receptors that do not present the epitope recognised by trastuzumab; (iii) active ER signalling that functions as an escape pathway in ER/HER2-positive cells; (iv) intrinsic alterations/variants of HER2 structure; (v) alterations in the apoptotic pathway that is inhibited by HER2 signalling (Luque-Cabal, García-Teijido et al. 2016).

Most mAbs can have different disease indications, as exemplified by tocilizumab, a humanised mAb against the human IL-6 receptor. Tocilizumab was initially approved for the treatment of rheumatoid arthritis and only recently used to treat the cytokine storm triggered during the novel disease COVID-19 caused by the SARS-CoV-2 virus (Buonaguro, Puzanov et al. 2020).

Table 1.4 – Mechanism of action (MoA) of the principal antibody-based drugs used in cancer treatment. List of the most relevant US FDA-approved therapeutic mAbs in use for cancer treatment with relative targets and MoAs. An updated list of approved mAbs is provided by www.antibodysociety.org. (CDC: complement-dependent cytotoxicity; ADCC: antibody-dependent cell mediated cytotoxicity; ADP: antibody-dependent phagocytosis). (Adapted from Shepard et al. 2017)

Antibody	Brand name	Target	Format	Mechanism of action	Therapeutic indication
<i>Adalimumab</i>	Humira	TNF-α	Human IgG1	Blocking	Crohn's disease, Rheumatoid arthritis, Psoriatic arthritis, Ankylosing spondylitis, Ulcerative colitis, Psoriasis, Hidradenitis suppurativa, Uveitis, Juvenile idiopathic arthritis
<i>Alemtuzumab</i>	Campath	CD52	Humanized IgG1	CDC, ADCC	Multiple sclerosis, Chronic lymphocytic leukemia
<i>Basiliximab</i>	Simulect	CD25	Chimeric IgG1	Blocking	Multiple sclerosis, Transplant rejection
<i>Belimumab</i>	Benlysta	BAFF	Human IgG1	Blocking	Systemic lupus erythematosus
<i>Bevacizumab</i>	Avastin	VEGF-A	Humanized IgG1	Angiogenesis inhibition	Macular degeneration and oedema, Colorectal cancer, Breast cancer, Glioblastoma, Renal cell carcinoma, Gastric cancer
<i>Bezlotoxumab</i>	Zinplava	<i>Clostridium</i>	Human IgG1	Blocking	<i>Clostridium difficile</i> infection
<i>Blinatumomab</i>	Blincyto	CD19/CD3	Bispecific T-cell engager (BiTE)	ADCC	<i>B-cell precursor acute lymphoblastic leukemia</i>
<i>Canakinumab</i>	Ilaris	Interleukin-1	Human IgG1	Blocking	<i>Rare inflammatory syndromes, active juvenile arthritis, gouty arthritis</i>
<i>Cetuximab</i>	Erbitux	EGFR	Chimeric IgG1	CDC, ADCC, Blocking	Colorectal cancer
<i>Infliximab</i>	Remicade	TNFα	Chimeric IgG1	Blocking	Crohn's disease
<i>Ipilimumab</i>	Yervoy	CTLA-4	Human IgG1	Depleting Treg cells	Metastatic melanoma
<i>Mepolizumab</i>	Nucala	IL-5	Humanized IgG1	Blocking	Severe eosinophilic asthma
<i>Natalizumab</i>	Tysabri	Alpha-4 integrin	Humanized IgG4	Blocking	Multiple sclerosis, Crohn's disease
<i>Nivolumab</i>	Opdivo	CD279/PD-1	Human IgG4	Neutralizing inhibitory signal in T cells	Melanoma, Non-small cell lung cancer, Renal cell carcinoma, Hodgkin lymphoma, Head and neck squamous carcinoma
<i>Obiltoxaximab</i>	Anthim	Anthrax toxin	Chimeric IgG1	Blocking	Exposure to <i>Bacillus anthracis</i> spores
<i>Obinutuzumab</i>	Gazyva	CD20	Humanized IgG1	ADCC, apoptosis induction	Rheumatoid arthritis, B-cell malignancies
<i>Omalizumab</i>	Xolair	IgE	Humanized IgG1	CDC, ADCC, ADP	Asthma
<i>Pembrolizumab</i>	Keytruda	PD-1	Humanized IgG4	Neutralizing inhibitory signal in T cells	Melanoma
<i>Rituximab</i>	Rituxan	CD20	Chimeric IgG1	CDC, ADCC, ADP	Non-Hodgkin lymphoma
<i>Tocilizumab</i>	Actemra	IL-6R	Humanized IgG1	Blocking	Rheumatoid arthritis
<i>Trastuzumab</i>	Herceptin	HER2	Humanized IgG1	Growth signal blocking; ADCC	Breast cancer
<i>Ustekinumab</i>	Stelara	P40 subunit of IL-12 and IL-23	Human IgG1	Blocking	Plaque and psoriatic arthritis, Crohn's disease
<i>Vedolizumab</i>	Entyvio	Alpha-4 integrin	Humanized IgG1	Blocking	Crohn's disease, ulcerative colitis

Since antibody molecules have a modular structure, it is possible to extract functional fragments to be used in therapy. Due to their reduced size, fragments of antibodies can easily penetrate target tissues or tumour masses (Nelson 2010), and have enhanced pharmacokinetic properties. The smaller size and the lack of glycosylation make the fragment easier and less costly to produce as the production can be carried out in bacteria. However, the fragments have a shorter circulating half-life and are quickly degraded because of the absence of the Fc domain. For the same reason they fail to induce antibody-dependent cell-mediated cytotoxicity (ADCC) or complement-dependent cytotoxicity (CDC) on their own compared to Fc mediated functions. To be effective, fragments need to be conjugated to an effector element.

To date, three types of antibody fragments have been produced (Figure 1.17). Fragment antigen binding (Fab) consist of the variable domain and the first constant region of both heavy and light chain and have a molecular weight of 50 kDa. The single-chain variable fragment (scFv) is a smaller (30 kDa) fusion protein consisting of the light and heavy chain variable regions held together by a linker peptide. Because of their smaller size, they show reduced stability. However, scFvs can be preferred for the easier production process. Single-domain antibodies (sdAbs – VHH/VH), also known as *nanobodies*, consist of a single monomeric variable (either light or heavy) antibody domain (Röthlisberger et al. 2005).

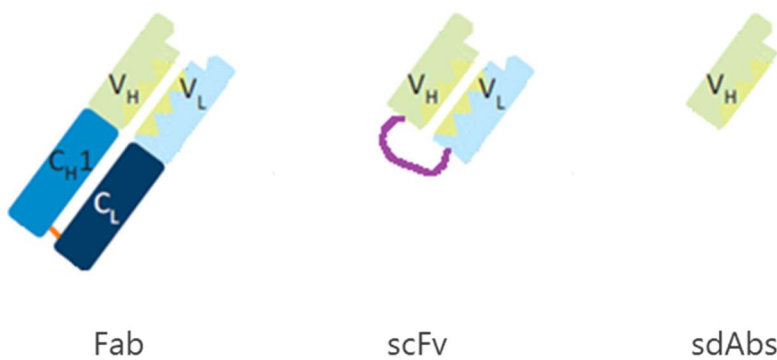


Figure 1.17 – Functional fragments of mAbs used for cancer treatment. The picture shows the main types of fragments derived by mAbs. Fab: fragment antigen binding; scFv: single-chain variable fragment; sdAbs: single-domain antibodies.

1.7.4 Bispecific and trispecific antibodies

Polyspecific monoclonal antibodies (PsMabs) are considered the next big thing for what concerns cancer immunotherapy. Indeed, psAbs are capable of binding to more than one antigen simultaneously. Basically, they hold effector cells of the immune system by hand and take them to the target tumour cells. PsMabs have shown a big potential to overcome the need of multiple combined therapies for treatment of neoplastic disease, especially in cold solid tumours. Interestingly, PsMabs development and production presents lower costs compared to CAR-T cells (Runcie, Budman et al. 2019).

They come in different forms ranging from fully antibodies to fragments. Bispecific mAbs (BsMabs) can bind simultaneously two different targets, one for each arm, while trispecific mAbs (tsMabs) are able to bind three different antigens simultaneously. BsMabs are classified as IgG-like, which keep the Fc region thus being able to exert Fc-mediated effector function, and non-IgG-like, whom therapeutic effect is exerted by the antigen binding capacity. Bispecific T-cell engagers (BiTEs) are an example of small fragment molecules, in which the single chain variable regions from two different mAbs are combined. In such molecule, one end binds to an effector cells while the other end binds the antigen on the target cell, thus increasing the antitumour effect. Advantages of such small molecules (50-60 kDa) are high specificity and tumour penetration (Runcie, Budman et al. 2018). Bispecific killer cell engagers (BiKEs) and trispecific killer cell engagers (TriKEs) are fragments containing the variable region of anti-CD16 and one or two, respectively, variable regions against the target of choice. Such constructs are designed to engage NK cells by binding to CD16 (Fc_γRIII) and take them in proximity of the target cell, thus enhancing tumour cell lysis (Felices, Lenvik et al. 2016).

Although the concept of CD3-targeting BsMabs was proposed for the first time in 1985, it took 30 years for the first treatment to be approved by the FDA (Benonisson, Altıntaş et al. 2019). CD3-bsMabs have been tested in murine melanoma models, where they induced T-cell and macrophage infiltration into immunologically ‘cold’ tumours. CD3- Blinatumomab is a bsMab, in which one arm binds to the CD19 protein expressed on acute lymphoblastic leukaemia cells, while the second arm targets CD3 domain of the TCR expressed on T-cells, thereby recruiting activated T-cell into proximity with target cells, achieving a stronger and more efficient immune response (Topp, Gökbüget et al. 2015). A phase II trial showed that blinatumomab improved (up to 40%) complete remission in patients with relapsed or

refractory acute lymphoblastic leukaemia. Nevertheless, the adverse event profile of blinatumomab is unique, in that presenting a significant toxicity with cytokine release syndrome (CRS) and toxicity events in the central nervous system (CNS) due to a neurotoxic cytokine release with consequent disruption of the blood-brain barrier (Lee, Chow et al. 2016). Several trials are currently testing CD3-bsMabs targeting antigens such as Carcino-Embryonic Antigen, EGFR, HER2, Mucin-1, and immune check points in solid tumours such as non-small cell lung cancer (NSCLC), breast cancer, and glioblastoma multiforme (GBM). A phase I trial of ertumaxomab, targeting HER2xCD3 confirmed a clinical response and safety in advanced breast, rectal, and gastric cancer patients (Haense, Atmaca et al. 2016). bsMabs fragments have also been tested for PCa treatment in the form of PSMAxCD3 diabodies, which are formed by the single chain Fv fragments against PSMA and CD3 connected by a small peptide linker (Bühler, Wolf et al. 2008). *In vivo* experiments on xenograft-SCID mouse model showed efficient inhibition of tumour growth.

However, nowadays there are no active clinical trials for tsMabs, although preclinical studies in multiple myeloma show promising results (Caraccio, Krishna et al. 2020).

1.8 EPCR as A Novel Marker for Aggressive PCa and Its Use in Therapy Design

The big question when developing a mAb-based therapy is which antigen to target. Identification of tumour markers is a powerful resource that can be used in cancer diagnosis, prognosis, for therapy response prediction and surveillance. In order to select the most appropriate target for cancer treatment it is important to screen the pros and cons linked to directing the immune system against the target.

As a result of the research conducted during this project, the human Endothelial Protein C receptor (EPCR) was selected as a suitable marker for antibody-based therapy of aggressive PCa. The following chapters will illustrate the journey started with the search of a marker for invasive PCa and gone through the generation of specific mAbs against it and their *in vitro* and *in vivo* test for antibody-mediated cell-dependent cytotoxicity (ACDC).

1.9 Aims and Objectives

Hypothesis

EPCR is a valid marker for metastatic prostate cancer. Targeting EPCR with specific mAbs can inhibit cell proliferation *in vitro* and tumour growth *in vivo*.

Aim

To develop monoclonal antibodies (mAbs) against the human Endothelial Protein C Receptor (EPCR) and evaluate their therapeutic potential by assessing their capacity to target and kill prostate cancer cells *in vitro* and *in vivo*.

Objectives

1. Confirm the role of EPCR in EMT and cancer progression by assessing the effect of knocking down EPCR expression in human prostate cancer cell lines on a range of functional properties associated with EMT and metastasis.
2. Generate mAbs against EPCR.
3. Identify clones having the best reactivity to EPCR and capacity to trigger the killing of prostate cancer cells *in vitro* and *in vivo*

2. Identification and Characterisation of EPCR as A Potential Target for Immunotherapy of Aggressive Prostate Cancer

2.1 Introduction

In the last 70 years, the systemic treatment of choice for newly diagnosed metastatic prostate cancer (PCa) has been androgen deprivation therapy (ADT). Treatment of hormone-sensitive PCa with ADT has been demonstrated to exert a selective pressure on the tumour population, quickly leading to the hormone-relapsed prostate cancer (HRPC) phenotype, which the patients spend the majority of their remaining lifetime in (Damodaran, Kyriakopoulos et al. 2017). HRPC progresses in all patients and it typically metastasises leading to poor prognosis and survival. Currently, immunotherapy represents a promising treatment option for these patients. Indeed, PCa is considered a suitable disease for immunotherapy treatment because of its relatively slow growth rate, which may allow the immune system enough time to produce a good response to treatment (Fernandez-Garcia, Vera-Badillo et al. 2015). In patients with advanced disease (metastatic HRPC), treatment with sipuleucel-T, anti-androgen drugs, chemotherapy, and radiotherapy have led to slightly improved clinical outcomes (C. Lee, Kantoff 2019). Nevertheless, generally no immune therapeutic treatment of mHRPC has delivered substantial improvements in patient OS (overall survival) or AWE (Alive Without Events – namely: radiographic and/or pain progression, chemotherapy initiation, or death) numbers (Gulley, Borre et al. 2019). Sipuleucel-T, a cell-based immune therapy, has been the first - and so far the only - immune therapeutic treatment for minimally symptomatic mHRPC that has increased OS, as showed in three double-blind randomized phase III clinical trials (Small et al. 2006; Higano et al. 2005). Only recently, a promising clinical trial for a new mAb-based therapeutic approach for mHRPC targeting PD1 started (Antonarakis et al. 2020). Indeed, the phase II KEYNOTE-199 study conducted in 2019 on the monotherapeutic use of pembrolizumab for immune checkpoint inhibition targeting PD1 in 285 mHRPC patients showed anti-tumour activity and encouraging OS estimates, with 1 in 20 men gaining up to two years of life.

Thus, despite the positive effects of various therapeutic combinations on the OS of patients with mHRPC (Table 2.1), advanced PCa remains incurable.

Table 2.1 Current FDA approved therapies for mHRPC. In this table, the different treatments and relative combinations for PCa are shown. Median overall survival (OS) and hazard ratio (HR) values are reported. (Adapted from Maia, Hansen 2017)

Agent	Setting (all mHRPC)	Comparator Arm	Median OS (months)	HR (p value)
<i>Docetaxel</i>	–	Mitoxantrone	18.9 m vs 16.5	HR 0.76 (p = 0.009)
<i>Cabazitaxel</i>	Post-docetaxel	Mitoxantrone	15.1 m vs 12.7	HR 0.70 (p < 0.001)
<i>Abiraterone</i>	Pre-docetaxel Post-docetaxel	Placebo + prednisone Placebo + prednisone	34.7 m vs 30.3 14.8 m vs 10.9	HR 0.81 (p = 0.0033) HR 0.65 (p < 0.001)
<i>Enzalutamide</i>	Pre-docetaxel Post-docetaxel	Placebo + prednisone Placebo + prednisone	32.4 m vs 30.2 18.4 m vs 13.6	HR 0.71 (p < 0.001) HR 0.63 (p = 0.001)
<i>Sipuleucel-T</i>	Pre/post- docetaxel, asymptomatic or minimally symptomatic	Placebo	25.8 m vs 21.7	HR 0.78 (p = 0.03)
<i>Radium-223</i>	Symptomatic bone metastasis only	Placebo	14.0 m vs 11.2	HR 0.70 (P = 0.002)

The aim of the current project was to identify a protein present on the cell membrane of PCa cells that can be used in targeted cytotoxic treatments mediated by mAbs, such as ADCC (Antibody-Dependent Cell Cytotoxicity) or possibly CDC (Complement-Dependent Cytotoxicity). ADCC and CDC are two important mechanisms of action of mAbs that are currently being exploited as very promising therapeutic approaches in cancer patients. ADCC and CDC are addressed in more detail in chapter 1 and the dedicated chapter 5. Adaptive immunity effector cells can react against antigens that are recognised by mAbs. Several classes of antigens have been identified based on their tumour-specific expression patterns (Vadakekolathu, Miles et al. 2014). Viral proteins, mutated proteins and proteins encoded by cancer-germline genes all present high tumour specificity. In order to direct immune reaction towards cancer cells, it is key to identify antigens as much as possible specific for neoplastic cells. If the expression of the selected target is shared by cancer and normal cells, basing a therapeutic strategy on it would trigger an immune response against both malignant and normal cells. The consequence of such reactions could be unwanted and potentially harmful side-effects and ultimately, depending on the systems that get affected, mild to severe impairment of the vital functions.

Some of the tumour-associated antigens (TAAs) for PCa are already known, such as prostate specific antigen (PSA), prostatic acid phosphatase (PAP), and prostate-specific membrane antigen (PSMA) (Arlen, Mohebtash et al. 2009). PSA has already been used in several targeted vaccine-based immunotherapies. Trial studies on sipuleucel-T showed 4.1-month increase in overall survival among men with asymptomatic or minimally symptomatic metastatic hormone-relapsed prostate cancer (Kantoff, Higano et al. 2010), whereas PROSTVAC did not show any effect on overall survival or alive without events numbers in mHCRP (Gulley et al. 2019).

Identifying a target specifically expressed on the surface of invasive PCa cells was a pivotal aim for this project. In a previous study conducted by Dr Regad and his team, the role of the cytoplasmic isoform of the promyelocytic leukaemia (cPML) protein in promoting EMT and invasion in PCa was investigated (Buczek, Miles et al. 2016). PML is known to exert a physiological tumour suppressive activity in cells and is mainly found in the nucleus, where it is involved in the formation of PML-nuclear bodies. In contrast, the presence of cytoplasmic PML correlates with cancer progression and poorer prognosis in PCa patients. There are 8 different isoforms of PML, most of which present an NLS (nuclear localisation signal) which anchors them in the nucleus, while only one presents the NES (nuclear export sequence) which allows its Exportin1-mediated translocation to the cytoplasm. To investigate the role of cPML in PCa cells, a lentiviral expression system was used to generate three PMLI mutant constructs stably expressed in DU145 and PC3 cell lines. The WT construct refers to the wild type protein, containing both NLS and NES, which were alternatively removed in each of the other two constructs generated, namely the PML Δ NLS and PML Δ NES (Figure 2.1).

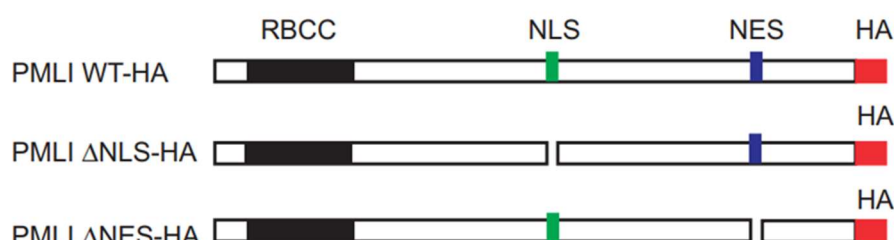


Figure 2.1 – PMLI mutant constructs. Schematic representation of PMLI WT, PMLI Δ NLS and PMLI Δ NES mutant constructs. All the three constructs are hemagglutinin-tagged. Wild type (WT) PML contains the nuclear localisation signal (NLS) and the nuclear export sequence (NES) which allow for its nuclear localisation and transport to the cytoplasm, respectively. Δ NLS mutants express the PML isoform without the NLS domain which determines the cytoplasmic localisation of the protein, contrarily to Δ NES mutants in which the PML isoform expressed without the NES domain anchors it in the nucleus (Adapted from Buczek et al. 2016).

As a result, the PML Δ NLS (lacking the NLS) protein was constitutively relocated in the cytoplasm, while the PML Δ NES (lacking the NES) protein was confined to the nucleus. Cells expressing the PML Δ NLS construct showed increased EMT characteristics, such as a mesenchymal phenotype and increased migration, in contrast to the cells expressing the PML Δ NES construct, which showed an induced markedly epithelial phenotype. Thus, the study provided evidence that cPML can drive a more invasive phenotype in PCa cells which is responsible for the tumour local invasion and occurs via TGF- β signalling activation. Taken together, these results suggest that such system can be a versatile *in vitro* model with which induce EMT PCa cells, thus making possible to investigate EMT effects (Di Biase, Miles et al. 2018). The rationale for this project was then to identify a potential target amongst the proteins that were up regulated exclusively in the cells with more mesenchymal phenotype and down regulated in the cells expressing epithelial phenotype.

2.2 Materials and Methods

2.2.1 Materials

2.2.1.1 Reagents

CELL CULTURE MEDIA	PROVIDER
DMEM	SLS (Lonza)
EMEM	SLS (Lonza)
F-12K	Gibco
RPMI 1640	SLS (Lonza)

CULTURE MEDIA SUPPLEMENTS	PROVIDER
Foetal calf serum (FCS)	Fisher (GE Healthcare)
L-Glutamine	SLS (Lonza)
D-glucose	Sigma
HEPES	SLS (Lonza)
Sodium Pyruvate	SLS (Lonza)

OTHER CELL CULTURE REAGENTS	PROVIDER
Dimethyl sulfoxide (DMSO)	Insight Biotechnology
Dulbecco's phosphate buffered saline (DPBS)	SLS (Lonza)
Trypan Blue solution (v/v 0.4%)	Sigma
Trypsin/Versene	SLS (Lonza)

CHEMICALS & BIOCHEMICALS	PROVIDER
Acetonitrile	Fluka Analytical
Agar	Bioline
Ammonium Persulphate (APS)	Geneflow
Ampicillin	Sigma
Bovine serum albumin (BSA)	Merck
Bromophenol blue	Arcos Organics
Clarity Western ECL Substrate	Bio Rad
Dithiothreitol (DTT)	Dithiothreitol (DTT)
Double distilled water (ddH ₂ O)	Barnstead, Nanopure Diamond
DPX mountant for histology	Sigma
Ethanol	Fisher Scientific
Ethyl alcohol absolute	VWR chemicals
Formic acid	Fluka analytical
Glycerol	Sigma
Glycine	Sigma
Haematoxylin	Sigma
Hydrochloric acid (HCl)	Fisher Scientific
Hydrogen peroxide	Sigma
Iodoacetamide (IAA) 0.55M	Sigma
Isoton II	Beckman Coulter
Nuclease-free water	Ambion
Skimmed milk	Marvel

Tetraethylammonium bromide (TEAB) 25mM	Sigma
Xylene	Fisher Scientific

IMMUNOCHEMICAL REAGENTS	PROVIDER
Alexa Fluor™ 488 conjugated donkey anti-rat IgG	Invitrogen
Alexa Fluor™ 488 conjugated goat anti-mouse IgG	Invitrogen
Anti-Mouse IgG HRP-linked Ab	Cell Signalling Technology
ImmEdge™ Pen	Vector
Mouse anti-human β-actin (clone 8H10D10)	Sigma
Mouse anti-human EPCR (clone ab56689)	Abcam
Mouse anti-human EPCR (clone M2)	Sigma
Precision Plus Protein WesternC Standards	Bio Rad
Precision Protein™ StrepTactin-HRP Conjugate	Bio Rad
Rat anti-human EPCR (clone NB600-963)	Novus Biologicals
VECTASHIELD® Antifade Mounting Medium with DAPI	Vector

REAGENT KITS	PROVIDER
Avidin/Biotin Blocking Kit	Vector Laboratories
DAB Peroxidase (HRP) Substrate Kit (with Nickel), 3,3'-diaminobenzidine	Vector Laboratories
DC Protein Assay	Bio Rad
FcR Blocking Reagent	Miltenyi Biotec
LIVE/DEAD™ Fixable Violet Dead Cell Reagent	Thermo Fisher Scientific
R.T.U. VECTASTAIN UNIVERSAL Elite ABC KIT	Vector Laboratories
RNeasy Mini Kit	Qiagen
QIAfilter Plasmid Midi	Qiagen

OTHERS	PROVIDER
DU145 human prostate cancer cell line	ATCC
FH1_ PROC R qRT-PCR forward primer	Merck
LNCaP human prostate cancer cell line	ATCC
Oligo-(dT) ₁₅ primers	Promega
PC3 human prostate cancer cell line	ATCC
PNT2 benign prostate epithelial cells immortalized with SV40	ATCC
Prostate Cancer Patient Tissue Micro Array (TMA)	Nottingham University Hospitals NHS Trust
RH1_ PROC R qRT-PCR reverse primer	Merck

2.2.1.2 Equipment

LABORATORY PLASTICS, GLASSWARE AND SHARPS	PROVIDER
Cell culture flasks (T25, T75, T175)	Sarstedt, UK
Conical flasks (50 mL, 100 mL)	Pyrex
Eppendorf tubes (0.5 mL, 1.5 mL, 2 mL)	Sarstedt, UK
12x75 mm polystyrene flow cytometry tubes	Tyco healthcare group
Falcon tubes (50 mL, 15 mL)	Sarstedt, UK
Filter tips (0.5-10 µL, 2-20 µL, 20-200 µL, 200-1000 µL)	Greiner bio-one/ Sarstedt
Flat-bottom culture dishes (6, 24, 96-well)	Sarstedt, UK

Micropipette tips (0.5-10 µL, 20-200 µL, 200-1000 µL)	Sarstedt, UK
Pipettes (5 mL, 10 mL, 25 mL)	Sarstedt, UK
PVDF blotting membrane (pore size 0.45 µm)	GE Healthcare, Life science
Screw-top tubes (15 mL, 50 mL)	Sarstedt
Serological pipettes	Sarstedt
Syringes (10 mL, 20 mL)	Becton Dickenson
Universal tubes (20 mL)	Greiner
Western blot filter paper	Schleicher-Schuell
0.45 µm syringe filter	Sartorius
0.22 µm syringe filter	Sartorius
40 µm nylon strainer	Greiner
70 µm nylon strainer	Greiner

LABORATORY EQUIPMENT	PROVIDER
4°C refrigerators	Lec
-20°C freezers	Lec
-80°C freezers	Revco/ Sanyo
96-well plate reader	Tecan
Autoclave	Rodwell
Cell culture incubator	Sanyo
Centrifuges	Sanyo, Eppendorf
CCD camera -Western blot imager	Syngene
Class II safety cabinets	Walker
Flow cytometer	Beckman Coulter
Haemocytometers	SLS
Heatblocks	Lab-Line
Light microscope	Nikon/Olympus
TripleTOF™ 6600 mass spectrometer	Sciex
Microcentrifuge	MSE
NanoDrop™ 8000 Spectrophotometer	Thermo scientific
pH meters	Metler Toledo
Pipettes and multichannel pipettes	Gilson, Star Labs, Eppendorf
Plate rocker	VWR, Stuart
Spectrophotometer for 96-well plate	Tecan ULTRA
Transfer tank	Bio Rad
Ultracentrifuge Optima TLX	Beckman
Ultrapure water dispenser	Barnstead
Vortex	Scientific industries
Water baths	Clifton
ZOOM® system incubator	Incucyte

SOFTWARE	PROVIDER
Aperio ImageScope	Leica Biosystems
Axiovision Microscopy Software 4.7.1. version	ZEISS
GraphPad Prism 8	Graph Pad software
Kaluza™ 3.1 version	Beckman Coulter
Morpheus	Broad Institute

nSolver™ Analysis Software (V.4.0)	NanoString Technologies Inc.
Reactome Analysis Tool	Reactome

2.2.1.3 Cell line growth media

DU145 COMPLETE MEDIUM	CONCENTRATIONS
EMEM	-
FCS	10%
L-glutamine	1%

LnCAP COMPLETE MEDIUM	CONCENTRATIONS
RPMI 1640	-
FCS	10%
L-glutamine	1 %
Glucose 45%	0.4 %
HEPES	1 %
Na Pyruvate	1 %

PC3 COMPLETE MEDIUM	CONCENTRATIONS
F-12K	-
FCS	10%

PNT2 COMPLETE MEDIUM	CONCENTRATIONS
RPMI 1640	-
FCS	10%
L-glutamine	1%

2.2.1.4 Buffers and gels

4X SDS-PAGE LOADING BUFFER	FOR 10 ML
1M Tris-HCl pH 6.8	2.4 mL
Sodium dodecyl sulfate (SDS)	0.8 g
Glycerol	4 mL
DTT	0.5 mL
Bromophenol blue	4 mg
ddH ₂ O	3.1 mL

5X SDS RUNNING BUFFER	FOR 1 L
Glycine	94 g
Tris base	15.1 g
10% SDS	50 mL
ddH ₂ O	Up to 1 L

5X Running buffer was diluted with ddH₂O to 1X working concentration prior use.

5% STACKING GEL	FOR 6 mL
ddH ₂ O	4.1 mL
30% Acrylamide mix	1.0 mL
1.0 M Tris (pH 6.8)	0.75 mL
10% SDS	0.06 mL
10% ammonium persulfate	0.06 mL
TEMED	0.006 mL

10X TRIS-BUFFERED SALINE (10 X TBS)	FOR 1 L
Trizma base	24.2 g
NaCl	80 g
ddH ₂ O	Up to 1 L
pH was adjusted to 7.6 with concentrated HCl.	

10% RESOLVING GEL	FOR 20 mL
ddH ₂ O	7.9 mL
30% Acrylamide mix	6.7 mL
1.5 M Tris (pH 8.8)	5 mL
10% SDS	0.2 mL
10% ammonium persulfate	0.2 mL
TEMED	0.008 mL

CITRATE BUFFER	FOR 1 L
Citric acid monohydrate	2.3 g
ddH ₂ O	Up to 1 L
pH was adjusted to 6 with concentrated HCl.	

ERIKA'S BUFFER WITH PROTEASE INHIBITOR	FOR 50 mL
Urea	28.5 g
Dithiothreitol (DTT)	1 g
N-Octyl-Beta-Glucopyranoside	0.5 g
ddH ₂ O	Up to 50 mL
Solution was mixed vigorously and sonicated until dissolved	
Proteinase Inhibitor cocktail	500 µL

RIPA BUFFER	FOR 50 mL
ddH ₂ O	47 mL
Sodium chloride	150 mM
Tris-HCl	50 mM
Triton-X-100	1% v/v
10% v/v Sodium deoxycholate	0.5% v/v
10% w/v SDS	0.1% v/v
pH was adjusted to 8.0	

TRANSFER BUFFER	FOR 2 L
Glycine	5.8 g
Tris base	11.6 g
10% SDS	0.75 g
Methanol	400 mL
ddH ₂ O	Up to 2 L

Transfer buffer was stored at 4°C.

TRIS-BUFFERED SALINE WITH TWEEN (TBST)	FOR 1 L
10X TBS	100 mL
ddH ₂ O	900 mL
Tween-20	1 mL

2.2.2 Methods

2.2.2.1 Routine cell culture

PNT2, DU145, PC3, and LNCaP cell lines were purchased from American Type Culture Collection (ATCC). All cell lines were cultured in their dedicated media. The PNT2 cell line was cultured in Roswell Park Memorial Institute 1640 (RPMI 1640) medium with 1% w/v L-Glutamine; DU145 cell line was cultured in Eagle's Minimum Essential Medium (EMEM) with 1% w/v L-Glutamine; PC3 cell line was cultured in Kaighn's Modification of Ham's F-12 Medium (F-12K); LNCaP cell line was cultured in RPMI 1640 Medium with 1% w/v L-Glutamine, 0.4% w/v Glucose 45%, 1% v/v HEPES, and 1% w/v Sodium Pyruvate. As a supplementary agent, 10% v/v foetal calf serum (FCS) was added to all media according to ATCC culture methods. No antibiotics were used. Each cell line was cultured at 37°C in the incubator containing 5% v/v CO₂ and humidified air. Cells were routinely passaged at 70-80% confluence. During passaging, cells were washed twice with Dulbecco's Phosphate Saline (DPBS) and detached by incubating with 0.25% w/v Trypsin- 0.53 mM EDTA solution for 5-15 min at 37°C. Equal amounts of cell-specific medium were added immediately upon cell detachment and cells were then centrifuged at 260 g for 5 min. Cell counting was carried out, by re-suspending a harvested cell pellet in 1-3 mL of cell-dedicated medium and re-suspending cell solution in Trypan blue 1:10. The haemocytometer was used to count the total number of living cells and excluded the number of dead cells (blue stained) from the count. The cell pellet was re-suspended in fresh medium and cells re-cultured in culture flasks by passaging. Stock of each cell line was prepared at approximately 1x10⁶ cell number in 1 mL FCS + 10% v/v DMSO (freezing medium) and stored at -80°C. As required, cells were thawed, gently re-suspended in 10 mL cell-dedicated medium and centrifuged at 150 g for

5 min. Cell pellets were then again gently re-suspended in fresh batch of cell-dedicated medium and plated in suitable dish. Medium changes ensured removal of DMSO from frozen cells sample and increased the viability of thawed samples.

2.2.2.2 Mass spectrometry analysis of differentially expressed proteins

2.2.2.2.1 Whole cell lysate preparation

In order to maximise protein yields from samples intended for MS analysis, Erika's Buffer was used for this experiment. Since the use of strong detergents such as SDS or Tween-20 to lyse cells could affect the quality of the lysate itself, cells were mechanically dissociated. The high concentration of urea in Erika's Buffer ensures protein denaturation, whereas DTT increases protein solubility by breaking down their secondary structure.

PML ΔNES and PML ΔNLS cells were cultured in six T75 flasks replicates until 90% confluency at 37°C in the incubator containing 5% v/v CO₂ and humidified air with FCS-free medium for 24 hours. Medium was then removed, and cells washed three times with cold DPBS. Any residual DPBS was carefully removed from the flasks, and 200 µL of Erika's lysis Buffer, supplemented with 1% v/v protease inhibitor was added directly to prevent protein degradation. Lysis buffer was spread across the entire cells and left to rest for 2 min. Cell lysates were collected into the corner of each flask using a cell scraper and then transferred into Eppendorf tubes. The tubes were transferred to an ice water bath for sonication at max power for 5 min. Then, samples were stored on ice for another 5 min. This step was repeated twice, and then samples were centrifuged for 10 min at 12,000 g and 4°C. Each supernatant (cell lysate) was removed carefully and stored in individual fresh tubes at -80°C.

2.2.2.2.2 Cell lysate protein quantification and MS analysis

The protein content of lysates was quantified using Bio-Rad Protein Assay according to the manufacturer's protocol. Protein Assay Dye Reagent Concentrate was diluted in 1:5 ratio with ddH₂O (such prepared was kept at 4°C for up to 2 weeks). Protein standards were prepared using different BSA protein concentrations (0.9-0.2 mg/mL) in EB+PI and 50 nM TEAB in 1:1 ratio. Controls included solutions of EB+PI and 50 nM TEAB in 1:1 ratio. Standard immediate absorbance was measured at 595 nm using TECAN ULTRA spectrophotometer. The average absorbance values from control wells were then subtracted from corresponding

test wells to remove the background signal. Sample protein concentrations were calculated as a reference to the standard curve.

2.2.2.3 Mass spectrometry sample preparation

Based on the quantification results, 50 µg of each sample was aliquoted to fresh tubes. 50 mM TEAB was added to each sample to the final volume of 93.5 µl. 1 µl of 0.5M DTT was added to each tube, mixed, and incubated at 56°C for 20 min. 2.7 µl of 0.55 M Iodoacetamide (IAA) was added to each tube, mixed, and incubated at RT in the dark for 15 min. Proteomic-grade Trypsin from porcine pancreas was dissolved in 1 nM HCl to the final concentration of 1 µg/mL vortexed and rested on ice. 1.8 µl Trypsin was added to each sample, vortexed thoroughly and incubated overnight at 37°C with shaking. HyperSep™ SpinTip Microscale SPE Extraction Tips (SPE tips) were wetted with 80% v/v Acetonitrile (ACN) in 0.1% v/v Formic Acid (FA) and centrifuged at 1500 g for 30 sec. Then, the same tips were wetted three times with 0.1% v/v FA and centrifuged at 1500 g for 30 sec. All trypsinized samples were topped up with 50 µl of 0.1% v/v FA, loaded on SPE tips and centrifuged at 550 g for 30 sec. All tips were then washed three times with 0.1% v/v FA and centrifuged at 550 g for 30 sec. Finally, samples were eluted with 3 aliquots of 50 µl 80% v/v ACN into a fresh Eppendorf tube. The samples were dried in vacuum dryer for about 1.5 hours at 60°C. Samples were then resuspended in 18 µl 5% v/v ACN in 0.1% v/v FA to the final sample concentration of 2 µg/µl.

2.2.2.4 Mass spectrometry analysis

Samples were then analysed on a SCIEX TripleTOF® 6600 mass spectrometer linked to an Eksigent nanoLC 425 HPLC system. The LC system was operating in micro flow (5 µl/min) and 3 µl of each sample was directly injected on a YMC 25 cm x 0.3 mm Triart-C18 column (12 nm, 3 µm particle size). Chromatographic separation was achieved over a 60-minute time frame for sequential window acquisition of all theoretical fragment ion spectra (SWATH) analysis and 87 min for Information Dependent Acquisition (IDA). The chromatography separation consisted of the following mobile phase gradients; 2% v/v mobile phase B (2% v/v acetonitrile, 5% v/v DMSO in 0.1% v/v FA) to 40% v/v over 50 min; to 80% v/v B at 55 min, held for 2 min, then returned to 2% v/v over 1 min. MS analysis was performed using two acquisition methods, IDA for spectral library generation and MS-SWATH data acquisition. The tandem MS spectra were searched using ProteinPilot 5.0 (SCIEX) with a Swissprot database containing human species at 1% False Discovery Rate (FDR) cut-off.

2.2.2.3 Expression of endogenous *PROCR* mRNA in normal tissues: Real-time quantitative PCR (qRT-PCR)

2.2.2.3.1 RNA extraction and cDNA synthesis

Total RNA was isolated from PNT, DU145, PC3 and LNCaP cells (grown and harvested as described in section 2.2.2.1) using the RNeasy Mini Kit (cat. #74104 - Qiagen) as described in the manufacturer's protocol and stored at -20°C. Quantitative and qualitative analysis of the RNA was then performed using the NanoDrop™ 8000 Spectrophotometer.

For each sample, 1.5 µg RNA, 1 µL of Oligo-(dT)₁₅ primers, and nuclease-free water (NFW) according to different samples concentrations was transferred to 0.5 mL Eppendorf reaction tubes, topping up to 10 µL final volume. Samples were mixed gently and incubated in a thermal block at 70°C for 5 min. Then, tubes were transferred immediately onto ice for 5 min. Meanwhile, the second master mix was prepared according to Table 2.2 below, calculating volumes based on the number of samples to test.

Table 2.2 – cDNA master mix. The table shows the volumes used to prepare the cDNA master mix for a single reaction tube.

Reagents	Volume for Single Reaction
RT 5x Buffer	5 µL
Reverse Transcriptase	1 µL
RNasin	0.7 µL
dNTPs	1 µL
NFW	7.3 µL
Total	15 µL

15 µL of the cDNA Master Mix was then added to each reaction tube with the RNA mix mixed thoroughly by gently pipetting up and down. Tubes were incubated in a water bath at 40°C for 60 min. After the incubation time, the reaction was inactivated by incubating the tubes in a thermal block at 95°C for 5 min. Finally, cDNA samples were stored at -20°C until use.

2.2.2.3.2 Primers reconstitution and efficiency test

PROCR forward and reverse primers were purchased from Merck (Table 2.3) and resuspended according to the manufacturer's recommendations by adding the accurate amount of NFW to each vial up to 100 pmol and vortexed. The vials were kept for 30 min to

dissolve completely. Aliquots with 10 pmol working solutions were prepared by adding 10 µL from the primer stock to 90 µL of NFW (1:10) dilution, and stored at -20°C.

Table 2.3 – *PROCR* primers specifications. The table provides the technical characteristics relative to Forward Human 1_ *PROCR* (FH1_ *PROCR*) and Reverse Human 1_ *PROCR* (RH1_ *PROCR*) primers used for all the Real-time quantitative PCR experiments in this thesis.

Oligo Name	Oligo #	Tm°	GC %	Sequence (5'-3')
FH1_ <i>PROCR</i>	8024281228-10/0	57.7	45	TTCTCTTCCCTAGACTGC
RH1_ <i>PROCR</i>	8024281228-10/1	58.8	45	CATATGAAGTCTTGGAGGC

Prior to their use in assays, primers were tested for their efficiency running a Real-Time quantitative PCR (qRT-PCR) on samples from DU145 cells, using 1:5 serial dilutions, and annealing at 58°C. Figure 2.2 shows the dilutions used and the results confirming efficient performance with the chosen configuration.

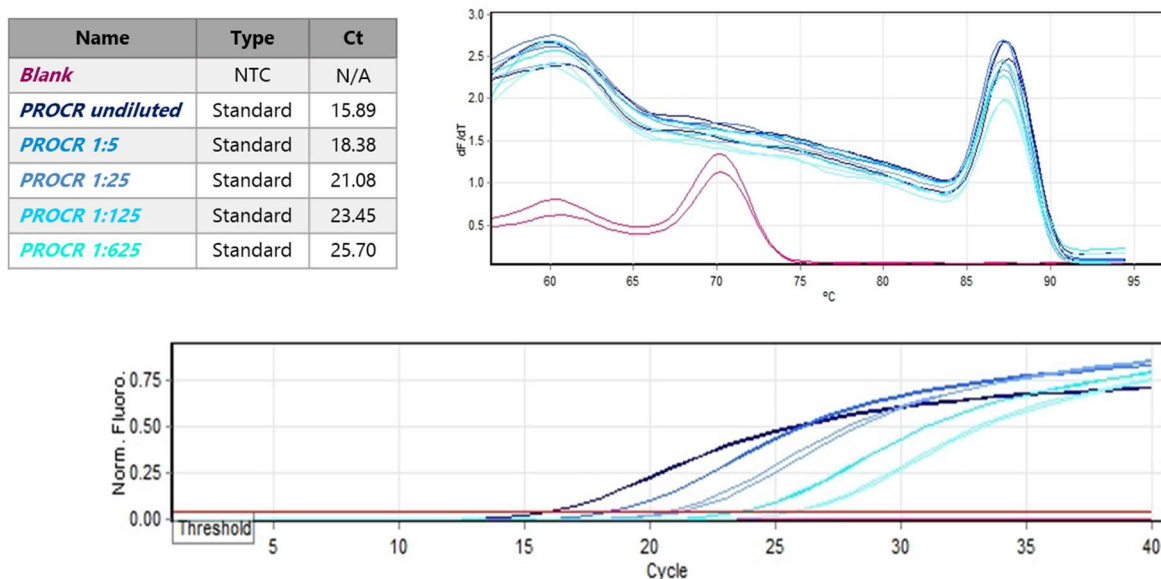


Figure 2.2 – Primer optimisation for Real-time quantitative PCR (qRT-PCR). The picture shows the dilutions used to perform the primer optimisation and the relative results with a single peak, confirming primer specificity.

Detailed protocol can be found in the next paragraph of this section.

2.2.2.3.3 Quantitative Real-Time PCR (qRT-PCR) reaction

A master mix was prepared by mixing the reagent in Table 2.4 below. The master mix was calculated according to the number of samples, plus two additional samples. For each cDNA sample, triplicates were calculated. In each sample levels of target mRNA (*PROCR*) as well control mRNA (*GUSB*) were analysed. *GUSB* was selected as housekeeping gene because of

its annealing temperature and Ct, which are comparable to *PROCR*, allowing the two genes to be analysed simultaneously in the same experiment run.

Table 2.4 – Real-time quantitative PCR (qRT-PCR) master mix. The table shows the volumes used to prepare a qRT-PCR master mix for a single reaction tube.

Reagents	Volume for 1X
iTaq™ Universal SYBR® Green Supermix	6.75 µL
Forward Primer (10 pmol)	0.5 µL
Reverse Primer (10 pmol)	0.5 µL
NFW	3.75 µL
Total	11.5 µL

11.5 µL of the master mix was pipetted carefully into labelled PCR tubes (kept on ice) and 1 µL of cDNA sample templates was added. The tubes were closed tightly and placed into QIAGEN's real-time PCR cycler, Rotor-Gene Q. Then, reaction was carried out using the primers temperature profile according to the conditions shown in Table 2.5 below. Acquisition on the green channel was set during the elongation step.

Table 2.5 – PCR conditions. The table shows the settings used to perform the PCR reaction.

PCR conditions	
Initial denaturation	5 min at 95°C
Denaturation	10 sec at 95°C
Annealing	15 sec at 58°C
Elongation	20 sec at 72°C
40 cycles	

For the analysis, the threshold was set on 0.04 and Ct (cycle threshold) values exported by Q-Rex Software. Finally, obtained data were analysed and normalised, and statistical analysis performed with Graph Pad Prism 8 software.

2.2.2.4 Expression of endogenous EPCR protein in normal tissues: Western Blot

2.2.2.4.1 Preparation of the cell lysates and protein quantification

PNT, DU145, PC3 and LNCaP cells were grown and harvested as described in section 2.2.2.1, and snap frozen in dry ice for 5 min. Pellets were then lysed by adding 100 µL

Radioimmunoprecipitation assay Buffer (RIPA Buffer) + 1% v/v protease inhibitors, subjected to 3 cycles of vortex, and then centrifuged at 10,000 g for 10 min at 4°C to remove any debris. Supernatants were transferred to fresh tubes and stored at -20°C.

Total protein concentration in all lysate samples were quantified using a DC Protein Assay (BioRad), a detergent-compatible colorimetric assay based on the Lowry assay method, according to the manufacturer's protocol.

As a reference, a stock solution of 2 mg/mL Bovine Serum Albumin (BSA) solution in RIPA buffer was prepared and used for serial dilutions (Table 2.6).

Table 2.6 – BSA standard curve. Each standard was prepared as 50 µL final volume.

Final concentration (mg/mL)	2 mg/mL BSA (µL)	Buffer (µL)
0	0	50
0.125	3.12	46.48
0.25	6.25	43.75
0.5	12.5	37.5
0.75	18.75	31.25
1	25	25
1.5	37.5	12.5
2	50	0

For each standard and unknown sample, 10 µL/well in triplicates in 96-well plates were used. 25 µL of working reagent was added to each well and mixed carefully by pipetting up and down, then 200 µL of reagent B was added to each well, then the plate was incubated in the dark at 37°C for 15 to 30 min. The absorbance was measured at 570 nm using a TECAN ULTRA spectrophotometer, and average values from control wells were then subtracted from corresponding test wells. Standard curves were then generated based on the absorbance intensity generated using the standard concentrations. Sample concentrations were calculated based on the standard curve.

2.2.2.4.2 Gel preparation and electrophoresis

First, SDS-PAGE was performed to separate the proteins in sample lysates. Gels were prepared as described in section 2.2.1.3 and immersed in a tank containing 1X SDS running buffer. For each sample, a volume of lysate sample equivalent to 30 µg protein per gel-lane was mixed with 5X Protein Loading Buffer at ratio 4:1, vortexed and incubated at 95°C for 5 min for protein denaturation. Denatured samples were carefully loaded on well-set gel

alongside 5 µL of Precision Plus Protein Western Standards. Once loaded, the samples were run at 60 V for 10-20 min (to allow proteins to pass through the stacking gel), and then the voltage was increased to 100 V to allow proteins to separate in the resolving gel.

2.2.2.4.3 Wet transfer

Once proteins had run through the gel (approximately 90 min), the electrophoresis was stopped. The gel was carefully removed from the tank and transferred onto a PVDF blotting membrane via “wet transfer”. First, PVDF membranes were cut into 8 x 6 cm pieces (fitting the size of the gel) and activated by soaking in methanol for 30 sec, water for 10 min, and transfer buffer for 15 min. Two pieces (per membrane) of filter paper of the same size were cut and soaked with transfer buffer. The “sandwich” was assembled using an assembly cassette, sponge, blotting mat, membrane, gel, blotting mat, sponge. All assembly parts listed above remained soaked with transfer buffer at all times. The assembly cassette was used to seal the construct and the “sandwich” was immediately inserted into a transfer tank filled with ice-cold transfer buffer. Proteins were transferred at 100 V for 1 hour at room temperature (RT).

2.2.2.4.4 Immunoprobining

After the transfer, membranes were removed from the assembly cassette and washed 3 times with DPBS, rocking for 10 min. Membranes were then blocked with 5% w/v Marvel skimmed milk in TBS for 1 hour rocking at RT. Membranes were then incubated with primary monoclonal antibodies at 4°C on the rocking platform overnight. The following day, the membranes were washed three times with TBST and incubated with the corresponding secondary antibodies for 1 hour on the rocking platform at RT. All antibody concentrations are shown in Table 2.7.

Following the incubation, the membranes were washed with TBST. Finally, membranes were incubated with Clarity Western ECL Substrate for a min prior to imaging using a CCD camera.

Table 2.7 – Antibodies and dilutions used in Western blot analysis.

Primary Ab	Dilution	Reference number	Clone	Supplier
Mouse anti-EPCR	1 µg/mL	WH0010544M3	M2	Sigma
Mouse anti-β-actin	1:1000	SAB1305567	8H10D10	Sigma
Secondary Ab	Dilution	Reference number	Clone	Supplier
Anti-Mouse IgG HRP-linked	1:1000	7076	Polyclonal	Cell Signalling
Ladder	Dilution			Supplier
Precision Protein™ StrepTactin-HRP Conjugate	1:5000			Bio Rad

2.2.2.5 Cell surface expression of endogenous EPCR protein in normal tissues: Flow Cytometry

2.2.2.5.1 Sample preparation

PNT, DU145, PC3 and LNCaP cells were grown, harvested, and counted as described in section 2.2.2.1, and 10×10^5 cells of each type were aliquoted to 12x75 mm polycarbonate flow cytometry tubes. 1 µL of LIVE/DEAD™ Fixable Violet Dead Cell Reagent was mixed with 1 mL of DPBS and added to each tube with cells (apart from the unstained control) and incubated at RT for 30 min. Cells were washed with 1 mL of DPBS and centrifuged at 400 g for 5 min. Supernatants were removed by gently flicking the tube and pellets were resuspended by gentle tapping. 5 µL of FcR Blocking reagent was mixed with 45 µL of PBS added to each tube and incubated at RT for 10 min. 50 µL primary monoclonal antibody was prepared in PBS as described in Table 2.8, taking into consideration that the final volume per tube is 100 µL thus adjusting antibody dilution accordingly, and added to each test tube except for the unstained and control tubes, and incubated at RT for 30 min. After incubation, cells were washed with 2 mL of PBS and centrifuged at 400 g for 5 min. Supernatants were removed from each sample and pellets were resuspended by gentle tapping. 100 µL of secondary antibody diluted in PBS was added to all but the ‘unstained’ tube, and samples incubated at RT for 30 min in the dark. After incubation, cells were washed with 2 mL of PBS and centrifuged at 400 g for 5 min. Supernatants were removed from each sample and pellets were resuspended by gentle tapping in 300 µL of ISOTON II™ flow cytometry sheath fluid shield fluid.

Table 2.8 – Primary and secondary antibodies used for flow cytometry analyses.

Primary Ab	Dilution	Reference number	Reference number	Supplier
Rat anti-EPCR	10 µg/mL	NB600-963	RCR-252	Novus Biologicals
Secondary Ab	Dilution	Reference number	Reference number	Supplier
Alexa Fluor™ 488 conjugated Donkey anti-rat IgG	1:500	A21208	Polyclonal	Invitrogen

2.2.2.5.2 Cell gating strategy and data acquisition

Prior to start the acquisition, a suitable strategy for gating was set, as shown in Figure 2.3. First, the cell population was distinguished based on its forward and side scatter intensities (FS and SS INT). Both these values together give an estimation of the cell size and granularity, respectively. At the bottom left corner of the dot plot are often found debris and dead cells with a lower level of FS. Setting a gate that excludes such events made possible to avoid collecting them. On this first gate then a second gate was applied to discriminate cell doublets. In such gate, single cells were selected plotting the FS intensity by its height. Viability of cells represents another important factor since dead cells can display an increased auto fluorescence and non-specific binding of antibodies. As a consequence, a viability stain was included in all analysis and data acquired on the viable population. The viability dye interacts with compromised cell membranes giving higher fluorescent signal, whereas live cells show very low/absent fluorescence intensity. Thus, a third gate excluded non-viable cells and data acquired from the viable population. Samples incubated with secondary antibody alone acted as a negative control, against which cells expressing EPCR could be identified. Data were acquired using a 10-color/3-laser Beckman Coulter Gallios™ flow cytometer and analyzed using Kaluza™ v1.3 data acquisition and analysis software (Beckman Coulter).

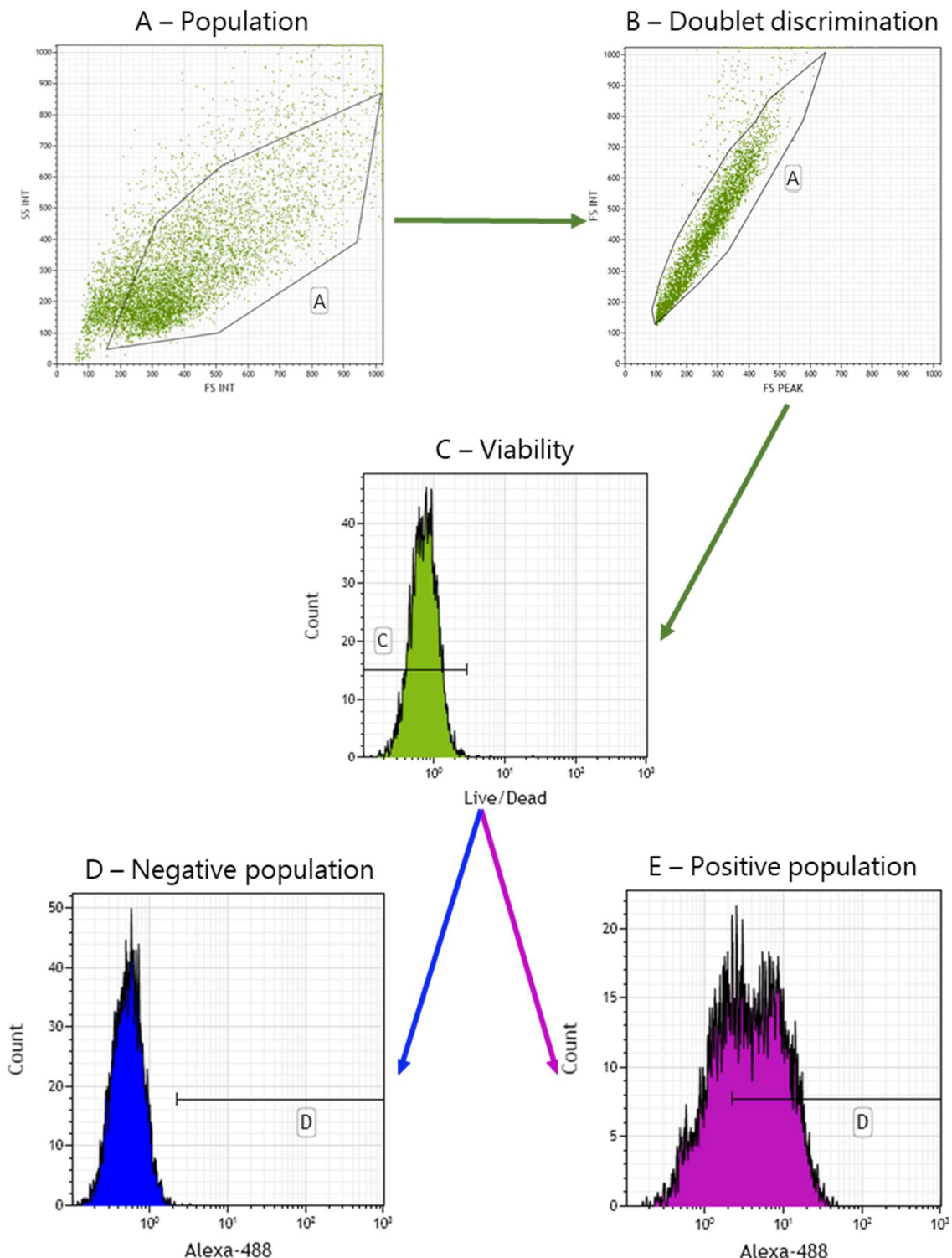


Figure 2.3 – Gating scheme for flow cytometric analysis. (A) SSC (side scatter) vs FSC (forward scatter) density plot was used to identify the target cell population based on cell's size and granularity. Each dot or point on the plot represents an individual cell. (B) Doublet gating was applied to discriminate single cells. (C) Cells were stained with a viability dye that enabled isolation of viable cells. A gate was applied to identify a specific population, in this case DU145 cells without (D) and with (E) anti-EPCR primary antibody.

2.2.2.6 Immunohistochemistry staining of Tissue Microarrays (TMAs)

PCa tissue microarrays (TMAs) were kindly provided by Dr Des Powe (Queen's Medical Centre, Nottingham University Hospitals NHS Trust). TMA slides were washed in several different solutions by immersing the TMA slide in a Coplin jar. TMAs slides were first

dewaxed with two changes of xylene, each for 5 min. TMAs slides were then washed with two changes of 100% v/v ethanol each for 4 min, 90% v/v ethanol for 4 min, 70% v/v ethanol for 4 min, and washed with dH₂O for 2 min. Slides were then washed with 3% v/v hydrogen peroxide in methanol for 10 min, and subsequently with dH₂O for 3 min. Slides were then placed in 1 L beaker filled with citrate antigen retrieval buffer, covered with a cling film, and boiled in the microwave for 30 min. Slides were left to cool at RT for 20 min and once cooled they were washed in TBST for 5 min. Slide sections were then outlined with ImmEdge™ waterproof pen. Following protocol refers to the use of the reagents from Avidin/Biotin Blocking Kit, DAB Peroxidase (HRP) Substrate Kit (with Nickel), 3, 3'-diaminobenzidine, pre-made buffers and antibodies. Slide sections were blocked with 2.5% v/v horse serum in TBST for 10 min. After incubation, serum was removed and slide sections were covered with Avidin-D solution and incubated for 15 min. After incubation, Avidin-D solution was removed and slides were washed with TBST for 2 min. Slides were subsequently covered with Biotin and incubated for 15 min. After incubation, Biotin was removed and slides covered with a mouse anti-human EPCR primary monoclonal antibody (clone CD201; Abcam - ab56689, IgG1) in 1:50 dilution in TBST + 2.5% horse serum and incubated overnight at 4°C. Following day, slides were washed with two changes of TBST for 10 min each, after which they were incubated with biotinylated universal secondary antibody that recognises mouse and rabbit IgG for 10 min. After incubation, slides were washed with two changes of TBST for 10 min each. Slide sections were then covered with ABC reagent and incubated for 5 min. After incubation, slides were washed with two changes of TBST for 10 min each. Slides were covered with peroxidase substrate DAB solution (premixed from 5 mL dH₂O + 3 drops Buffer solution + 4 drops DAB Substrate + 2 drops Hydrogen Peroxidase) and incubated for 6 min. After incubation, DAB solution was removed and slides were washed with dH₂O. Slides were then covered with haematoxylin and incubated for 1 min and subsequently washed with running tap water for 5 min. Slides were then washed with 70% v/v ethanol for 4 min, 90% v/v ethanol for 4 min, two changes of 100% v/v ethanol each for 4 min and two changes of 100% v/v xylene for 4 min. Finally, slides were dried from the excess of liquid, covered with a few drops of DPX mountant for histology solution and then with coverslip. High-resolution TMA slides scans were taken by NanoZoomer 2.0-HT Whole Slide Imager a digital pathology slide scanner and viewed in NDPView2 software.

2.3 Results

2.3.1 Identification of the target: the human EPCR

In the *in vitro* induced-EMT DU145 model, the expression of the PML Δ NES construct drove a marked epithelial phenotype and reduced the invasive potential. On the other hand, the expression of PML Δ NLS led to the activation of early EMT events and increased invasive behaviour in cells. As EMT is considered to be one of the first step towards the formation of metastases, and is necessary for cancer cells to become invasive, we decided to investigate different patterns of protein expression in cells undergoing EMT and not-EMT cells using mass spectrometry analysis of lysates from DU145 PML Δ NLS and PML Δ NES mutants. Differential protein expression in PML Δ NES vs. PML Δ NLS mutants was assessed and eventually a panel of proteins with significant (p -value <0.005) expression fold change was generated (Figure 2.4 and Table 2.9). Candidate target proteins were selected with fold change values between 0 and 0.5, indicating proteins that are up regulated in PML Δ NLS mutant. Amongst these proteins, the target candidate was selected based on its subcellular location, relative expression in tissues and in PCa (Table 2.10).

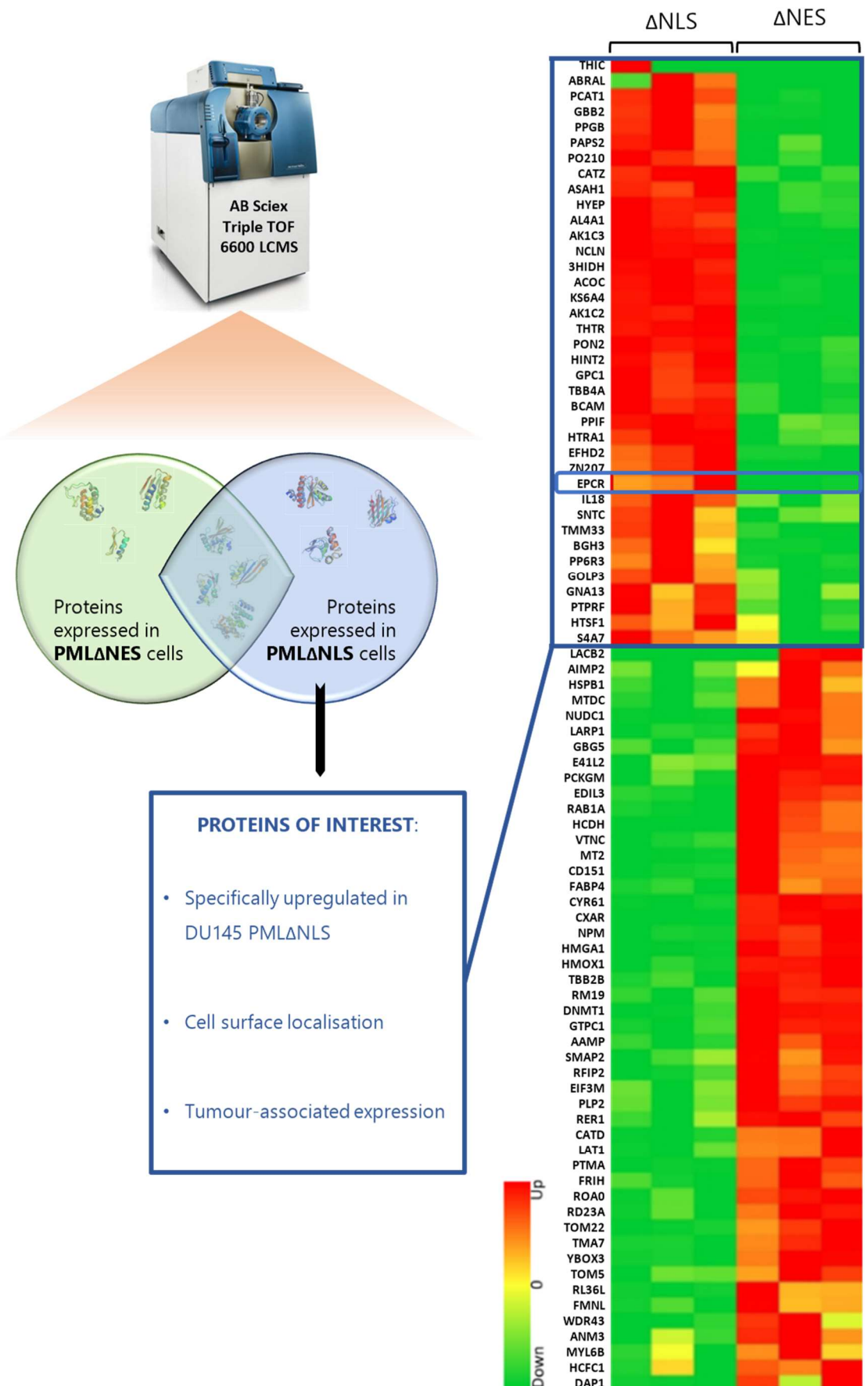


Figure 2.4 – Schematic representation of the process for the identification of target and results.
 SWATH/DIA quantitative proteomics was performed with AB Sciex TripleTOF™ 6600 LCMS on whole lysates from DU145 PML Δ NLS / PML Δ NES cells (left panel). Heat-map representing the proteins listed in Table 3.2 (right panel).

Table 2.9 – Proteins differentially expressed in DU145 PMLΔNES vs PMLΔNLS. Proteins with logarithmic fold change (LFC) between +/-0.5 and p-value<0.005 were selected. Upregulated (**blue** table) and downregulated (**red** table) proteins in DU145 PMLΔNES are ranked according to fold change.

Entry name	UniProt accession	Fold change	p-value	Protein name
DAP1	P51397	63.40	3.73E-02	Death-associated protein 1
MT2	P02795	22.90	7.44E-04	Metallothionein-2
PTMA	P06454	11.20	2.05E-04	Prothymosin alpha
FRIH	P02794	11.10	5.64E-04	Ferritin heavy chain
TBB2B	Q9BVA1	8.81	4.37E-05	Tubulin beta-2B chain
RM19	P49406	8.71	1.17E-04	39S ribosomal protein L19, mitochondrial
DNMT1	P26358	8.68	2.63E-05	DNA (cytosine-5)-methyltransferase 1
CD151	P48509	7.57	8.40E-04	CD151 antigen
MTDC	P13995	7.55	1.77E-03	Bifunctional methylenetetrahydrofolate dehydrogenase
FABP4	P15090	6.69	1.62E-03	Fatty acid-binding protein
HMGA1	P17096	6.08	6.95E-06	High mobility group protein
RFIP2	Q7L804	6.06	7.86E-04	Rab11 family-interacting protein 2
PLP2	Q04941	5.76	7.65E-04	Proteolipid protein 2
TOM5	Q8N4H5	5.63	3.47E-03	Mitochondrial import receptor subunit TOM5 homolog
HMOX1	P09601	5.27	7.52E-06	Heme oxygenase 1
RER1	O15258	4.93	2.32E-03	Protein RER1
AAMP	Q13685	4.72	1.81E-04	Angio-associated migratory cell protein
ZN207	O43670	4.69	3.05E-03	BUB3-interacting and GLEBS motif-containing protein
NUDC1	Q96RS6	4.62	4.32E-04	NudC domain-containing protein 1
ROA0	Q13151	4.59	3.06E-04	Heterogeneous nuclear ribonucleoprotein A0
EFHD2	Q96C19	4.38	5.26E-06	EF-hand domain-containing protein D2
LARP1	Q6PKG0	4.38	4.63E-04	La-related protein
EIF3M	Q7L2H7	4.30	1.89E-03	Eukaryotic translation initiation factor 3 subunit M
YBOX3	P16989	4.26	5.33E-04	Y-box-binding protein 3
GBG5	P63218	4.22	1.79E-03	Guanine nucleotide-binding protein G subunit gamma-5
FMNL	O95466	4.20	1.21E-02	Formin-like protein 1
E41L2	O43491	4.17	1.40E-03	Band 4.1-like protein 2
ANM3	O60678	4.10	1.05E-02	Protein arginine N-methyltransferase 3
GTPC1	Q9GZT8	4.08	5.82E-05	NIF3-like protein 1
RL36L	Q969Q0	3.95	1.04E-02	60S ribosomal protein L36a-like
TOM22	Q9NS69	3.87	1.12E-03	Mitochondrial import receptor subunit TOM22 homolog
RD23A	P54725	3.86	9.12E-04	UV excision repair protein RAD23 homolog A
LAT1	Q01650	3.80	2.33E-03	Large neutral amino acids transporter small subunit 1
EDIL3	O43854	3.79	5.32E-05	EGF-like repeat and discoidin I-like domain-containing protein 3
VTNC	P04004	3.72	3.86E-04	Vitronectin
CYR61	O00622	3.53	2.32E-06	CCN family member 1
ABRAL	Q9P1F3	3.52	9.45E-03	Costars family protein ABRAL
NPM	P06748	3.49	1.72E-05	Nucleophosmin
PCKGM	Q16822	3.45	2.65E-04	Phosphoenolpyruvate carboxykinase
MYL6B	P14649	3.45	3.89E-02	Myosin light chain 6B
WDR43	Q15061	3.43	2.62E-02	WD repeat-containing protein 43
THIC	Q9BWD1	3.38	3.61E-04	Acetyl-CoA acetyltransferase, cytosolic
SMAP2	Q8WU79	3.37	4.75E-03	Stromal membrane-associated protein 2

Entry name	UniProt accession	Fold change	p-value	Protein name
TMA7	Q9Y2S6	3.34	6.93E-04	Translation machinery-associated protein 7
RAB1A	P62820	3.28	4.85E-04	Ras-related protein Rab-1A
HCFC1	P51610	3.27	3.69E-02	Host cell factor 1
AIMP2	Q13155	3.24	3.14E-02	Aminoacyl tRNA synthase complex-interacting multifunctional protein 2

Entry name	UniProt accession	Fold change	p-value	Protein name
THTR	Q16762	0.32	3.04E-07	Thiosulfate sulfurtransferase
PCAT1	Q8NF37	0.32	5.04E-05	Lysophosphatidylcholine acyltransferase 1
GBB2	P62879	0.32	4.61E-04	Guanine nucleotide-binding protein G subunit beta-2
S4A7	Q9Y6M7	0.31	4.24E-02	Sodium bicarbonate cotransporter 3
5NTC	P49902	0.31	9.93E-03	Cytosolic purine 5'-nucleotidase
PPIF	P30405	0.30	3.75E-04	Peptidyl-prolyl cis-trans isomerase F, mitochondrial
HTSF1	O43719	0.30	2.66E-02	HIV Tat-specific factor 1
BGH3	Q15582	0.29	1.19E-02	Transforming growth factor-beta-induced protein ig-h3
PP6R3	Q5H9R7	0.29	3.69E-03	Serine/threonine-protein phosphatase6 regulatory subunit3
PTPRF	P10586	0.28	2.94E-03	Receptor-type tyrosine-protein phosphatase F
CATZ	Q9UBR2	0.28	8.65E-05	Cathepsin Z
ASAH1	Q13510	0.28	9.23E-05	Acid ceramidase
GPC1	P35052	0.28	4.08E-05	Glycan-1
GNA13	Q14344	0.27	1.27E-02	Guanine nucleotide-binding protein subunit alpha-13
HINT2	Q9BX68	0.26	4.49E-05	Histidine triad nucleotide-binding protein 2, mitochondrial
HYEP	P07099	0.25	3.25E-05	Epoxide hydrolase 1
BCAM	P50895	0.23	2.68E-05	Basal cell adhesion molecule
PON2	Q15165	0.22	2.58E-05	Serum paraoxonase/arylesterase 2
IL18	Q14116	0.22	2.41E-03	Interleukin-18
PAPS2	O95340	0.22	8.40E-04	3'-phosphoadenosine 5'-phosphosulfate synthase 2
HCDH	Q16836	0.21	1.36E-04	Hydroxyacyl-coenzyme A dehydrogenase, mitochondrial
TBB4A	P04350	0.21	7.04E-05	Tubulin beta-4A chain
ACOC	P21399	0.21	4.89E-07	Cytoplasmic aconitate hydratase
KS6A4	Q75676	0.21	6.18E-07	Ribosomal protein S6 kinase alpha-4
HTRA1	Q92743	0.20	3.25E-04	Serine protease HTRA1
PO210	Q8TEM1	0.20	2.22E-04	Nuclear pore membrane glycoprotein 210
CXAR	P78310	0.19	2.67E-06	Coxsackievirus and adenovirus receptor
TMM33	P57088	0.19	3.27E-03	Transmembrane protein 33
PPGB	P10619	0.18	2.63E-04	Lysosomal protective protein
CATD	P07339	0.17	1.34E-06	Cathepsin D
GOLP3	Q9H4A6	0.17	4.68E-03	Golgi phosphoprotein 3
3HIDH	P31937	0.17	1.69E-06	3-hydroxyisobutyrate dehydrogenase, mitochondrial
EPCR	Q9UNN8	0.17	2.70E-03	Endothelial protein C receptor
LACB2	Q53H82	0.14	1.55E-06	Endoribonuclease LACTB2
AK1C3	P42330	0.13	8.04E-07	Aldo-keto reductase family 1 member C3
HSPB1	P04792	0.13	5.06E-07	Heat shock protein beta-1
AL4A1	P30038	0.11	2.98E-05	Delta-1-pyrroline-5-carboxylate dehydrogenase
AK1C2	P52895	0.04	6.28E-07	Aldo-keto reductase family 1 member C2
NCLN	Q969V3	0.04	2.14E-08	Nicalin

Table 2.10 – Final candidate target selection process. Candidate proteins were screened based on the selection criteria determined in the study, identified in 3 steps. Information about subcellular location and relative expression in tissues was obtained from UniProt and the Human Protein Atlas, respectively.

Protein	Localisation On Membrane (Uniprot AND GO)		Expression in normal tissues		Expression in PCa	
THTR	Mitochondrion	✗	--	✗	--	✗
PCAT1	Plasma Membrane, ER, Cytosol, Golgi Apparatus, Lysosome	✓	Medium/high	✗	--	✗
GBB2	Cytosol, Plasma Membrane, Lysosome	✓	Medium/high	✗	--	✗
S4A7	Plasma Membrane	✓	Low	✓	Not detected	✗
5NTC	Cytosol	✗	--	✗	--	✗
PPIF	Mitochondrion	✗	--	✗	--	✗
HTSF1	Nucleus	✗	--	✗	--	✗
BGH3	Secreted	✗	--	✗	--	✗
PP6R3	Nucleus, Cytosol, Plasma Membrane	✓	High	✗	--	✗
PTPRF	Plasma Membrane	✓	Medium/high	✗	--	✗
CATZ	Lysosome, ER, Plasma Membrane	✓	Medium/high	✗	--	✗
ASAH1	Lysosome, Nucleus	✗	--	✗	--	✗
GPC1	Plasma Membrane, Endosome, Cytosol, Golgi Apparatus, Lysosome, Nucleus	✓	Low/medium	✗	--	✗
GNA13	Nucleus, Cytosol, Plasma Membrane	✓	Medium/high	✗	--	✗
HINT2	Nucleus, Mitochondrion	✗	--	✗	--	✗
HYEP	ER	✗	--	✗	--	✗
BCAM	Plasma Membrane	✓	Medium	✗	--	✗
PON2	Plasma Membrane	✓	Medium/high	✗	--	✗
IL18	Secreted	✗	--	✗	--	✗
PAPS2	Cytosol	✗	--	✗	--	✗
HCDH	Nucleus, Mitochondrion	✗	--	✗	--	✗
TBB4A	Cytosol	✗	--	✗	--	✗

Protein	Localisation On Membrane (Uniprot AND GO)		Expression in normal tissues		Expression in PCa	
ACOC	Cytosol, ER, Mitochondrion, Golgi Apparatus	✗	--	✗	--	✗
KS6A4	Nucleus, Cytosol	✗	--	✗	--	✗
HTRA1	Cytosol, <i>Plasma Membrane</i>	✓	Low/medium	✗	--	✗
PO210	Nucleus, ER	✗	--	✗	--	✗
CXAR	Nucleus, <i>Plasma Membrane</i>	✓	Medium	✗	--	✗
TMM33	Nucleus, ER	✗	--	✗	--	✗
PPGB	Lysosome, ER	✗	--	✗	--	✗
CATD	Lysosome, Endosome	✗	--	✗	--	✗
GOLP3	Mitochondrion, Golgi Apparatus	✗	--	✗	--	✗
3HIDH	Mitochondrion	✗	--	✗	--	✗
EPCR	Plasma Membrane	✓	Low	✓	Detected	✓
LACB2	Mitochondrion	✗	--	✗	--	✗
AK1C3	Cytosol	✗	--	✗	--	✗
HSPB1	Nucleus, Cytosol	✗	--	✗	--	✗
AL4A1	Mitochondrion	✗	--	✗	--	✗
AK1C2	Cytosol	✗	--	✗	--	✗
NCLN	ER	✗	--	✗	--	✗

Eventually, from the list of potential candidates, EPCR was the only protein meeting the criteria for selection, such as cell surface expression limited to invasive PCa cells and low or absent expression in normal tissues, thus it was chosen for further validation.

EPCR, also known as CD201, is a type 1 transmembrane N-glycosylated protein encoded by the *PROCR* gene, which consists of 4 exons and is located on chromosome 20q-11.2 (Figure 2.5) (Oganesyan, Oganesyan et al. 2002; Fukudome, Esmon 1994). EPCR protein is mainly expressed on the endothelium of the large blood vessels – with exception of the liver sinusoidal endothelium and the spleen – and with lower levels on the microvascular endothelium (Mohan Rao, Esmon et al. 2014).

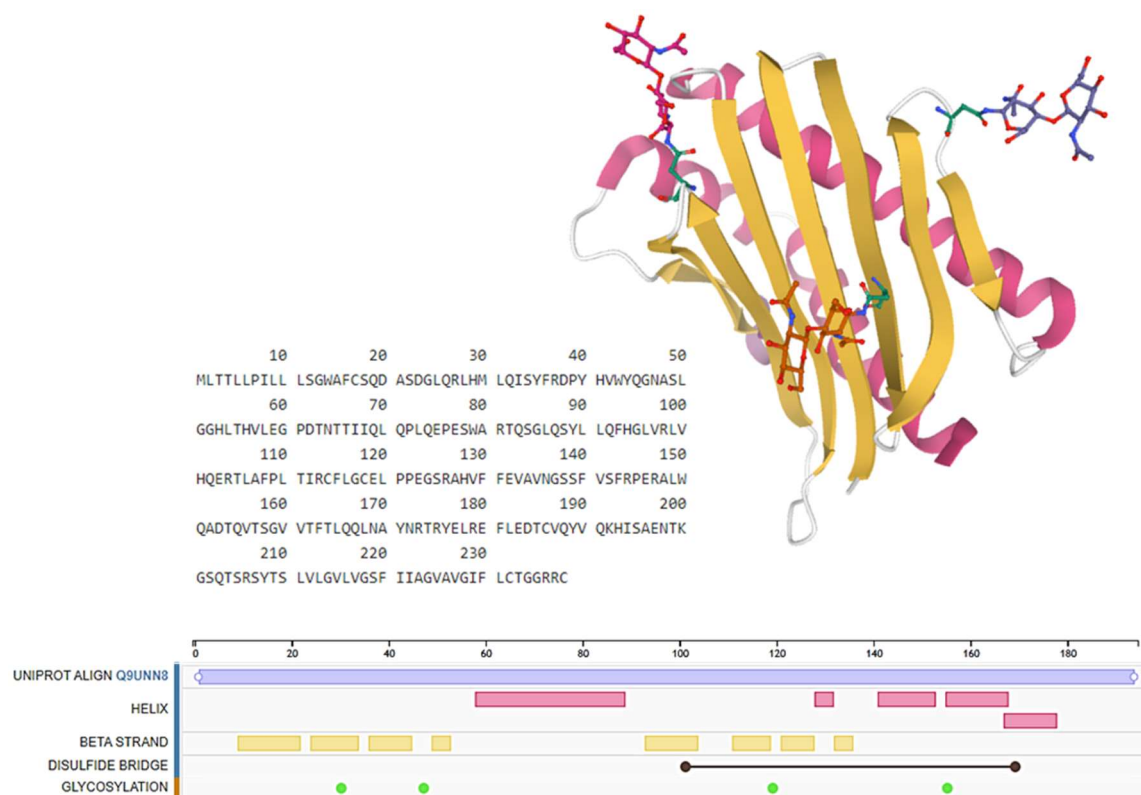


Figure 2.5 – Representation of the human EPCR protein. 3D-view of the Crystal Structure of the Endothelial Protein C Receptor molecule. The protein presents nine β -strands (yellow) and four α -helix structures (pink). The four glycosylations are also represented in the figure. (Adapted from <https://www.uniprot.org/>)

According to the Human Protein Atlas database, EPCR protein expression in different tissues with low levels and no expression is detected in normal prostate tissue (Figure 2.6-A). However, EPCR protein is expressed at medium levels in PCa specimens (Figure 2.6-B).

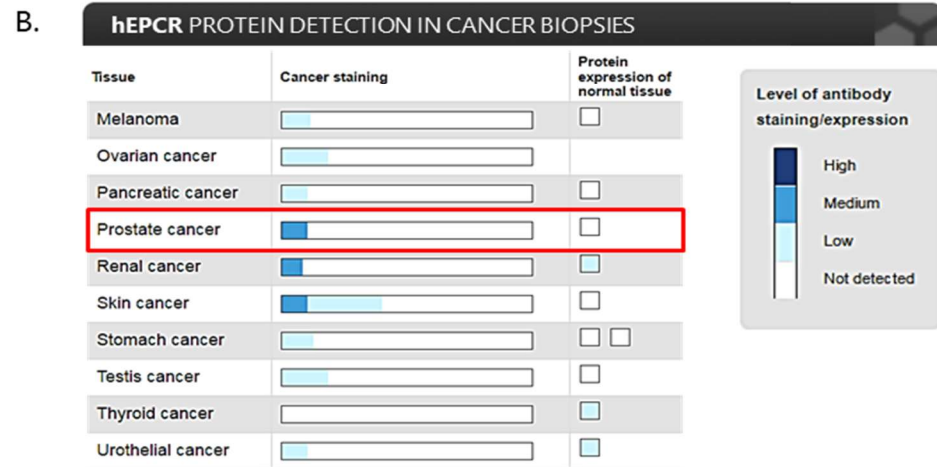
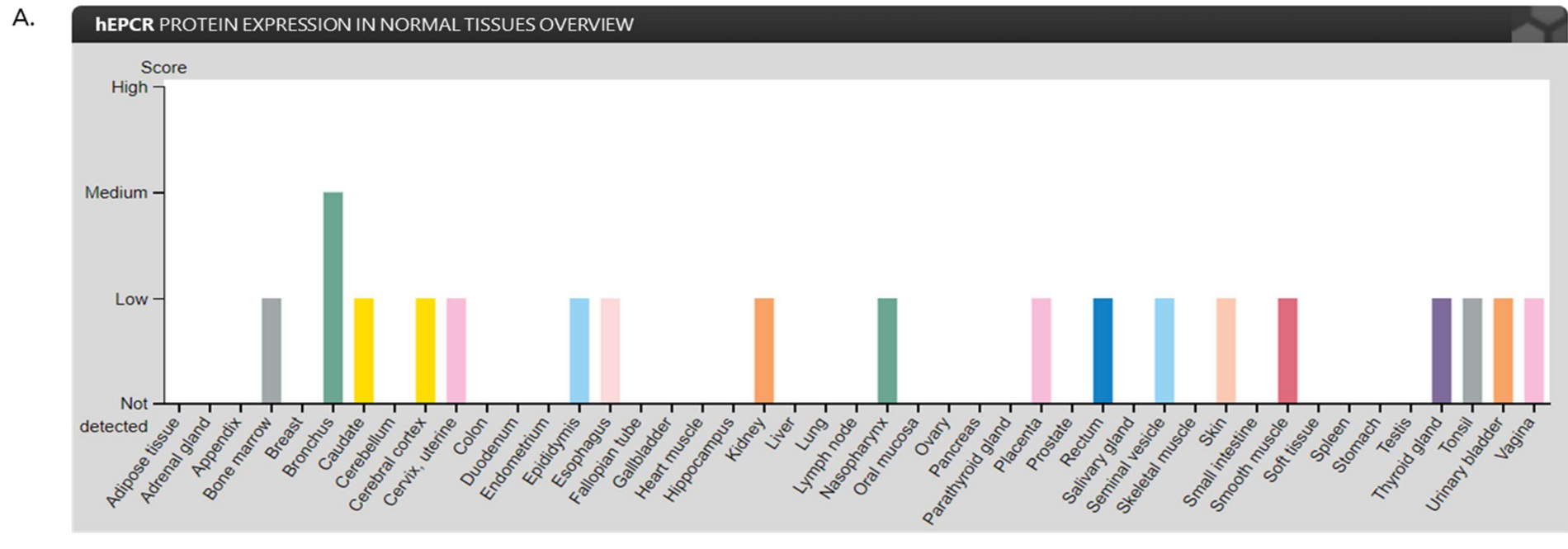


Figure 2.6 – EPCR protein expression in normal tissues and cancer biopsies.

(A) - The panel shows EPCR protein expression in human normal tissues derived from antibody-based protein profiling using immunohistochemistry. Protein expression is low or not detected in all the tissues considered, except for bronchus in which EPCR expression is scored as medium. (B) - Immunohistochemistry analysis using a tissue microarray-based analysis show that EPCR protein expression in prostate cancer is detected with medium levels. Adapted from the *Human Protein Atlas* (<https://www.proteinatlas.org/>).

2.3.2 Differential expression of EPCR in benign and prostate cancer cells

In order to assess whether EPCR expression was limited to PCa or is also expressed by benign prostate epithelial cells, relative levels of both transcript and protein expression in non-malignant (PNT2) and cancer (DU145, PC3, and LNCaP) prostate cell lines were analysed. PNT2 cells were selected as control cell line for the first part of this study because they derive from normal human prostate. However, such cell line was initially established by immortalisation transfecting the primary cell line with SV40, which sequestrates pRB and p53 (tumour suppressor proteins) thus extending the otherwise limited cellular lifespan of the target cell line (Liu et al. 2009). Nevertheless, PNT2 cells are widely used as a model of well differentiated human prostate epithelium (Berthon et al. 1995).

Real-time qPCR analysis was used to determine the relative endogenous expression levels of *PROCR* mRNA in total RNA samples extracted from lysates of the cell lines under study. The values for the relative levels of mRNA were obtained as the ratio of *PROCR/GUSB* Ct values and then normalised assigning value 1 to the levels of mRNA expression in PNT2 cells. PNT2 cells were used as a reference since they represent a benign immortalised adult prostatic epithelial cell line, thus the level of *PROCR* mRNA in this cell line was set as 1. In comparison to PNT2 benign prostate cells, levels of *PROCR* mRNA were increased in DU145 and PC3 cells, namely 3 and 2 folds, and negligible in LNCaP (Figure 2.7).

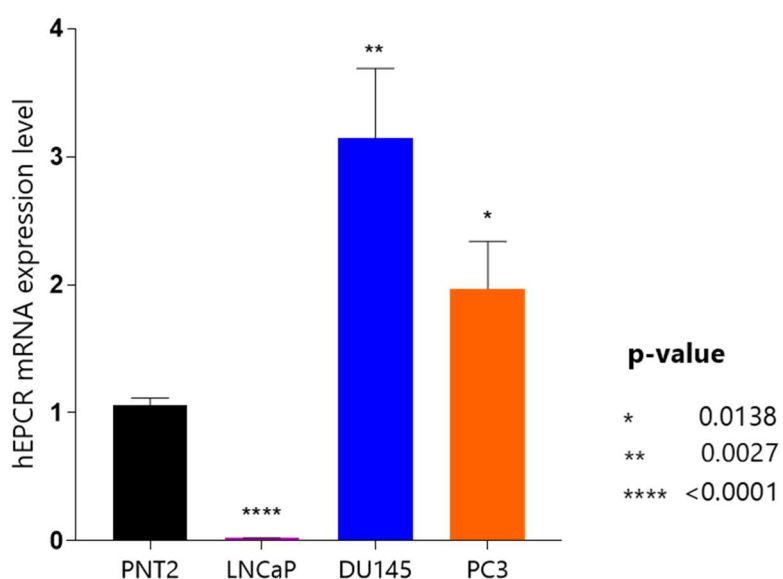


Figure 2.7 – Relative *PROCR* mRNA expression levels in benign and PCa cell lines. Bar graph showing results of real time qPCR analysis of *PROCR* mRNA expression levels in benign (PNT2) and PCa cell lines (LNCaP – DU145 – PC3). Data reported as mean Ct values \pm SD and representative of three independent experiments giving similar results (n=3). Values were normalised on *GUSB* mRNA expression in all the cell lines and relative *PROCR* mRNA expression in cell lines was obtained setting level of expression in PNT2 as 1. Statistical significance was calculated between control and each test group using unpaired t-test and indicated as asterisk.

In order to assess whether the expression pattern of EPCR is maintained also at protein level, the relative levels of EPCR protein in whole cell lysates from the same benign and cancer prostate cell lines was assessed by Western blot. Each sample was used at a quantity of 30 μ g per well. As a positive control a lysate from NIH/3T3 EPCR+ was used (data not shown), in which *PROCR* gene was knocked-in (kindly gifted by the team of Prof. H.M. Jäck from the University of Erlangen). The levels of EPCR protein detected were normalised on the values of the loading control gene β -actin. The analysis confirms that the levels of expression of EPCR protein in DU145 and PC3 cells are significantly higher compared to the levels in benign prostate cells (Figure 2.8).

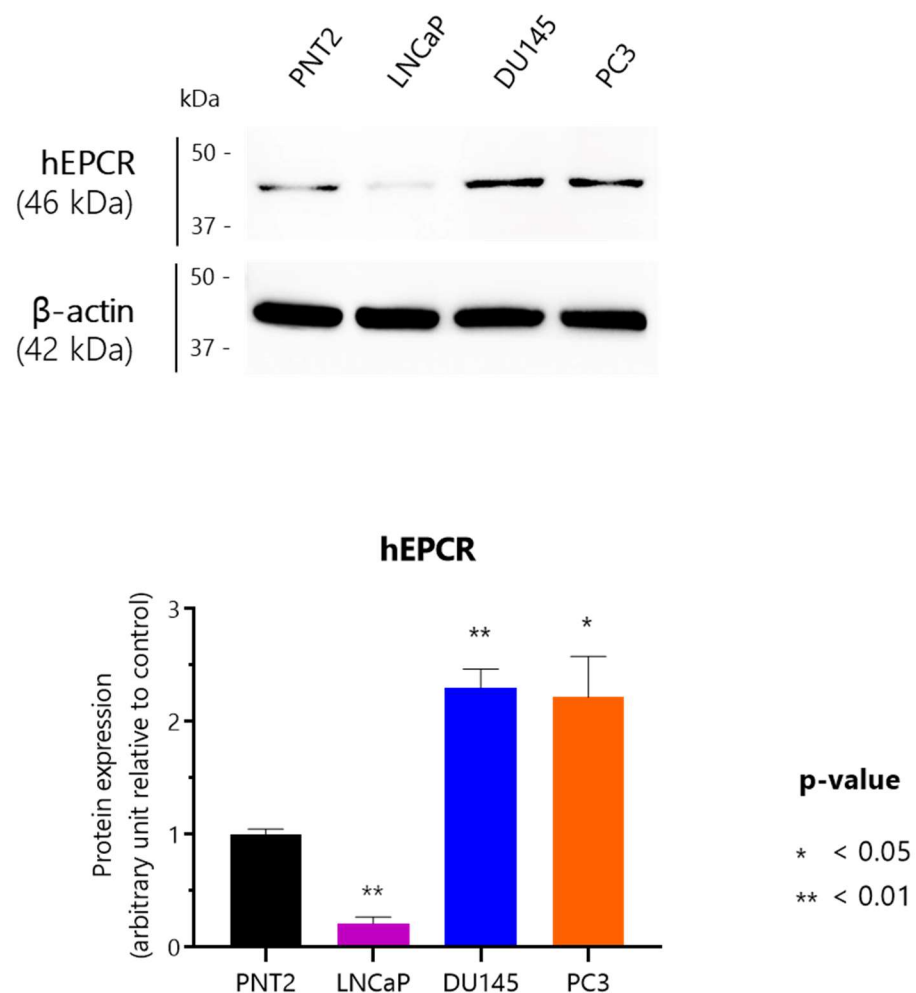


Figure 2.8 – Relative EPCR protein expression levels in benign and PCa cell lines. Immunoblot (top) showing EPCR protein expression in benign (PNT2) and PCa cell lines (LNCaP – DU145 – PC3). The relative band is at the expected value of ~46 kDa. Data reported as mean \pm SD and are representative of three independent experiments giving similar results (n=3). Values were normalised on β -actin expression in all the cell lines and plotted in a bar graph (bottom). Statistical significance was calculated between control and each test group using unpaired t-test and indicated as asterisks.

EPCR protein expression in LNCaP cells is significantly increased compared to the level of the relative transcript.

For EPCR to be conclusively selected as a PCa-associated marker to use as target for antibody-based therapies, we needed to demonstrate its localisation on the cell surface. For this purpose, EPCR expression by the cell lines was determined by flow cytometry using a commercially available monoclonal antibody against the human EPCR. Cells were not fixed or permeabilised during the staining process in order to maintain the cytoplasmic membrane and only the expression by viable cells was examined. In this way, the results reflect the abundance of the protein only on the cell surface.

The results showed in Figure 2.9 refer to the expression of EPCR on benign prostate epithelial cells (PNT2) and PCa cells. Intensity of the fluorescence from control (incubated only with the secondary antibody) and stained populations were overlaid together, and results collected as MFI. PNT2 cells fluorescence emission did not show any significant shift, with a MFI of 0.65. In contrast, all the PCa cells were shown to be positive for EPCR, albeit to differing degrees and with LNCaP cells showing a non significant MFI value difference when compared to PNT2 value. These results further confirm previous results obtained with transcript analysis and Western blot.

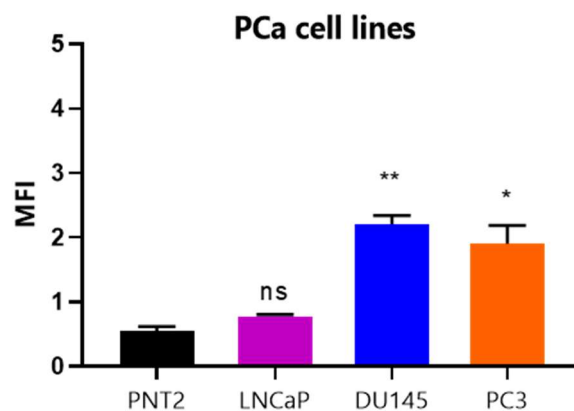
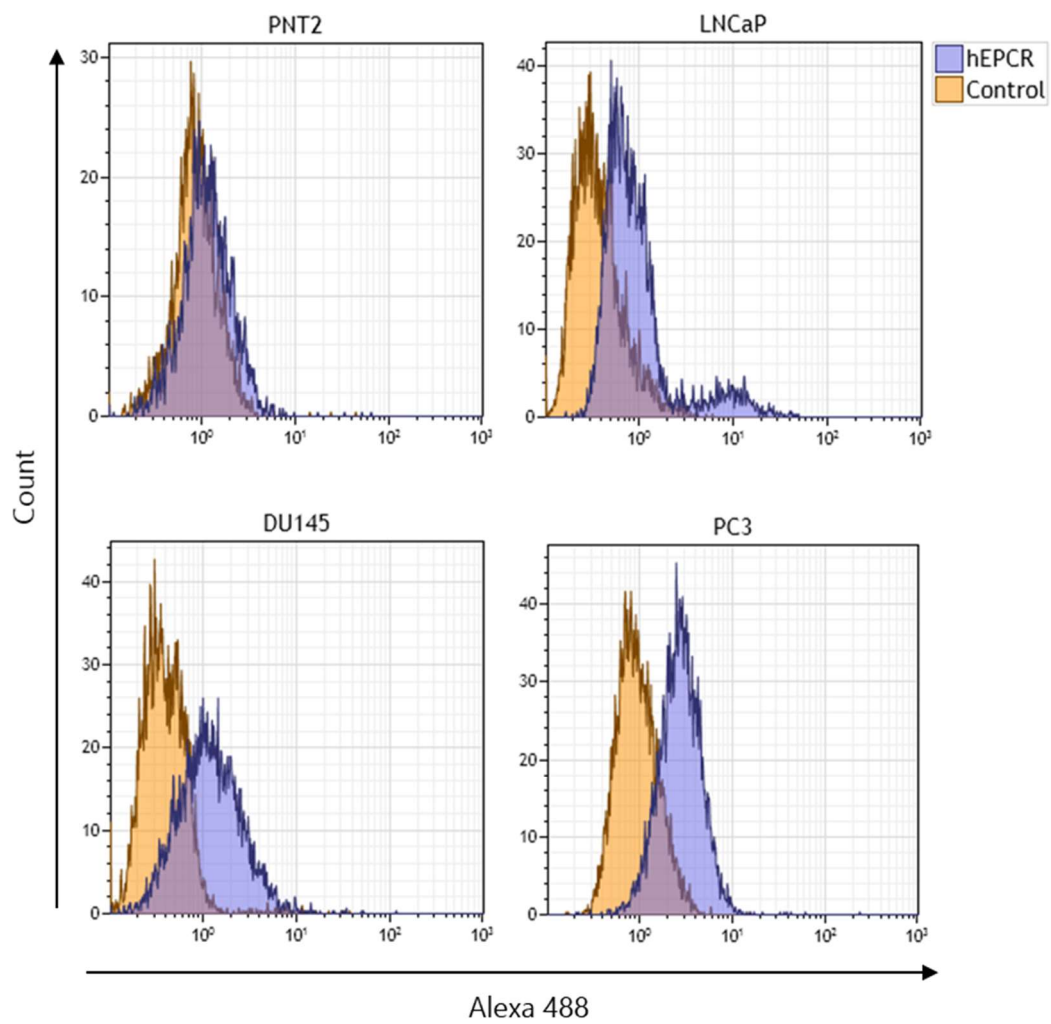


Figure 2.9 – Cell surface expression of EPCR. Flow cytometry analysis of EPCR expression on cell surface of benign (PNT2) and cancer (LNCaP – DU145 – PC3) prostate cell lines. **Orange** shading represents tracks obtained with specific EPCR primary antibody; **blue** shading shows control cells treated with only secondary antibody. Values represent percentage of positive cells gated against the control population in which no primary antibody was used. Data are reported as mean \pm SD and are representative of three independent experiments giving similar results ($n=3$) and plotted in a bar graph (bottom). Statistical significance was calculated between control and each test group using unpaired t-test and indicated as asterisks (ns= non-significant p-value > 0.05, * = p-value < 0.05, ** = p-value < 0.01).

2.3.3 Evaluation of EPCR as a novel PCa biomarker

As shown so far in this chapter, EPCR expression is up regulated in prostatic malignant cell lines. Such evidence led to the question of whether EPCR could be suggested as a biomarker specific for invasive PCa with a clinical application for prognosis and diagnosis, correlating the protein expression with pathologic parameters and clinical outcome in patients. In order to address this question, immunohistochemistry analysis was conducted on tissue microarrays (TMAs) with specimens from a cohort of almost 200 PCa patients.

The mouse anti-EPCR primary antibody from Abcam (Ab56689) was first optimised at different dilutions and then used to probe the TMAs at 2 µg/mL. The slides were then scanned at high resolution and the scans analysed by an expert immunopathologist for tumours scoring and grading (Figure 2.10). Unfortunately, the analysis reported an unspecific staining as the protein was observed in different cellular compartments in contrast to its expected localisation on the cytoplasmic membrane. Indeed, the micrographs show sparse staining in cytoplasm and little or no staining on the plasma membrane.

Such dual localisation of the protein, combined with our expectation of focussing the investigation on the cell surface fraction of EPCR, made the analysis not straightforward to perform. For this reason, it was not possible to score the specimens and obtain an effective correlation between protein expression and tumour grade.

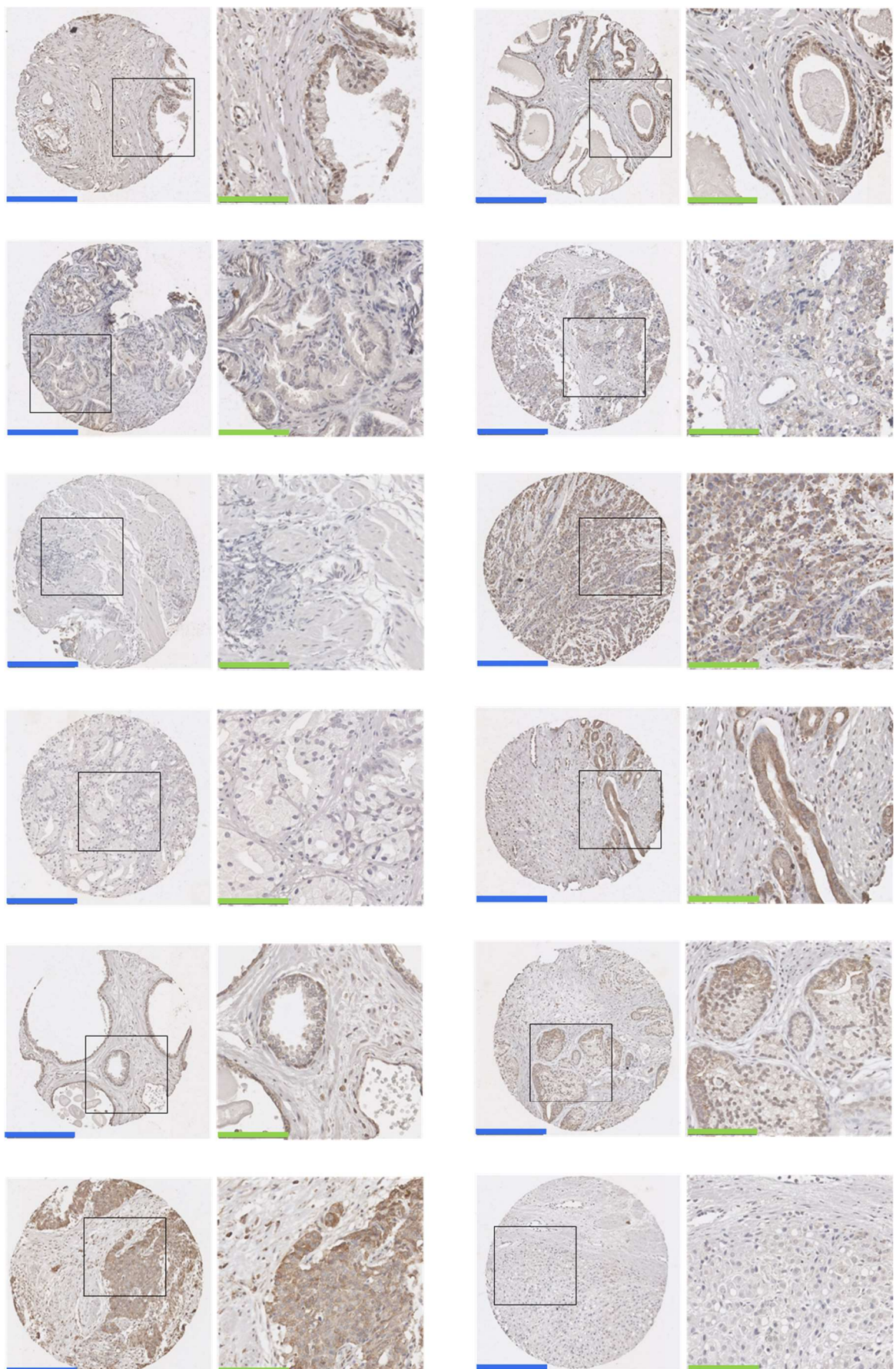


Figure 2.10 – Immunohistochemistry analysis of EPCR expression in PCa biopsies. To the purpose of this analysis, TMAs with specimens from PCa patients (kindly provided by Dr D Powe, Queen's Medical Centre, Nottingham University Hospitals NHS Trust). Blue bars indicate 250 µm and green bars indicate 100 µm. EPCR staining appears as a brown colour, nuclei were counterstained in blue.

2.4 Discussion

Data presented in this chapter support the eligibility of EPCR as a potential cell surface target for antibody-based therapy since the up regulation of EPCR protein expression in PCa cells compared to benign prostate epithelial cells correlates with increased EMT phenotype. In a study on the expression of EPCR in PCa cells, Menschikowski and colleagues (Menschikowski, Hagelgans et al. 2011) reported a correlation between the expression of EPCR in PCa cell lines and their invasiveness. In agreement with these findings, data collected in the present chapter confirm that EPCR is up regulated in DU145 and PC3 cells compared to benign prostate epithelial cells, whereas only a subpopulation of LNCaP cells expresses EPCR. Studies on LNCaP cells, linked cellular heterogeneity to androgen stimulation. Indeed, such studies highlighted the presence of cellular subpopulations in LNCaP showing differential growth rates and stem-like features (Horning et al. 2018). Such evidence could explain the presence of a subpopulation expressing EPCR at high levels in our *in vitro* model. Similar up regulation of EPCR was found in colon and renal cell carcinomas as well as in melanomas, correlating with poor response to chemotherapy (Menschikowski et al. 2011). Low levels of expression of EPCR protein showed in normal tissues further supports the choice of EPCR as a target for immunotherapy in PCa. Moreover, a previous study on use of blocking mouse mAbs anti-EPCR *in vivo* in primates to investigate the role of EPCR in protein C activation showed no significant side-effects (Taylor, Peer et al. 2001). Such study supports the concept of EPCR as a potential target for therapeutic mAbs development, acting as a valid preclinical study model for use of targeting mAbs *in vivo*, providing evidence about the potential safety of targeting EPCR.

EPCR plays a crucial role in the activation of protein C (PC) anticoagulant pathway by presenting the protein C to the activating thrombin-TM complex (Stearns-Kurosawa, Kurosawa et al. 1996). Although the main localisation of EPCR is on the cell membrane, a small fraction of the protein is also localised intracellularly in recycling vesicles, where internalisation of the EPCR-PC/aPC (activated protein C) regulates protein C activation. Notwithstanding the fact that it is localised on the plasma membrane, it is known that EPCR can also be found perinuclearly in dense cytoplasmic aggregates (Nayak, Sen et al. 2009). A soluble form of EPCR can also be released upon metalloproteolysis (Xu, Qu et al. 2000). Soluble EPCR is 4 kDa smaller than the intact protein and its concentration in plasma is about 100 ng/mL. Recent studies demonstrated that EPCR activity is regulated also by

ligands other than protein C (Figure 2.11) (Pendurthi, Rao 2018). Due to its short cytoplasmic tail, EPCR signalling is indirect and modulated via its localisation into lipid rafts and caveolae in which EPCR can get in close proximity to signal mediators (Nayak et al. 2009). The three-dimensional protein shows a structural homology with the major histocompatibility class 1/CD1 protein family (Esmon 2004), which is also responsible for its role in the inflammatory process, one of the relevant players in tumour progression. EPCR has recently been identified as a marker of human hematopoietic stem cells (HSCs) - (Subramaniam, Talkhoncheh et al. 2019) and of multipotent mouse mammary stem cells (MaSCs) - (Wang, Cai et al. 2015). EPCR expression in endothelial cells promotes vascular barrier protection and stability strengthening the endothelial walls so to prevent extravasation during cancer invasion, via binding to Factor VIIa (Sundaram, Keshava et al. 2014). Nevertheless, EPCR role in cancer is considerably complex. Indeed, EPCR expression patterns have been found altered in several cancers correlating with clinical outcome, with its over expression of EPCR in breast, ovarian, and lung cancers correlating with increased tumour growth and metastasis formation (Pendurthi, Rao 2018).

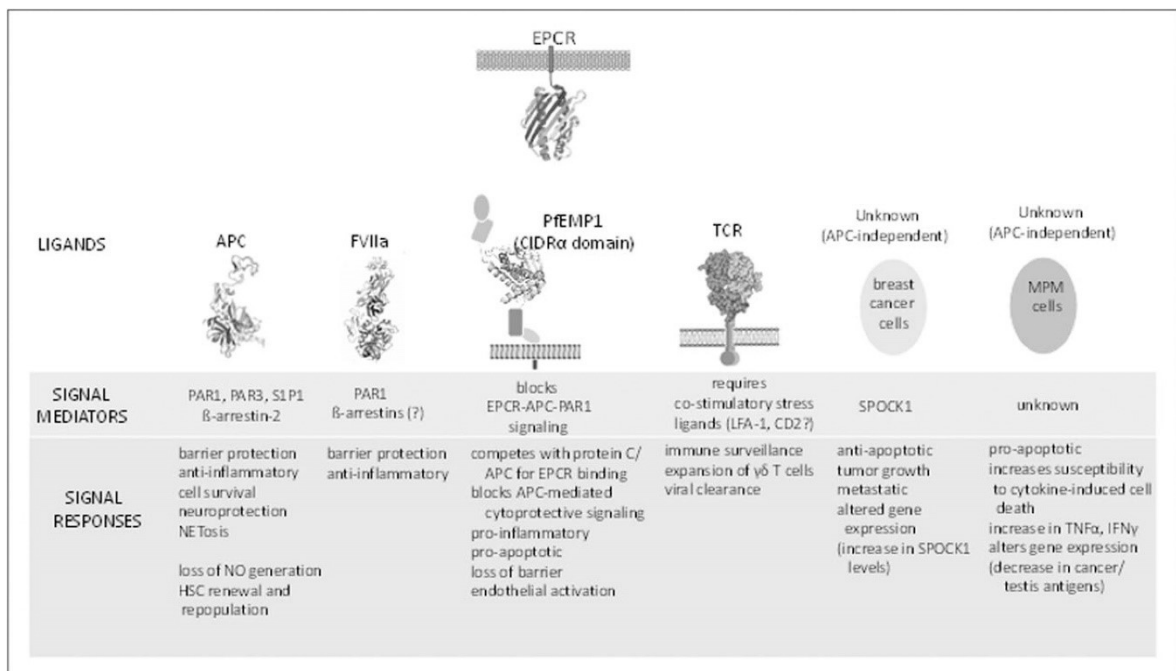


Figure 2.11 – Ligands of EPCR and related signalling responses. The picture shows the known ligands of EPCR and the relative signal responses. (Adapted from Pendurthi, Rao 2018).

Despite its demonstrated role during progression of several cancers, there is also evidence about EPCR promoting apoptosis in malignant pleural mesothelioma (MPM) cells, thus exerting a negative regulation on its tumorigenicity (Keshava, Rao et al. 2015).

The use of EPCR as a biomarker for cancers has already been confirmed in lung cancer, investigating its expression in TMAs of lung carcinoma biopsies, and correlating it to histopathological and clinical parameters (Heng, Mu et al. 2013). Unfortunately, our attempt to translate the use of EPCR in clinical practice validating it as a biomarker for PCa was not successful for technical reasons. Indeed, due to the unspecific staining obtained in the TMAs following IHC targeting EPCR, it was not possible to analyse EPCR expression in PCa specimens to investigate whether any relationship between EPCR expression and clinical parameters in PCa patients exist. Consequently, this keeps the door open to future attempt to address this point by changing the protocol used for the staining and/or the primary antibody used to probe the tissues.

3. Investigating the Role of EPCR in Prostate Cancer Progression

3.1 Introduction

Several studies demonstrate the role played by EPCR in disease progression in cancers of different origins. Abnormal expression of EPCR correlates with clinical outcome and worse prognosis in tumours including lung (Antón, Molina et al. 2012), glioblastoma and leukaemia (Tsuneyoshi, Fukudome et al. 2001), breast (Beaulieu, Church 2007), ovarian (Ducros, Mirshahi et al. 2012), and colon (Scheffer, Flens et al. 2002).

Research to investigate the contribution of EPCR to the tumour proliferation and invasion has been conducted in different cancer models, like breast (Perurena, Zandueta et al. 2017) and gastric cancer (Wang, Tang et al. 2018). Interestingly, EPCR silencing in breast cancer model led to decreased tumorigenicity and metastatic potential, suggesting that EPCR could be involved in the activation of the EMT program in malignant cells (Perurena et al. 2017).

The correlation between EPCR over expression and malignant phenotype in *in vitro* prostate models has already been investigated in literature (Menschikowski et al. 2011) and confirmed in our model as well, as shown in the previous chapter where the results obtained indicated that EPCR endogenous expression is increased in prostate cancer (PCa) cells compared to benign epithelial prostate cells.

To elucidate the role of EPCR in tumour proliferation and invasion, stable knockdown of EPCR was carried out in PCa cells and functional studies conducted in order to investigate whether a link between EPCR expression in PCa cells and EMT exists. DU145 and PC3 cell lines were selected over LNCaP cells based on their higher EPCR endogenous expression levels and intrinsic metastatic potential. Cells were transduced with a 2nd-generation lentiviral system (Song, Yang 2010) expressing short hairpin RNAs (shRNAs) targeting EPCR. The lentiviral particles determine stable integration of the shRNA sequence into the target genome allowing for more extensive and reliable laboratory tests (Manjunath, Wu et al. 2009).

3.2 Materials and Methods

3.2.1 Materials

3.2.1.1 Reagents

CELL CULTURE MEDIA	PROVIDER
EMEM	SLS (Lonza)
F-12K	Gibco
DMEM	SLS (Lonza)
Opti-MEM	Gibco

CULTURE MEDIA SUPPLEMENTS	PROVIDER
Foetal calf serum (FCS)	Fisher (GE Healthcare)
L-Glutamine	SLS (Lonza)
D-glucose	Sigma
HEPES	SLS (Lonza)
Sodium Pyruvate	SLS (Lonza)

OTHER CELL CULTURE REAGENTS	PROVIDER
Dimethyl sulfoxide (DMSO)	Insight Biotechnology
Dulbecco's phosphate buffered saline (DPBS)	SLS (Lonza)
Trypan Blue solution (v/v 0.4%)	Sigma
Trypsin/Versene	SLS (Lonza)
Puromycin	Sigma

CHEMICALS & BIOCHEMICALS	PROVIDER
Agar	Bioline
Ammonium Persulphate (APS)	Geneflow
Ampicillin	Sigma
Bovine serum albumin (BSA)	Merck
Bromophenol blue	Arcos Organics
Clarity Western ECL Substrate	Bio Rad
Double distilled water (ddH ₂ O)	Barnstead, Nanopure Diamond
Dithiothreitol (DTT)	Sigma
Ethanol	Fisher Scientific
Ethyl alcohol absolute	VWR chemicals
Glycerol	Sigma
Glycine	Sigma
Haematoxylin	Sigma
Hexadimethrine bromide solution	Sigma
Hydrochloric acid (HCl)	Fisher Scientific
Isoton II	Beckman Coulter
Lipofectamine 3000	Thermo Fisher Scientific
Nuclease-free water	Ambion
Paraformaldehyde	Thermo Fisher Scientific

IMMUNOCHEMICAL REAGENTS	PROVIDER
Alexa Fluor™ 488 conjugated donkey anti-rat IgG	Invitrogen
Alexa Fluor™ 488 conjugated goat anti-mouse IgG	Invitrogen
Anti-Mouse IgG HRP-linked Ab	Cell Signalling Technology
Anti-Rabbit IgG HRP-linked Ab	Cell Signalling Technology
Mouse anti-human β-actin (clone 8H10D10)	Sigma
Rabbit anti-human β-catenin (clone 8480P)	Cell Signalling
Rabbit anti-human E-cadherin (clone 3195S)	Cell Signalling
Rabbit anti-human N-cadherin (clone 13116P)	Cell Signalling
Rabbit anti-human Vimentin (clone 5741S)	Cell Signalling
Rabbit anti-human ZO-1 (clone 8193S)	Cell Signalling
Mouse anti-human EPCR (clone ab56689)	Abcam
Mouse anti-human EPCR (clone M2)	Sigma
Precision Plus Protein WesternC Standards	Bio Rad
Precision Protein™ StrepTactin-HRP Conjugate	Bio Rad
Rat anti-human EPCR	Novus Biologicals

REAGENT KITS	PROVIDER
FcR Blocking Reagent	Miltenyi Biotec
LIVE/DEAD™ Fixable Violet Dead Cell Reagent	Thermo Fisher Scientific
QIAGEN QIAfilter Plasmid Midi	QIAGEN

OTHERS	PROVIDER
DU145 Human Prostate Cancer Cell Line	ATCC
HEK-293T Human Embryonic Kidney	ATCC
PC3 Human Prostate Cancer Cell Line	ATCC
MISSION® pLKO.1 puro	Sigma
MISSION® hEPCR shRNAs	Sigma
psPAX2	Addgene
pMD2.G	Addgene
PL-SIN-EF1α-EGFP	Addgene

3.2.1.2 Equipment

LABORATORY PLASTICS, GLASSWARE AND SHARPS	PROVIDER
Cell culture flasks (T25, T75, T175)	Sarstedt, UK
Conical flasks (50 mL, 100 mL)	Pyrex
Eppendorf tubes (0.5 mL, 1.5 mL, 2 mL)	Sarstedt, UK
12x75 mm polystyrene flow cytometry tubes	Tyco healthcare group
Falcon tubes (50 mL, 15 mL)	Sarstedt, UK
Filter tips (0.5-10 µL, 2-20 µL, 20-200 µL, 200-1000 µL)	Greiner bio-one/ Sarstedt
Flat-bottom culture dishes (6, 24, 96-well)	Sarstedt, UK
Micropipette tips (0.5-10 µL, 20-200 µL, 200-1000 µL)	Sarstedt, UK
Pipettes (5 mL, 10 mL, 25 mL)	Sarstedt, UK
PVDF blotting membrane (pore size 0.45 µm)	GE Healthcare, Life science
Screw-top tubes (15 mL, 50 mL)	Sarstedt
Serological pipettes	Sarstedt
Syringes (10 mL, 20 mL)	Becton Dickenson

Universal tubes (20 mL)	Greiner
Western blot filter paper	Schleicher-Schuell
0.45 µm syringe filter	Sartorius
0.22 µm syringe filter	Sartorius
40 µm nylon strainer	Greiner
70 µm nylon strainer	Greiner

LABORATORY EQUIPMENT	PROVIDER
4°C refrigerators	Lec
-20°C freezers	Lec
-80°C freezers	Revco/ Sanyo
96-well plate reader	Tecan
Autoclave	Rodwell
Bacterial cell orbital incubator	Stuart
Bacterial cell culture plate incubator	Genlab
Cell culture incubator	Sanyo
Centrifuges	Sanyo, Eppendorf
CCD camera -Western blot imager	Syngene
Class II safety cabinets	Walker
Countess II Automated Cell Counter	Invitrogen
Flow cytometer	Beckman Coulter
Haemocytometers	SLS
Heatblocks	Lab-Line
Light microscope	Nikon/Olympus
TripleTOF™ 6600 mass spectrometer	Sciex
Microcentrifuge	MSE
NanoDrop™ 8000 Spectrophotometer	Thermo scientific
pH meters	Metler Toledo
Pipettes and multichannel pipettes	Gilson, Star Labs, Eppendorf
Plate rocker	VWR, Stuart
Spectrophotometer for 96-well plate	Tecan ULTRA
Transfer tank	Bio Rad
Ultracentrifuge Optima TLX	Beckman
Ultrapure water dispenser	Barnstead
Vortex	Scientific industries
Water baths	Clifton
ZOOM® system incubator	Incucyte

SOFTWARE	PROVIDER
Aperio ImageScope	Leica Biosystems
Axiovision Microscopy Software 4.7.1. version	ZEISS
GraphPad Prism 8	Graph Pad software
Kaluza™ 3.1 version	Beckman Coulter
Morpheus	Broad Institute
nSolver™ Analysis Software (V.4.0)	NanoString Technologies
Reactome Analysis Tool	Reactome

3.2.1.3 Cell line growth media

DU145 COMPLETE MEDIUM	CONCENTRATIONS
EMEM	-
FCS	10%
L-glutamine	1%

HEK-293T COMPLETE MEDIUM	CONCENTRATIONS
DMEM	-
FCS	10%
L-glutamine	1%

PC3 COMPLETE MEDIUM	CONCENTRATIONS
F-12K	-
FCS	10%

3.2.1.4 Buffers and gels

4X SDS-PAGE LOADING BUFFER	FOR 10 mL
1M Tris-HCl pH 6.8	2.4 mL
Sodium dodecyl sulfate (SDS)	0.8 g
Glycerol	4 mL
DTT	0.5 mL
Bromophenol blue	4 mg
ddH ₂ O	3.1 mL

5X SDS RUNNING BUFFER	FOR 1 L
Glycine	94 g
Tris base	15.1 g
10% SDS	50 mL
ddH ₂ O	Up to 1 L

5X Running buffer was diluted with ddH₂O to 1X working concentration prior use.

5% STACKING GEL	FOR 6 mL
ddH ₂ O	4.1 mL
30% Acrylamide mix	1.0 mL
1.0 M Tris (pH 6.8)	0.75 mL
10% SDS	0.06 mL
10% ammonium persulfate	0.06 mL
TEMED	0.006 mL

10X TRIS-BUFFERED SALINE (10 X TBS)	FOR 1 L
Trizma base	24.2 g
NaCl	80 g
ddH ₂ O	Up to 1 L

pH was adjusted to 7.6 with concentrated HCl.

10% RESOLVING GEL	FOR 20 mL
ddH ₂ O	7.9 mL
30% Acrylamide mix	6.7 mL
1.5 M Tris (pH 8.8)	5 mL
10% SDS	0.2 mL
10% ammonium persulfate	0.2 mL
TEMED	0.008 mL

ERIKA'S BUFFER WITH PROTEASE INHIBITOR	FOR 50 mL
Urea	28.5 g
Dithiothreitol (DTT)	1 g
N-Octyl-Beta-Glucopyranoside	0.5 g
ddH ₂ O	Up to 50 mL
Solution was mixed vigorously and sonicated until dissolved	
Proteinase Inhibitor cocktail	500 µL

LB AGAR PLATE WITH AMPICILLIN	FOR 500 mL
NaCl	5 g
Tryptone	5 g
Yeast Extract	2.5 g
Agar	7.5 g
ddH ₂ O	Up to 500 mL
Autoclaved, cooled down to 50°C	
Ampicillin	50 mg

LB BROTH	FOR 500 mL
NaCl	5 g
Tryptone	5 g
Yeast Extract	2.5 g
ddH ₂ O	Up to 500 mL
Autoclaved, cooled down to 50°C	
Ampicillin	50 mg

TRANSFER BUFFER	FOR 2 L
Glycine	5.8 g
Tris base	11.6 g
10% SDS	0.75 g
Methanol	400 mL
ddH ₂ O	Up to 2 L

TRIS-BUFFERED SALINE WITH TWEEN (TBST)	FOR 1 L
10X TBS	100 mL
ddH ₂ O	900 mL
Tween-20	1 mL

TRIS-EDTA (TE) BUFFER	FOR 500 ML
1 M Tris (pH 8)	5 mL
0.5 M EDTA (pH8)	1 mL
ddH ₂ O	Up to 500 mL

3.2.2 Methods

3.2.2.1 Routine cell culture

DU145 and PC3 cell lines were purchased from American Type Culture Collection (ATCC). All cell lines were cultured in their dedicated media. The DU145 cell line was cultured in Eagle's Minimum Essential Medium (EMEM) with 1% w/v L-Glutamine; PC3 cell line was cultured in Kaighn's Modification of Ham's F-12 Medium (F-12K). As a supplementary agent, 10% v/v foetal calf serum (FCS) was added to all media according to ATCC culture methods. For EPCR transfection, HEK-293T (human embryonic kidney) cell line (purchased from American Type Culture Collection (ATCC) was used. HEK-293T cells were cultured in Dulbecco's Modified Eagle Medium (DMEM) medium supplemented with 1% L-Glutamine and 10% foetal calf serum (FCS). No antibiotics were used during the routine cell culture. Cells were incubated at 37°C in a humidified atmosphere with 5% CO₂. Cells were routinely passaged at 70-80% confluence. During passaging, cells were washed twice with Dulbrecco's Phosphate Saline (DPBS) and detached through incubation with 0.25% (w/v) Trypsin- 0.53 mM EDTA solution for 5-15 min at 37°C. Equal amounts of cells-specific media were added immediately upon cell detachment and cells were then centrifuged at 260 g for 5 min. Cell counting was carried out by re-suspending a harvested cell pellet in 1-3 mL of cell-culture media and re-suspending cell solution in Trypan blue at 1:10 ratio. The haemocytometer was used to count the total number of living cells and excluded the number of dead cells (blue stained) from the count. The cell pellet was re-suspended in fresh media and cells were re-cultured in culture flasks by passaging. Stock of each cell line was prepared at approximately 1x10⁶ cell number in 1 mL FCS + 10% DMSO (freezing medium) and stored at -80°C for future use. Upon need, cells were thawed, gently re-suspended in 10 mL cell-dedicated medium, and centrifuged at 150 g for 5 min. Cell pellets were then again gently re-suspended in fresh batch of cell-dedicated media and plated in suitable dish. This step of media changes was performed to ensure removal of DMSO from frozen cells sample and to increase the viability of thawed samples.

3.2.2.2 Silencing of EPCR in DU145 and PC3 cells

The outline of this procedure is shown on Figure 3.1 below.

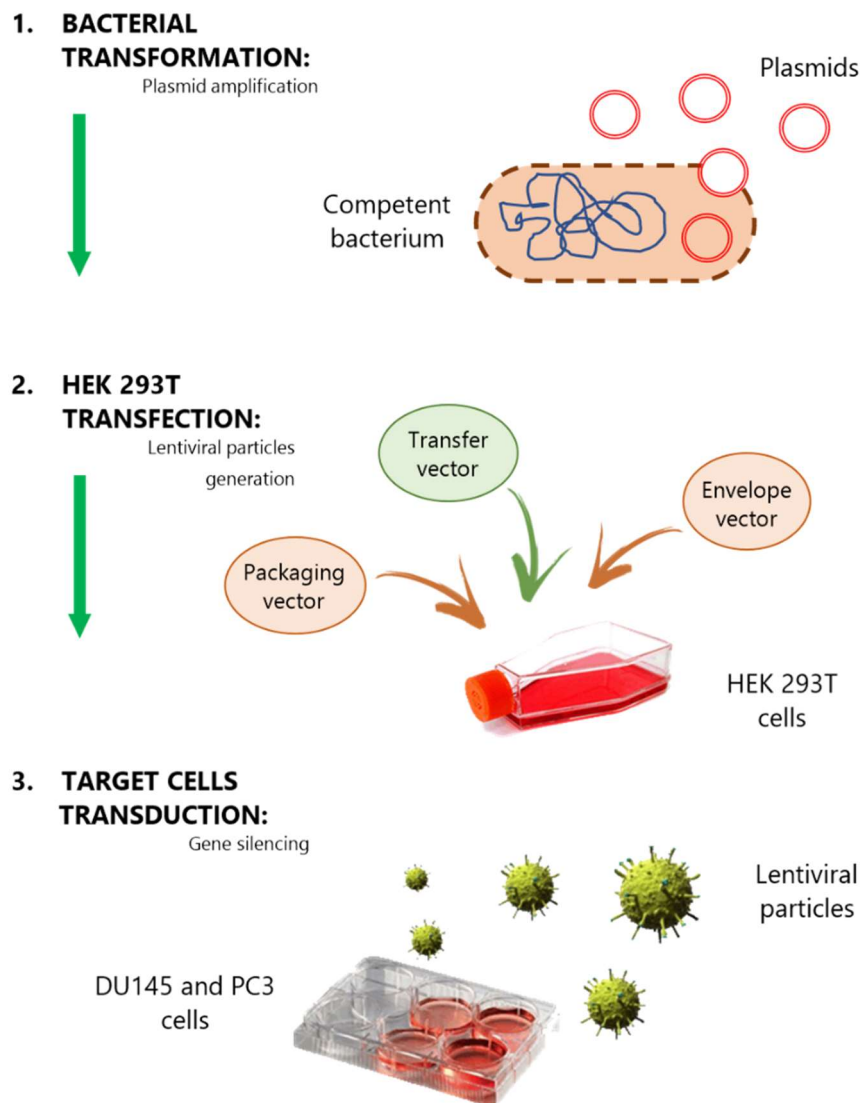


Figure 3.1 - Workflow for the generation of stable knockdowns for EPCR. Plasmids required for the generation of lentiviral particles were amplified in competent bacteria and then isolated. Lentiviral particles used to silence EPCR expression in target PCa cells were generated using HEK-293T transfection system and lentiviral vectors envelope psPAX2 and packaging pMD2.G. Such lentiviral particles were eventually used to transduce the shRNAs-containing plasmids into the recipient cells, namely DU145 and PC3, used to perform functional studies.

3.2.2.2.1 Target cell line antibiotic kill curve

DU145 and PC3 cells were grown to 50% confluence in 1 mL of cell-dedicated medium in 24-well culture plates and incubated overnight at 37°C. After incubation, the medium was replaced with fresh medium containing varying concentrations of puromycin antibiotic as well as without antibiotic for the negative control. Each concentration was maintained in duplicates as indicated in the 24-well plate format (Figure 3.2), and the medium with antibiotic replaced every 48 hours. Cells were cultured for 7 days, and then cell viability in

each well was determined by cell counter (Invitrogen™ Countess™ II Automated Cell Counter). The concentration of antibiotic that completely blocks the growth of cells for both lines was found at 1 µg/mL.

	1	2	3	4	5	6
A	0 µg/mL	0 µg/mL	0.25 µg/mL	0.25 µg/mL	0.50 µg/mL	0.50 µg/mL
B	0.75 µg/mL	0.75 µg/mL	1.00 µg/mL	1.00 µg/mL	1.25 µg/mL	1.25 µg/mL
C	1.50 µg/mL	1.50 µg/mL	1.75 µg/mL	1.75 µg/mL	2.00 µg/mL	2.00 µg/mL
D	2.25 µg/mL	2.25 µg/mL	2.50 µg/mL	2.50 µg/mL	2.75 µg/mL	2.75 µg/mL

Figure 3.2 – Schematic guide for selection antibiotic optimal concentration. Representation of 24-well plate setup for puromycin titration for determining working selection concentration.

3.2.2.2.2 Competent bacteria transformation for plasmid amplification

Lentiviral vectors MISSION® pLKO.1-puro empty vector (at 500 ng/µL), EPCR-shRNA1, -shRNA2, -shRNA3, -shRNA4, and -shRNA5 (at 20 ng/µL – Table 3.1) in DNA format were purchased from Sigma. Lentiviral vectors envelope psPAX2 and packaging pMD2.G, and transduction positive control PL-SIN-EF1 α -EGFP in bacteria as agar stab format were obtained from Addgene. XL1-B super-competent bacteria was used for transformation and plasmid amplification were gently thawed on ice. 100 µL of cells were added to a pre-chilled round bottom tube for each clone to be transformed. PLKO.1-puro and EPCR-shRNA plasmids were diluted at 20 ng/µL, and 5 µL was transferred to each of the reaction tubes collecting 5 µg of plasmid mix. Each transformation reaction was gently mixed without pipetting by swirling and incubated on ice for 30 min. The transformation reactions were then heat shocked at 42°C for 45 sec before being placed in ice for 2 min. 250 µL of RT LB Broth were added to each reaction. Each transformation reaction was shaken horizontally at 200 rpm, 37°C for 1 hour. 200 µL of each transformation reaction was spread on pre-warmed LB-agar selective plates containing 50 µg/mL ampicillin, and incubated overnight at 37°C. PsPAX2, pMD2.G, and PL-SIN-EF1 α -EGFP single colonies were picked from stab culture, plated in LB-agar selective plates containing 50 µg/mL ampicillin, and incubated overnight at 37°C. After incubation, single colonies for each plasmid were then inoculated in 50 mL LB-broth containing 50 µg/mL ampicillin and cultured overnight at 37°C with shaking. Cell cultures with visible cloudy bacterial growth were used for plasmid isolation using QIAGEN QIAfilter Plasmid Midi according manufacturer protocol. Isolated plasmids were quantified using Nanodrop 8000 Spectrophotometer and stored in TE buffer at -20°C.

3.2.2.3 HEK-293T cell transfection

HEK-293T (human embryonic kidney cells containing SV40 T-antigen) cells were grown to 90% confluence in 4 mL of cell-dedicated medium in T25 flasks. On first day, 20 µL Lipofectamine 3000 and 500 µL OPTIMEM medium were incubated for 30 min at RT (L+O mixture). 6 µg of the packaging plasmid psPAX2 and 2 µg of the envelope expressing plasmid pMD2.G were mixed with 500 µL OPTIMEM medium (psPAX2 + pMD2.G + O). 8 µg of each plasmid of interest (pLKO.1-puro empty vector, EPCR-shRNA1, -shRNA2, -shRNA3, -shRNA4, and -shRNA5, and PL-SIN-EF1 α -EGFP) were added to each psPAX2 + pMD2.G + O mixture, mixed with pre-incubated L+O mixture and finally added to each of HEK-293T T25 flask with 4 mL of cell-culture medium, and incubated at 37°C for 16 hours. On second day, medium was changed in each HEK-293T flask with 5 mL of fresh HEK-293T-dedicated medium. On third day, fractions of medium (F1) from transfected HEK-293T cell culture were collected, centrifuged at 300g for 10 min to remove any floating cells, filtered through 40 µm nylon strainers to further remove any residual particles. Filtered fractions were aliquoted in 1 mL portions and stored at -20°C for short term storage. On fourth day of transfection, a second fraction (F2) was collected and stored in similar manner.

3.2.2.4 Infection of target PCa cell lines

DU145 and PC3 cell lines were grown to 60% confluence in 6-well culture plates. 1 mL of collected lentiviral supernatant was combined with 1 mL of cell line-dedicated medium and 16 µL Hexadimethrine bromide solution (1 mg/mL in 0.9% NaCl), and then added to DU145 and PC3 cells that were incubated at 37°C overnight. The following day, fresh medium was added. The cells were infected with supernatants from F1 that contained the lentiviral constructs pLKO.1-puro empty vector, EPCR-shRNA1, -shRNA2, -shRNA3, -shRNA4, and -shRNA5, and PL-SIN-EF1 α -EGFP, and were further grown in cell line-dedicated media. The efficiency of infection of the positive control PL-SIN-EF1 α -EGFP plasmid-expressing cells was assessed by observing the expression of the Enhanced Green Fluorescence Protein (EGFP) at 488 nm emission wavelength using a Carl Zeiss PALM MicroBeam fluorescent microscope. 48 hours after infection, DU145 and PC3 cells were treated with cell-dedicated media supplemented with puromycin (1 µg/mL) to select cells that had efficiently integrated the lentiviral constructs.

Table 3.1 – Specification of the MISSION® shRNA clones used to perform gene silencing in target cells.

The Table shows details of the region on the *PROCR* gene targeted by each shRNA. All the clones used for the purpose of this technique were already validated in previous studies.

	Clone ID	Target Seq	Match Position	Match Region	Forward Oligo Sequence	Reverse Oligo Sequence
shRNA 1	TRCN000 0377417	GAATCACC TGAGGCCT CAAA	1259	3UTR	CCGGGAATCACCTGA GCGTTCAAACCTGA GTTGAACGCCTCAG GTGATTCTTTG	AATTCAAAAAGAAC ACCTGAGGCCTCAA ACTCGAGTTGAACG CCTCAGGTGATTTC
shRNA 2	TRCN000 0369969	TTTGCTGA ATTAGTCT GATAA	1157	3UTR	CCGGTTGCTGAATTA GTCTGATAACTCGAGT TATCAGACTAATTCAAG CAAATTTTG	AATTCAAAAATTGCT GAATTAGTCTGATAAC TCGAGTTATCAGACTA ATTCAAGCAAA
shRNA 3	TRCN000 0300564	TGGCCTCC AAAGACTT CATAT	287	CDS	CCGGTGGCCTCCAAA GACTTCATATCTCGAG ATATGAAGTCTTGAG GCCATTTTG	AATTCAAAAATGGCC TCCAAGACTTCATAT CTCGAGATATGAAGT CTTGGAGGCCA
shRNA 4	TRCN000 0300553	GCAGCAG CTCATGC CTACAA	713	CDS	CCGGGCAGCAGCTCA ATGCCTACAACCTGA GTTGTAGGCATTGAG CTGCTGCTTTTG	AATTCAAAAAGCAGC AGCTCAATGCCTACA ACTCGAGTTGTAGGC ATTGAGCTGCTGC
shRNA 5	TRCN000 0061378	TGGCCTCC AAAGACTT CATAT	287	CDS	CCGGTGGCCTCCAAA GACTTCATATCTCGAG ATATGAAGTCTTGAG GCCATTTTG	AATTCAAAAATGGCC TCCAAGACTTCATAT CTCGAGATATGAAGT CTTGGAGGCCA

3.2.2.3 Assessment of silencing of EPCR in DU145 and PC3 cells

3.2.2.3.1 Real-time quantitative PCR (qRT-PCR)

Total RNA for this experiment was isolated from cells expressing pLKO.1-puro, EPCR-shRNA1, -shRNA2, -shRNA3, -shRNA4, and -shRNA5 relative to both DU145 and PC3 lines. Samples were processed and analysed according to the protocol described in section 2.2.2.3.

3.2.2.3.2 Flow cytometry

DU145 and PC3 pLKO.1-puro, EPCR-shRNA1, -shRNA2, -shRNA3, -shRNA4, and -shRNA5 cells were used for this experiment. Cells were processed and analysed according to the protocol described in section 2.2.2.5.

3.2.2.3.3 Western blot

Total protein lysate for this experiment was isolated from cells expressing pLKO.1-puro, EPCR-shRNA1, -shRNA2, -shRNA3, -shRNA4, and -shRNA5 relative to both DU145 and PC3

lines. Samples were processed and analysed according to the protocol described in section 2.2.2.4.

For each sample, 30 µg of total-proteins lysates were equally loaded and separated by SDS-PAGE prior transfer to activated PVDF membrane. During each experiment, two membrane were produced to assess, respectively, EPCR and β-actin protein expression. Each membrane was incubated with the corresponding primary antibody diluted in 5% milk-TBS buffer separately, followed by anti-mouse secondary antibody according to dilutions showed in Table 3.2. Washes with TBST buffer were performed after incubation with primary and secondary antibodies.

Table 3.2 – List of the antibodies used in Western blot analysis. Antibodies and standards used to perform the immunoblotting are indicated with relative working dilutions.

Primary Ab	Dilution	Reference number	Clone	Supplier
Mouse anti-EPCR	1 µg/mL	WH0010544M3	M2	Sigma
Mouse anti-β-actin	1:1000	SAB1305567	8H10D10	Sigma
Secondary Ab	Dilution	Reference number	Clone	Supplier
Anti-Mouse IgG HRP-linked	1:1000	7076	Polyclonal	Cell Signalling
Ladder	Dilution			Supplier
Precision Protein™ StrepTactin-HRP Conjugate	1:5000			Bio Rad

3.2.2.4 Effects of EPCR silencing on cell proliferation and clonogenicity

3.2.2.4.1 Incucyte® cell confluence proliferation assay

For this assay, pLKO.1-puro, EPCR-shRNA1 and EPCR-shRNA4 relative to both DU145 and PC3 lines were used and the protocol provided by the manufacturer applied. Cells were cultured and harvested, according to the protocol described in section 2.2.2.4, at below 80% confluence. Cells were then resuspended at 1.0×10^5 cells/mL density, 100 µL of such prepared cell suspension were transferred to each well (1.0×10^4 cells/mL) of a transparent 96-well flat bottom plate in four replicates, so that the cell confluence by day 1 was 20%. Then, plate was transferred to the Incucyte ZOOM® system incubator, allowed to warm to 37°C for 30 min, and scanned in Phase Contrast at every hour, for a total of 80 time points collected.

3.2.2.4.2 Colony Formation Assay (CFA)

The clonogenic assay was used to assess the differences in reproductive viability between control and knockdown cells.

For this assay, pLKO.1-puro, EPCR-shRNA1 and EPCR-shRNA4 relative to both DU145 and PC3 lines were used. Cells were plated in 6-well plates at a density of 1.0×10^3 cells per well. Plates were then cultured for one week according to protocol described in section 2.2.2.4. Cell medium was then removed, and cells carefully washed with DPBS avoiding cell detachment. DPBS was removed from the wells, and cells were fixed with 4% paraformaldehyde for 15 min at RT. Paraformaldehyde was then removed and cells stained with 0.5% crystal violet solution for 30 min at RT. Tap water was used to carefully wash the cells and then removed, plates were left to dry in normal air at RT. A picture for each well was taken with a camera, and then analysed using the count and Plot Histograms of Colony Size (countPHICS) software.

3.2.2.5 Effects of EPCR silencing on cell migration and invasion

3.2.2.5.1 Cell migration and invasion assay

For this assay, pLKO.1-puro, EPCR-shRNA1 and EPCR-shRNA4 relative to both DU145 and PC3 lines were used. Cultrex® 96 Well BME Cell Migration and Invasion Assay was used following the manufacturer's recommendations (Trevigen, Gaithersburg, MD, USA). Each transwell chamber presented 8 μm pores in the polyethylene terephthalate (PET) bottom, which could be occluded with basal membrane extract (BME) to test the ability of cells to degrade a biological matrix. Therefore to perform the migration assay the chambers were left without coating, while for the invasion assay each insert was coated with 1X BME. Twenty-four hours prior the beginning of the assay, cells were starved in dedicated medium with 0.5% FCS. Top chambers of the invasion device used to perform the invasion assay were coated with 50 μL 1X basal membrane extract (BME) solution and incubated overnight at 37°C, whilst the top chambers on the same device used to perform the migration assay were left empty. Cells were cultured to 80% confluence on the day of the assay and harvested according to protocol described in section 2.2.2.1, the pellet washed with 1X Wash Buffer, counted, and resuspended at 1×10^6 cells/mL in dedicated medium with 0.5% FCS. Coated top chambers were aspirated and 50 μL of cells added to each well used for both migration and invasion assay (final cell density 5×10^4 cells/well. 150 μL of complete

dedicated medium (with 10% FCS) was added to each bottom chamber. The plate was finally incubated at 37°C for 24 hours. On day two, top chambers were aspirated and washed with 100 µL of 1X Wash Buffer. Bottom chambers were aspirated too, and each well washed twice with 200 µL 1X Wash buffer. 100 µL of Cell Dissociation Solution/Calcein-AM was added to bottom chamber, top chamber device assembled, and such prepared plate incubated at 37°C for one hour. Finally, top chamber was removed, and plate read at 485 nm excitation, 520 nm emission with Infinite M200 Pro TECAN (Tecan Group Ltd, Männedorf, Switzerland). Percentage of relative migration and invasion was calculated comparing values obtained from wild type versus knock down cell populations.

3.2.2.6 Effects of EPCR silencing on EMT and cancer progression

3.2.2.6.1 EMT markers

The expression of EMT marker was assessed on control (Empty vector) and knockdown (shRNA1 and shRNA4) cells in both DU145 and PC3 lines.

Table 3.3 – List of the antibodies used in Western Blot analysis for EMT markers. Antibodies and standards used to perform the immunoblotting are indicated with relative working dilutions.

Primary Ab	Dilution	Reference number	Clone	Supplier
Rabbit anti-β-Catenin	1:500	D10A8	8480P	Cell Signalling
Rabbit anti-E-cadherin	1:500	24E10	3195S	Cell Signalling
Rabbit anti-N-cadherin	1:500	D4R1H	13116P	Cell Signalling
Rabbit anti-Vimentin	1:500	D21H3	5741S	Cell Signalling
Rabbit anti-ZO1	1:500	D7D12	8193S	Cell Signalling
Mouse anti-β-actin	1:1000	SAB1305567	8H10D10	Sigma
Secondary Ab	Dilution	Reference number	Clone	Supplier
Anti-Mouse IgG HRP-linked	1:1000	7076	Polyclonal	Cell Signalling
Anti-Rabbit IgG HRP-linked	1:1000	7074S	Polyclonal	Cell Signalling
Ladder	Dilution			Supplier
Precision Protein™ StrepTactin-HRP Conjugate	1:5000			Bio Rad

Cell lysates preparation as well as the immunoblot assay were performed as described in section 2.2.2.4.

Antibodies used for the assay are showed in Table 3.3.

3.2.2.6.2 mRNA profiling with the NanoString PanCancer Progression technology

Gene expression profile of DU145 pLKO.1-puro (Empty vector) and EPCR-shRNA4 cells was assessed using the PanCancer Progression Panel, which consists of 770 genes (606 pathway genes, 124 cancer driver genes, and 40 reference genes). This assay was carried out according to the manufacturer instructions. Total RNA for this experiment was isolated from DU145 pLKO.1-puro (Empty vector) and EPCR-shRNA4 cell populations using Qiagen RNAeasy columns. Cells were cultured in four T25 flasks replicates and harvested as described in section 2.2.2.1. Samples were processed and analysed according to the protocol described in section 2.2.2.3. High quality of total RNA samples was assessed using Nanodrop 8000, and 150 ng of total RNA from each sample were used for setting up NanoString probe hybridisation overnight for 20 hours at 65°C. The reaction Master Mix was prepared according to Table 3.4 below.

Table 3.4 – NanoString probe hybridisation master mix. Table specifies the volume of reagents (experimental tubes) for single reaction. All reagents listed in this Table are included in the PanCancer Progression Panel kit.

Reagents	Volume for Single Reaction
RNA sample	5 µL (up to 150 ng)
Reporter probe	8 µL
Capture probe	2 µL

After the overnight hybridisation completed, excess probes were removed using nCounter® Prep Station, magnetic beads and hybridised mRNA/probe were immobilised on a streptavidin-coated cartridge. The processed cartridge was subsequently scanned using an nCounter® digital analyser platform for the generation of the raw data with a high-resolution scan 555 fields of view (fov). Raw data were processed with nSolver Analysis Software (V.4.0), imaging quality control (QC), mRNA positive control QC and Normalization QC checked. All samples were within the quality parameters of NanoString gene expression assays. Differential expression, pathway scoring, and cell type scoring were performed using nSolver advance analysis module V. 2.0.115. Normalisation of the data was performed using the geNorm algorithm for the selection of the best housekeeping genes. Genes which

showed ≥ 2 , fold change in their expression with a BY (Benjamini Yekutieli) p-value ≤ 0.05 were considered significant between the group.

3.2.2.6.2 Quantitative proteomics analysis of differentially expressed proteins following EPCR silencing in DU145 cells

MS analysis was conducted on DU145 pLKO.1-puro (Empty vector) and EPCR-shRNA4 cells according to the protocol described in section 2.2.2.2.

3.3 Results

3.3.1 Assessment of effective EPCR silencing in DU145 and PC3 cells

To study the role of EPCR in PCa, DU145 and PC3 cells were transduced with lentivirus particles encoding EPCR-targeting shRNAs. EPCR expression levels were stably silenced using five different EPCR-targeting shRNAs as described in the Materials and Methods section. As a negative control to carry along with the EPCR-targeting shRNAs, the empty vector consisting in the pLKO.1-puro backbone was used. Such vector does not contain any shRNA insert and is therefore a valid negative control to assess the EPCR silencing-specific effect of transduction on cells. All the lentiviral vectors used for this study contain the gene for the puromycin resistance, allowing cells that have taken the plasmid and successfully integrated its genetic content to survive in culture media added with puromycin, thus being positively selected.

Firstly, the efficacy of gene silencing was assessed at the transcriptome level. Three cell passages post antibiotic selection, total RNA was extracted from each cell line to validate the effective knockdown, and RT-qPCR performed on cDNA obtained from 1.5 µg of RNA. In both DU145 and PC3 cells, shRNA1 and shRNA4 significantly reduced EPCR mRNA expression (around 75% for shRNA1 and 77% for shRNA4 in DU145 and around 94% for shRNA1 and 86% for shRNA4 in PC3) showing higher efficiency (Figure 3.3).

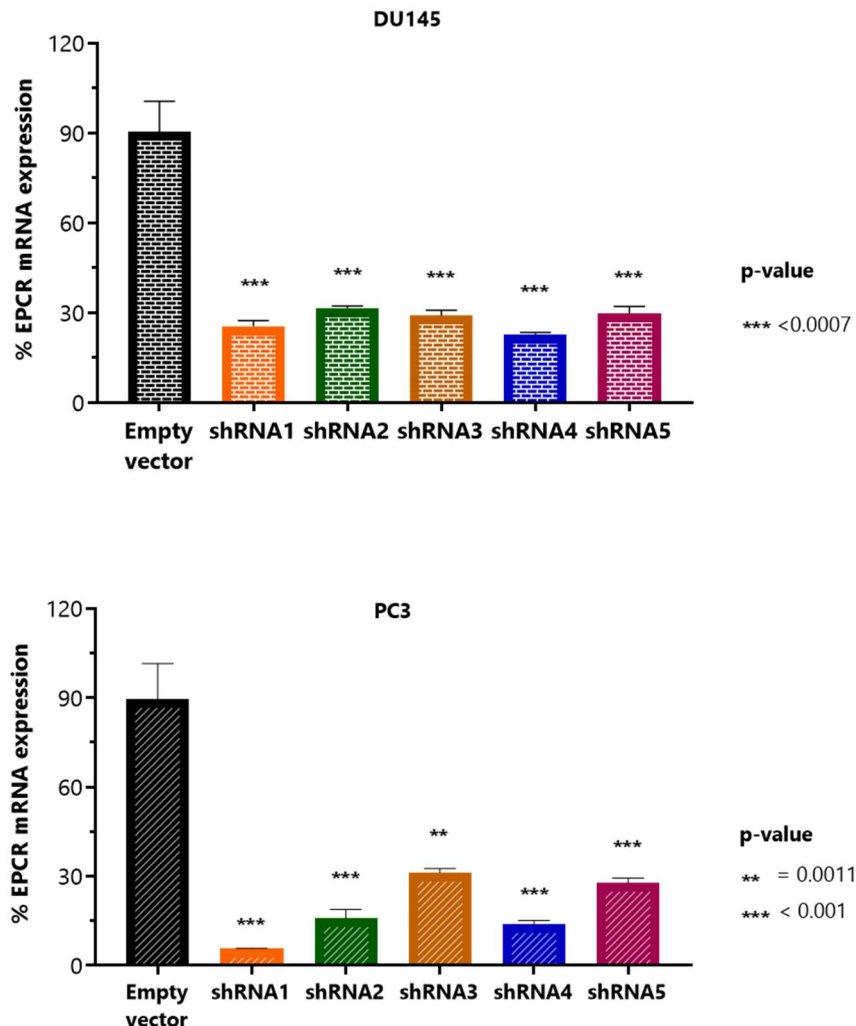
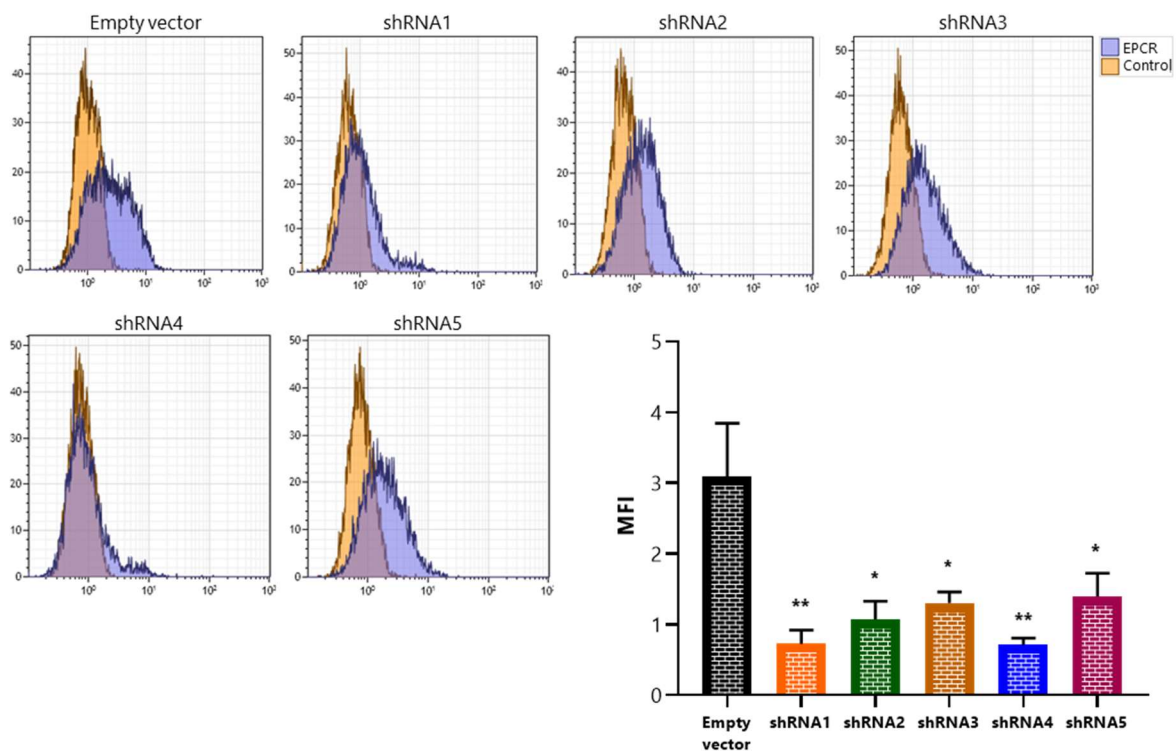


Figure 3.3 – Expression of EPCR mRNA in DU145 and PC3 cells following silencing knockdowns with EPCR shRNAs. Quantitative PCR on mRNA samples from DU145 (top) and PC3 (bottom) in control (pLKO.1) and EPCR shRNAs cells. Data are reported as mean \pm SD and are representative of three independent experiments giving similar results ($n=3$). Values were normalised on GUSB mRNA expression in all the cell lines. Statistical significance was calculated between control and each test group using *t-test* and indicated as asterisk (** = p-value < 0.01 , *** = p-value < 0.001).

A preliminary assessment of the reduction of EPCR protein expression on the cell surface was performed using flow cytometry (FCM) experiments using shRNA control cell line and five EPCR knockdown cell lines. Fixation and permeabilization steps were excluded from flow cytometry workflow to specifically assess the surface EPCR expression. Therefore, results obtained are relative to the fraction of EPCR protein present on the membrane alone. A similar trend to the transcript level was observed on a protein level on cell surface in FCM experiments in both DU145 (Figure 3.4-A) and PC3 cells (Figure 3.4-B), thus confirming successful and efficient knockdown of EPCR.

A.



B.

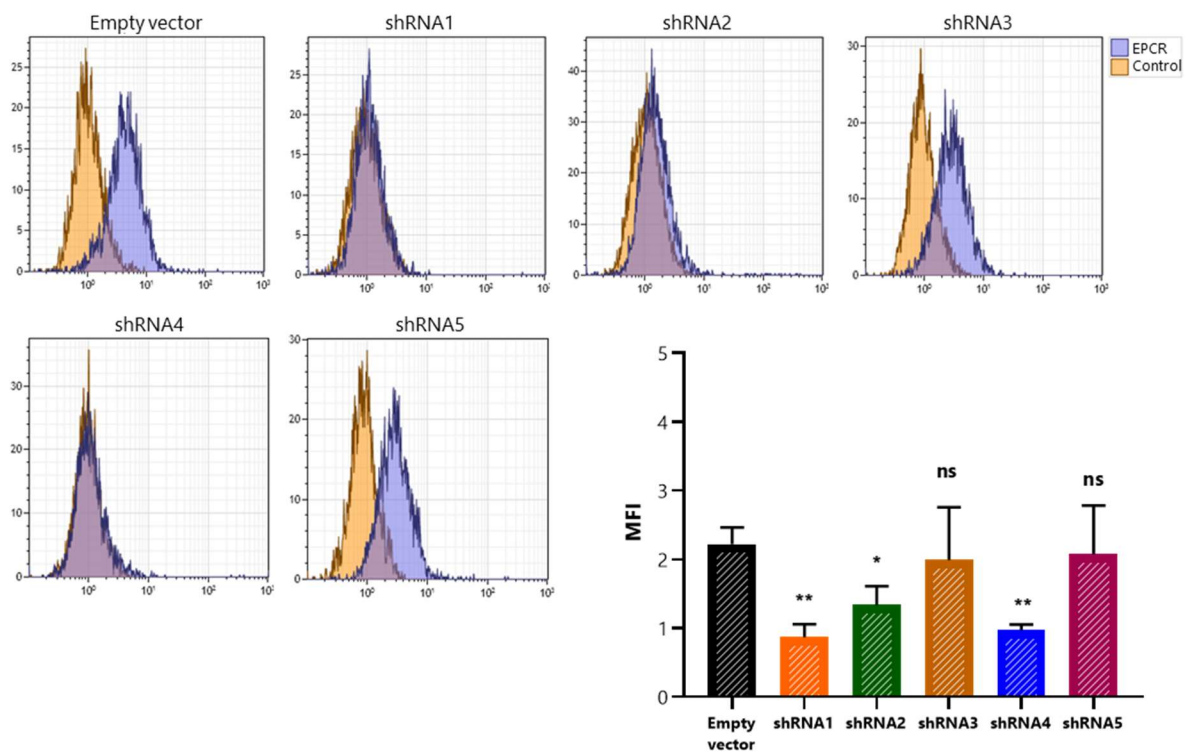


Figure 3.4 – Expression of EPCR in DU145 and PC3 cells following knockdowns with EPCR shRNAs. FCM analysis of EPCR protein expression in control (pLKO.1) and EPCR shRNAs DU145 (A) and PC3 (B) cells (top of each panel). Data are reported as mean \pm SD and are representative of three independent experiments giving similar results ($n=3$) and plotted in a bar graph (bottom of each panel). Values represent the mean fluorescence intensity (MFI) against the control population in which no primary antibody was used. Statistical significance was calculated between control and each test group using t-test and indicated as asterisks (ns= non-significant > 0.05 , * = p -value < 0.05 , ** = p -value < 0.01).

Indeed, shRNA1 and shRNA4 constructs determined a reduction of the mean fluorescence intensity (MFI) from 3.09 of the control to 0.72 and 0.71 respectively in DU145 and from 2.84 of the control to 0.9 and 1.03 respectively in PC3.

For this reason, EPCR knockdown constructs 1 and 4 (shRNA1 and shRNA4) were selected for further investigation and pLKO.1-puro (Empty Vector) used as negative control (Figure 3.5).

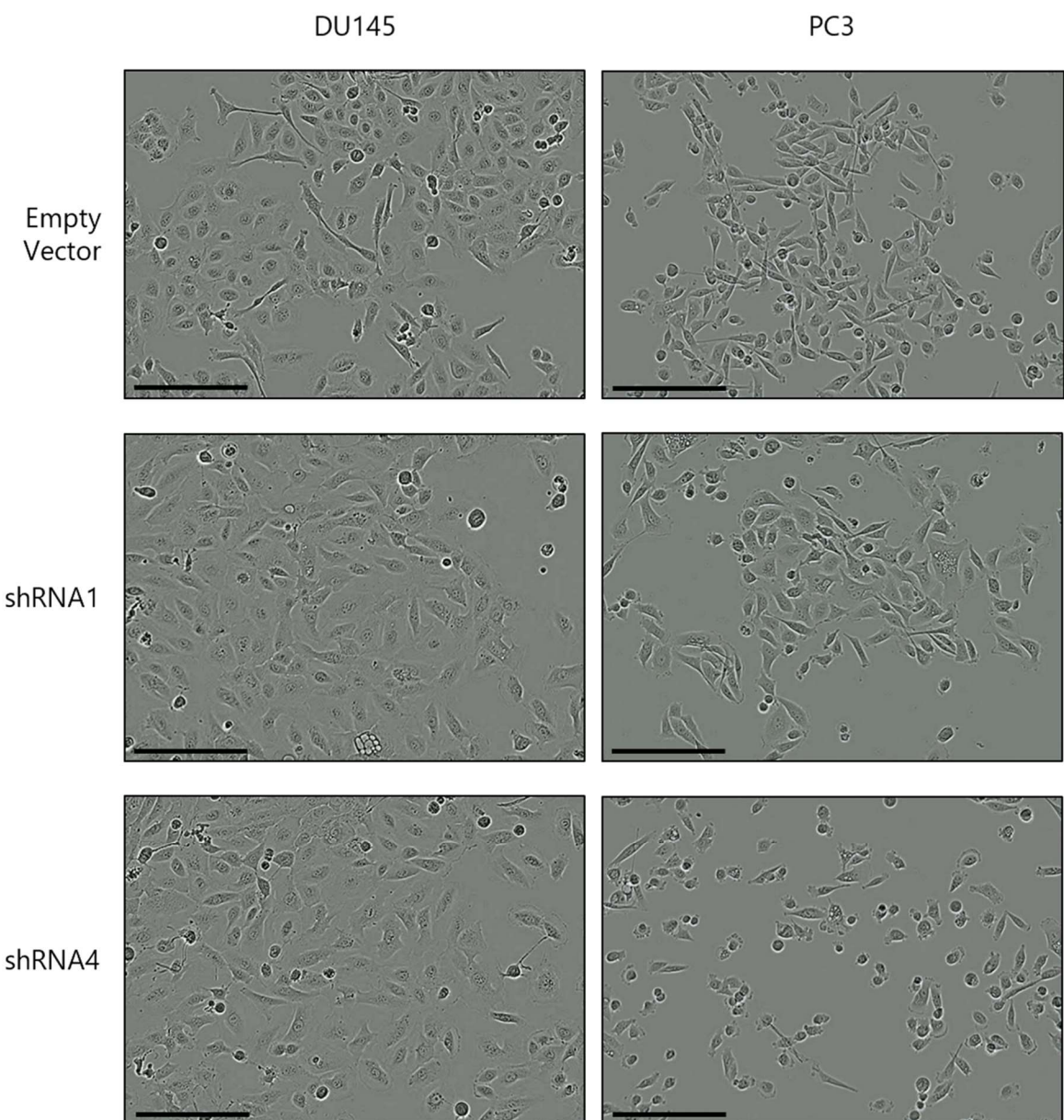


Figure 3.5 – Micrographs showing wild type and EPCR knock down populations of DU145 and PC3 cells.
It is possible to observe changes of morphology in each cell line upon silencing of EPCR, with wild type populations exhibiting a more elongated shape. Pictures were taken at the same time point across for each cell line. Scale bars refer to 100 µm.

The total EPCR protein expression levels after silencing with the shRNA1 and shRNA4 constructs in DU145 and PC3 cells were assessed by Western blot analysis (Figure 3.6).

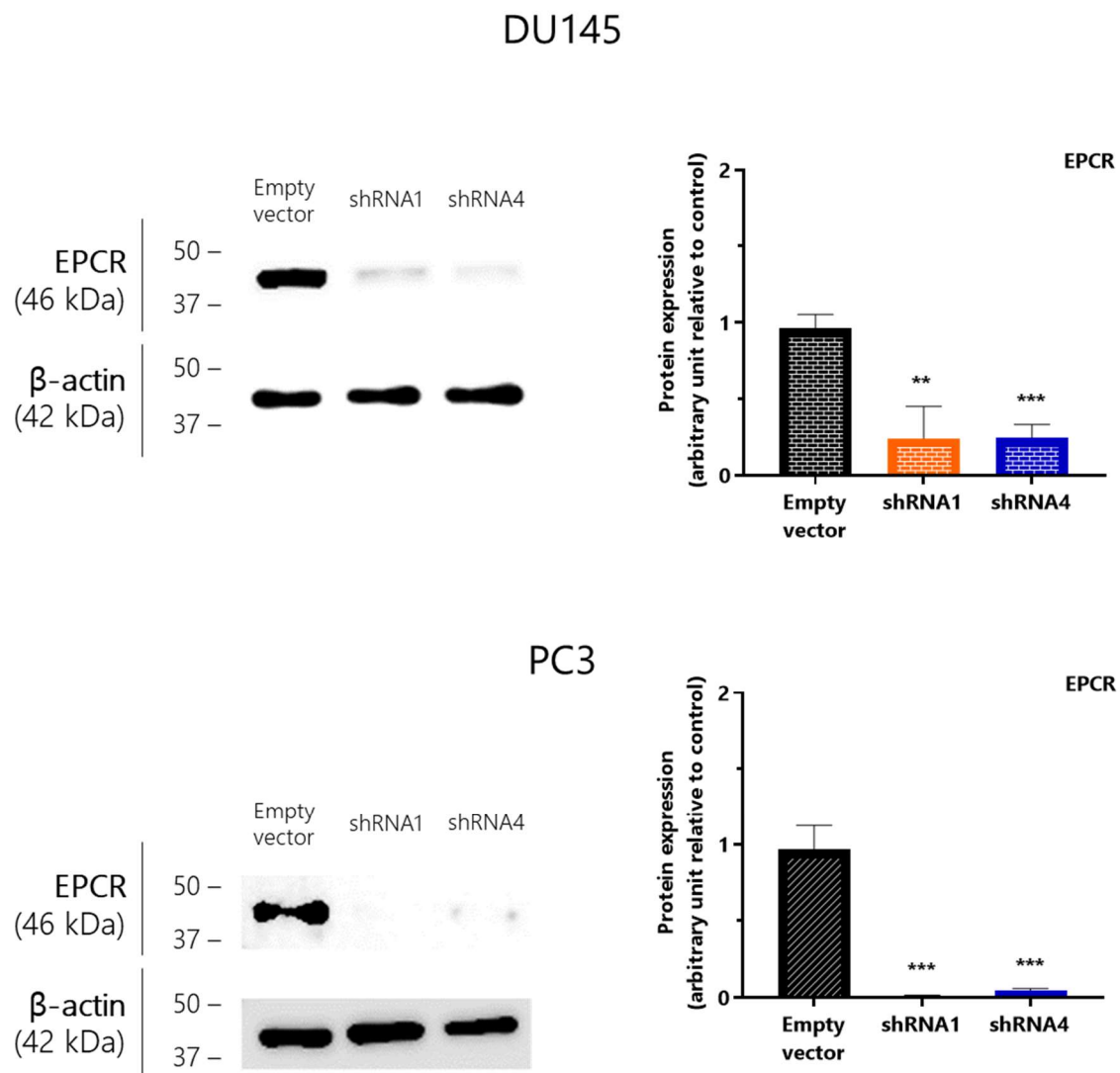


Figure 3.6 – Expression of EPCR in DU145 and PC3 cells following knockdowns with EPCR shRNAs. Immunoblot (top) showing EPCR protein expression in control (pLKO.1) and EPCR shRNA1 and shRNA4 in DU145 and PC3 cells (left). EPCR relative band is at the expected value of 46 kDa. Data reported as mean \pm SD and are representative of three independent experiments giving similar results ($n=3$). Values were normalised on β-actin expression in all the cell lines and plotted in a bar graph (right). Statistical significance was calculated between control and each test group using t-test and indicated as asterisks (**= p-value < 0.01, *** = p-value < 0.001).

Figure 3.6 shows how the decreased EPCR protein expression was successfully verified in both shRNA1 and shRNA4 constructs, with the control cells giving a band at the expected molecular weight of ~46 kDa (Liaw, Mather et al. 2001), further confirming the highly efficient knockdown with both constructs in DU145 and PC3 cells.

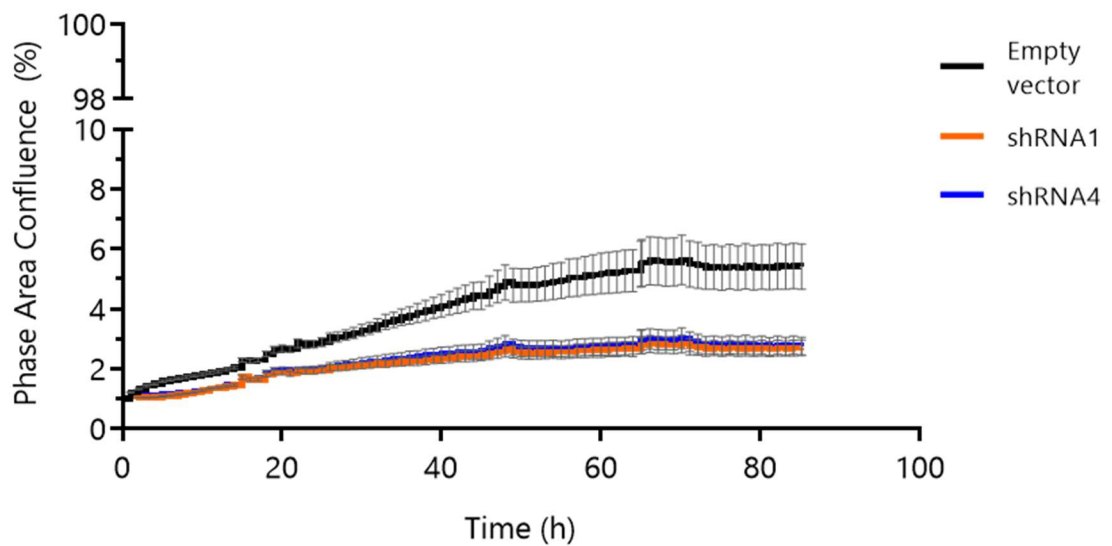
3.3.2 Effects of EPCR silencing on cell proliferation and clonogenicity

To determine whether silencing EPCR affected cell proliferation in the cell lines under study, a proliferation assay was set up using the Incucyte technology according to the manufacturer's protocol and as shown in section 3.3.2. Incucyte is a live cell imaging and analysis system that allows for a more accurate and detailed cell-growth analysis by collecting the cell growth data in designated time intervals.

To measure cell proliferation over time, cell confluence percentage was detected using Incucyte (Essen BioScience, Ann Arbor, MI, USA) software by phase-contrast images. Data are presented as mean percentage of phase area confluence for time point, and normalised to time 0.

Figure 3.7 shows the results for the proliferation assay. The experiment was performed once, in order to provide stronger and clearer results, repetition of such experiment needs to be performed in the future.

DU145



PC3

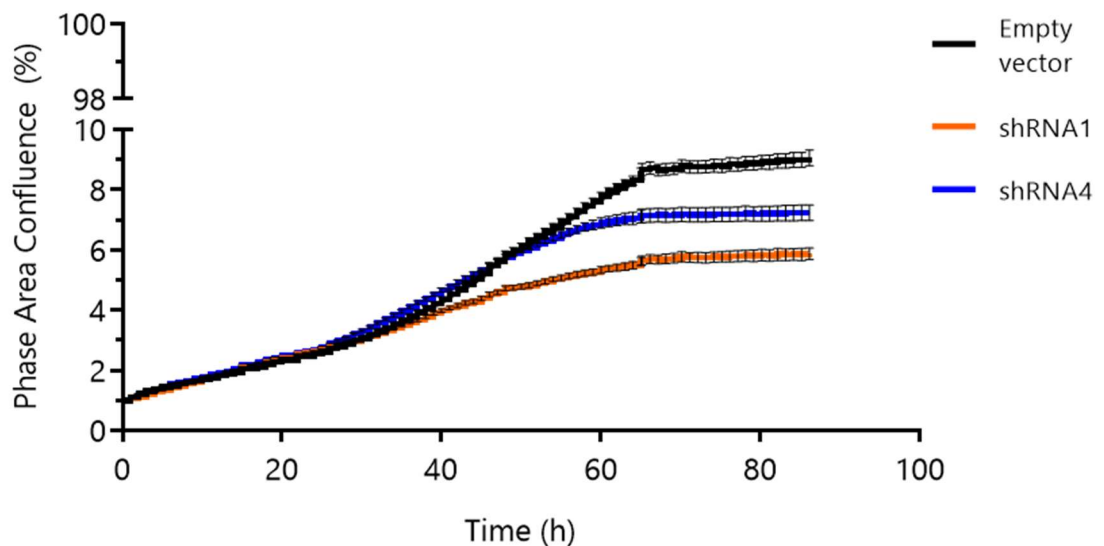


Figure 3.7 – Proliferation growth curve in DU145 and PC3 cells following knockdowns with EPCR shRNAs.
 IncuCyte Cell Proliferation Assay on DU145 and PC3 negative control, shRNA1, and shRNA4 knockdowns. Each data point represents four replicates within the same experiment. Values represent the mean percentage phase area confluence \pm SD for each time point and were normalised to the initial value at time 0. This experiment was performed once.

In order to assess the ability of cells to produce progeny, such as a single cell forming a colony of 50 or more cells, a CFA was performed. Results suggest that EPCR expression correlates with higher clonogenic potential. Indeed, in both DU145 and PC3 control lines showed higher number of colonies compared to the knockdown lines (Figure 3.8). In this assay shRNA1 showed higher ability to affect cell potential of unlimited division compared to shRNA4. Interestingly, these results show a similar pattern to the one observed during the proliferation assay, with the shRNA1 interfering more effectively with cell replication.

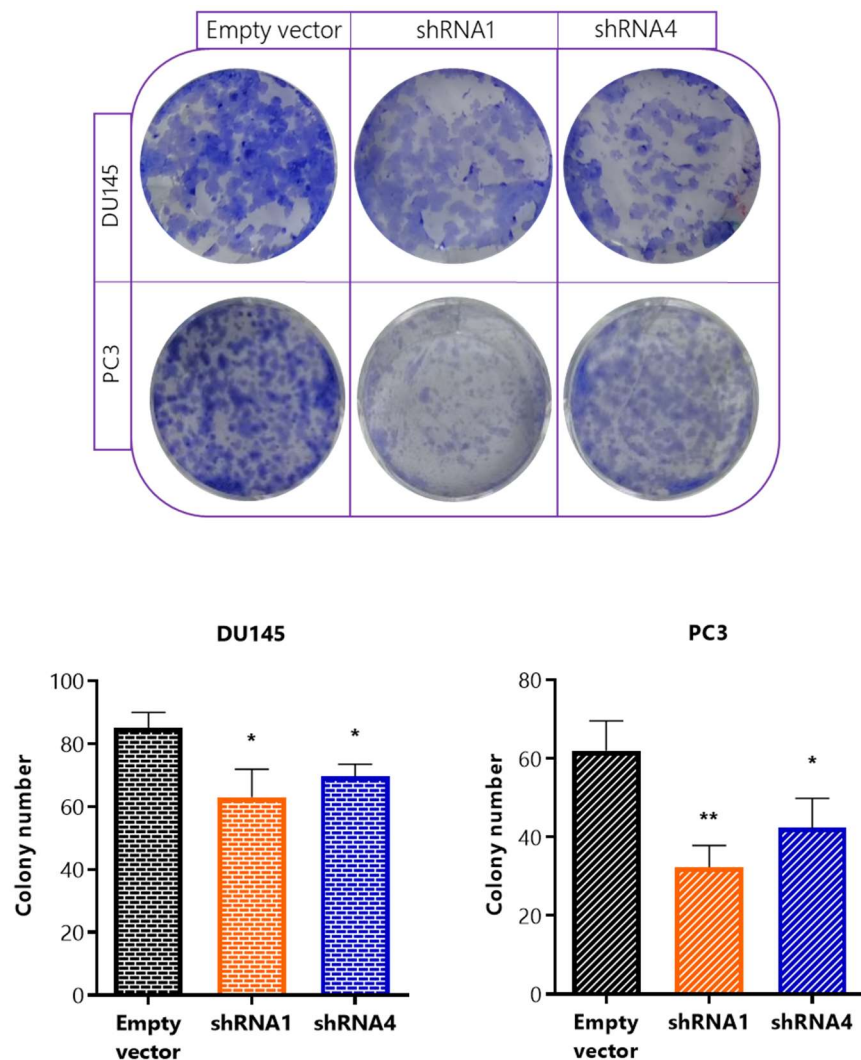


Figure 3.8 – Colony formation assay. Picture showing colonies formed after a week of incubation (top). Cells were fixed with 4% formaldehyde and then stained using crystal violet. Data reported as mean \pm SD ($n=3$) of colony number. Statistical significance was calculated between control and each test group using t-test and indicated as asterisks (* = p -value < 0.5 , ** = p -value < 0.01).

3.3.3 Effects of EPCR silencing on cell migration and invasion

The knockdowns were further studied for their effect on cell migratory and invasive ability. Transwell migration and invasion assays were performed using the Cultrex BME Cell Invasion Assay kit, as described in the section 3.2.2.5.1 of this chapter.

Silencing of EPCR with shRNA1 and shRNA4 resulted in a significant reduction of the migration potential in both DU145 and PC3 cells (Figure 3.9 – left panel).

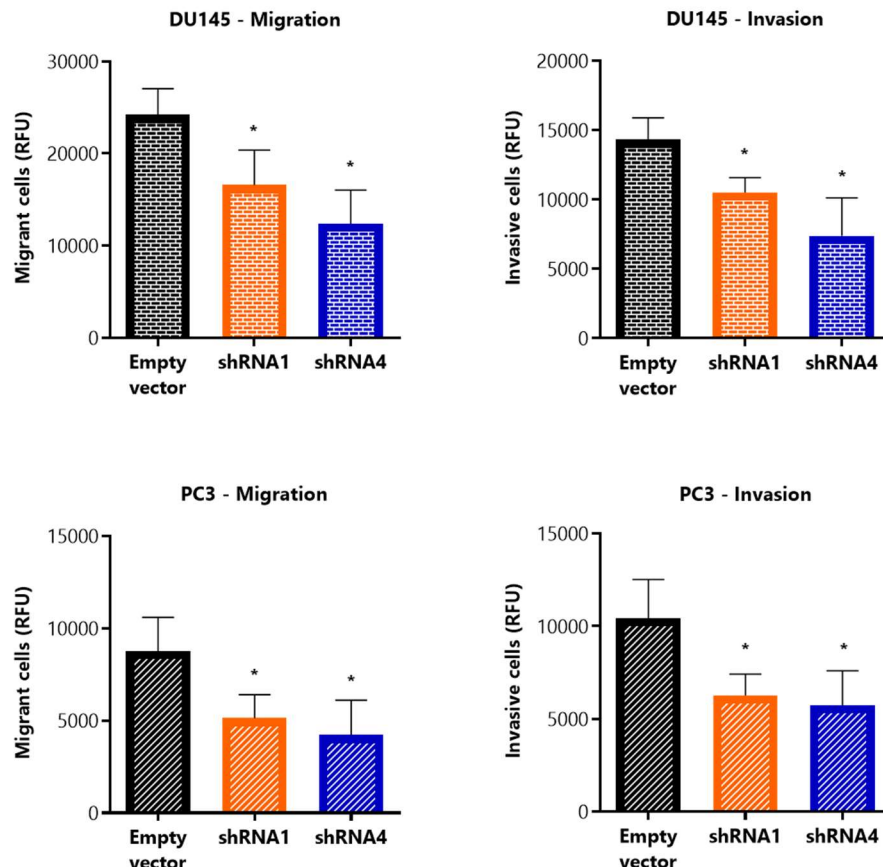


Figure 3.9 – Cell migration and invasion assays. Quantification of DU145 (top) and PC3 (bottom) cell migration (left) and invasion (right) was obtained by measuring the fluorescence emitted by the transmigrated cells in the wells of the bottom plate treated with Calcein-AM. Data are reported as mean \pm SD and are representative of three independent experiments giving similar results ($n=3$). Statistical significance was calculated between control and each test group using t-test and indicated as asterisks (* = p-value < 0.5).

Similarly, invasion ability was significantly reduced in both knockdowns of DU145 and PC3 (Figure 3.9 – right panel).

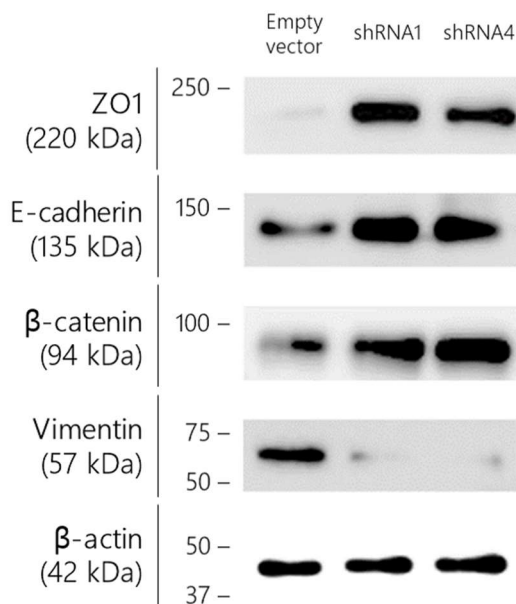
3.3.4 Effects of EPCR silencing on EMT and cancer progression

3.3.4.1 EMT markers expression modulation upon EPCR silencing

The results so far suggested that the silencing of EPCR has a significant effect on tumour proliferation, cell cologenicity, migration and invasion in PCa cells (DU145 and PC3). In order to clarify the role of EPCR in PCa progression we investigated its potential role in the EMT process. To do so, the protein expression levels of most common EMT markers reported in the literature were assessed in whole cell lysates of shRNA1 and shRNA4 constructs in both DU145 and PC3 cells. Epithelial markers analysed in DU145 cells for the purpose of this section are ZO1, E-cadherin, β -catenin, whereas vimentin was used as a mesenchymal marker since N-cadherin could not be detected, in accordance with existing literature (Fontana, Raimondi et al. 2019). Instead, in PC3 cells E-cadherin and β -catenin were selected as epithelial markers, whereas N-cadherin and vimentin were selected as mesenchymal markers.

Interestingly, results strongly suggest that following EPCR silencing a modulation of the endogenous pattern of EMT markers protein expression in PCa cells occurred. Figure 3.10 and 3.11 clearly show the inverse pattern of protein expression in controls (Empty vector) compared to the knockdown (shRNA1 and shRNA4) lines, respectively in DU145 and PC3 cells. Indeed, epithelial markers such as ZO1, E-cadherin, and β -catenin showed highly significant increased expression in the DU145 knockdown cell populations. Conversely, the protein level of the mesenchymal marker vimentin was significantly decreased in the knockdown lines compared to the control populations in DU145 cells.

A.



B.

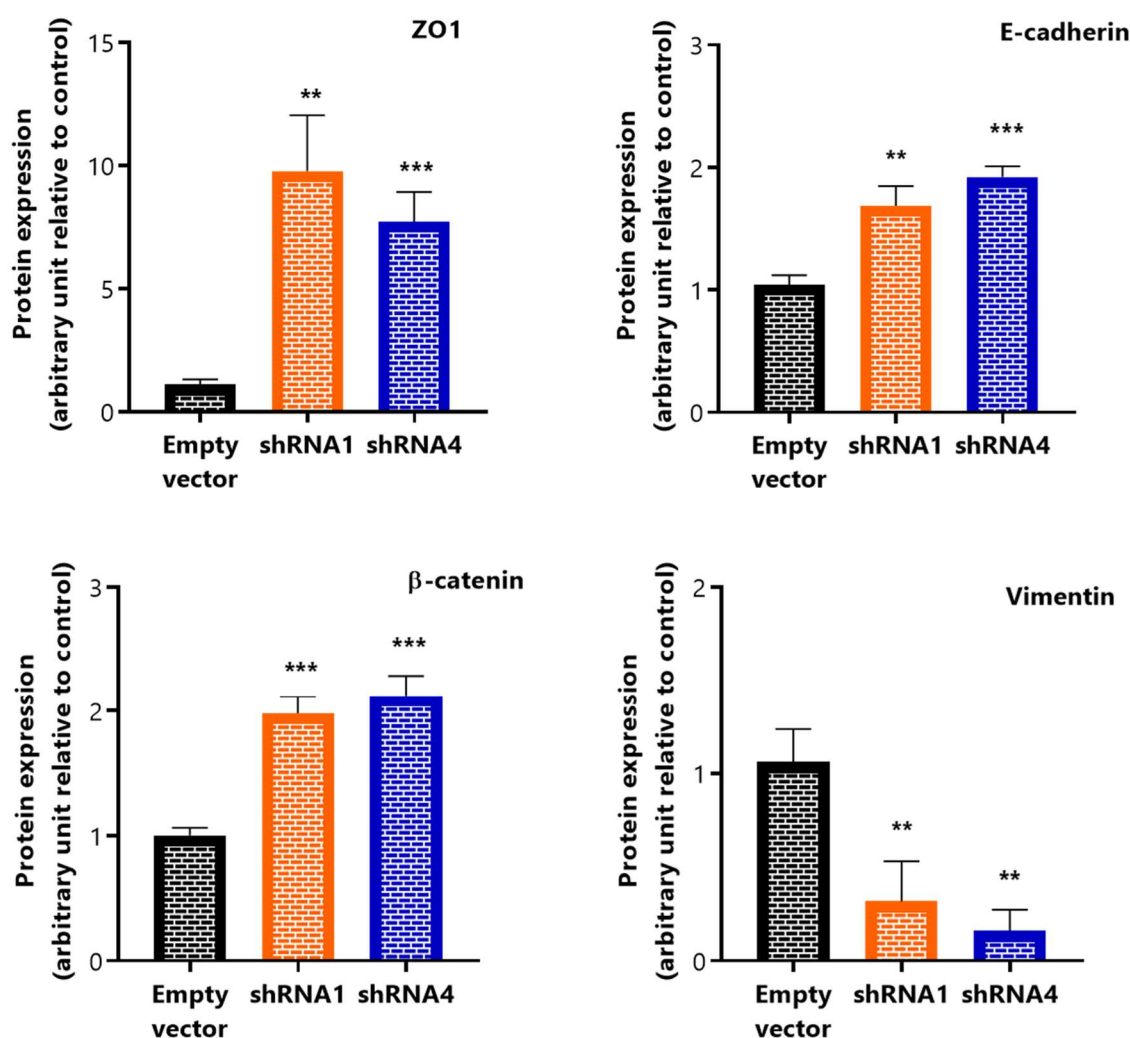
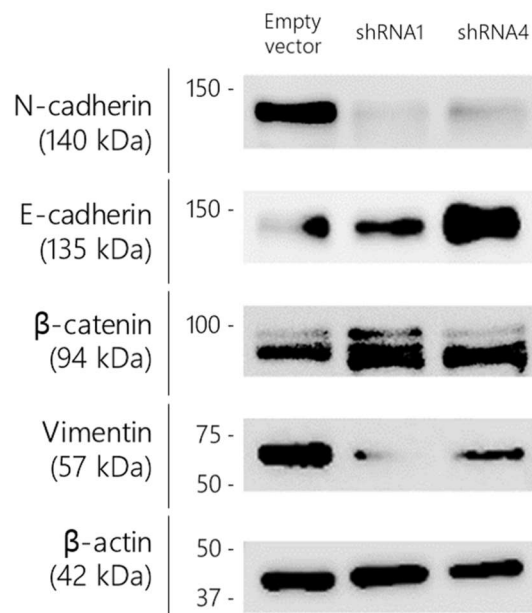


Figure 3.10 – Western blot of EMT markers in DU145 cells. (A.) Analysis of ZO1 (220 kDa), E-cadherin (135 kDa), β -catenin (94 kDa), and Vimentin (57 kDa) is shown in the top panel. β -actin (42 kDa) was used as protein loading control. (B.) Values were normalised against β -actin expression in all the cell lines and plotted in a bar graph (bottom). Data are reported as mean \pm SD and are representative of three independent experiments giving similar results ($n=3$). Statistical significance was calculated between control and each test group using t-test and indicated as asterisks (**= p-value < 0.01, *** = p-value < 0.001).

A.



B.

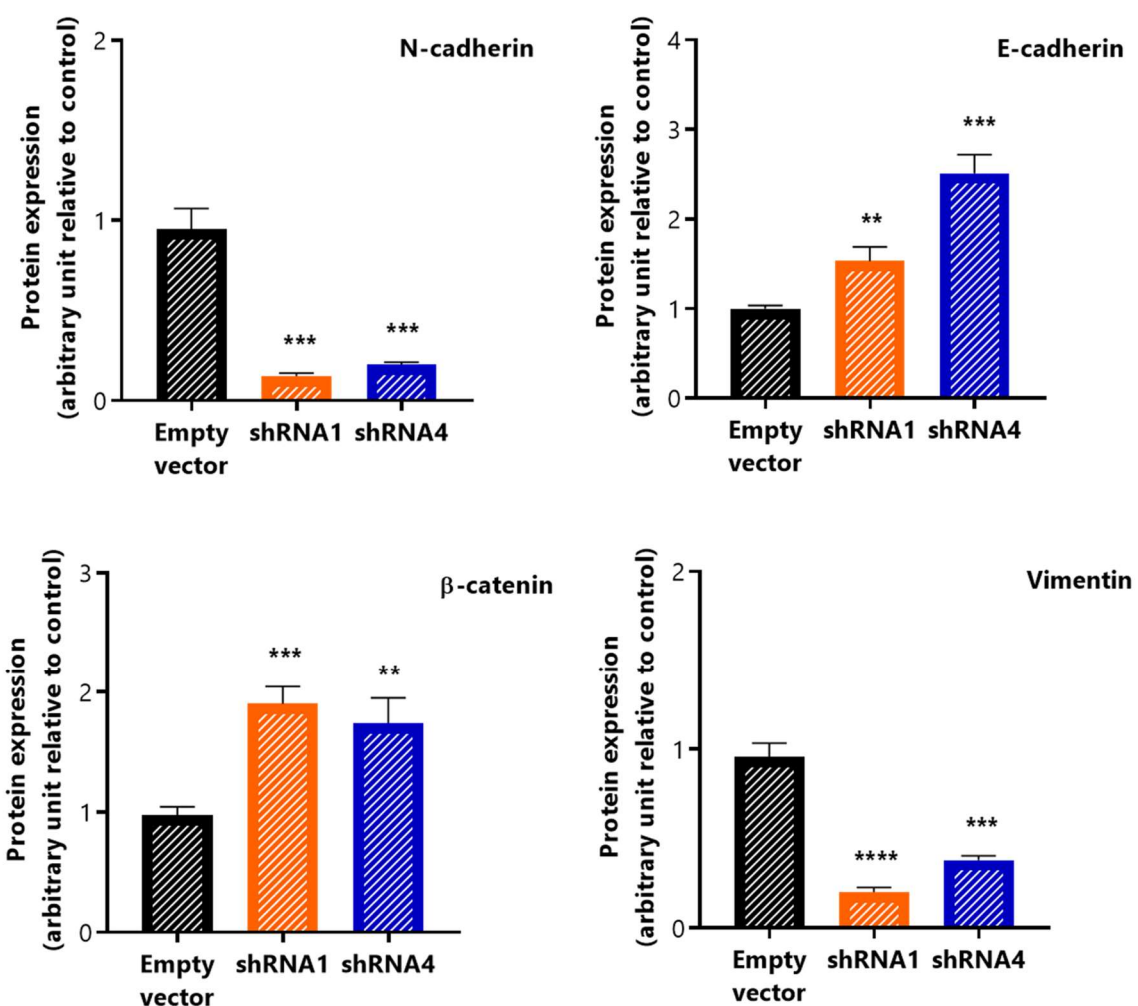


Figure 3.11 – Western blot of EMT markers in PC3 cells. (A.) Analysis of N-cadherin (140 kDa), E-cadherin (135 kDa), β -catenin (94 kDa), and Vimentin (57 kDa) is shown in the top panel. β -actin (42 kDa) was used as protein loading control. **(B.)** Values were normalised against β -actin expression in all the cell lines and plotted in a bar graph (bottom). Data reported as mean \pm SD and are representative of three independent experiments giving similar results ($n=3$). Statistical significance was calculated between control and each test group using t-test and indicated as asterisks (**= p -value < 0.01, *** = p -value < 0.001, **** = p -value < 0.0001).

3.3.4.2 Profile changes in mRNA expression after EPCR knock down

To profile a wide pool of genes involved in cancer progression, total RNA samples were analyzed using the NanoString nCounter® FLEX platform and the nSolver® software (alpha version 4.0). This system utilizes a novel digital barcode technology for direct multiplexed measurement of analytes with high levels of precision and sensitivity (<1 copy per cell). For high-throughput direct mRNA counting in this study, the *PanCancer Progression* panel was used. It contains probes to screen for the expression of 770 genes (606 pathway genes, 124 cancer driver genes, and 40 reference genes) representing 13 canonical cancer pathways covering the major steps in the cancer progression process: angiogenesis, extracellular matrix remodeling (ECM), epithelial-to-mesenchymal transition (EMT) and metastasis (Table 3.5).

Table 3.5 – PanCancer Progression Panel pathways. Details of the processes within the themes used to identify each gene's contribution.

Angiogenesis	ECM	EMT	Metastasis
<ul style="list-style-type: none">• Angiogenesis Response• Blood Coagulation• Negative Regulation of Angiogenesis• Regulation of Angiogenesis• Sprouting Angiogenesis• Positive Regulation of Angiogenesis• Vasculogenesis• VEGFA Signalling	<ul style="list-style-type: none">• Basal Lamina• Basement Membrane• Collagen Family• ECM Structure• Fibrosis• Integral to Membrane• Plasma Membrane• ECM Receptor Interaction• LOX Remodelling• MMP Remodelling	<ul style="list-style-type: none">• EMT• Cell Differentiation• Cell Motility• Cell Adhesion• EMT to Metastasis• TGFB Signalling	<ul style="list-style-type: none">• Metastasis Response• Metastasis Suppressors• HIF1A Signalling• Hypoxia Response• Regulation of Metabolism• Carbon Cancer Metabolism• Cell Proliferation• Cell Growth Factors• Choline Cancer Metabolism• Cell Cycle
277 genes	254 genes	269 genes	173 genes

For this assay, DU145 cell line was selected due to the relatively higher expression of endogenous EPCR, and shRNA4 was selected as knockdown due to the overall most significant effects on cancer progression features (i.e. cell proliferation, migration and invasion potential, EMT markers expression). Total RNA samples were extracted from whole-cell lysates of control (Empty vector) and knock down (shRNA4) DU145 cells, for a total of four individual samples for each cell line. For this assay, RNA samples were loaded to the nCounter® Prep Station according to the manufacturer's instructions with a concentration of 100ng/5mL each as described in section 3.2.2.6.2. Data were collected by the nCounter® Digital Analyser and analysed using the NanoString nSolver analysis software.

The 770 genes investigated in the PanCancer panel were analysed for their differential expression in shRNA4 versus control cell populations. The most significantly modulated genes were sorted by p-value and the top 20 were selected. Figure 3.12 shows the top 20 selected genes sorted by \log_2 fold change with detailed relative expression (\log_{10}) across each of the four replicates.

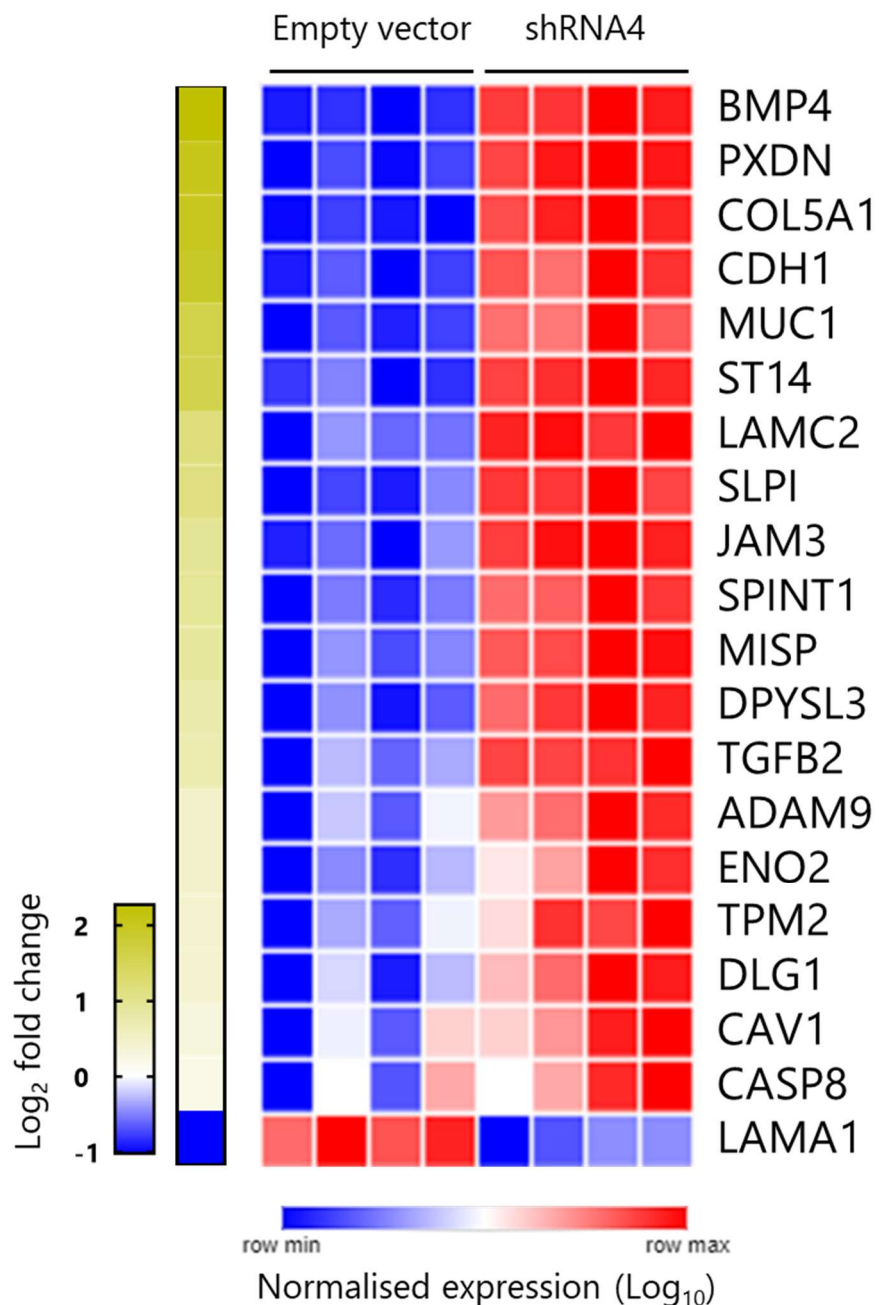


Figure 3.12 – Profile changes in mRNA expression after EPCR knock down with shRNA4 in DU145 cells.
Heatmap showing the top 20 significantly modulated genes in knock down (shRNA4) DU145 against baseline of control DU145 (Empty vector). Values across rows indicate relative \log_{10} mRNA expression. Genes were ordered according to their \log_2 fold expression value for treated vs. control, shown as colour gradient in the bar above the heatmap. Created with the online software Morpheus, <https://software.broadinstitute.org/morpheus>.

Table 3.6 – Top 20 significant p-value genes. The genes are shown as up-regulated (blue) and down-regulated (red) based on the fold change expressed as \log_2 . For each modulated gene, involved pathways are listed according to analysis carried out with NanoString nSolver analysis software.

Gene name	Fold change	p-value	Pathway involved
BMP4	2.27	3.08E-08	Cell Proliferation, Cell Growth Factor, Sprouting Angiogenesis, Stem Cell Associated, TGFB Signalling
PXDN	2.02	2.02E-08	ECM Structure
COL5A1	1.99	9.10E-07	Basement Membrane, Cell Adhesion, Cell Growth Factor, Collagen Family, ECM Receptor Interaction, ECM Structure, Vasculogenesis
CDH1	1.93	2.64E-06	Cell Adhesion, Epithelial to Mesenchymal Transition, Integral to Membrane, Metastasis Suppressors, MMP Remodelling, Plasma Membrane, Stem Cell Associated
MUC1	1.61	4.97E-06	Cell Cycle, Epithelial to Mesenchymal Transition, Plasma Membrane
ST14	1.59	7.72E-06	Epithelial to Mesenchymal Transition, Plasma Membrane
LAMC2	1.16	7.50E-06	Cell Adhesion, ECM Receptor Interaction
SLPI	1.12	4.18E-06	ECM Structure, Epithelial to Mesenchymal Transition
JAM3	0.942	1.11E-06	Angiogenesis Response, Cell Adhesion, Epithelial to Mesenchymal Transition
SPINT1	0.933	6.15E-07	Epithelial to Mesenchymal Transition, Vasculogenesis
MISP	0.853	3.37E-07	Epithelial to Mesenchymal Transition
DPYSL3	0.747	3.10E-06	Epithelial to Mesenchymal Transition, Metastasis Suppressors
TGFB2	0.702	4.93E-06	Angiogenesis Response, Cell Cycle, Cell Proliferation, Cell Differentiation, Cell Growth Factor, ECM Structure, Epithelial to Mesenchymal Transition, Hypoxia Response, TGFB Signalling
ADAM9	0.469	5.16E-06	Cell Adhesion, Cell Growth Factor, Collagen Family, Integral to Membrane, MMP Remodelling, Plasma Membrane
ENO2	0.469	5.24E-06	HIF1A Signalling, Plasma Membrane
TPM2	0.442	7.02E-06	Epithelial to Mesenchymal Transition
DLG1	0.423	2.31E-06	Basal Lamina, Cell Adhesion, Cell Cycle, Cell Proliferation, Cell Differentiation, Plasma Membrane
CAV1	0.311	2.90E-07	Angiogenesis Response, Cell Adhesion, Cell Proliferation, Epithelial to Mesenchymal Transition, Hypoxia Response, Integral to Membrane, Plasma Membrane, Stem Cell Associated
CASP8	0.211	2.73E-06	Angiogenesis Response, Metastasis Suppressors, MMP Remodelling
LAMA1	-1.02	1.17E-06	Basement Membrane, Cell Adhesion, ECM Receptor Interaction, ECM Structure

Table 3.6 shows the top 20 significant p-value differentially expressed genes alongside with the relative pathways affected by each gene. The analysis revealed that upon EPCR silencing the most significantly modulated genes were involved mainly in Cell Adhesion, EMT, and Angiogenesis.

3.3.4.3 Analysis of the effect of EPCR silencing on cellular protein expression in DU145 cells

To investigate further the effects of EPCR silencing at protein level, a quantitative proteomics profiling mass spectrometry (MS) analysis was performed on the same cell populations analysed with NanoString technology. The aim of the proteomics experiment was to identify the proteins whose endogenous expression patterns were altered following EPCR silencing and quantify their relative expression levels. Therefore, MS analysis was performed on both DU145 expressing the Empty vector and DU145 expressing the knockdown construct shRNA4 cell populations. The MS analysis was carried on whole cell lysates samples as described in section 3.2.2.6.2 of this chapter. Data obtained were analysed applying the 1% false discovery rate (FDR). From the analysis conducted, 3512 protein IDs were obtained. Information about protein identities was retrieved from UniProt Knowledgebase (UniProtKB). Eventually, the most modulated proteins were selected with 0.5 fold change \log_2 value and 50% confidence cut-off. Applying such criteria, 100 significantly modulated proteins were selected (Table 3.7).

Table 3.7 – The list of proteins differentially expressed in whole cell lysate from DU145 EPCR knockdown (EPCR shRNA4) vs. DU145 control (Empty vector) cell populations. The table offers the list of the 100 most significantly modulated genes out of 3512 modulated genes, obtained applying 0.5 fold change \log_2 and 50% confidence cut-off. Proteins listed in the red table are upregulated in knockdown vs. control cell populations, whereas the blue table shows downregulated proteins in knockdown vs. control cell populations.

Protein ID	Gene name	Fold change	Confidence level (%)	Protein names
P35527	KRT9	2.33	85	Keratin, type I cytoskeletal 9
P61457	PCBD1	2.18	56	Pterin-4-alpha-carbinolamine dehydratase
Q9BW04	C1orf116	1.88	68	Specifically androgen-regulated gene protein
Q04828	AKR1C1	1.80	69	Aldo-keto reductase family 1 member C1
P13645	KRT10	1.74	86	Keratin, type I cytoskeletal 10
P04264	KRT1	1.67	86	Keratin, type II cytoskeletal 1
P35908	KRT2	1.53	77	Keratin, type II cytoskeletal 2 epidermal
P40222	TXLNA	1.35	51	Alpha-taxilin
Q07866	KLC1	1.31	78	Kinesin light chain 1
Q01469	FABP5	1.14	80	Fatty acid-binding protein 5
Q9BWJ5	SF3B5	1.07	61	Splicing factor 3B subunit 5
Q13206	DDX10	1.05	55	Probable ATP-dependent RNA helicase DDX10
P40616	ARL1	1.03	60	ADP-ribosylation factor-like protein 1

Protein ID	Gene name	Fold change	Confidence level (%)	Protein names
Q16775	HAGH	0.99	52	Hydroxyacylglutathione hydrolase, mitochondrial
P05787	KRT8	0.99	87	Keratin, type II cytoskeletal 8
O00151	PDLIM1	0.97	95	PDZ and LIM domain protein 1
O75146	HIP1R	0.95	56	Huntingtin-interacting protein 1-related protein
Q01995	TAGLN	0.91	50	Transgelin
Q9H2U1	DHX36	0.89	56	ATP-dependent DNA/RNA helicase DHX36
Q96EQ0	SGTB	0.87	77	Small glutamine-rich tetratricopeptide repeat-containing protein beta
Q14195	DPYSL3	0.87	85	Dihydropyrimidinase-related protein 3
P80723	BASP1	0.86	54	Brain acid soluble protein 1
P62633	CNBP	0.85	87	Cellular nucleic acid-binding protein
Q6KB66	KRT80	0.83	85	Keratin, type II cytoskeletal 80
Q14192	FHL2	0.82	74	Four and a half LIM domains protein 2
P24844	MYL9	0.81	88	Myosin regulatory light polypeptide 9
P23497	SP100	0.79	63	Nuclear autoantigen Sp-100
P05783	KRT18	0.76	97	Keratin, type I cytoskeletal 18
P55884	EIF3B	0.74	50	Eukaryotic translation initiation factor 3 subunit B
O95361	TRIM16	0.74	54	Tripartite motif-containing protein 16
P31949	S100A11	0.74	87	Protein S100-A11
Q14019	COTL1	0.71	65	Coactosin-like protein
P67936	TPM4	0.70	87	Tropomyosin alpha-4 chain
P68366	TUBA4A	0.70	93	Tubulin alpha-4A chain
Q92599	SEPTIN8	0.70	70	Septin-8
Q4V328	GRIPAP1	0.68	54	GRIP1-associated protein 1
O95218	ZRANB2	0.67	65	Zinc finger Ran-binding domain-containing protein2
P23284	PPIB	0.66	79	Peptidyl-prolyl cis-trans isomerase B
P31947	SFN	0.66	80	14-3-3 protein sigma
P63241	EIF5A	0.66	83	Eukaryotic translation initiation factor 5A-1
O60502	OGA	0.65	77	Protein O-GlcNAcase
P06748	NPM1	0.65	55	Nucleophosmin
P06703	S100A6	0.65	62	Protein S100-A6
P42345	MTOR	0.65	55	Serine/threonine-protein kinase mTOR
Q9NQC3	RTN4	0.64	71	Reticulon-4
Q96T51	RUFY1	0.64	54	RUN and FYVE domain-containing protein 1
P09651	HNRNPA1	0.64	54	Heterogeneous nuclear ribonucleoprotein A1
Q16719	KYNU	0.64	69	Kynureninase
Q9UHB6	LIMA1	0.63	86	LIM domain and actin-binding protein 1
P32320	CDA	0.63	91	Cytidine deaminase
O95260	ATE1	0.63	59	Arginyl-tRNA--protein transferase 1
P25685	DNAJB1	0.62	60	DnaJ homolog subfamily B member 1
Q6GMV3	PTRHD1	0.61	58	Putative peptidyl-tRNA hydrolase PTRHD1
P09493	TPM1	0.60	83	Tropomyosin alpha-1 chain
O00170	AIP	0.59	53	AH receptor-interacting protein
P51114	FXR1	0.59	63	Fragile X syndrome-related protein 1
O43491	EPB41L2	0.58	83	Band 4.1-like protein 2
P04080	CSTB	0.58	85	Cystatin-B
P62158	CALM	0.57	52	Calmodulin

Protein ID	Gene name	Fold change	Confidence level (%)	Protein names
O75828	CBR3	0.57	64	Carbonyl reductase [NADPH] 3
Q9Y3X0	CCDC9	0.57	56	Coiled-coil domain-containing protein 9
O75347	TBCA	0.57	67	Tubulin-specific chaperone A
P13693	TPT1	0.57	53	Translationally-controlled tumor protein
Q13501	SQSTM1	0.56	90	Sequestosome-1
Q9NR12	PDLIM7	0.55	57	PDZ and LIM domain protein 7
O60701	UGDH	0.55	91	UDP-glucose 6-dehydrogenase
Q15185	PTGES3	0.54	67	Prostaglandin E synthase 3
Q15582	TGFB1	0.54	65	Transforming growth factor-beta-induced protein
Q96T37	RBM15	0.54	56	Putative RNA-binding protein 15
Q13630	TSTA3	0.53	56	GDP-L-fucose synthase
P62328	TMSB4X	0.53	59	Thymosin beta-4
Q8IVT2	MISP	0.53	58	Mitotic interactor and substrate of PLK1
P48506	GCLC	0.53	61	Glutamate--cysteine ligase catalytic subunit
Q86WR7	PROSER2	0.52	56	Proline and serine-rich protein 2
Q96HC4	PDLIM5	0.51	80	PDZ and LIM domain protein 5

Protein ID	Gene name	Fold change	Confidence level (%)	Protein names
Q9BTW9	TBCD	-0.50	51	Tubulin-specific chaperone D
Q96T76	MMS19	-0.50	53	MMS19 nucleotide excision repair protein homolog
P40926	MDH2	-0.51	72	Malate dehydrogenase, mitochondrial
Q96AG4	LRRC59	-0.58	63	Leucine-rich repeat-containing protein 59
P13995	MTHFD2	-0.58	57	Bifunctional methylenetetrahydrofolate dehydrogenase/cyclohydrolase, mitochondrial
P53597	SUCLG1	-0.58	51	Succinate--CoA ligase subunit alpha
P42785	PRCP	-0.61	53	Lysosomal Pro-X carboxypeptidase
P08243	ASNS	-0.61	50	Asparagine synthetase [glutamine-hydrolyzing]
Q9UM22	EPDR1	-0.61	89	Mammalian ependymin-related protein 1
P63173	RPL38	-0.63	73	60S ribosomal protein L38
P02795	MT2A	-0.67	67	Metallothionein-2
P35232	PHB	-0.70	89	Prohibitin
P48047	ATP5PO	-0.72	59	ATP synthase subunit O, mitochondrial
Q9UMX0	UBQLN1	-0.75	51	Ubiquilin-1
P04792	HSPB1	-0.80	85	Heat shock protein beta-1
Q99877	H2BC15	-0.81	57	Histone H2B type 1-N
P16104	H2AX	-0.88	87	Histone H2AX
Q92995	USP13	-0.99	54	Ubiquitin carboxyl-terminal hydrolase 13
Q6FI13	H2AC18-/19	-1.21	65	Histone H2A type 2-A
O00425	IGF2BP3	-1.48	68	Insulin-like growth factor 2 mRNA-binding protein 3
P55210	CASP7	-2.28	53	Caspase-7
Q96QR8	PURB	-2.97	52	Transcriptional activator protein Pur-beta
Q9BTM9	URM1	-3.37	54	Ubiquitin-related modifier 1
Q9NQ88	TIGAR	-4.11	52	Fructose-2,6-bisphosphatase TIGAR
P58107	EPPK1	-4.20	53	Epiplakin

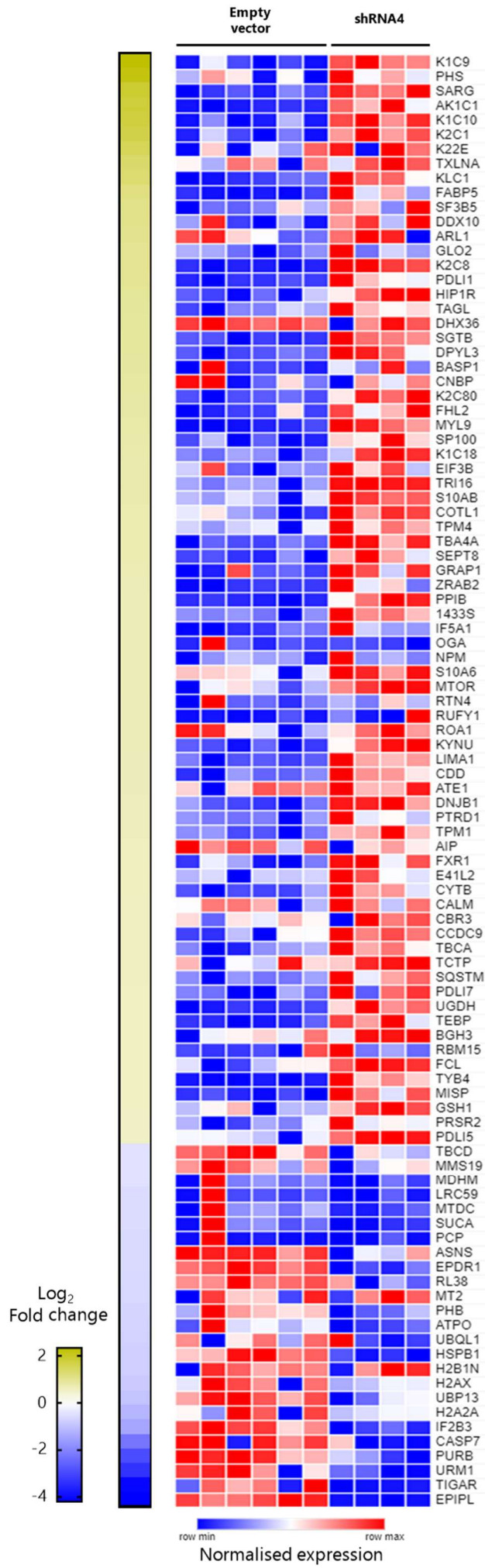


Figure 3.13 – Heatmap showing the top 100 significantly modulated proteins in shRNA4 vs. control DU145 cells. Heatmap shows 75 genes upregulated, and 25 genes downregulated in EPCR knockdown (shRNA4) vs. control (Empty vector) DU145 cell population. Proteins were selected with 0.5 log₂ fold-change and 50% confidence cut-off.

Figure 3.13 shows the heatmap created using the online software "Morpheus" with the 75 proteins upregulated and 25 downregulated in the shRNA4 versus the control samples, sorted by \log_2 fold change, with the relative normalised \log_{10} expression values for each replicate.

In order to investigate further the effect of EPCR silencing on protein expression modulation, the results obtained by the MS analysis were utilised to perform an expression analysis using the Analysis Tool on *Reactome.org*. Protein IDs and relative \log_2 fold change values were used to produce a scaled coloured overlay over Reactome pathway diagram, to visualise relative expression levels (Figure 3.14). 75 out of 100 identifiers in the sample were found in Reactome, where 482 pathways were hit by at least one of them. All identifiers were matched with the species '*Homo sapiens*' and resource 'UniProt'.

A list of the 25 most relevant pathways was generated based on the relative expression of proteins in the knockdown cell population (Table 3.8). Amongst the most significantly affected pathways are 'Formation of the cornified envelope' and 'Keratinisation' due to the down regulation of 7 members of the Keratin protein family in the knockdown cell population. 'RHO GTPases activate PKNs' and 'RHO GTPases Effectors' are also affected by EPCR silencing. Interestingly, the up regulated proteins responsible for the modulation of the majority of the pathways significantly are histone H2A and H2B variants.

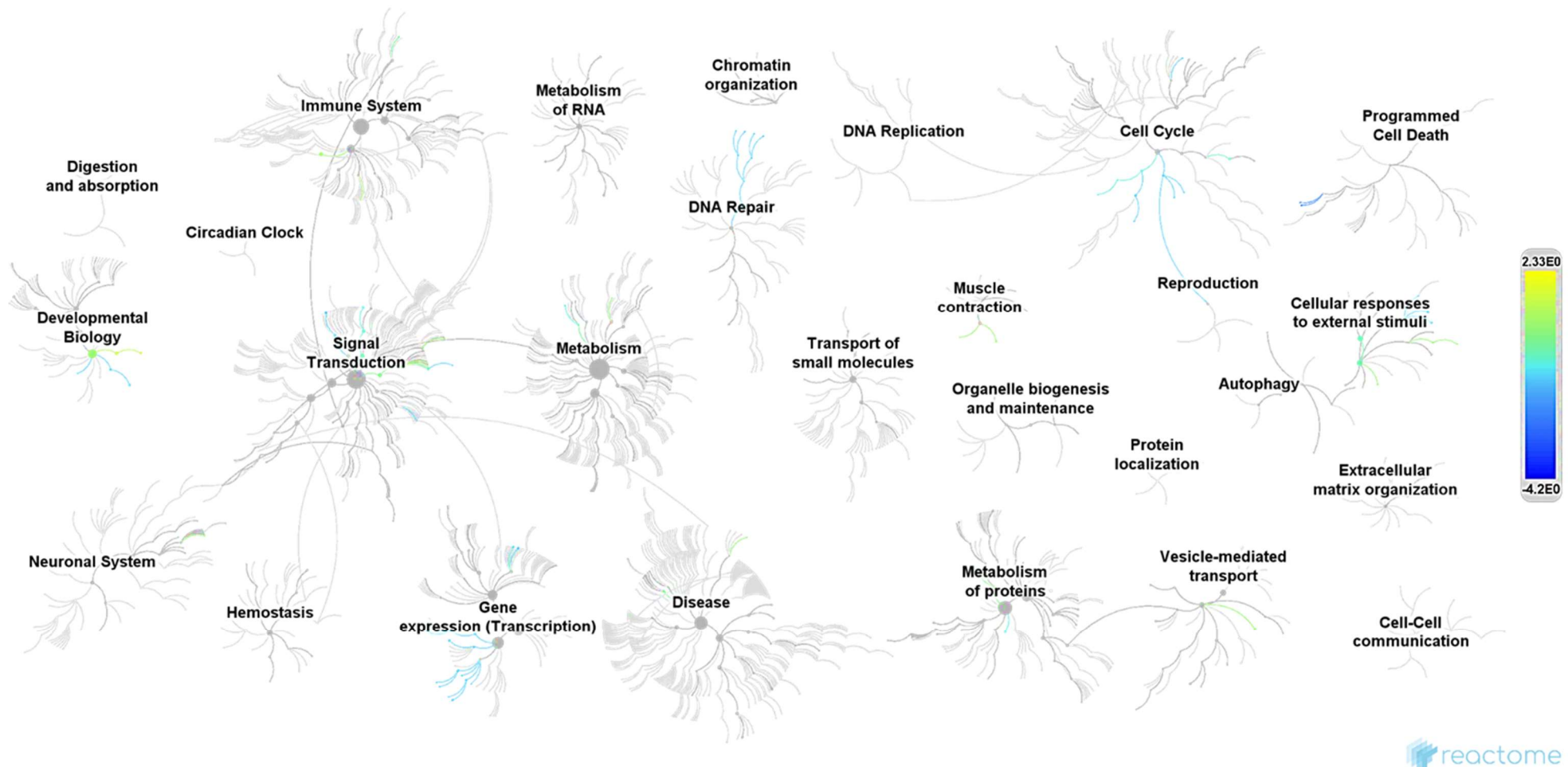


Figure 3.14 – Genome-wide overview of the Reactome pathway analysis. The diagram shows a genome-wide overview of the results of the pathway analysis. Pathways are arranged in a hierarchy, the centre of each of the circular "bursts" being the root of one top-level pathway. Each step away from the centre represents the next level lower in the pathway hierarchy. The colour code denotes over-representation of that pathway in the input dataset. Light grey signifies pathways that are not significantly over-represented. (<https://reactome.org/>)

Table 3.8 – Pathways regulated by proteins differentially expressed in EPCR knockdown (shRNA4) vs. control (Empty vector) cell populations. The following table shows the 25 most relevant pathways (p-value <0.01) sorted by p-value. **Blue** indicates upregulated genes and **red** downregulated proteins in shRNA4 vs. control cells.

Pathway name	Protein names	Entities found	p-value
Formation of the cornified envelope	Keratin, type II cytoskeletal 8, Keratin, type I cytoskeletal 9, Keratin, type I cytoskeletal 10, Keratin, type II cytoskeletal 80, Keratin, type I cytoskeletal 18, Keratin, type II cytoskeletal 2 epidermal, Keratin, type II cytoskeletal 1	7 / 129	1.52E-04
RHO GTPases activate PKNs	Histone H2AX, Histone H2B type 1-N, 14-3-3 protein sigma, Histone H2A type 2-A, Myosin regulatory light polypeptide 9	5 / 63	2.52E-04
Smooth Muscle Contraction	Tropomyosin alpha-1 chain, Tropomyosin alpha-4 chain, Myosin regulatory light polypeptide 9, Calmodulin	4 / 39	4.14E-04
Post-chaperonin tubulin folding pathway	Tubulin-specific chaperone D, Tubulin-specific chaperone A, Tubulin alpha-4A chain	3 / 23	0.001
HSF1-dependent transactivation	Serine/threonine-protein kinase mTOR, Prostaglandin E synthase 3, DnaJ homolog subfamily B member 1	3 / 24	0.001
Deposition of new CENPA-containing nucleosomes at the centromere	Histone H2AX, Histone H2B type 1-N, Nucleophosmin, Histone H2A type 2-A	4 / 54	0.001
Nucleosome assembly	Histone H2AX, Histone H2B type 1-N, Nucleophosmin, Histone H2A type 2-A	4 / 54	0.001
Aryl hydrocarbon receptor signalling	AH receptor-interacting protein, Prostaglandin E synthase 3	2 / 7	0.002
RUNX1 regulates genes involved in megakaryocyte differentiation and platelet function	Histone H2AX, Histone H2B type 1-N, Histone H2A type 2-A, Myosin regulatory light polypeptide 9	4 / 66	0.003
RNA Polymerase I Promoter Opening	Histone H2AX, Histone H2B type 1-N, Histone H2A type 2-A	3 / 32	0.003
Keratinisation	Keratin, type II cytoskeletal 8, Keratin, type I cytoskeletal 9, Keratin, type I cytoskeletal 10, Keratin, type II cytoskeletal 80, Keratin, type I cytoskeletal 18, Keratin, type II cytoskeletal 2 epidermal, Keratin, type II cytoskeletal 1	7 / 217	0.003
Packaging Of Telomere Ends	Histone H2AX, Histone H2B type 1-N, Histone H2A type 2-A	3 / 33	0.003
DNA methylation	Histone H2AX, Histone H2B type 1-N, Histone H2A type 2-A	3 / 34	0.003

Pathway name	Protein names	Entities found	p-value
Activated PKN1 stimulates transcription of AR (androgen receptor) regulated genes KLK2 and KLK3	Histone H2AX, Histone H2B type 1-N, Histone H2A type 2-A	3 / 36	0.004
SIRT1 negatively regulates rRNA expression	Histone H2AX, Histone H2B type 1-N, Histone H2A type 2-A	3 / 37	0.004
RHO GTPase Effectors	Histone H2AX, Histone H2B type 1-N, 14-3-3 protein sigma , Histone H2A type 2-A, Myosin regulatory light polypeptide 9 , Kinesin light chain 1 , Tubulin alpha-4A chain , Calmodulin	8 / 295	0.005
Cleavage of the damaged purine	Histone H2AX, Histone H2B type 1-N, Histone H2A type 2-A	3 / 38	0.005
Depurination	Histone H2AX, Histone H2B type 1-N, Histone H2A type 2-A	3 / 39	0.005
Recognition and association of DNA glycosylase with site containing an affected purine	Histone H2AX, Histone H2B type 1-N, Histone H2A type 2-A	3 / 39	0.005
Amyloid fibre formation	Histone H2AX, Histone H2B type 1-N, Histone H2A type 2-A, Transforming growth factor-beta-induced protein ig-h3	4 / 80	0.006
PRC2 methylates histones and DNA	Histone H2AX, Histone H2B type 1-N, Histone H2A type 2-A	3 / 42	0.006
Cleavage of the damaged pyrimidine	Histone H2AX, Histone H2B type 1-N, Histone H2A type 2-A	3 / 42	0.006
Depyrimidination	Histone H2AX, Histone H2B type 1-N, Histone H2A type 2-A	3 / 42	0.006
Recognition and association of DNA glycosylase with site containing an affected pyrimidine	Histone H2B type 1-N, Histone H2A type 2-A	3 / 42	0.006
Attenuation phase	Prostaglandin E synthase 3 , Dnaj homolog subfamily B member 1	2 / 14	0.007

3.4 Discussion

In this chapter, results of functional studies conducted to investigate EPCR involvement in PCa progression are presented. Stable EPCR knockdowns were generated in DU145 and PC3 cell lines, which were chosen as *in vitro* PCa models due to their significant expression of EPCR. Firstly, for each construct efficiency of EPCR silencing was assessed at the transcript level, then the absence of the protein from the cell surface confirmed by flow cytometry. Subsequently, cell populations showing the two most efficient knockdowns were selected to perform the functional studies. Collectively, the findings show that silencing of EPCR significantly reduce cell proliferation and clonogenic potential in both DU145 and PC3 cell lines. Such results are consistent with studies conducted in other cancer models. Indeed, EPCR knockdown was showed to inhibit cell proliferation in gastric cancer cells (Wang, Yang et al. 2018) and to have a tumorigenic and prometastatic activity in breast cancer (Perurena et al. 2017). Perurena and colleagues analysed a cohort of 286 breast cancer patients, finding a correlation between EPCR high expression levels and poor clinical outcome. Moreover, they showed that EPCR silencing affected cell growth in 3D cultures but not 2D cultures of several breast cancer cell lines. Their study also provided evidence about EPCR silencing reducing metastasis formation in bone and lungs.

Furthermore, cell migration and invasion potential was assessed upon EPCR silencing. Results presented in this chapter show that the intrinsic invasive potential in both DU145 and PC3 cells was impaired following the loss of EPCR protein. Similar results were obtained in PCa by Menschikowski and colleagues during a study on EPCR transient knockdown (Menschikowski et al. 2011). The relationship between EPCR expression and invasive behaviour in cancers of different origins is widely reported in the literature. *In vivo* studies in human and murine xenograft breast cancer models show that silencing of EPCR significantly reduced the occurrence of bone metastases (Perurena et al. 2017). Cell proliferation and migration was demonstrated to be negatively affected by EPCR silencing in gastric cancer due to the failure of EPCR to mediate activation of protease-activated receptor 1 (PAR1) and the consequent inhibition of ERK1/2 (Wang et al. 2018).

To further characterise EPCR involvement in early stage of cancer progression, evaluation of EMT was conducted since such process is the first step in tumour progression and metastasis cascade. Thus, Western blot analysis of the expression of a panel of EMT-associated markers,

namely β -catenin, E-cadherin, N-cadherin, vimentin, and ZO1 was performed. β -catenin, E-cadherin, and ZO1 represent the key markers of EMT due to their role in assembling of cell junctions. Particularly, downregulation of E-cadherin is one of the main initiation signals of EMT (Acloque, Adams et al. 2009b). Nevertheless, role of E-cadherin in EMT and cancer progression is controversial due to the contrasting findings in several studies. Studies conducted in DU145 and PC3 cells revealed that E-cadherin was upregulated in a highly invasive subpopulation displaying stem cell features (Bae, Parker et al. 2011). However, contrasting studies showed that E-cadherin downregulation in PCa cells leads to opposite effects on cell migration and invasion (Zhou, Yan et al. 2009; Chunthapong, Seftor et al. 2004). Western blot analysis performed in the present study revealed that epithelial markers were up regulated in knockdown cell populations whereas mesenchymal markers showed a decreased expression in knockdowns compared to control cell populations. The same trend was shared by both shRNA1 and shRNA4 across DU145 and PC3 cell lines. Particularly, upregulation of mesenchymal markers such as N-cadherin and vimentin is reported to be a signature on CTCs in patients with mHRPC (Armstrong, Marengo et al. 2011). Recent study in DU145 and PC3 cells reports that upregulation of epithelial markers and simultaneous downregulation of mesenchymal markers enhanced cell migration and invasion (Wang, Wang et al. 2017), in agreement with our findings.

Interestingly, a correlation between EPCR reduced expression and the expression pattern of the EMT markers was showed in multipotent mammary stem cells (MaSCs) in a murine model. Indeed, Wang and colleagues demonstrated that a subpopulation of basal MaSCs positive for EPCR exhibit EMT features, such as decreased expression of epithelial markers and increased expression of mesenchymal ones, linking such population with breast cancer initiation (Wang et al. 2015). An interesting remark about the relationship between EPCR expression, EMT, and cell stemness in cancer progression is the role of EPCR as a marker for stem cells in human breast (Schaffner, Yokota et al. 2013) and prostate (Montanari, Rossetti et al. 2017) cancers. Notably, EMT mechanisms were studied mainly in cells derived from secondary lesions, such is the case of DU145 and PC3 cells. Interesting recent study of spontaneous EMT in PCa showed that primary cell lines can be a more suitable and appropriate model for the purpose. Indeed, data collected by Harner-Foreman and colleagues indicate that Type 3 EMT features can be shared by both aggressive stem-like and non-aggressive non-stem-like cells (Harner-Foreman, Vadakekolathu et al. 2017). Thus, it is important to highlight that previous understandings regarded EMT as a binary state in

cell identity whereas recent developments suggest EMT as a more dynamic spectrum, meaning that transforming cancer cells can at any stage display different epithelial and/or mesenchymal markers expression in the so-called partial or hybrid EMT state (Liao, Yang 2020).

In order to obtain a broader understanding of the effects that EPCR silencing has on the transcriptome expression in PCa cells, mRNA profiling analysis was conducted on one of the knockdown cell populations generated in DU145 cell line. Results obtained provide an interesting overall picture of the effects of EPCR silencing, yet partially questioning the evidence collected by the previous functional studies. Analysis of the individual genes that are significantly modulated in populations under study provides a closer insight into the pathways affected and the consequent effect on cell behaviour. As summarised in the PanCancer Progression panel gene list specifications, genes such as CAV1, DPYSL3, JAM3 fall into the mesenchymal spectrum, whereas CDH1 (E-cadherin), MUC1, SPINT1, ST14 belong to the epithelial spectrum. Interestingly, the fold change measured of the epithelial genes in the present experiment is relatively higher than the mesenchymal ones. DLG1 gene, upregulated in the knockdown cell population, is involved in adherens junction assembly and cell cycle, acting as an essential tumour suppressive gene (Chalmers, Whitley et al. 2012). Loss of DLG1 has been shown to correlate with poor prognosis in several cancers (Sandoval, Graham et al. 2013). BMP4, also upregulated in knockdown cell population, is a member of the TGFB superfamily with reported dual role in cancer (Bach, Park et al. 2017). Studies on murine PCa xenografts showed BMP4 high expression to promote bone metastasis formation (Lee, Cheng et al. 2011).

Pathway analysis conducted on MS results in the present study highlighted that proteins involved in the most significantly modulated pathways are keratins, a subgroup of the Intermediate Filament proteins family. Keratins are recognised as epithelial cell markers and have been showed to regulate several cellular functions, such as apico-basal polarization, motility, and signalling (Karantza 2011). In their study, Fortier and colleagues showed that loss of Keratins 8/18 (K8/18) in endometrial, hepatocellular, and cervical carcinomas is associated with increased cell migration and chemoresistance (Fortier, Asselin et al. 2013). Interestingly, such processes, commonly underlying cancer progression's early stage EMT, were in place without any modulation in EMT markers expression. Keratins (K) are used to discriminate between basal and luminal cells in normal human prostate epithelium, with the

epithelial markers K8/18 expressed in luminal cells and K5/18 expressed in basal cells. Interestingly, prostate metastases were showed to be consistently expressing K18 (van Leenders, Geert, et al. 2001). Expression of K8/18 proteins has also been correlated with invasion and poor prognosis in oral squamous cell carcinomas (Fillies, Werkmeister et al. 2006). In the present study, keratin proteins appear to be downregulated in EPCR knockdown DU145 cells, which can be interpreted as a sign of decreased epithelial phenotype in the examined population, although, as previously mentioned, K18 downregulation can be expected to combine with decreased invasive behaviour.

The most overrepresented modulated proteins in the pathway analysis belong to the histone family, all of which have been found upregulated in the knockdown cell population. H2A and H2B form one of the core subunits in the nucleosome (Placek, Harrison et al. 2005). H2A.X, a H2A variant, is involved in activation of DNA-damage repair pathways and its downregulation is associated with tumorigenesis (Jeggo, Löbrich 2007). Furthermore, it has been demonstrated to regulate EMT and signalling in colon cancer metastasis. Indeed, silencing of H2A.X was reported to be inducing mesenchymal-like features and EMT transcription factors activation in human colon cancer cells (Weyemi, Redon et al. 2016).

Rho GTPase pathway is another significantly modulated one in our pathway analysis. EPCR role in Rho GTPase pathway has been studied in gastric cancer. Recent studies showed a correlation between the inhibition of the aPC/EPCR/PAR-1 axis by ALEX1 and decreased cell proliferation and metastasis formation in both gastric and lung cancer (Pang, Li et al. 2018). Such ALEX-1 activity was reported to be linked to the consequent attenuation of the Rho GTPase signalling pathway. Such pathway figures amongst the most significantly modulated ones in the pathway analysis performed with Reactome.

The EPCR-mediated PAR-1 activation has great relevance in cancer progression and its cytoprotective effects have been extensively demonstrated in recent studies and correlated with anti-apoptotic activity (Mohan Rao et al. 2014). Interestingly, EPCR overexpression and recombinant human activated protein C (rhaPC) administration in murine metastatic melanoma models reduced lung and liver metastases, highlighting the complex and multivocal role of the aPC/EPCR axis (Bezuhly, Cullen et al. 2009). In their study on the effects of EPCR knockdown on breast cancer progression, Perurena and colleagues found that silencing human EPCR had no effect on cell cycle progression *in vitro*, while it led to a significant reduction of the primary tumour growth in *in vivo* experiments (Perurena, Zandueta et al. 2017). This study showed that the reduction of tumour growth, in knockdown

cells in both *in vitro* and *in vivo* setups, was independent of activated protein C (aPC) binding, thus indicating that other EPCR-ligands may be involved in EPCR-mediated signalling (Perurena et al. 2017). Moreover, relapse-free analysis in a cohort of 392 breast cancer patients showed that patients with high expression of EPCR had significantly shorter relapse-free times. EPCR was demonstrated to play a role in relevant cancer processes in previous studies. Indeed, EPCR knockdown in gastric cancer was shown to significantly inhibit cell proliferation and migration and promote apoptosis. Furthermore, given its key role as a negative regulator of blood coagulation, EPCR is considered to enhance tumour cells growth potential by enabling malignant cells to maintain an anti-coagulant environment (Tsuneyoshi et al. 2001).

Surprisingly, a case was documented in which EPCR plays a different role in cancer progression. Indeed, in malignant pleural mesothelioma (MPM) ectopic expression of EPCR acts as a tumour suppressor (Keshava, Sahoo et al. 2013).

Taken together the results presented herein show that a relationship between EPCR expression and the proliferative and invasive behaviour of DU145 and PC3 cells, as well as its connection to the EMT process, exists. Our findings are in agreement with the data present in literature.

In conclusion, EPCR emerges as a promising therapeutic target in aggressive PCa. Based on such premise, the following step during the present project consisted in generating new monoclonal antibodies directed against EPCR in order to test them for the application in therapeutic treatment of malignant PCa. The aim being the halt of metastasis formation by targeting cells undergoing EMT. Results will be presented and discussed in the following chapter.

4. Generation, Characterisation, and Validation of Monoclonal Antibodies Targeting EPCR

4.1 Introduction

The novel hybridoma methodology presented by Milstein and Köhler 45 years ago in *Nature*, triggered a revolution in the biomedical research fields.

In their work, for which they were awarded the Nobel Prize in Physiology or Medicine in 1984, Milstein and Köhler described how to produce large amounts of monoclonal antibodies with a desired specificity using hybridomas. Indeed, before the publication of their work it was not possible to isolate single antibodies (targeting specific portion of an antigen) from the pool of polyclonal antibodies generated by the body's immune system targeting an entire antigen. Previous studies showed that single myeloma cells were producing mono-specific antibodies and that it was possible to fuse two myeloma cells generating a functioning hybrid cell able to produce antibodies from both parental cells (Kunkel, Slater et al. 1951; Cotton, Milstein 1973). Unfortunately, the hybrids obtained had a short lifespan, which resulted in poor yield and subsequent recovery. To overcome such limitations, Milstein and Köhler developed a novel approach in which they generated a hybridoma by fusing myeloma cells with splenocytes and cultured these in appropriate selection medium. Therefore, hybridomas show the unlimited division potential of myeloma cells combined with the ability of splenocytes to produce specific antibodies (Köhler, Milstein 1975). The consistency of mAbs across batches, together with the flexibility of epitope targeting they offer, has made them one of the most versatile and fine tool for *in vivo* research (Zaroff, Tan 2019). Nowadays, mAbs are widely used in clinical research, diagnostic and therapeutic field such as in the detection of disease-specific biomarkers, and therapeutic agents, either as naked or conjugated molecules.

MAbs generated using the hybridoma technology have many benefits. To start with, mAbs are biologically refined molecules, which means that they have already gone through the so-called affinity maturation (AM), which is key for a host's immune system to select antibodies with higher affinity for the specific antigen. Somatic hypermutations (SHM) are mutations occurring in the DNA region relative to the CDRs encoding for the variable region of the antibody, the region responsible for the specificity of the antibody for its target. As a consequence of such mutations, several antibody clones able to recognise the same target

but with different affinities are generated and only the ones with the best affinity are selected eventually and expanded (Peled, Kuang et al. 2008). Such process occurs naturally in the host body and B cells harvested from secondary lymphatic organs – such as lymph nodes and spleen- are producing the final matured antibodies. Another consequence of the generation of mAbs in an animal host rather than *in vitro* also involves a natural pairing of light and heavy variable regions with constant domains of the same class, which leads to a lower level of immunogenicity of the molecule (Steinwand, Droste et al. 2014).

Although mAbs can be generated in different host mammals - such as rats, rabbits, mice, or monkeys -, the most commonly used are BALB/c mice because of their high immune reactivity and the availability of compatible fusion partner cells, which ensure chromosomal stability in the resulting hybridomas. Figure 4.1 shows the main steps involved in the process of mAbs generation using the hybridoma technology that was used for this project.

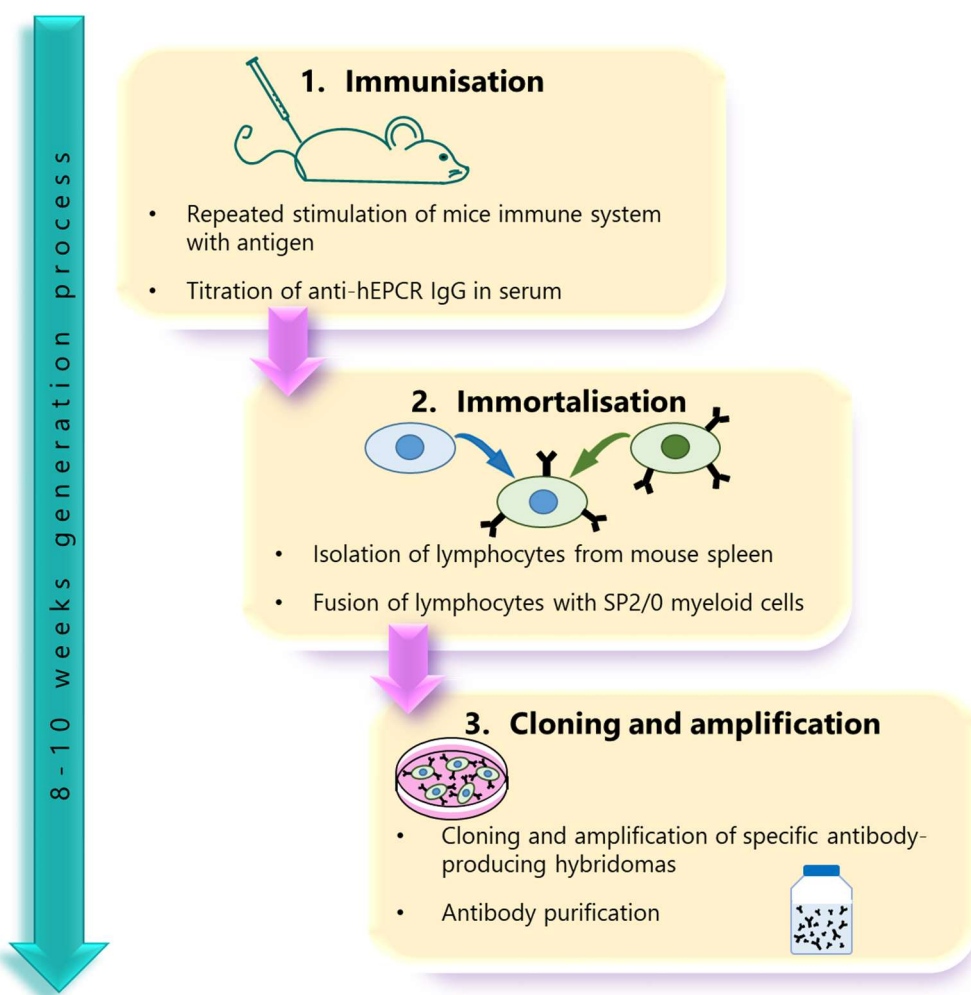


Figure 4.1 – Overview of the mAbs generation process. Generation of mAbs can be a time-consuming process due the considerable length of the individual steps, namely: (1) immunisation of host (in this project mice were used) with the target antigen, (2) generation of immortalised hybrid cells able to produce antibodies; (3) cloning and amplification of hybridomas producing specific antibodies against the desired antigen.

One of the main goals in antibody generation for therapeutic purpose is to obtain stereospecific mAbs. Indeed, mAbs can target the epitope either as a linear or conformational type. While a linear epitope is recognised in the primary structure of the antigen (2D configuration), conformational epitopes depend on the 3D configuration of the antigen determined by the secondary and tertiary protein structure. The type of epitope recognised by a specific mAb depends largely on the strategy used to immunise the mice. Adjuvants used in combination during the antigen administration can be responsible of altering its protein structure, leading to mAbs generated against antigens in a non-native conformation.

The first step of mAbs generation with hybridoma technology is the immunisation of the mice with the target antigen. Based on the characteristics of the targeted molecule, different approaches can be adopted in order to optimise the immunisation step, such as the use of either whole cells, recombinant proteins, or DNA fragments. For the purpose of the present study, the stimulation of the immune response in the host organism was achieved using the recombinant human EPCR protein (Figure 4.2). The recombinant protein used for this part of the project refers to the extracellular domain of the human EPCR (aa 1-209), with a polyhistidine tag added at the C-terminus, and was synthesised by expression in HEK 293T cells. That means that the folding and the post-translational modifications of the recombinant protein are similar to the human native form.

The antigen was administrated in combination with Alum, an aluminium salt-based reagent used as adjuvant in vaccines for two main purposes. Alum acts as a slow-release antigen-storage depot that prolongs the exposure of the immune system to the antigen. Alum also has a mild irritant effect, enhancing the stimulation of the immune system recruiting leukocytes. Therefore, the overall effect of the adjuvant is to increase the immunogenicity of the target-antigen without stimulating CD8 T cell responses (Shaw, Feinberg 2013). Once the presence of the specific antibodies against the target is confirmed in the serum of immunised mouse, B cells are isolated from the spleen and used for the cell immortalisation step.

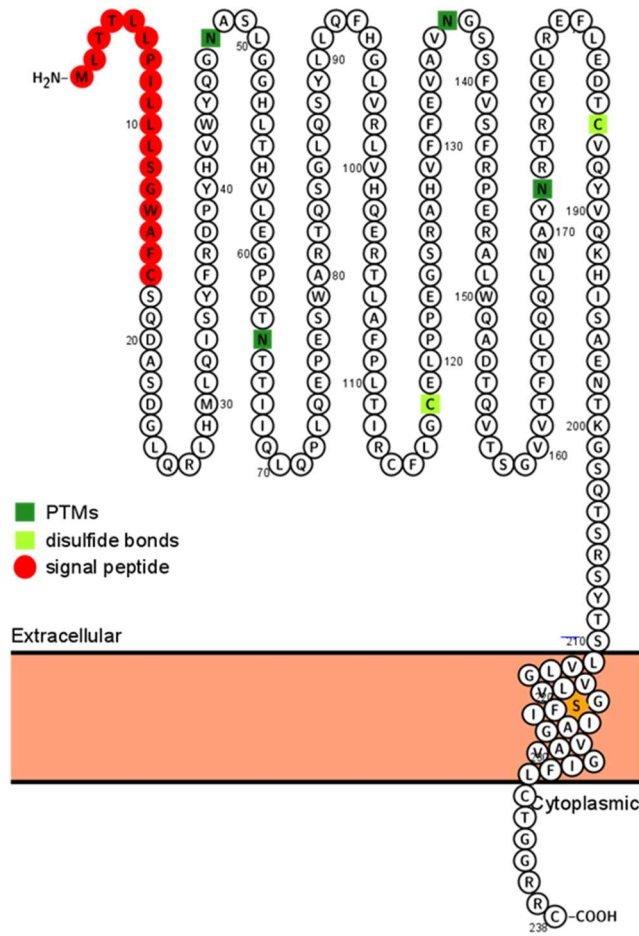


Figure 4.2 – Human EPCR protein. The picture represents the amino acid sequence of the human EPCR protein. Highlighted in red, amino acids (1-17) forming the signal peptide that is cleaved before the protein addressing to the membrane or before protein secretion. Highlighted dark green are the protein post-translational modifications (PTMs) that consist in the four N-glycosylations. Highlighted light green are the two cysteine residues (118, 186) involved in the disulphide bond. (Generated with Protter <http://wlab.ethz.ch/protter/start/> - (Omasits, Ahrens et al. 2014).

Fusion can be performed using three different methods. The first method traditionally used is the chemical fusion, performed using polyethylene glycol (PEG) that enables the fusion of membranes from two adjacent cells acting as a dehydrating agent. A second method is based on the use of viral agents, such as Sendai and vesicular stomatitis virus. The last and most efficient method is the electro cytofusion, which was used for the present project. Mouse B cells isolated from the spleen of the immunised host are fused with immortal myeloma cells SP2/0, also known as SP2/0-Ag-14, derived from the fusion of a BALB/c mouse spleen cell and a mouse myeloma cell. SP2/0 are used as fusion partner cells to generate hybridomas because they originate from the same strain of the mouse used for the immunisation, also they are sensitive to the HAT (hypoxanthine-aminopterin-thymine) media supplement and resistant to 8-azaguanine (Shulman, Wilde et al. 1978). After cell fusion, the generated hybrid cells undergo a selection step based on their ability to

synthesise nucleotides using the salvage pathway (Hnasko, Stanker 2015). Normally, cells can synthesise the nucleotides they require either *de novo* or recycling the denatured nucleotides already present in the cells through the salvage pathway. A key enzyme in such pathway is the hypoxanthin-guanin-phosphoribosyl-transferase (HGPRT), of which myeloma cells are deficient. The aminopterin, a component of the HAT selective medium, blocks the *de novo* synthesis of nucleotides thanks to the action of aminopterin. This means that myeloma cells are not able to synthesise nucleotides using either of the pathways, therefore they cannot survive in presence of HAT. On the other hand, the salvage pathway is fully functional in the antibody-producing lymphocytes so they can survive, but only for a short period of approximately 7 days. Therefore, only hybridomas can survive indefinitely and produce antibodies (Figure 4.3).

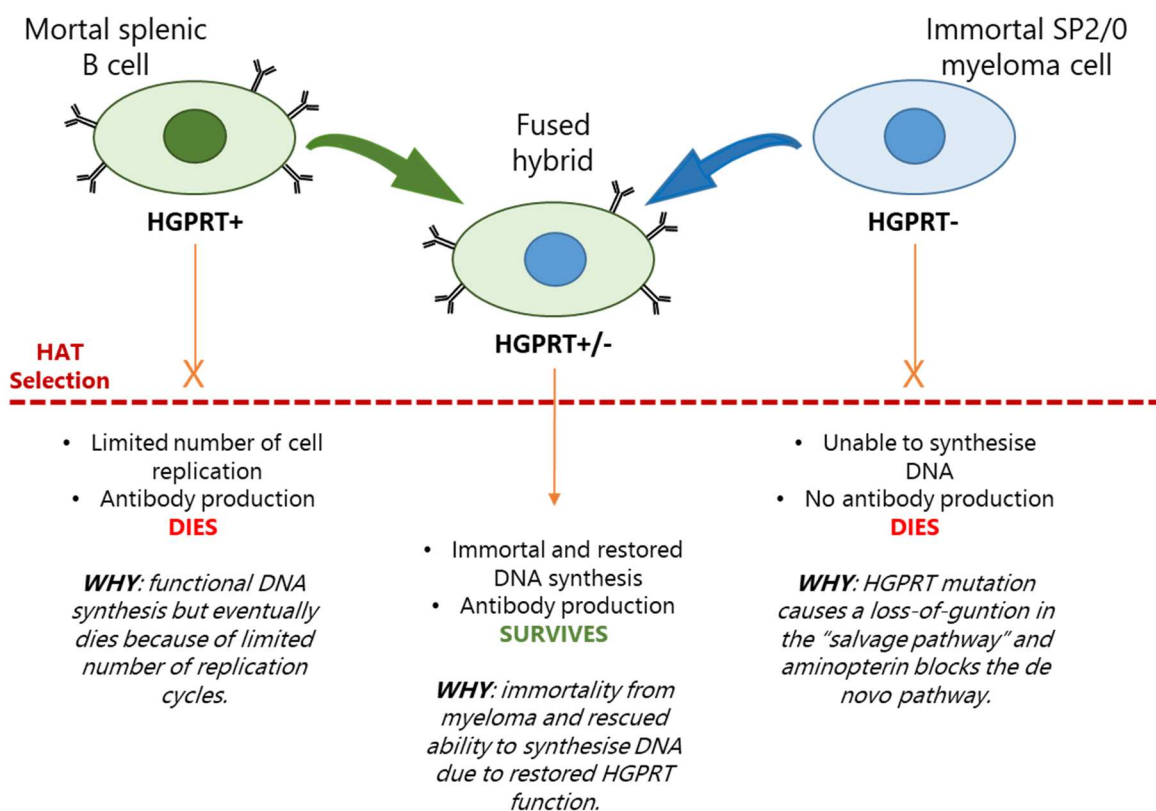


Figure 4.3 – HAT selection for hybridomas. Immortal hybrid cells able to produce antibodies are generated by fusing antibody producing B cells with immortalised myeloma cells and selected adding HAT supplement to the culture medium. Aminopterin prevents *de novo* purine nucleotides synthesis. Normal cells, such as B cells, can activate the salvage pathway to synthesise nucleotides using hypoxanthine and thymine precursors, but they die after few replication cycles. Conversely, myeloma cells are transformed cells able to survive through undetermined replication cycles but cannot survive in presence of aminopterin due to the lack of salvage pathways enzymes such as HGPRT. Correctly fused hetero-hybrid cells (myeloma + B cell) inherit the immortal phenotype proper of the parent myeloma cell and retain the HGPRT enzyme, which supports the nucleotide synthesis through salvage pathway, and the ability to produce IgG from the parental B cell. HAT: hypoxanthine-aminopterin-thymine; HGPRT: hypoxanthin-guanin-phosphoribosyl-transferase.

Hybridomas from the cell fusion produce mAbs with varying specificity and affinity to the target antigen. Thus, screening of hybridomas for the isolation of desired clone is the third important step in mAbs generation. Isolated hybridomas are then scaled up, subsequently, to produce high amounts of target-specific mAbs that can be purified, characterised and validated.

In the present chapter, the process followed for the successful generation of new mAbs targeting the human EPCR using the hybridoma technology is illustrated. This chapter also demonstrates how the purified EPCR antibodies were validated as reagents for various research application used in several analytical platforms. Its utility in clinical and therapeutic space is also explored.

4.2 Materials and Methods

4.2.1 Materials

4.2.1.1 Reagents

CELL CULTURE MEDIA	PROVIDER
EMEM	SLS (Lonza)
RPMI 1640	SLS (Lonza)
DMEM	SLS (Lonza)
CD-Hybridoma medium	Gibco

CULTURE MEDIA SUPPLEMENTS	PROVIDER
2-mercaptoethanol	Gibco
Foetal calf serum (FCS)	Fisher (GE Healthcare)
L-Glutamine	SLS (Lonza)
HEPES	SLS (Lonza)
Sodium Pyruvate	SLS (Lonza)
OPI Media Supplement	Sigma
HAT Media Supplement (50×) Hybri-Max	Sigma
Pen/strep antibiotic solution	SLS (Lonza)
Puromycin	Sigma

OTHER CELL CULTURE REAGENTS	PROVIDER
Dimethyl sulfoxide (DMSO)	Insight Biotechnology
Dulbecco's phosphate buffered saline (DPBS)	SLS (Lonza)
Trypan Blue solution (v/v 0.4%)	Sigma
Trypsin/Versene	SLS (Lonza)

CHEMICALS & BIOCHEMICALS	PROVIDER
Ammonium Persulphate (APS)	Geneflow
Bovine serum albumin (BSA)	Merck
Bromophenol blue	Arcos Organics
Double distilled water (ddH ₂ O)	Barnstead, Nanopure Diamond
Mannitol	Sigma
Nuclease-free water	Ambion
Ethyl alcohol absolute	VWR chemicals
Glycerol	Sigma
Glycine	Sigma
ISOTON II™	Beckman Coulter
Clarity Western ECL Substrate	Bio Rad
Ethanol	Fisher Scientific
Hydrochloric acid (HCl)	Fisher Scientific
Sulfuric Acid (H ₂ SO ₄)	Sigma

IMMUNOCHEMICAL REAGENTS	PROVIDER
Alexa Fluor™ 488 conjugated donkey anti-rat IgG	Invitrogen
Alexa Fluor™ 488 conjugated goat anti-mouse IgG	Invitrogen

Anti-Mouse IgG HRP-linked Ab	Cell Signalling Technology
Goat anti-mouse IgG unlabelled	Southern Biotech
Mouse anti-human EPCR (clone ab56689)	Abcam
Mouse anti-human EPCR (clone M2)	Sigma
Normal Mouse Immunoglobulin	PeproTech
PE rat anti-human CD319 (clone 162.1)	Biolegend
PE mouse anti-human EPCR (clone RCR-401)	Biolegend
Precision Plus Protein™ WesternC™ Blotting Standards	Bio Rad
Precision Protein™ StrepTactin-HRP Conjugate	Bio Rad
Purified Peptide Library	GeneScript
Rat anti-mouse EPCR (clone RCR-252)	Novus Biologicals
ImmEdge™ Pen	Vector
VECTASHIELD® Antifade Mounting Medium with DAPI	Vector

REAGENT KITS	PROVIDER
Protein G GraviTrap	GE Healthcare
Slide-A-Lyzer dialysis cassettes (10K, 12-30 mL)	Thermo scientific
FcR Blocking Reagent	Miltenyi Biotec
LIVE/DEAD™ Fixable Violet Dead Cell Reagent	Thermo Fisher Scientific
TMB Substrate Set	Biolegend

OTHERS	PROVIDER
38 B9 murine pro-B-cell line	ATCC
Alum	Thermo Scientific
BALB/c mice	Trianni Mouse™
DU145 human prostate cancer cell line	ATCC
EPCR Protein, Human, Recombinant (His Tag)	Sino Biological
NIH 3T3 murine fibroblast	ATCC
SP2/0 Hybridoma: B lymphocyte	ATCC

4.2.1.2 Equipment

LABORATORY PLASTICS, GLASSWARE AND SHARPS	PROVIDER
Cell culture flasks (T25, T75, T175)	Sarstedt, UK
Conical flasks (50 mL, 100 mL)	Pyrex
Eppendorf tubes (0.5 mL, 1.5 mL, 2 mL)	Sarstedt, UK
12x75 mm polystyrene flow cytometry tubes	Tyco healthcare group
Falcon tubes (50 mL, 15 mL)	Sarstedt, UK
Filter tips (0.5-10 µL, 2-20 µL, 20-200 µL, 200-1000 µL)	Greiner bio-one/ Sarstedt
Flat-bottom culture dishes (6, 24, 96-well)	Sarstedt, UK
Micropipette tips (0.5-10 µL, 20-200 µL, 200-1000 µL)	Sarstedt, UK
Pipettes (5 mL, 10 mL, 25 mL)	Sarstedt, UK
PVDF blotting membrane	GE Healthcare, Life science
Screw-top tubes (15 mL, 50 mL)	Sarstedt
Serological pipettes	Sarstedt
Syringes (10 mL, 20 mL)	Becton Dickenson
Universal tubes (20 mL)	Greiner
Western blot filter paper	Schleicher-Schuell

LABORATORY EQUIPMENT	PROVIDER
4°C refrigerators	Lec
-20°C freezers	Lec
-80°C freezers	Revco/ Sanyo
96-well plate reader	Tecan
Cell culture incubator	Sanyo
Centrifuges	Sanyo, Eppendorf
CCD camera -Western blot imager	Syngene
Class II safety cabinets	Walker
ECFG21 Super Electro Cell Fusion Generator	Nepa Gene
Fluorescence microscope	ZEISS
Flow cytometer	Beckman Coulter
Haemocytometers	SLS
Heat blocks	Lab-Line
Light microscope	Nikon/Olympus
Microcentrifuge	MSE
NanoDrop™ 8000 Spectrophotometer	Thermo scientific
pH meters	Metler Toledo
Pipettes and multichannel pipettes	Gilson, Star Labs, Eppendorf
Plate rocker	VWR, Stuart
Spectra max 190 Microplate Reader	Molecular Devices
Spectrophotometer for 96-well plate	Tecan ULTRA
Transfer tank	Bio Rad
Ultracentrifuge Optima TLX	Beckman
Ultrapure water dispenser	Barnstead
Vortex	Scientific industries
Water baths	Clifton

SOFTWARE	PROVIDER
Aperio ImageScope	Leica Biosystems
Axiovision Microscopy Software 4.7.1. version	ZEISS
GraphPad Prism 8	Graph Pad software
Kaluza™ 3.1 version	Beckman Coulter

4.2.1.3 Cell line growth media

38 B9 COMPLETE MEDIUM	CONCENTRATIONS
RPMI 1640	-
FCS	10%
L-glutamine	2 %
Na Pyruvate	1 %
2-MercaptoEtOH	0.1%
Pen/strep	1%

NIH 3T3 COMPLETE MEDIUM		CONCENTRATIONS
DMEM	-	-
FCS	10%	
L-glutamine	2 %	
Na Pyruvate	1 %	
Pen/strep	1%	

SP2/0 COMPLETE MEDIUM		CONCENTRATIONS
RPMI 1640	-	
FCS	10%	

R0+ FUSION MEDIUM		CONCENTRATIONS
RPMI 1640	-	
L-glutamine	2%	
Na Pyruvate	1%	
2-MercaptoEtOH	0.1%	
Pen/strep	1%	

R10+ FUSION MEDIUM		CONCENTRATIONS
RPMI 1640	-	
FCS	10% v/v	
L-glutamine	2%	
OPI supplement	1%	
HAT supplement	1 vial/500 mL medium	
Na Pyruvate	1%	
2-Mercaptoethanol	0.1%	
Penicillin-Streptomycin	1%	

4.2.1.4 Buffers and gels

ECF BUFFER		CONCENTRATIONS
Mannitol	0.3 M	
CaCl ₂	0.1 mM	
MgCl ₂	0.1 mM	

PURIFICATION BINDING BUFFER		CONCENTRATIONS
Sodium Phosphate pH 7.0	20 mM	
Na ₂ HPO ₄ ·7H ₂ O	12 mM	
NaH ₂ PO ₄ ·H ₂ O	8 mM	
pH was adjusted to 7.0 and the solution volume brought to 250 mL with nanopure ddH ₂ O		

PURIFICATION ELUTION BUFFER		CONCENTRATIONS
Glycine	0.1 M	
HCl	Volume needed to adjust the pH	
pH was adjusted to 2.7 and the solution volume brought to 100 mL with nanopure ddH ₂ O		

PURIFICATION NEUTRALISING BUFFER	CONCENTRATIONS
Trizma-base	1 M
HCl	Volume needed to adjust the pH
pH was adjusted to 9.0 and the solution volume brought to 20 mL with nanopure ddH ₂ O	

GEL FIXING BUFFER	CONCENTRATIONS
Methanol	46% v/v
Acetic acid	7% v/v
Buffer was prepared in ddH ₂ O	

COOMASSIE STAINING BUFFER	CONCENTRATIONS
Methanol	46% v/v
Acetic acid	7% v/v
Coomassie Blue R-250	0.1% w/v
Buffer was prepared in ddH ₂ O	

GEL DE-STAINING BUFFER	CONCENTRATIONS
Methanol	5% v/v
Acetic acid	7.5% v/v
Buffer was prepared in ddH ₂ O	

ELISA COATING BUFFER	CONCENTRATIONS
Na ₂ CO ₃	15 mM
NaHCO ₃	35 mM
Buffer was prepared in ddH ₂ O and pH adjusted to 9.6	

ELISA WASHING BUFFER	CONCENTRATIONS
DPBS	1X
Tween-20	0.05% v/v
Buffer was prepared in ddH ₂ O	

ELISA BLOCKING BUFFER	CONCENTRATIONS
DPBS	1X
FCS	2% w/v
Buffer was prepared in ddH ₂ O	

4X SDS-PAGE LOADING BUFFER	FOR 10 mL
1M Tris-HCl pH 6.8	2.4 mL
Sodium dodecyl sulphate (SDS)	0.8 g
Glycerol	4 mL
DTT	0.5 mL
Bromophenol blue	4 mg
ddH ₂ O	3.1 mL

RIPA BUFFER	FOR 50 ML
ddH ₂ O	47 mL
Sodium chloride	150 mM
Tris-HCl	50 mM
Triton-X-100	1% v/v
10% v/v Sodium deoxycholate	0.5% v/v
10% w/v SDS	0.1% v/v
pH was adjusted to 8.0	

5% STACKING GEL	FOR 6 ML
ddH ₂ O	4.1 mL
30% w/v Acrylamide mix	1.0 mL
1.0 M Tris (pH 6.8)	0.75 mL
10% w/v SDS	0.06 mL
10% w/v Ammonium persulfate	0.06 mL
TEMED	0.006 mL

10% RESOLVING GEL	FOR 20 ML
ddH ₂ O	7.9 mL
30% Acrylamide mix	6.7 mL
1.5 M Tris (pH 8.8)	5 mL
10% SDS	0.2 mL
10% ammonium persulfate	0.2 mL
TEMED	0.008 mL

5X SDS RUNNING BUFFER	FOR 1 L
Glycine	94 g
Tris base	15.1 g
10% SDS	50 mL
ddH ₂ O	Up to 1 L

Buffer was diluted with ddH₂O to 1X working concentration prior use.

TRANSFER BUFFER	FOR 2 L
Glycine	5.8 g
Tris base	11.6 g
10% w/v SDS	0.75 g
Methanol	400 mL
ddH ₂ O	Up to 2 L

Transfer buffer was stored at 4°C.

10X TRIS-BUFFERED SALINE (10 X TBS)	FOR 1 L
Trizma base	24.2 g
NaCl	80 g
ddH ₂ O	Up to 1 L

pH was adjusted to 7.6 with concentrated HCl.

TRIS-BUFFERED SALINE WITH TWEEN (TBST)	FOR 1 L
10X TBS	100 mL
ddH ₂ O	900 mL
Tween-20	1 mL

4.2.2 Methods

4.2.2.1 Routine cell culture

DU145 cell line was purchased from American Type Culture Collection (ATCC). 38 B9 (murine pro-B-cell line), NIH 3T3 (murine fibroblast), and SP2/0 (Hybridoma: B lymphocyte) cell lines were kindly provided by Prof. Dr. Hans-Martin Jäck (Department of Medicine - Division of Immunology, University Hospital Erlangen). All cell lines were cultured in their dedicated media. The DU145 cell line was cultured in Eagle's Minimum Essential Medium (EMEM) with 1% w/v L-Glutamine, 10% v/v foetal calf serum (FCS) was added according to ATCC culture methods. The 38 B9 wild type (wt) cell line was cultured in Roswell Park Memorial Institute 1640 (RPMI 1640) medium with 10% w/v FCS, 2% w/v L-Glutamine, 1% w/v sodium pyruvate, 0.1% w/v 2-mercaptoethanol, 1% w/v Pen/strep; NIH 3T3 wt cell line was cultured in Dulbecco's Modified Eagle Medium (DMEM) medium supplemented with 10% w/v FCS, 2% w/v L-Glutamine, 1% w/v sodium pyruvate, 1% w/v Pen/strep. 38 B9 EPCR⁺ and NIH 3T3 EPCR⁺ cells were cultured in dedicated media supplemented with 5 µg/mL of puromycin. Hybridomas generated were cultured in R10 medium, RPMI 1640 medium supplemented with 10% w/v FCS, 2% w/v L-Glutamine, 1% w/v OPI supplement, 1 vial/500 mL medium HAT supplement, 1% w/v sodium pyruvate, 0.1% w/v 2-mercaptoethanol, 1% w/v Pen/strep. Each cell line was cultured at 37°C in the incubator containing 5% v/v CO₂ and humidified air.

Cells were routinely passaged at 70-80% confluence. During passaging, adherent cells were washed twice with Dulbecco's Phosphate Saline (DPBS) and detached by incubating with 0.25% w/v Trypsin- 0.53 mM EDTA solution for 5-15 min at 37°C. Equal amounts of cell-specific medium were added immediately upon cell detachment. 38 B9 and hybridoma suspension cells were collected without trypsinisation. All cell lines were then centrifuged at 260 g for 5 min. Cell counting was carried out by re-suspending a harvested cell pellet in 1-3 mL of cell-dedicated medium and re-suspending cell solution in Trypan blue 1:10. The haemocytometer was used to count the total number of living cells and excluded the number of dead cells (blue stained) from the count. The cell pellet was re-suspended in fresh medium and cells re-cultured in culture flasks by passaging. Stock of each cell line was

prepared at approximately 1×10^6 cell number in 1 mL FCS + 10% v/v DMSO (freezing medium) and stored at -80°C. As required, cells were thawed, gently re-suspended in 10 mL cell-dedicated medium and centrifuged at 150 g for 5 min. Cell pellets were then again gently re-suspended in fresh batch of cell-dedicated medium and plated in suitable dish. Medium changes ensured removal of DMSO from the frozen cells samples and increased the viability of thawed samples.

4.2.2.2 Generation of mouse mAbs against human EPCR

The hybridomas used as part of this project were generated as a collaboration with the team of Prof. Hans-Martin Jäck, Head of the Division of Immunology at the University of Erlangen (Germany). Professor Jäck offered his facilities and expertise to complete the entire process of specific antibody-producer hybridomas.

4.2.2.1 Mouse immunisation with EPCR recombinant protein

For this part of the study, two 6-months old BALB/c mice, namely CA19 and CA20, with HHKKLL IgG profile were used and the standard immunisation protocol with multiple boosts applied (Table 4.1). Mice were kept in IVC-cages under pathogen-free conditions in the Franz-Penzoldt Centre animal facility of the University of Erlangen-Nürnberg. After the first administration of the target-antigen, four boosts were performed in order to activate the host's immunological memory. The recombinant EPCR (human PROCR-His Tag, Sino Biological, ref. 13320-H08H) was delivered in the mice together with Alum, diluted 1:1 with DPBS.

Table 4.1 – Panel of immunisation steps. Mice were primed with an initial dose of recombinant human EPCR (rhEPCR) protein as antigen, in a solution with Alum adjuvant in DPBS. Immunisation was repeated boosting mice with lower doses of protein in adjuvant in order to keep the immune memory. Boosts were repeated close to the day of fusion. Final boost is performed with a solution of antigen alone in DPBS.

Week	Action	Antigen + adjuvant
0	Priming	30 µg rhEPCR + 100 µL Alum
4	Boost #1	20 µg rhEPCR + 100 µL Alum
13	Boost #2	20 µg rhEPCR + 100 µL Alum
17	Boost #3	20 µg rhEPCR + 100 µL Alum
21	Final boost	20 µg rhEPCR w/o Alum

Blood samples were collected from mice before the immunisation and at different time points after the priming. Samples were allowed to clot for 30 min at room temperature, and

then centrifuged at 2,000 g for 10 min at 4°C in order to separate serum. The supernatants were transferred in a fresh Eppendorf tube and stored at -20°C.

4.2.2.2 Test for presence of mouse anti-EPCR in serum with Enzyme-Linked Immunosorbent Assay (ELISA)

Indirect ELISA was used to investigate the presence of antibodies against human EPCR in sera isolated from the two mice immunised. Such assay consists in the direct adsorption of the target antigen to the wells of a multiwell plate that is then probed with a primary antibody followed by the detection through a secondary anti-IgG antibody conjugated with horseradish peroxidase (HRP). In presence of hydrogen peroxide, HRP enzyme oxidises the substrate generating a colour change that is detectable by a spectrophotometer (Figure 4.4).

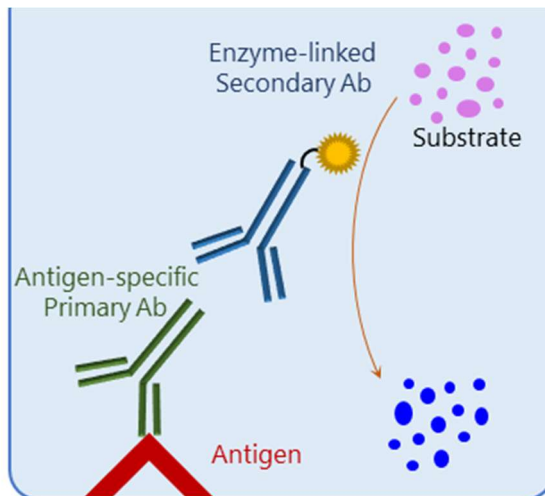


Figure 4.4 – Indirect ELISA for specific anti-EPCR IgG detection in purified antibodies. The picture represents the molecules involved during the reaction developing in a well. Antigen of interest is immobilised in wells of a 96-well plate. In case antibodies specific for that antigen are present in the probing solution they will bind to the well bottom. Detection happens by probing with a secondary antibody specific against the Fc region of the primary antibody, conjugated with HRP enzyme. When an appropriate substrate is added, a colour change is produced. The signal is detected with a spectrophotometer.

Mid-absorption 96-wells plates were coated with 50 µL/well of antigen in coating buffer with a dilution of 0.5 µg/mL at 4°C overnight. As antigen, the same human EPCR recombinant protein administered to mice for immunisation was used, upon reconstitution at 0.5 µg/µL in ddH₂O. On the day of the assay, plates were washed with washing buffer three times and blocked with 150-200 µL/well of blocking buffer for 30 min at RT. Buffer was discarded and wells probed with 50 µL/well undiluted sera isolated from mice CA19 and CA20. Plates were incubated for 1 hour at RT, after which wells were washed with washing buffer three times. 50 µL/well of secondary anti-mouse IgG-HRP antibody in blocking buffer (Table 4.2) was added to each well and the plate incubated 1 hour at RT, after which wells

were washed with washing buffer three times. 100 µL of 3,3',5,5'-Tetramethylbenzidine (TMB) substrate were transferred to each well and let react at RT. As soon as the colour change was occurring, the reaction was blocked adding 50 µL/well of 2N sulphuric acid. The absorbance was measured at 450 nm using a TECAN ULTRA spectrophotometer.

Table 4.2 – Secondary antibody used for ELISA analysis. The table reports the details and dilution of the antibodies used.

Coating	Working Dilution	Reference number	Reconstitution buffer
Human EPCR recombinant protein (Sino Biological)	0.5 µg/mL	13320-H08H	ddH ₂ O
Primary pAb	Working Dilution		Mouse
Serum	Undiluted		CA19
Serum	Undiluted		CA20
Secondary pAb	Working Dilution	Reference number	Clone
Anti-Mouse IgG HRP-linked	1:3000	7076	Polyclonal
Diluent: blocking buffer			

4.2.2.2.3 Test for presence of mouse anti-EPCR in serum with flow cytometry

Flow cytometry (FCM) was used to assess the presence of specific anti-EPCR antibodies in the serum isolated from immunised mice.

38 B9 (wt and EPCR⁺) and NIH 3T3 (wt and EPCR⁺) cells were grown, harvested, and counted as described in section 4.2.2.1. 1x10⁶ cells of each type were aliquoted to 12x75 mm polycarbonate flow cytometry tubes. 1 µL of LIVE/DEAD™ Fixable Violet Dead Cell Reagent was mixed with 1 mL of DPBS and added to each tube with cells (apart from the unstained control) and incubated at RT for 30 min. Cells were washed with 1 mL of DPBS and centrifuged at 400 g for 5 min at room temperature. Supernatants were removed by gently flicking the tubes and pellets were resuspended by gentle tapping. 5 µL of FcR Blocking reagent was mixed with 45 µL of PBS added to each tube and incubated at RT for 10 min. Primary monoclonal antibodies and sera (diluted 1:200 in DPBS, for a final dilution of 1:400 in the sample tubes) were prepared in PBS as described in Table 4.3, and 50 µL added to the respective test tube. Dilutions were calculated taking into consideration that the final volume per tube is 100 µL and the need to adjust the antibody dilution accordingly.

Table 4.3 – Primary and secondary monoclonal antibodies used for flow cytometry analyses. The table represents a list of the antibodies and their dilutions used.

Primary mAb	Working Dilution	Reference number	Clone	Supplier
PE rat anti-human CD319	10 µg/mL	331806	162.1	Biolegend
PE mouse anti-human EPCR	10 µg/mL	351903	RCR-401	Biolegend
Pre-immune Serum from mouse CA20	1:400	N/A	N/A	N/A
Fusion Serum from mouse CA20	1:400	N/A	N/A	N/A
Secondary pAb	Working Dilution	Reference number	Clone	Supplier
Alexa Fluor™ 488 conjugated goat anti-mouse IgG	1:200	A11001	polyclonal	Invitrogen
Diluent: DPBS				

All the samples were incubated at RT for 30 min. After incubation, cells were washed with 2 mL of PBS and centrifuged at 400 g for 5 min. Supernatants were removed from each sample and pellets were resuspended by gentle tapping. 100 µL of secondary antibody diluted in PBS (Table 4.3) was added only to the test tubes, except the unstained in which DPBS only was added, and all samples incubated at RT for 30 min in the dark. After incubation, cells were washed with 2 mL of PBS and centrifuged at 400 g for 5 min. Supernatants were removed from each sample and pellets were resuspended by gentle tapping in 300 µL of ISOTON II™ flow cytometry sheath fluid. Data were acquired using a 10-color/3-laser Beckman Coulter Gallios™ flow cytometer and analyzed using Kaluza™ v1.3 data acquisition and analysis software (Beckman Coulter).

4.2.2.2.4 Fusion of B-cells with fusion cell-partner

On the day of the fusion, 3-6 days after the final boost, spleen was taken from the mouse, transferred to a 70 µm cell strainer placed in a petri dish in sterile conditions and cells mechanically separated by compressing the tissue through the mesh of the strainer using a 5 mL syringe plunger. B cells and SP2/0 cells were counted as described in section 4.2.2.1. 9.5×10^7 cells from each line were collected and washed once in warm R0+ medium and then centrifuged at 300 g for 10 min at RT.

Both pellets were combined and washed twice with 20 mL warm ECF buffer then resuspended in 6.4 mL ECF buffer. Cell suspension was transferred to the sterile

electrofusion chamber of the ECFG21 Super Electro Cell Fusion Generator (Nepa Gene) and the program started according to the manufacturer's recommendations (Table 4.4).

Table 4.4 – Parameters setting for fusion ECFG21 Super Electro Cell Fusion Generator. This table summarises the setting used to perform electro cell fusion.

AC					
Voltage: 80			Duration: 60 sec		
Post Fusion AC					
Duration: 12 sec			Decay: OFF		
DC Pulse					
Voltage	Length	Interval	No of cycles	Decay	Polarity
1,300	30 µsec	0.5 sec	2	10%	+

The Electro Cell Fusion Generator allows for significantly (25-100 times) higher cell fusion efficiency than PEG (polyethylene glycol). When the alternating current is delivered, cells align side to side forming several chains within which the fusion between cells is realised by 2-step DC pulses with voltage decay.

After completion of the fusion, cells were collected from the chamber and transferred in a tube with 20 mL warm R0+, and incubated 10 min at RT. Cells were then centrifuged at 300 g for 10 min at RT. The pellet was then resuspended in 500 mL R10+ and cells plated in 96-wells plates as following:

- 40 plates with $1,8 \times 10^4$ cells in 200 µL per well;
- 50 plates with 8×10^3 cells in 200 µL per well.

Plates were then incubated at 37°C with 5% v/v CO₂ and humidified air for about two weeks before the start of the hybridoma screening.

4.2.2.5 Hybridomas visual screening

Plates were observed under microscope for growing hybridoma colonies. Usually, it takes 7-14 day for the colonies to become visible. 150 µL of cell culture supernatant (CSN) was collected from each well containing one single colony for further analysis with ELISA and FCM.

4.2.2.6 Screening for IgG-secreting hybridomas through Enzyme-Linked Immunosorbent Assay (ELISA)

Sandwich ELISA was used to optimise screening for the presence of IgG antibodies in CSN samples from high numbers of hybridoma clones. Such assay consists in the direct

adsorption of the target antigen to the wells of a multiwell plate that is then probed with a primary antibody followed by the detection through a secondary anti-IgG antibody conjugated with horseradish peroxidase (HRP). In the presence of hydrogen peroxide, HRP oxidises the substrate generating a colour change that is detectable by a spectrophotometer (Figure 4.5).

For this experiment, CSNs from hybridoma clones were tested. Mid-absorption 96-wells plates were coated with 50 µL/well of anti-mouse IgG unlabelled in coating buffer with a dilution of 1 µg/mL at 4°C overnight. On the day of the assay, plates were washed with washing buffer three times and blocked with 150-200 µL/well of blocking buffer for 30 min at RT. Buffer was discarded and wells probed with CSNs from growing hybridoma clones.

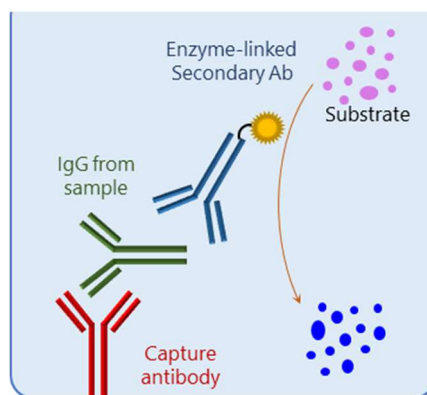


Figure 4.5 – Sandwich ELISA for IgG detection in hybridoma CSNs. The picture represents the molecules involved during the reaction developing in a well. A capture antibody anti-mouse IgG is immobilised in wells of a 96-well plate. Any mouse IgG molecule present in the probing solution will bind to the well bottom. Detection happens by probing with a secondary antibody specific against the Fc region of the primary antibody, conjugated with HRP enzyme. When an appropriate substrate is added, a colour change is produced. The signal is detected with a spectrophotometer.

Additionally, 50 µL/well normal mouse IgG was used as positive control at a concentration of 0.2 µg/mL in blocking buffer (Table 4.5). For each growing hybridoma clone, 50 µL of CSN was carefully collected and transferred to each of the antigen-coated well. Then, the plate was incubated for 1 hour at RT, after which wells were washed with washing buffer three times. 50 µL/well of secondary anti-mouse IgG-HRP antibody in blocking buffer (1:3000) was added to each well and the plate incubated 1 hour at RT, after which wells were washed with washing buffer three times. 100 µL of 3,3',5,5'-Tetramethylbenzidine (TMB) substrate were transferred to each well and the reaction allowed to proceed at RT. Colour was let developing for 5 min, then the reaction was stopped adding 50 µL/well of 2N sulphuric acid. The absorbance was measured at 450 nm using a Spectra max 190 spectrophotometer.

Table 4.5 – Antigen, primary and secondary monoclonal antibodies used for ELISA analysis. The table represents a list of the Immunoglobulin standard and antibodies with relative dilutions used.

Coating	Working Dilution	Reference number	Clone	Supplier
Goat anti-mouse IgG unlabelled	1 µg/mL	1030-01	Polyclonal	Southern Biotech
Primary mAb	Working Dilution	Reference number	Clone	Supplier
Normal Mouse Immunoglobulin	0.2 µg/mL	500-M00	Polyclonal	PeproTech
Hybridoma CSNs	N/A	N/A	Any growing hybridoma	N/A
Secondary pAb	Working Dilution	Reference number	Clone	Supplier
Anti-Mouse IgG HRP-linked	1:3000	7076	Polyclonal	Cell Signalling
Diluent: ELISA blocking buffer				

4.2.2.7 Hybridoma reactivity assessment using flow cytometry analysis

Hybridoma clones that tested positive for the production of specific anti-EPCR antibodies were then further analysed with flow cytometry. 38 B9 (wt and EPCR⁺) and NIH 3T3 (wt and EPCR⁺) cells were grown, harvested, and counted as described in section 4.2.2.1.

10x10⁵ cells of each type were aliquoted to 12x75 mm polycarbonate flow cytometry tubes. 1 µL of LIVE/DEAD™ Fixable Violet Dead Cell Reagent was mixed with 1 mL of DPBS and added to each tube with cells (apart from the unstained control) and incubated at RT for 30 min. Cells were washed with 1 mL of DPBS and centrifuged at 400 g for 5 min. Supernatants were removed by gently flicking the tube and pellets were resuspended by gentle tapping. 5 µL of FcR Blocking reagent was mixed with 45 µL of PBS added to each tube and incubated at RT for 10 min. 50 µL primary monoclonal antibodies was prepared in PBS as described in Table 4.6, taking into consideration that the final volume per tube is 100 µL thus adjusting antibody dilution accordingly, and added to each control tube except for the unstained and test tubes.

Table 4.6 – Primary and secondary monoclonal antibodies used for flow cytometry analyses. The table represents a list of the antibodies and their dilutions used.

Primary mAb	Working Dilution	Reference number	Clone	Supplier
PE rat anti-human CD319	10 µg/mL	331806	162.1	Biolegend
PE mouse anti-human EPCR	10 µg/mL	351903	RCR-401	Biolegend
Hybridoma CSNs	Undialuted	N/A	Any growing hybridoma	N/A
Secondary pAb	Working Dilution	Reference number	Clone	Supplier
Alexa Fluor™ 488 conjugated goat anti-mouse IgG	1:500	A11001	polyclonal	Invitrogen
Diluent: DPBS				

50 µL serum was added to each test tube except for the unstained and control tubes. All the samples were incubated at RT for 30 min. After incubation, cells were washed with 2 mL of PBS and centrifuged at 400 g for 5 min. Supernatants were removed from each sample and pellets were resuspended by gentle tapping. 100 µL of secondary antibody diluted in PBS was added only to the secondary control tubes and tubes treated with sera, and samples incubated at RT for 30 min in the dark. After incubation, cells were washed with 2 mL of PBS and centrifuged at 400 g for 5 min. Supernatants were removed from each sample and pellets were resuspended by gentle tapping in 300 µL of ISOTON II™ flow cytometry sheath fluid. Data were acquired using a 10-color/3-laser Beckman Coulter Gallios™ flow cytometer and analysed using Kaluza™ v1.3 data acquisition and analysis software (Beckman Coulter).

4.2.2.2.8 Hybridoma cloning by limiting dilution

In order to obtain stable populations derived from single clones of hybridomas, a single-cell-cloning technique was applied using limiting dilutions. Hybridomas were grown, harvested, and counted as described in section 4.2.2.1. Cells were plated in 96-well plates with a dilution of 0.03 cells/well. 5 culture plates were used for each hybridoma. 15 cells were resuspended in 120 mL of dedicated medium and 250 µL of such suspension aliquoted to each well. Eventually, plates were cultured at 37°C in the incubator containing 5% v/v CO₂ and humidified air for 4-7 days without changing the medium and then observed for growth of isolated clones.

4.2.2.3 Characterisation and validation of newly generated mouse mAbs against human EPCR

4.2.2.3.1 Hybridoma sequencing

Hybridomas were sent for sequencing at Absolute Antibody (Oxford, UK). For each hybridoma, two cryovials containing 3×10^6 cells were frozen in liquid nitrogen and then shipped to the company.

Sequencing was performed by whole transcriptome shotgun sequencing (RNA-Seq). This is a proprietary approach to antibody sequencing developed exclusively at Absolute Antibody (Figure 4.6). Total RNA is extracted from cells and a barcoded cDNA library generated through RT-PCR using a random hexamer. Next Generation Sequencing is performed on an Illumina HiSeq sequencer.

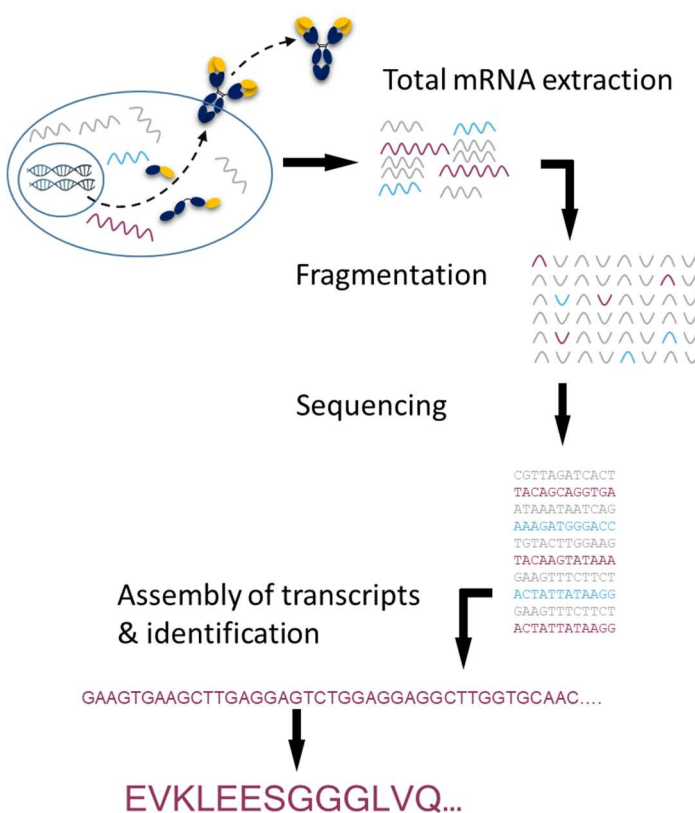


Figure 4.6 – Hybridoma sequencing approach developed by Absolute Antibody. Schematic representing the high throughput (NGS) hybridoma sequencing performed on the selected clones. (Image courtesy of Absolute Antibody. <https://absoluteantibody.com/custom-services/antibody-sequencing/hybridoma-sequencing/>)

4.2.2.3.2 Antibody purification from hybridoma CSNs

Hybridoma clones JvGCRC-H61.3, JvGCRC-H589.9, JvGCRC-H599.5 and JvGCRC-H754.6 were bulked up and cultured in big volumes of dedicated medium in order to purify

antibodies from the CSN. For this purpose, 500 mL of R10+ medium was used and hybridoma cultured until 80-90% confluent. Cells were then pelleted and resuspended in 500 mL of CD-Hybridoma medium, a protein-free medium specifically formulated to support the growth of hybridomas for antibody production. Hybridomas were cultured until approximately 1/3 were dead, and then pelleted and the CSN collected for the purification with Protein G GraviTrap columns according to manufacturer's recommendations (Figure 4.7). The pH of the sample was checked and adjusted to 7.0 using HCl before application of the sample to the column, in order for it to be equal to the pH of the binding buffer. The bottom tip of the rProtein G Sepharose columns was cut off and the top cap removed. Column storage solution was poured off and the column placed in the workmate column stand for equilibration with 10 mL of binding buffer. After equilibration, the sample was added to the column and let flow through by gravity. Columns were then washed adding 15 mL binding buffer and the flow through discarded. Eventually, the antibodies were eluted by adding 6 mL of elution buffer to the columns. Such solution has a very low pH (2.7) which allows the disruption of the ionic and hydrogen bonds between antibody and Protein G. 1.2 mL of neutralising buffer was added to the collection tubes used in order to increase the pH in the eluted solution and preserve the antibodies.

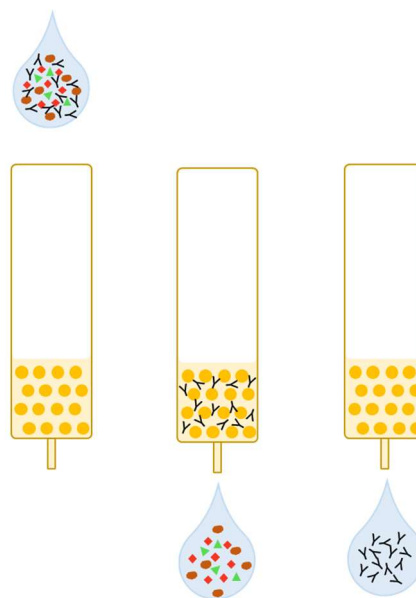


Figure 4.7 – Antibody purification steps overview. CSNs collected from hybridomas were run through rProtein G Sepharose columns by gravity flow. Antibodies binds with high specificity to rProtein G while other molecules are discarded in the flow-through. Columns are then washed, and antibodies eluted and neutralised.

4.2.2.3.2.1 Antibody dialysis for buffer exchange against DPBS

After elution, the purified antibodies were dialysed against DPBS using the Slide-A-Lyzer dialysis cassettes with molecular weight cut-off of 10 kDa and volume range of 12-30 mL

according to manufacturer's recommendation. Cassettes were soaked in DPBS for 1-2 min in order to hydrate the membranes. Samples were loaded into the cassettes using a syringe, carefully avoiding piercing the membrane. Samples were then dialysed in cold DPBS for 2 hours at 4°C. Buffer was then changed to fresh DPBS 3 times, performing the last dialysis overnight at 4°C, after which samples were withdrawn from the cassettes, aliquoted in 1.5 mL tubes and stored at -80°C until quantification.

4.2.2.3.2.2 Antibody quantification and purity analysis by SDS-PAGE

Purified antibodies JvGCRC-H61.3, JvGCRC-H589.9, JvGCRC-H754.6 and JvGCRC-H599.5 were quantified through protein assay, according to the procedure described in section 2.2.2.4.1. SDS gels were prepared as described in section 2.2.1.3 and immersed in a tank containing 1X SDS running buffer. For each sample, a volume of lysate sample equivalent to 30 µg protein per gel-lane was mixed with 5X Protein Loading Buffer at ratio 4:1, vortexed and incubated at 95°C for 5 min for protein denaturation. Denatured samples were carefully loaded on well-set gel alongside 5 µL of Precision Plus Protein Western Standards. Once loaded, the samples were run at 60 V for 10-20 min (to allow proteins to pass through the stacking gel), and then the voltage was increased to 100 V to allow proteins to separate in the resolving gel. Next, the SDS gel was fixed in 50 mL fixing buffer for 1 hour and then stained in 50 mL Coomassie staining buffer for 1 hour, on rocking plate at room temperature. Eventually, the gel was destained in 50 mL de-staining buffer for 24 hours on rocking plate at room temperature. A digital photograph of the gel was taken with a camera device.

4.2.2.3.3 Application of purified mAbs in Western blotting

DU145, cells were grown and harvested as described in section 4.2.2.1, and snap frozen in dry ice for 5 min. Pellets were then lysed by adding 100 µL RIPA Buffer + 1% v/v protease inhibitors, subjected to 3 cycles of vortex, and then centrifuged at 10,000 g for 10 min at 4°C to remove any debris. Supernatants were transferred to fresh tubes and stored at -20°C. Total protein concentration in all lysate samples were quantified using a DC Protein Assay (BioRad), a detergent-compatible colorimetric assay based on the Lowry assay method, according to the manufacturer's protocol. As a reference, a stock solution of 2 mg/mL Bovine Serum Albumin (BSA) solution in RIPA buffer was prepared and used for serial dilutions (Table 4.7). For each standard and unknown sample, 10 µL/well in triplicates in 96-well plates were used. 25 µL of working reagent was added to each well and mixed carefully by pipetting up and down, then 200 µL of reagent B was added to each well, then the plate

was incubated in the dark at 37°C for 15 to 30 min. The absorbance was measured at 570 nm using a TECAN ULTRA spectrophotometer, and average values from control wells were then subtracted from corresponding test wells. Standard curves were then generated based on the absorbance intensity measured using the standard concentrations. Sample concentrations were calculated based on the standard curve.

Table 4.7 – Generation of protein standards. The volume of reagents used to create the serial dilution of the standards in Protein Assay. The final volume calculated for each point is 50 µL.

Final concentration (mg/mL)	2 mg/mL BSA (µL)	Buffer (µL)
0	0	50
0.125	3.12	46.48
0.25	6.25	43.75
0.5	12.5	37.5
0.75	18.75	31.25
1	25	25
1.5	37.5	12.5
2	50	0

4.2.2.3.3.1 Gel preparation and electrophoresis

First, SDS-PAGE was performed to separate the proteins in sample lysates. Gels were prepared (see section 4.2.1.3) and immersed in a tank containing 1X SDS running buffer. For each sample, a volume of lysate sample equivalent to 30 µg protein per gel-lane was mixed with 5X Protein Loading Buffer (see section 4.2.1.3) at ratio 4:1, vortexed and incubated at 95°C for 5 min for protein denaturation. Denatured samples were carefully loaded on well-set gel alongside 5 µL of Precision Plus Protein™ WesternC™ Blotting Standards. Once loaded, the samples were run at 60 V for 10-20 min (to allow proteins to pass through the stacking gel), and then the voltage was increased to 100 V to allow proteins to separate in the resolving gel.

4.2.2.3.3.2 Wet transfer

Once proteins had run through the gel (approximately 90 min), the electrophoresis was stopped. The gel was carefully removed from the tank and transferred onto a PVDF blotting membrane via “wet transfer”. First, PVDF membranes were cut into 8x6 cm pieces (fitting the size of the gel) and activated by soaking in methanol for 30 sec, water for 10 min, and transfer buffer for 15 min. Two pieces (per membrane) of filter paper of the same size were cut and soaked with transfer buffer. The “sandwich” was assembled using an assembly cassette, sponge, blotting mat, membrane, gel, blotting mat, sponge. All assembly parts

listed above remained soaked with transfer buffer at all times. The assembly cassette was used to seal the construct and the “sandwich” was immediately inserted into a transfer tank filled with ice-cold transfer buffer. Proteins were transferred at 100 V for 1 hour at room temperature (RT).

4.2.2.3.3.3 Immunopropbing

After the transfer, membranes were removed from the assembly cassette and washed 3 times with DPBS, rocking for 10 min. Membranes were then blocked with 5% w/v Marvel skimmed milk in TBST for 1 hour rocking at RT. Membranes were then incubated with primary antibodies at 4°C on the rocking platform overnight. The following day, the membranes were washed three times with TBST and incubated with the corresponding secondary antibodies for 1 hour on the rocking platform at RT. Antibodies were diluted in 5% w/v Marvel skimmed milk in TBS at concentrations shown in Table 4.8.

Following the incubation, the membranes were washed with TBST. Finally, membranes were incubated with Clarity Western ECL Substrate for one min prior to imaging using a CCD camera.

Table 4.8 – Antibodies and dilutions used in Western Blot analysis. The table represents a list of the antibodies and their dilutions used.

Primary mAb	Working Dilution	Reference Number	Clone	Supplier
Mouse anti-human EPCR	1 µg/mL	WH0010544M3	M2	Sigma
Purified mouse anti-human EPCR	1 µg/mL	N/A	JvGCRC-H61.3	N/A
Purified mouse anti-human EPCR	1 µg/mL	N/A	JvGCRC-H589.9	N/A
Purified mouse anti-human EPCR	1 µg/mL	N/A	JvGCRC-H754.6	N/A
Purified mouse anti-human EPCR	1 µg/mL	N/A	JvGCRC-H599.5	N/A
Ladder	Working Dilution	Reference Number	Supplier	
Precision Plus Protein™ WesternC™ Blotting Standards	5 µL/well	161-0376	Bio Rad	
Secondary pAb	Working Dilution	Reference Number	Supplier	
Anti-Mouse IgG HRP-linked	1:1000	7076	Cell Signalling	
Anti-Ladder	Working Dilution	Reference Number	Supplier	
Precision Protein™ StrepTactin-HRP Conjugate	1:5000	161-0380	Bio Rad	

4.2.2.3.4 Application of purified mAbs in flow cytometry assay

In order to assess the ability of purified anti-EPCR antibodies to bind to EPCR expressed on the surface of target cells, FCM analysis was performed. Prior to that, a titration of the purified mAbs was performed. The same protocol was applied to both analyses.

DU145 cells were grown, harvested, and counted as described in section 4.2.2.1. 10×10^5 DU145 cells were aliquoted to each 12x75 mm polycarbonate flow cytometry tubes. 1 μL of LIVE/DEAD™ Fixable Violet Dead Cell Reagent was mixed with 1 mL of DPBS and added to each tube with cells (apart from the unstained control) and incubated at RT for 30 min. Cells were washed with 1 mL of DPBS and centrifuged at 400 g for 5 min. Supernatants were removed by gently flicking the tube and pellets were resuspended by gentle tapping. 5 μL of FcR Blocking reagent was mixed with 45 μL of DPBS added to each tube and incubated at RT for 10 min. 50 μL primary antibody was prepared in DPBS for each antibody to test as described in Table 4.9, taking into consideration that the final volume per tube is 100 μL thus adjusting antibody dilution accordingly, and added to each test tube except for the unstained and control tubes, and incubated at RT for 30 min.

After incubation, cells were washed with 2 mL of PBS and centrifuged at 400 g for 5 min. Supernatants were removed from each sample and pellets were resuspended by gentle tapping. 100 μL of secondary antibody diluted in PBS was added to all but the 'unstained' tubes, and samples incubated at RT for 30 min in the dark. After incubation, cells were washed with 2 mL of DPBS and centrifuged at 400 g for 5 min. Supernatants were removed from each sample and pellets were resuspended by gentle tapping in 300 μL of ISOTON II™ flow cytometry sheath fluid. Data were acquired using a 10-color/3-laser Beckman Coulter Gallios™ flow cytometer and analysed using Kaluza™ v1.3 data acquisition and analysis software (Beckman Coulter).

Table 4.9 – Primary and secondary monoclonal antibodies used for flow cytometry. Antibodies and their dilutions used during the antibody titration and the target recognition specificity assays.

Antibody Titration Assay				
Primary mAb	Working Dilutions Tested	Reference number	Clone	Supplier
Rat anti-human EPCR	<ul style="list-style-type: none"> • 0.1 µg/mL • 0.25 µg/mL • 0.5 µg/mL • 1 µg/mL • 3 µg/mL • 6 µg/mL 	NB600-963	RCR-252	Novus Biological
Purified mouse anti-human EPCR		N/A	JvGCRC-H61.3	N/A
Purified mouse anti-human EPCR		N/A	JvGCRC-H589.9	N/A
Purified mouse anti-human EPCR		N/A	JvGCRC-H754.6	N/A
Purified mouse anti-human EPCR		N/A	JvGCRC-H599.5	N/A
Secondary pAb	Working Dilution	Reference number	Clone	Supplier
Goat anti-Mouse IgG (H+L) Secondary Antibody, Alexa Fluor® 488 conjugate	1:1000	A-11001	Polyclonal	Invitrogen
Alexa Fluor™ 488 conjugated Donkey anti-rat IgG	1:500	A21208	Polyclonal	Invitrogen
Diluent: DPBS				

Target Recognition Specificity Assay				
Primary mAb	Working Dilution	Reference number	Clone	Supplier
Rat anti-human EPCR	1 µg/mL	NB600-963	RCR-252	Novus Biological
Purified mouse anti-human EPCR	3 µg/mL	N/A	JvGCRC-H61.3	N/A
Purified mouse anti-human EPCR	3 µg/mL	N/A	JvGCRC-H589.9	N/A
Purified mouse anti-human EPCR	1 µg/mL	N/A	JvGCRC-H754.6	N/A
Purified mouse anti-human EPCR	3 µg/mL	N/A	JvGCRC-H599.5	N/A
Secondary pAb	Working Dilution	Reference number	Clone	Supplier
Goat anti-Mouse IgG (H+L) Secondary Antibody, Alexa Fluor® 488 conjugate	1:1000	A-11001	Polyclonal	Invitrogen
Alexa Fluor™ 488 conjugated Donkey anti-rat IgG	1:500	A21208	Polyclonal	Invitrogen
Diluent: DPBS				

4.2.2.3.5 Application of purified mAbs in immunofluorescence

DU145 cells were grown, harvested, and counted as described in section 4.2.2.1. Cells were washed twice with DPBS, centrifuging at 400g for 5 min every time. Cells were then resuspended at a density of 2.5×10^6 cells/mL and 200 µL of such solution was transferred to each 1.5 mL test tube. Cells were centrifuged at 400g for 5 min, supernatants were removed and discarded and cells blocked with 200 µL DPBS + 10% w/v BSA for 1 hour at RT on rocker. After incubation, cells were washed three times with 500 µL DPBS (each time centrifuged at 400 g for 5 min with supernatants removal). 100 µL of diluted primary antibody solution (Table 4.10) was added and samples were incubated at 4°C overnight on rocker. The following day, cells were washed three times with 1000 µL DPBS and centrifuged at 400 g for 5 min. 100 µL of diluted secondary antibody solution was added to each tube and samples were incubated for 1 hour at RT in the dark on rocker. Finally, cells were washed three times (500 µL DPBS followed by a centrifugation at 400 g for 5 min) and resuspended in 100 µL DPBS. Several glass slides were wiped with ethanol and their edges were marked with the ImmEdge™ Pen (to keep cells in solution in the middle). Approximately 50 µL of cell-containing solution was transferred in the middle of the glass slide and mixed with Vectashield Antifade Mounting Medium with DAPI drops.

Table 4.10 – Primary and secondary monoclonal antibodies used for Immunofluorescence. Antibodies and dilutions used.

Primary mAb	Working Dilution	Reference number	Clone	Supplier
Mouse anti-human EPCR	1 µg/mL	ab56689	CD201	Abcam
Purified mouse anti-human EPCR	1 µg/mL	N/A	JvGCRC-H61.3	N/A
Purified mouse anti-human EPCR	1 µg/mL	N/A	JvGCRC-H589.9	N/A
Purified mouse anti-human EPCR	1 µg/mL	N/A	JvGCRC-H754.6	N/A
Purified mouse anti-human EPCR	1 µg/mL	N/A	JvGCRC-H599.5	N/A
Secondary pAb	Working Dilution	Reference number	Clone	Supplier
Goat anti-Mouse IgG (H+L) Secondary Antibody, Alexa Fluor® 488 conjugate	1:1000	A-11001	Polyclonal	Invitrogen
Diluent: 10% w/v BSA in DPBS				

Finally, a long rectangle cover slip was mounted on the top and the edges of the cover slip and the glass slide were gently sealed with nail varnish. Such prepared slides were kept in

the dark to prevent bleaching of secondary antibodies-attached fluorophores. Controls were prepared with secondary antibody only. The names and dilutions of antibodies used in these experiments are shown in Table 4.10. Slides were viewed under fluorescent microscope and the exposure for each fluorophore was adjusted to the controls (with secondary antibodies only).

4.2.2.3.6 Application of purified mAbs in Enzyme-Linked Immunosorbent Assay (ELISA)

Indirect ELISA (see section 4.2.2.2) was used to assess the ability of the purified mAbs to recognise and bind to their antigen EPCR. Prior to that, a titration of the purified mAbs was performed. The same protocol was applied to both analyses. Mid-absorption 96-wells plates were coated with 50 µL/well of antigen in coating buffer with a dilution of 0.5 µg/mL at 4°C overnight. As antigen, the same human EPCR recombinant protein administered to mice for immunisation was used, upon reconstitution at 0.5 µg/µL in ddH₂O. On the day of the assay, plates were washed with washing buffer three times and blocked with 150-200 µL/well of blocking buffer for 30 min at RT. Buffer was discarded and wells probed with primary antibodies. Primary mouse monoclonal anti-EPCR used as positive control and purified mAbs were prepared as shown in Table 4.11. Plate was incubated 1 hour at RT, after which wells were washed with washing buffer three times. 50 µL/well of secondary anti-mouse IgG-HRP antibody in blocking buffer (1:3000) was added to each well and the plate incubated 1 hour at RT, after which wells were washed with washing buffer three times. 100 µL of 3,3',5,5'-Tetramethylbenzidine (TMB) substrate were transferred to each well and let react at RT.

Colour was let developing for 5 min, then the reaction was blocked adding 50 µL/well of 2N sulphuric acid. The absorbance was measured at 450 nm using a TECAN ULTRA spectrophotometer.

Table 4.11 – Primary and secondary monoclonal antibodies used for ELISA analysis. Antibodies and dilutions used during the antibody titration and the target recognition specificity assays.

Antibody Titration Assay				
Coating	Working Dilution	Reference number	Reconstitution buffer	Supplier
Human EPCR recombinant protein	0.5 µg/mL	13320-H08H	ddH ₂ O	Sino Biological
Primary mAb	Working Dilutions Tested	Reference number	Clone	Supplier
Mouse anti-human EPCR	• 0.1 µg/mL	WH0010544M3	M2	Sigma
Purified mouse anti-human EPCR	• 0.25 µg/mL	N/A	JvGCRC-H61.3	N/A
Purified mouse anti-human EPCR	• 0.5 µg/mL	N/A	JvGCRC-H589.9	N/A
Purified mouse anti-human EPCR	• 1 µg/mL	N/A	JvGCRC-H754.6	N/A
Purified mouse anti-human EPCR	• 3 µg/mL	N/A	JvGCRC-H599.5	N/A
Purified mouse anti-human EPCR	• 6 µg/mL	N/A		
Secondary pAb	Working Dilution	Reference number	Clone	Supplier
Anti-Mouse IgG HRP-linked	1:3000	7076	Polyclonal	Cell Signalling
Diluent: blocking buffer				

Target Recognition Specificity Assay				
Coating	Working Dilution	Reference number	Reconstitution buffer	Supplier
Human EPCR recombinant protein	0.5 µg/mL	13320-H08H	ddH ₂ O	Sino Biological
Primary mAb	Working Dilution	Reference number	Clone	Supplier
Mouse anti-human EPCR	3 µg/mL	WH0010544M3	M2	Sigma
Purified mouse anti-human EPCR	3 µg/mL	N/A	JvGCRC-H61.3	N/A
Purified mouse anti-human EPCR	3 µg/mL	N/A	JvGCRC-H589.9	N/A
Purified mouse anti-human EPCR	3 µg/mL	N/A	JvGCRC-H754.6	N/A
Purified mouse anti-human EPCR	3 µg/mL	N/A	JvGCRC-H599.5	N/A
Secondary pAb	Working Dilution	Reference number	Clone	Supplier
Anti-Mouse IgG HRP-linked	1:3000	7076	Polyclonal	Cell Signalling
Diluent: blocking buffer				

4.2.2.3.7 Epitope mapping

In order to map the epitope targeted by each purified mAbs on EPCR an indirect ELISA was performed. Plates were coated with different peptides generated by breaking down EPCR's extracellular domain sequence. Set 1 comprised 12 peptides covering amino acids 18 to 202, each of which was 20 residues long and overlapped by 5 residues with each other. Set 2 comprised 19 peptides covering amino acids 18 to 210, each of which was 15 residues long and overlapped by 5 residues with the adjacent ones (Table 4.12). Amino acids 1 to 17 refer to the signal peptide, therefore they were not considered for the epitope mapping, as well as the transmembrane domain of EPCR (amino acids 211 to 238).

Table 4.12 – Library of Overlapping Peptides of EPCR Generated for Epitope Mapping of Purified Antibodies.

SET 1		SET 2	
Length: 20 aa Overlapping: 5 aa		Length: 15 aa Overlapping: 5 aa	
Amino acid positions	Peptide sequence	Amino acid positions	Peptide sequence
18-37	SQDASDGLQLRLHMLQISYFR	18-32	SQDASDGLQLRLHMLQ
33-52	ISYFRDPYHVWYQGNASLGG	28-42	LHMLQISYFRDPYHV
48-67	ASLGGHLTHVLEG PDTNTTI	38-52	DPYHVWYQGNASLGG
63-82	TNTTIIQLQPLQEPESWART	48-62	ASLGGHLTHVLEGPD
78-97	SWARTQSGLQS YLLQFHGLV	58-72	LEG PDTNTTI IQLQP
93-112	FHGLVRLVH QERTLA FPLTI	68-82	IQLQP LQEPESWART
108-127	FPLTIRCFLGCELPPEG SRA	78-92	SWARTQSGLQS YLLQ
123-142	EGSRAHVFFEVAVNGSSFVS	88-102	SYLLQFHGLVRLVHQ
138-157	SSFVSFRPERALWQADTQVT	98-112	RLVHQERTLA FPLTI
153-172	DTQVTSGVVTFTLQQLNAYN	108-122	FPLTIRCFLGCELP
168-187	LNAYNRTRYELREFLEDTCV	118-132	CELPPEG SRAHVFF
183-202	EDTCVQYVQKHISAENTKGS	128-142	HVF FEVA VNGSSFVS
		138-152	SSFVSFRPERALWQA
		148-162	ALWQADTQVTSGVVT
		158-172	SGVVTFTLQQLNAYN
		168-182	LNAYNRTRYELREFL
		178-192	LREFLEDTCVQYVQK
		188-202	QYVQKHISAENTKGS
		198-210	NTKGSQTSRSYTS

Mid-absorption 96-wells plates were coated with 50 µL/well of the full-length protein as well as two sets of linear peptides in coating buffer with a dilution of 1 µg/mL at 4°C overnight (Table 4.13). On the day of the assay, plates were washed with washing buffer three times and blocked with 150-200 µL/well of blocking buffer for 30 min at RT. Buffer was discarded and wells probed with 50 µL/well control and purified mAbs at dilutions

specified in Table 4.13. Then, the plate was incubated 1 hour at RT, after which wells were washed with washing buffer three times. 50 µL/well of secondary anti-mouse IgG-HRP antibody in blocking buffer (1:3000) was added to each well and the plate incubated 1 hour at RT, after which wells were washed with washing buffer three times. 100 µL of 3,3',5,5'-Tetramethylbenzidine (TMB) substrate were transferred to each well and let react at RT. As soon as the colour change was occurring, the reaction was blocked adding 50 µL/well of 2N sulphuric acid. The absorbance was measured at 450 nm using a Spectra max 190 spectrophotometer.

Table 4.13 – Antigen, primary and secondary monoclonal antibodies used for ELISA analysis. The table represents a list of the Immunoglobulin standard and antibodies with relative dilutions used.

Coating	Working Dilution	Reference number	Reconstitution buffer	Supplier
Human EPCR recombinant protein	1 µg/mL	13320-H08H	ddH ₂ O	Sino Biological
Purified Peptide Library	1 µg/mL	SC1487	DMSO	GeneScript
Primary mAb	Working Dilution	Reference number	Clone	Supplier
Mouse anti-human EPCR	3 µg/mL	WH0010544M3	M2	Sigma
Purified mouse anti-human EPCR	3 µg/mL	N/A	JvGCRC-H61.3	N/A
Purified mouse anti-human EPCR	3 µg/mL	N/A	JvGCRC-H589.9	N/A
Purified mouse anti-human EPCR	3 µg/mL	N/A	JvGCRC-H754.6	N/A
Purified mouse anti-human EPCR	3 µg/mL	N/A	JvGCRC-H599.5	N/A
Secondary pAb	Working Dilution	Reference number	Clone	Supplier
Anti-Mouse IgG HRP-linked	1:3000	7076	Polyclonal	Cell Signalling
Diluent: ELISA blocking buffer				

4.3 Results

4.3.1 Generation and selection of hybridoma clones producing specific mAbs against human EPCR

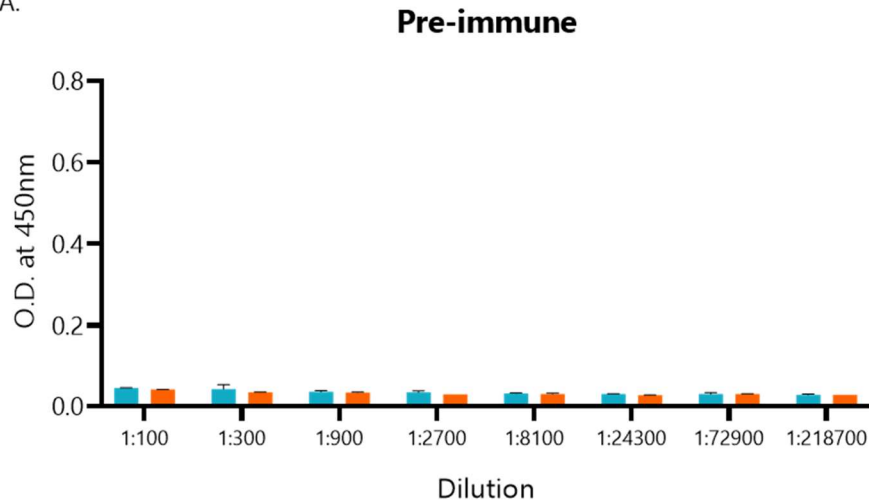
4.3.1.1 Mice immunisation with target antigen

Two mice, namely CA19 and CA20, were immunised according to the protocol described in section 4.2.2.2.1.

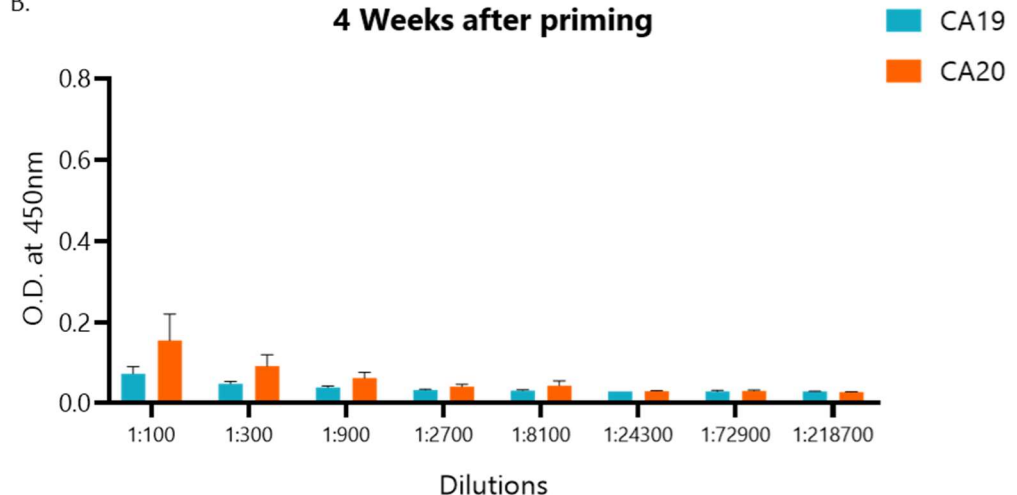
Subsequently, the titre of the specific anti-human EPCR antibodies in sera isolated from both mice before immunisation, four weeks after the first administration and 1 week after the final boost was analysed by ELISA using serial dilutions for each sample as represented in Figure 4.8-D.

No antibody was detected in both mice before the immunisation procedure (Figure 4.8-A), whereas four weeks after the first boost antibodies are still detectable in the serum from both mice (Figure 4.8-B), confirming that the antigen was able to stimulate antibody secretion. Eventually, levels of anti-human EPCR antibodies were checked after the final boost (Figure 4.8-C). Mouse CA20 showed higher levels of antibodies compared to mouse CA19. For this reason, mouse CA20 was selected for the cell fusion.

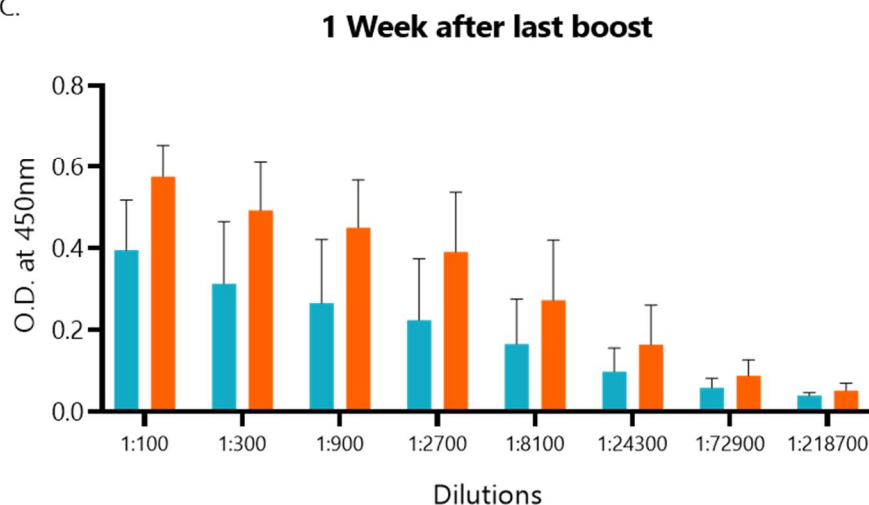
A.



B.



C.



D.

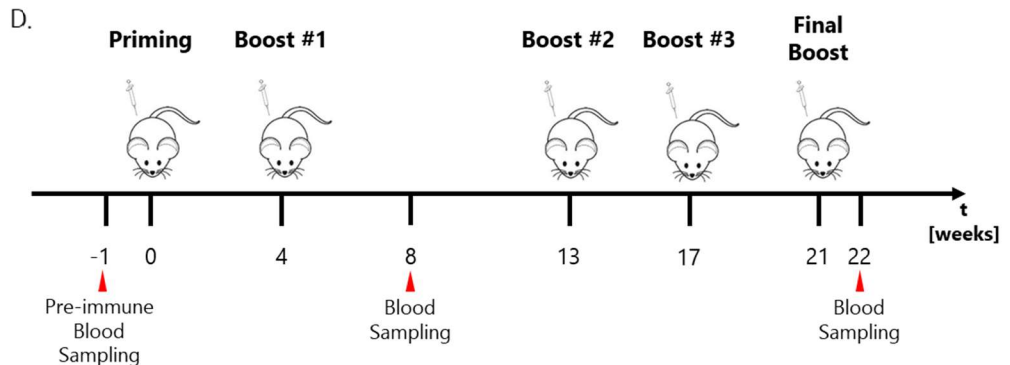


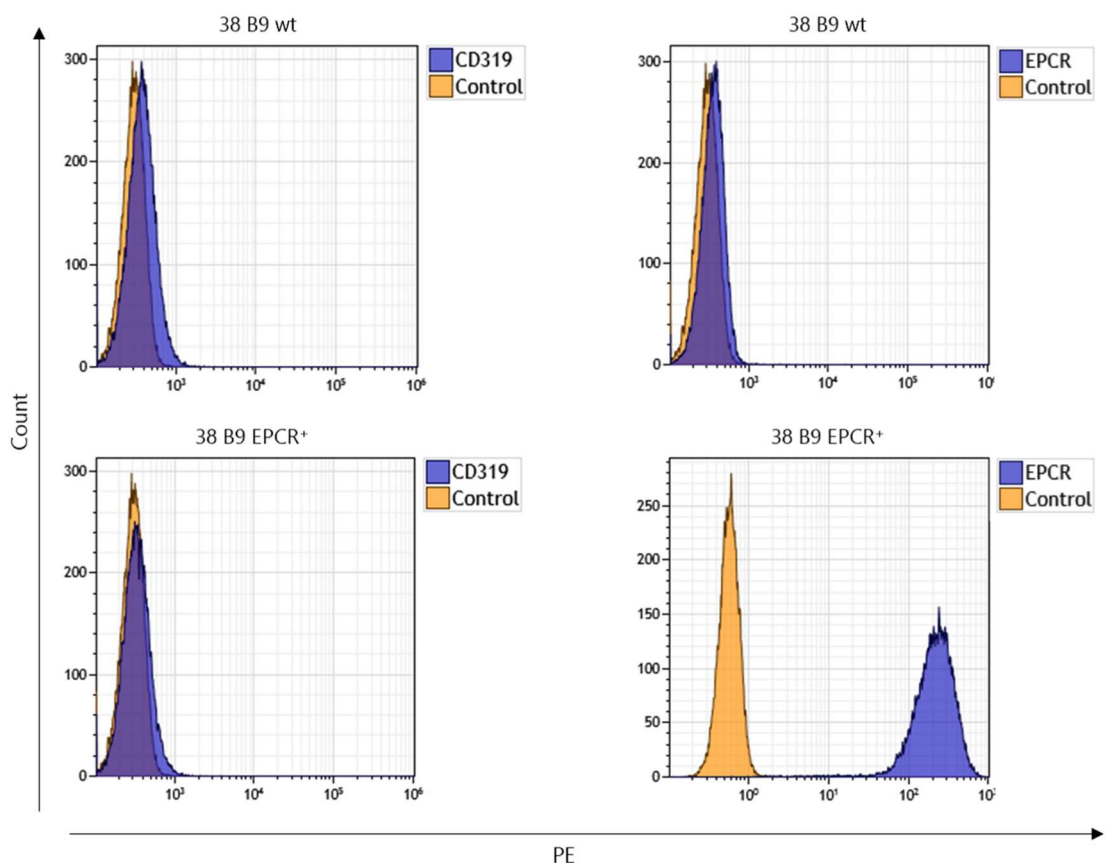
Figure 4.8 – Antibody titre in sera isolated from immunised mice. Titre of anti-human EPCR specific antibodies was evaluated by ELISA in sera samples from mice CA19 (blue bars) and CA20 (orange bars) collected at different time points: (A.) before immunisation, (B.) four weeks after the first shot of antigen and (C.) one week after the last boost. (D.) Immunisation and bleeding scheme.

At the end of the immunisation period, the presence of anti-human EPCR IgG in the serum of mouse CA20 was assessed using flow cytometry. The serum samples were tested on two murine cell lines, namely 38 B9 and NIH 3T3, that normally lack the expression of the human EPCR, transfected with EPCR knock-in construct (EPCR⁺) were used. Moreover, wt 38 B9 and NIH 3T3 cell lines were used as negative controls for the expression of EPCR on the cell surface. Commercial primary antibodies were used as controls. Anti-human CD319 antibody was used as negative control as the target cells do not express such protein, whereas the commercial anti-human EPCR was used as positive control for EPCR expression on target cells. Both control antibodies were conjugated with PE fluorophore, thus no secondary antibody was used. For sera staining, a secondary anti-mouse IgG antibody conjugated with FITC fluorophore was used. Figure 4.9 shows the complete set of positive and negative controls combined for the staining of wt and EPCR⁺ 38 B9 and NIH 3T3 cells, respectively. Upon incubation with anti-CD319, no signal was detected either in wt or EPCR⁺ cells. As expected, incubation with anti-EPCR produced a significant shift in the signal detected in EPCR⁺ cells, but not in wt cells, thus confirming the specificity of expression of EPCR in both 38 B9 and NIH 3T3 EPCR⁺ constructs.

Figure 4.10 refers to the probing of the cell lines with samples of sera collected from mice before immunisation and after the last boost, showing that the signals detected met the requirements for the fusion. Indeed, the pre-immune serum did not give any signal in either wt or EPCR⁺ of both 38 B9 and NIH 3T3 cell lines. As expected, incubation with the serum collected after the last boost produced a detectable signal only in the EPCR⁺ construct in both 38 B9 and NIH 3T3 cells. Particularly, the signal obtained incubating cells with sera is lower compared to the signal obtained using the control antibody against EPCR, this is possibly due to the higher dilution of the antibody in sera samples.

The results obtained confirmed the success of the immunisation, allowing the generation of antibodies process to proceed to the next step, the electro cell fusion.

A.



B.

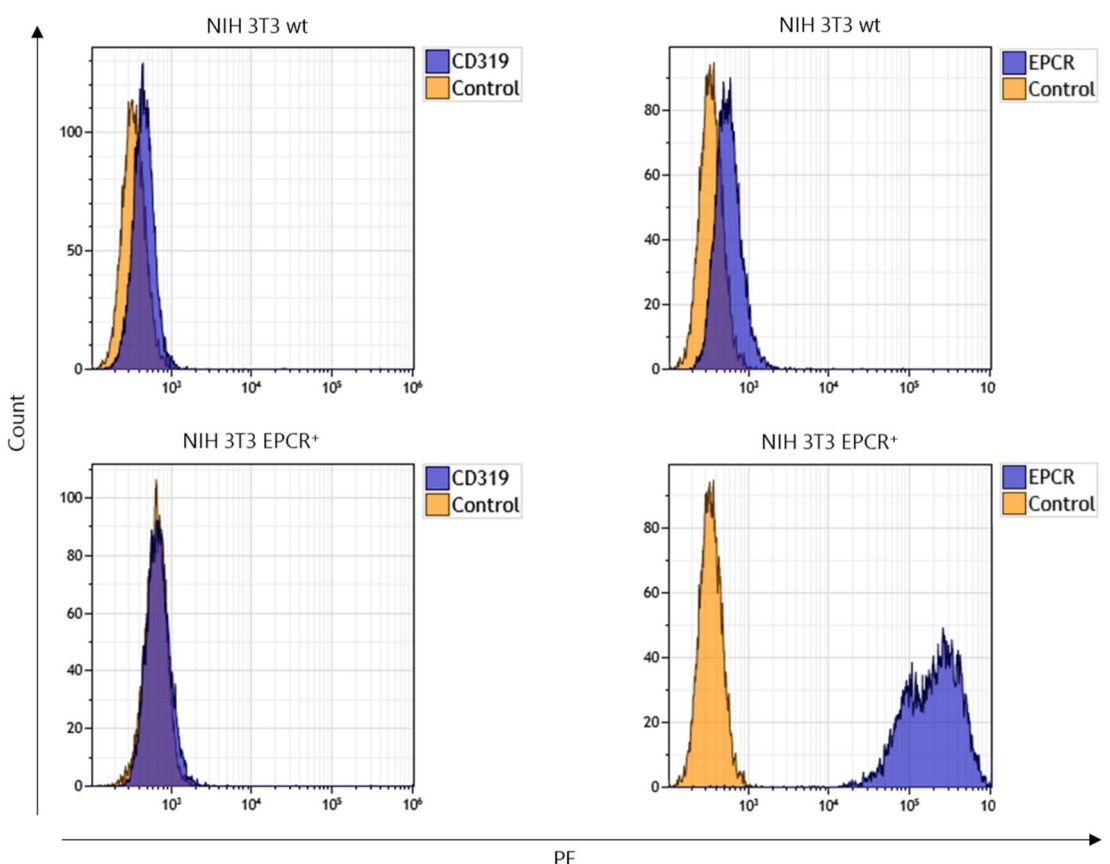


Figure 4.9 – Full panel of control tests on 38 B9 and NIH 3T3 cells. The panel shows that EPCR⁺ cells specifically express the human EPCR protein in both 38 B9 (A.) and NIH 3T3 (B.) lines. **Orange** shading represents tracks obtained with specific EPCR primary antibody; **blue** shading shows control cells treated with only secondary antibody.

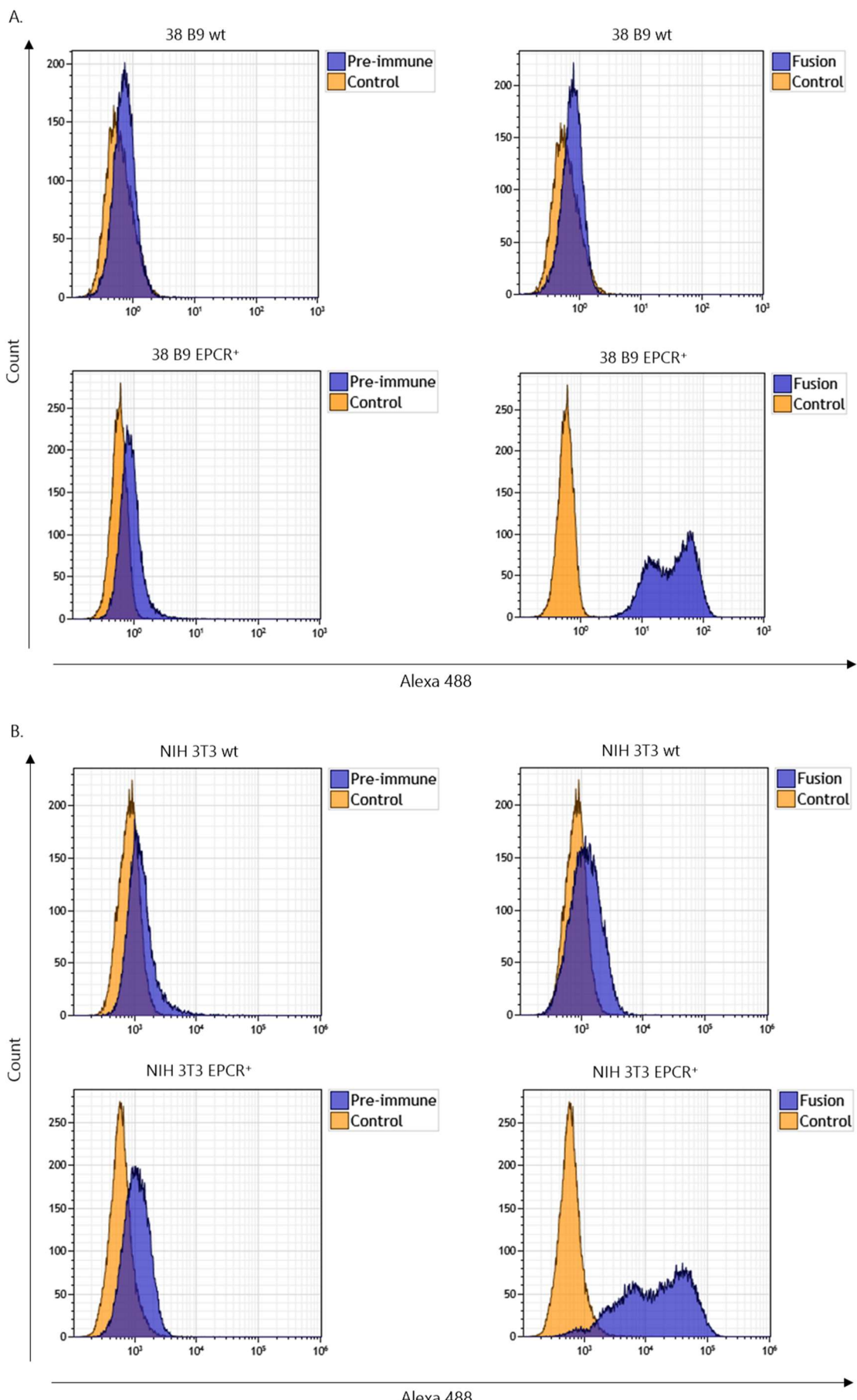


Figure 4.10 – Full panel of sera tests on 38 B9 and NIH-3T3 cells. The panel shows that anti-human EPCR specific antibodies are present in the sera of mouse CA20 on the day of fusion, confirmed on both 38 B9 (A.) and NIH 3T3 (B.) cell lines. **Orange** shading represents tracks obtained with specific EPCR primary antibody; **blue** shading shows control cells treated with only secondary antibody.

4.3.1.2 Cell fusion, selection and primary screening

After the fusion, cells were washed, plated in ~100 96-well plates at two different very low densities and incubated in selective medium until the first colonies become visible. Once the colonies start to appear, it is possible to have hundreds of new ones to test each day (Figure 4.11). However, hybridomas tend to be very unstable in the early stages after fusion, developing mutations and losing chromosomes, which can lead to impairment of cell proliferation and loss of antibody production. For this reason, it is crucial to identify positive clones and stabilise them by limiting dilution. Furthermore, cloning increases the likelihood to isolate monoclonal colonies.

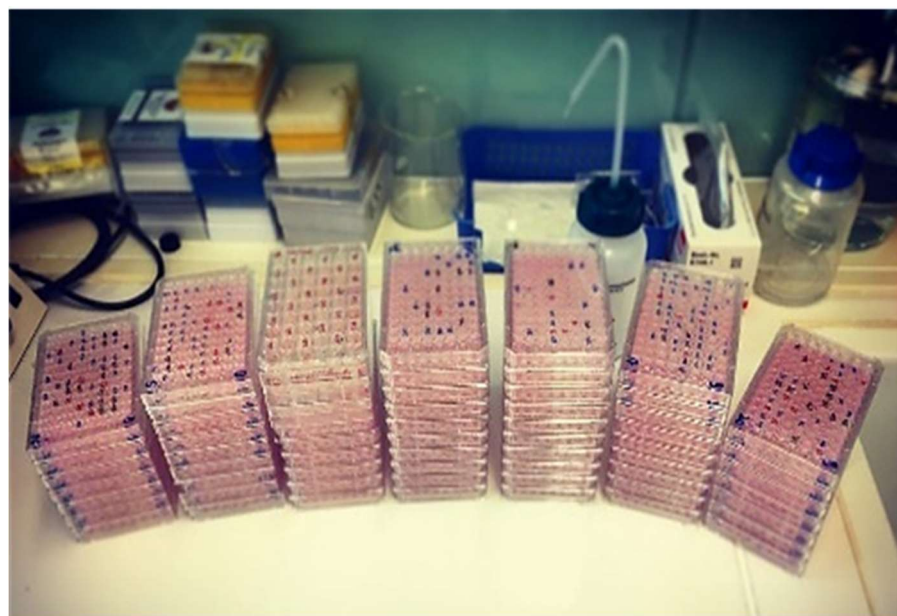


Figure 4.11 – Hybridoma cell cultures. At each round of fusion, ~100 plates containing hybridomas were cultured. Most of the clones produced non-specific antibodies or did not generate any colonies, thus the yield of EPCR specific hybridomas is extremely low.

Due to the high number of hybridomas found each day, a faster approach to screen for production of antibodies was applied, which consists in analysing each new growing clone first for its ability to secrete IgG - by testing the relative undiluted CSN it in a sandwich ELISA (Figure 4.12) - and then test only the IgG-producing clones for the specificity against EPCR with flow cytometry analysis.

Eventually, 572 out of the 1,300 hybridomas screened were positive for IgG production and were then tested for their specificity towards EPCR by flow cytometry analysis in wt and EPCR⁺ 38.B9 and NIH 3T3 cells.

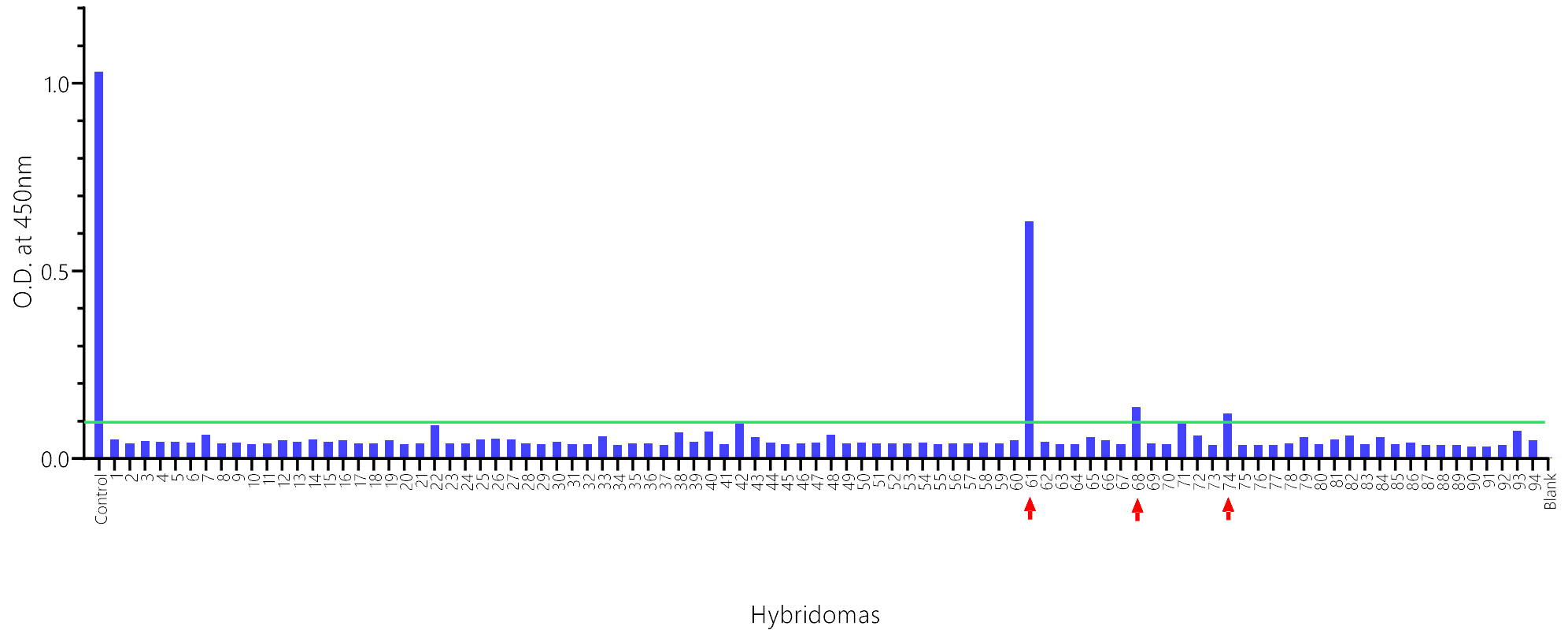


Figure 4.12 – Screening of hybridoma CSNs with ELISA. Example of a plate of hybridomas screened. Only hybridomas showing an absorbance signal higher than 0.1 (green line) were selected for the flow cytometry analysis (red arrows). Undiluted CSNs were used for this assay. As a control, normal mouse IgG at a known concentration (0.2 µg/mL) was used. Identities (IDs) of the hybridomas that were found positive for the expression of IgG molecules are listed in the table included. Optical density (O. D.) was measured at 450 nm. Values are given as single measurement for positive controls and IgG-specific signals from CSNs.

Of all the hybridomas tested, 19 showed specificity for EPCR following flow cytometry analysis. Such hybridomas were then expanded and tested at every passage, as hybridomas can either stop proliferating or lose the ability to produce antibodies. Only six hybridomas continued to produce antibodies. In order to ensure cell stability and monoclonality of the antibodies, hybridomas were cloned by limiting dilution (0.3 cells per well) in 96-well plates and bulked up. Two clones for each hybridoma were eventually selected for further experiments and sent to the John van Geest Cancer Research Centre for antibody production, characterisation, and validation.

Once received, one clone from each hybridoma was cultured and relative CSNs analysed by flow cytometry, while the second clone was stored in liquid nitrogen as a backup. Selected clones were 61.3, 74.2, 589.9, 599.5, 754.6, and 1222.15. Figure 4.13 shows the positive signal obtained with each clone on both EPCR⁺ 38 B9 and NIH 3T3 cell lines with flow cytometry analysis.

Specificity of binding was simultaneously confirmed by the absence of staining on wt cell populations. Interestingly, the shift obtained analysing each CSN was not the same for every clone. Indeed, clones 61.3, 74.2 and 589.9 produced a differential degree of staining in 38 B9 EPCR⁺ cells. Moreover, clone 599.5 was the one amongst all different clones to produce a less homogenous signal in NIH 3T3 EPCR⁺ cells. Such differences in signals could be due to different epitopes recognised by each antibody, different concentration of antibody in CSN, and affinity strength of antibody-antigen binding. Indeed, a subpopulation of 38 B9 EPCR⁺ cells show significantly lower expression of EPCR protein, potentially due to a difference in the specific epitope they express compared to the one recognised by the antibody tested.

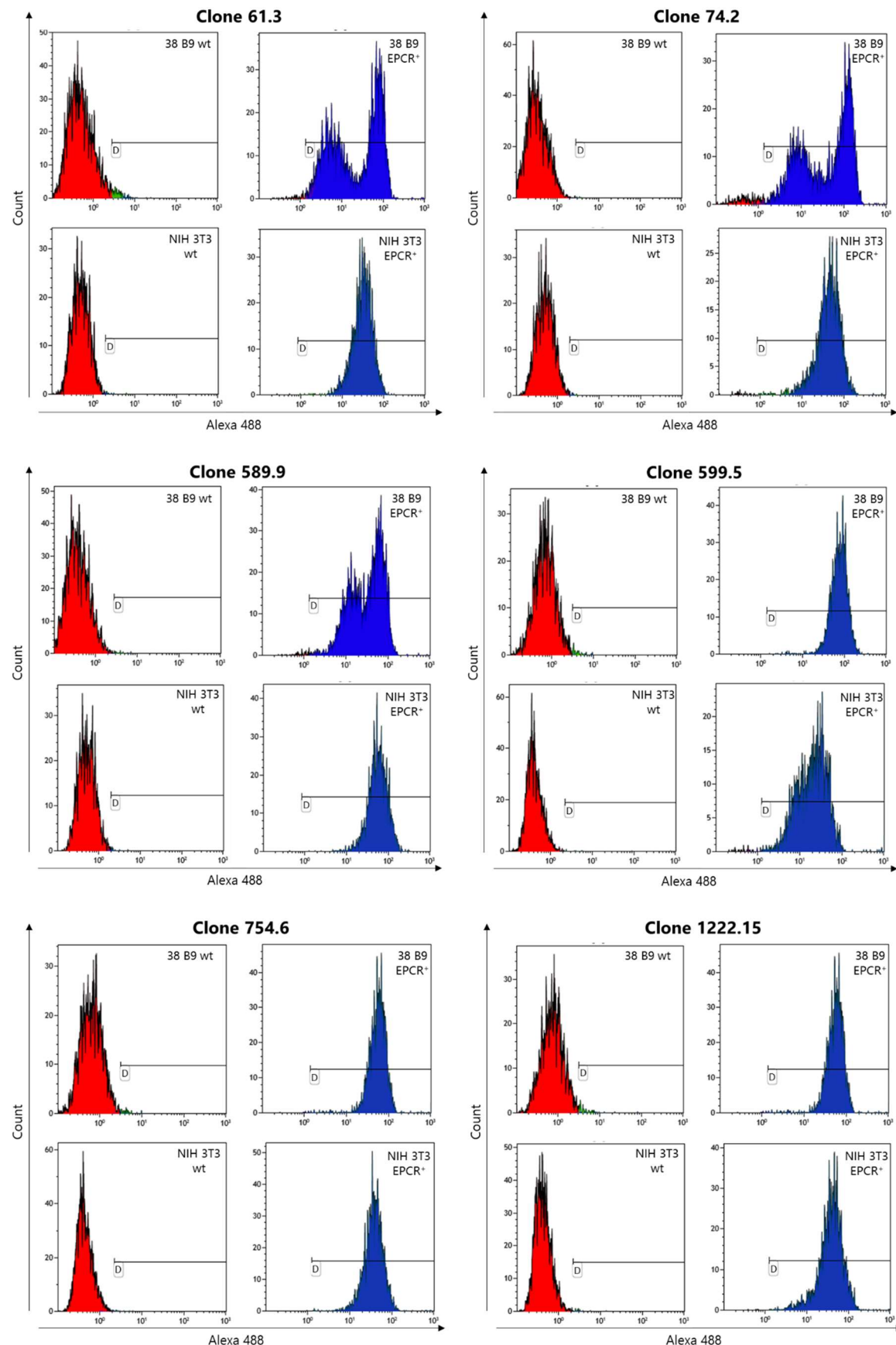


Figure 4.13 – Flow cytometry analysis of anti-human EPCR specific subclones. CSNs from hybridoma cultures were analysed with flow cytometry on wt and EPCR⁺ 38 B9 and NIH 3T3 cell lines in order to assess presence of antibodies from samples and their specificity.

4.3.2 Sequencing of newly generated anti-human EPCR mAbs

Sequencing of our hybridomas was performed externally through a specialised company named Absolute Antibody (Redcar, UK). Contigs obtained following RNA-seq of the hybridomas were assembled using an Absolute Antibody proprietary approach, and data mined for antibody sequences identifying all viable antibody sequences. Variable heavy and variable light domains were identified separately. The species and isotype of the identified antibody genes were confirmed. Sequences were compared with known aberrant antibody genes that are present in many hybridomas and these genes were removed from analysis when necessary. For each chain, the variable domain was reported. The heavy chain and light chain type were identified based on the sequence of the constant domain. The data were automatically filtered to only report antibody genes with an abundance of greater than 1%, based on the relative measurement obtained in transcripts per million. Moreover, CDR-1, -2, and -3 regions within both light and heavy variable sequences were identified according to the standard Kabat identification scheme (Johnson, Wu 2000). As variable regions are responsible for epitope binding, it is crucial to know the correct sequences in order to maintain antibody affinity and specificity.

Most relevant details for the six hybridomas sequenced are represented in Table 4.14. All hybridomas were sequenced as murine IgG1 heavy chain and kappa light chain, apart from 74.2 that presented lambda light chain.

Table 4.14 – Sequencing of anti-EPCR hybridomas. Hybridomas were sequenced by Absolute Antibody company. Heavy and light chain type was identified for each hybridoma. Amino acidic sequence was provided for both heavy and light variable chains. Complementarity determining region (CDR) domains are highlighted within the variable sequences: CDR1 in green, CDR2 in orange and CDR3 in purple. HC: heavy chain; VH: variable heavy chain; LC: light chain; VL: variable light chain.

Hybridoma	Primary heavy chain protein sequence			Primary light chain protein sequence	
	HC type	VH	LC type	VL	
61.3	Mouse IgG1	QVQLQQWGAGLLKPSETSLTCAVYGGSFSGYYWSWIRQPPGKG LEWIGEINHSGSTNYNPSLKSRTVISVDTSKNQFSLKLSSVTAADTA VYYCARRQLIASSYAFDIWGQGTMVTVSS	Mouse kappa	EIVMTQSPATLSLSPGERATLSCRASQSVTTRYLSWYQQKPGQAP RLLIYGASTRATGIPARFTGSGSGTDFTLTISSLQPEDFAYYCQQD YNLFTFGPGTKVDIK	
74.2	Mouse IgG1	EVQLVESGGGLVKPGGSLRLSCAASGFTFSNAWMTWVRQAPGK GLDWVGRIKSKTDGTTDYAAPVKGRFTISRDDSKNTLYLQMHSL KTEDTAVYYCTTDPTYSSGSYYIYYYGMDVWGQGTTVTVSS	Mouse lambda	QAVVTQESALTTSPGETVTLTCRSSTGAVTSNYANWVQEKPDLH FTGLIGGTNNRAPGVPARFSGSLIGDKAALTITGAQTEDEAIYFCAL WYSNHWVFGGGTKLTVL	
589.9	Mouse IgG1	EVQLLESGGGLVQPGGSLRLSCAASGFTFSYYAMSWVRQAPGKGL EWVSGSSGSGSAFYADFVKGRFTISRDISKNTFLQMNSLRAEDT AVYYCAKEGTISMAFDIWGQGTTVTVSS	Mouse kappa	AIQMTQSPSSLSASVGDRVITCRASQGIRNDLGWYQQKPGKAP KLLICAASSLQSGVPSRFSGRGSGTDFTLTISSLQPEDFATYYCLQDY NYPRTFGQGTKEIK	
599.5	Mouse IgG1	QVQLQESGPGLVQPSETSLTCTVSGGSISYYWSWIRQPPGKLE WIGYIYYSGSTNYNPSLKSRTVISVDTSKNQFSLKLSSVTAADTAVY YCARDQVNGWYRTGFDYWGQGTLTVSS	Mouse kappa	EIVMTQSPATLSLSPGERATLSCRASQSVSSGYLSWYQQKPGQAP RLLIYGASTRATGIPARFSGSGSGTDFTLTISSLQPEDFAAYYCQQD YNLPYTFGRGSKLEIK	
754.6	Mouse IgG1	QVQLVESGGGLVTPGGSLRLSCAASGFTSDYYMTWIRQAPGKGL EWVSYISNSGYTIYYAESVKGRFTISRDNNAKSSLYLQMNSLRAEDT AVYYCARDEVSFYYGLDVWGQGTTVTVSS	Mouse kappa	DIQMTQSPSSLSASAGDRVITCRASQGIRDDLWYQQKPGQAP KRLIYAASSLQSGVPSRFSGRGSGSTEFTLTISSLQPEDFATYYCLQHN SYPYTFGQGTKEIK	
1222.15	Mouse IgG1	EVQLLESGGGLVQPGGSLRLSCAASGFTFRSYVMSWVRQAPGKG LEWVSAISGSGGSTHYADSVKGRFTISRDNNSKNTLYLQMNSLRAE DTAAYYCAKEGYDIVTGYFKDYYGLDWGQGTTVTVSS	Mouse kappa	DIQMTQSPSSLSASEGDRVITCRASQGIKKDLGWYQQKPGKAPK RLIYAASSLQSGVPSRFSGRGSGSTEFTLTISSLQPEDFATYYCLQHNT YPFTFGPGTKVDIK	

4.3.3 Validation of purified anti-human EPCR mAbs

4.3.2.1 Purification of mAbs from hybridoma cell culture supernatants

Sequencing revealed hybridoma 74.2 as having a lambda light chain, which is less favourable than the kappa chain (as explained in section 4.4) thus it was not selected for subsequent purification. Likewise, hybridoma 1222.15 was not considered for purification due to the partial integrity of its heavy chain sequence. This means that the full constant domain sequence was not fully identified, which does not affect the validity of the variable domain sequence, but it is simply a reflection of the fact that the data has become truncated in the constant domain region.

Eventually, only 4 hybridomas were selected for further validation. Clones 61.3, 589.9, 599.5 and 754.6 were scaled up to produce large quantities of mAbs that were purified as described in section 4.2.2.3.2.

Purified mAbs, renamed as JvGCRC-H61.3, JvGCRC-H589.9, JvGCRC-H599.5 and JvGCRC-H754.6, were analysed by SDS-PAGE gel for their integrity and purity.

In Figure 4.14 both the heavy and light chains of each mAb are visible at the correct molecular weights of 50 and 25 kDa, respectively. No other contaminant proteins were detected.

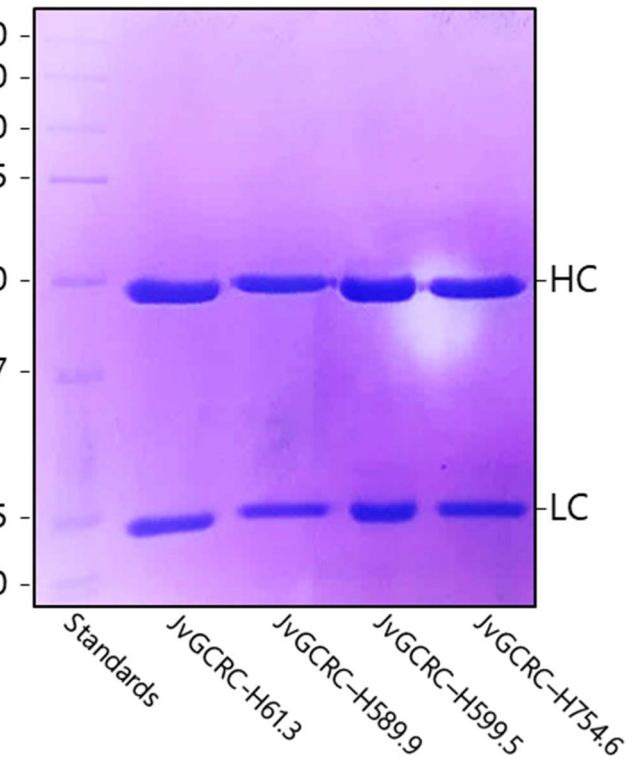


Figure 4.14 – SDS-PAGE of purified anti-EPCR mAbs. Antibodies produced by the selected clones were purified from CSNs. The SDS-PAGE gel shows the heavy chain (HC) of 50 kDa and the light chain (LC) of 25 kDa, as expected.

Purified mAbs were validated for application in several assays of molecular biology, such as immunoblotting, flow cytometry, ELISA and immunofluorescence. All the purified mAbs performed well for the applications in which they were tested.

4.3.3.2 Application of purified mAbs in Western blot

Purified antibodies were tested for Western blot, as described in section 4.2.2.3.3. The aim was to demonstrate that our purified antibodies are specific to EPCR when bound to a membrane on which samples containing the target protein were transferred. For this purpose, DU145 wt cell lysates were used as substrate and a commercial antibody (Sigma) used as a positive control. Figure 4.15 shows that all the purified antibodies were able to selectively bind to EPCR on the membrane at the expected weight and with no background staining.

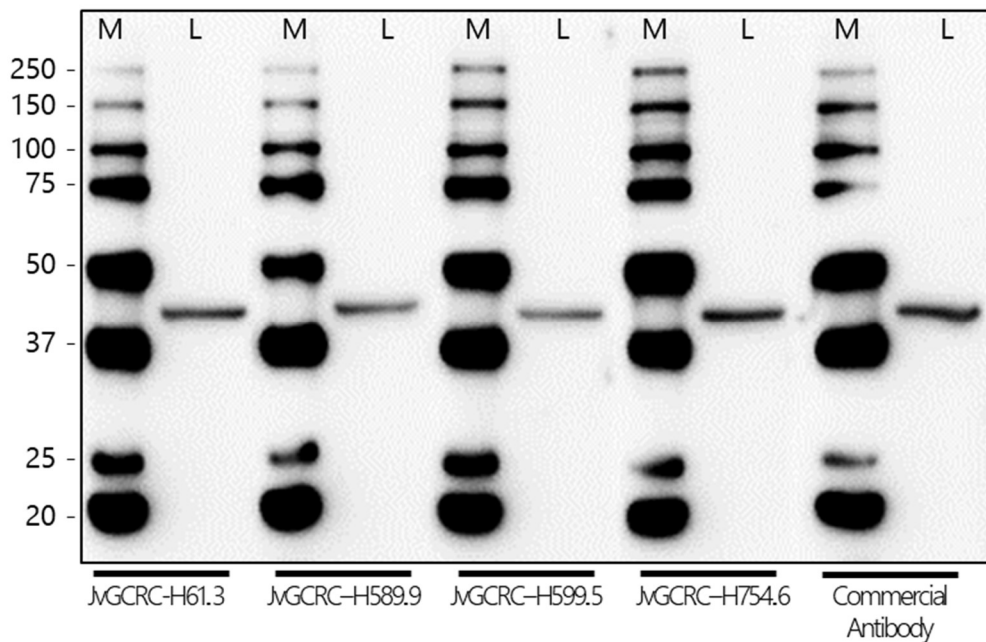


Figure 4.15 – Validation of purified antibodies against human EPCR in Western blotting. 30 µg of proteins from DU145 cell lysates were transferred to each well. Following protein transfer, membranes were incubated over night with each mAb diluted at 1 µg/mL in 5% w/v non-fat dry milk in TBS. EPCR (~46 kDa) was detected on blots blocked with 5% w/v non-fat dry milk in TBST. M: marker; L: lysate.

4.3.3.3 Application of purified mAbs in flow cytometry

Titration of purified mAbs was performed to find the best concentration to use in flow cytometry assays as described in section 4.2.2.3.4. Based on the results obtained (Figure 4.16), concentrations of 1 µg/mL for control (Novus Biological) and JvGCRC-H599.5 antibodies and 3 µg/mL for purified antibodies JvGCRC-H61.3, JvGCRC-H589.9 and JvGCRC-H754.6 were selected.

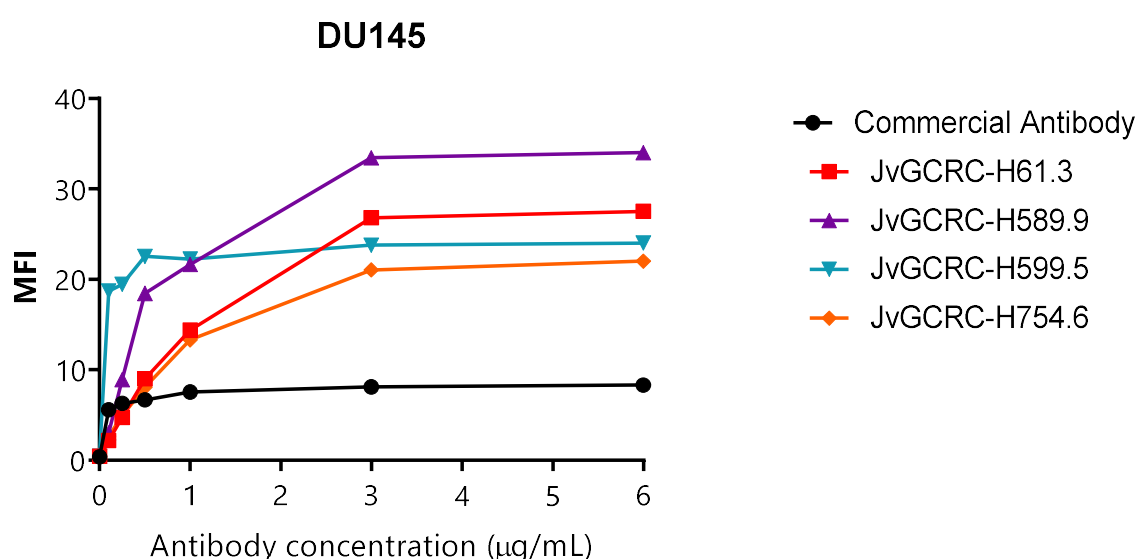


Figure 4.16 – Antibody Titration for Flow Cytometry Analysis. Flow cytometry analysis was performed testing different concentrations of primary antibodies (0.1 – 0.25 – 0.5 – 1 – 3 – 6 µg/mL) on DU145 wt cells. following mAbs binding to EPCR expressed on cell surface a fluorescent signal is detected. Data are reported as mean fluorescence intensity (MFI) values.

Eventually, flow cytometry analysis of purified antibodies to confirm their target recognition specificity was performed on wt and EPCR⁺ DU145 cells. For this assay, previously identified working concentrations were used. Intensity of the fluorescence from control (incubated only with the secondary antibody) and stained populations were overlaid together, and results collected as median fluorescence intensity, as shown in Figure 4.16.

By the analysis of values obtained in both cell lines, all the purified mAbs showed specific binding to EPCR, albeit to differing degrees. Such evidence can be explained considering differential abundance of the EPCR form bearing the specific epitope recognised by each mAb in target cell populations. Interestingly, clone JvGCRC-H61.3 was able to recognise a small population expressing high levels of EPCR in DU145 shRNA4, indicated by the red arrow in Figure 4.17.

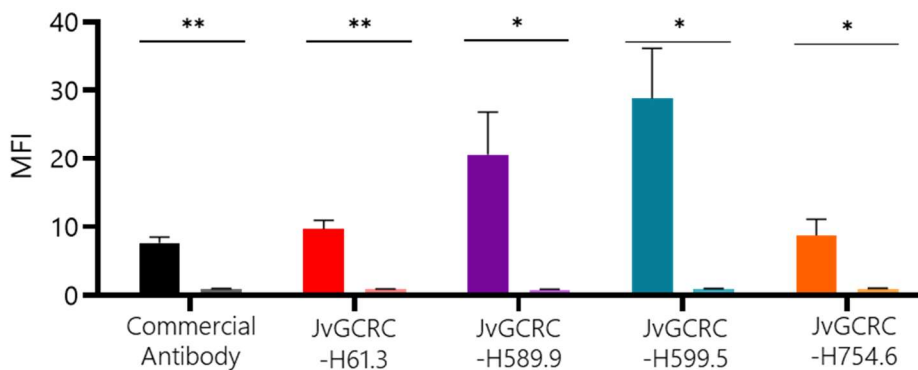
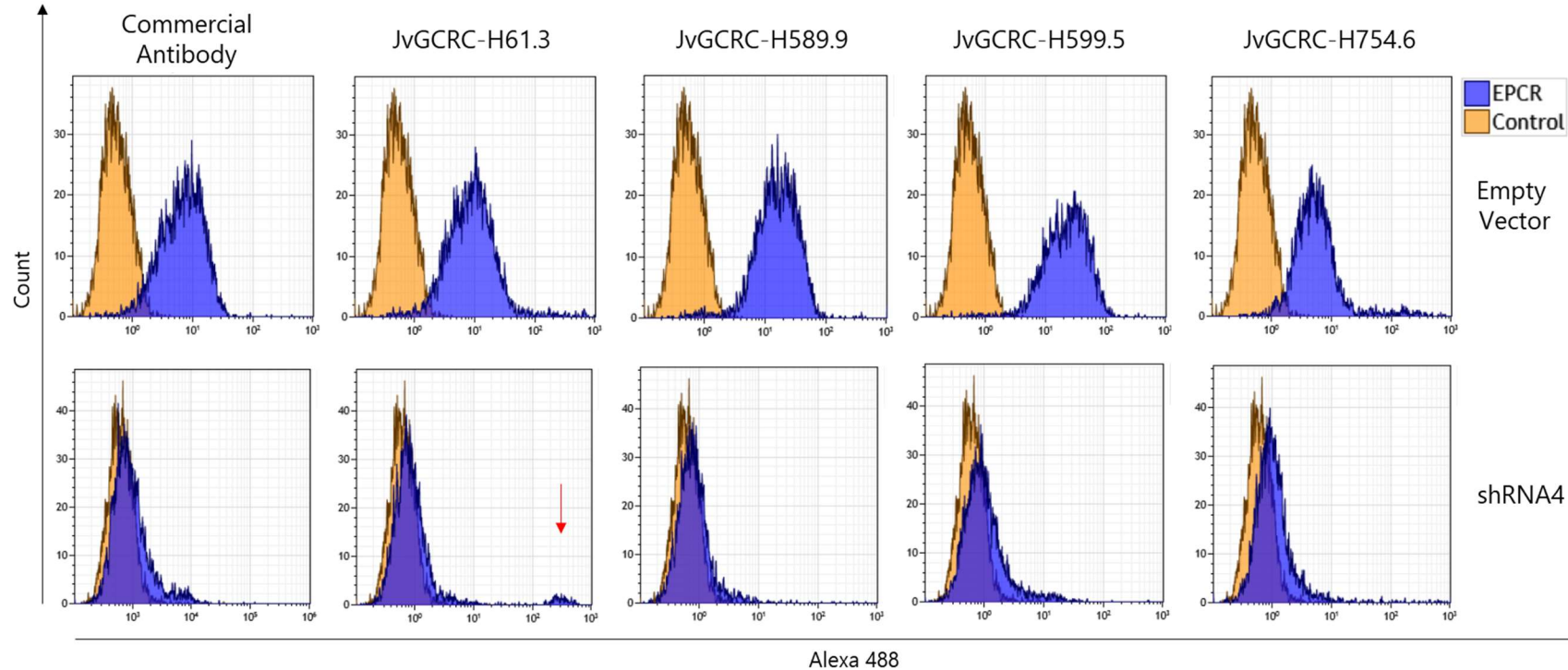


Figure 4.17 – Validation of purified antibodies against human EPCR in Flow Cytometry analysis. Orange shading represents tracks obtained with specific EPCR primary antibody; blue shading shows control cells treated with only secondary antibody. Red arrow indicates a subpopulation recognised by clone JvGCRC-H61.3. Data are reported as mean fluorescence intensity (MFI) values in the bar graph.

4.3.3.4 Application of purified mAbs in immunofluorescence

Purified mAbs were tested for application in immunofluorescence, as described in section 4.2.2.3.5. DU145 wt cells were used to verify specificity as they show known target expression levels. Since EPCR is a membrane protein, cells were not fixed or permeabilised. EPCR presents a typical dotted staining in immunofluorescence specimens, which is visible in Figure 4.18.

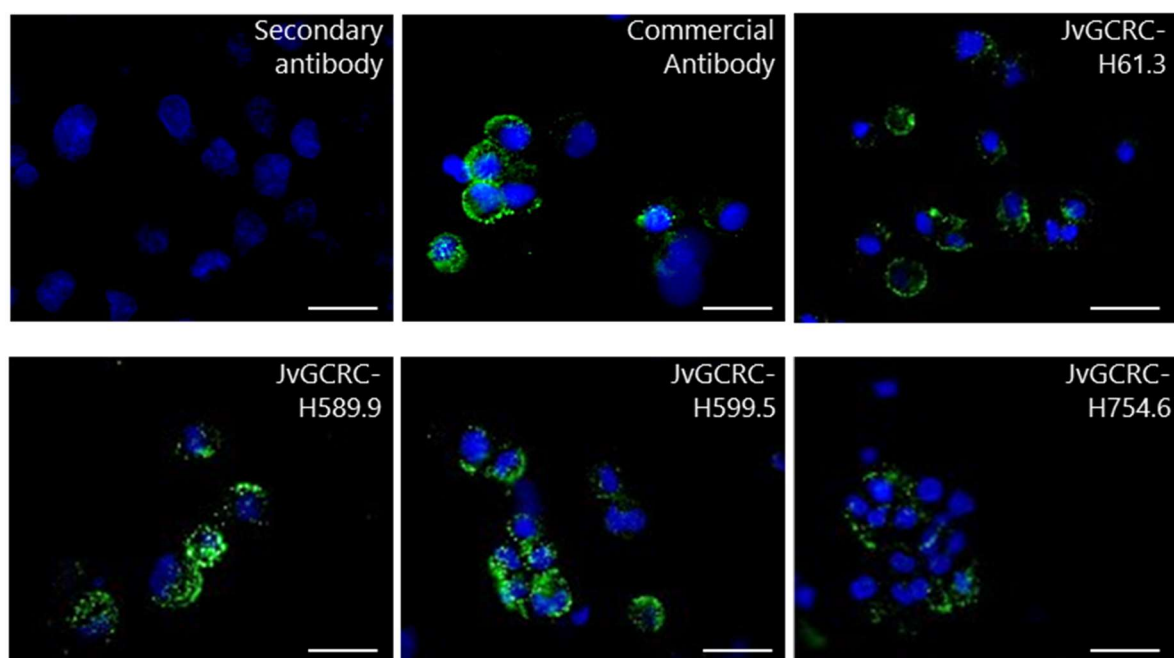


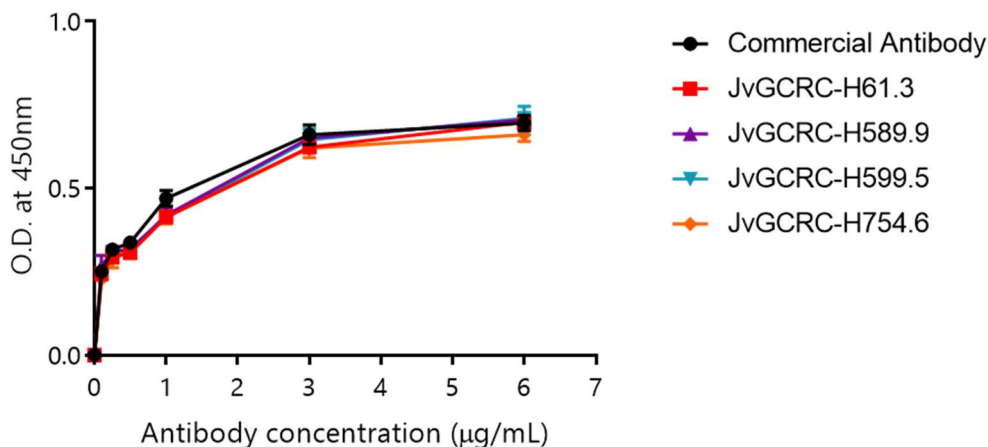
Figure 4.18 – Validation of purified antibodies against human EPCR in Immunofluorescence. Purified antibodies were tested on DU145 wild type cells at a dilution of 1 µg/mL in blocking buffer. EPCR on cells was labelled with control (Abcam) and purified mAbs (green), while nuclei were stained with DAPI (blue). Staining with secondary antibody only was used as negative control. Representative images were taken at 20x magnification with scale bars indicating 40 µm.

The purified mAbs performed well when used to label EPCR on DU145 cells for immunofluorescence assays. The pattern of expression of EPCR obtained with the purified mAbs matches the expected pattern produced using the commercial antibody (Abcam) as a positive control. Indeed, upon labelling, EPCR labelling confirmed target subcellular localisation prediction on the cell membrane and with the characteristic dotted labelling pattern.

4.2.3.4 Application of purified mAbs in ELISA

Titration of purified mAbs was performed using ELISA, as described in section 4.2.2.3.6. Based on the results obtained (Figure 4.19), a concentration of 3 µg/mL was selected for all the antibodies tested.

A.



B.

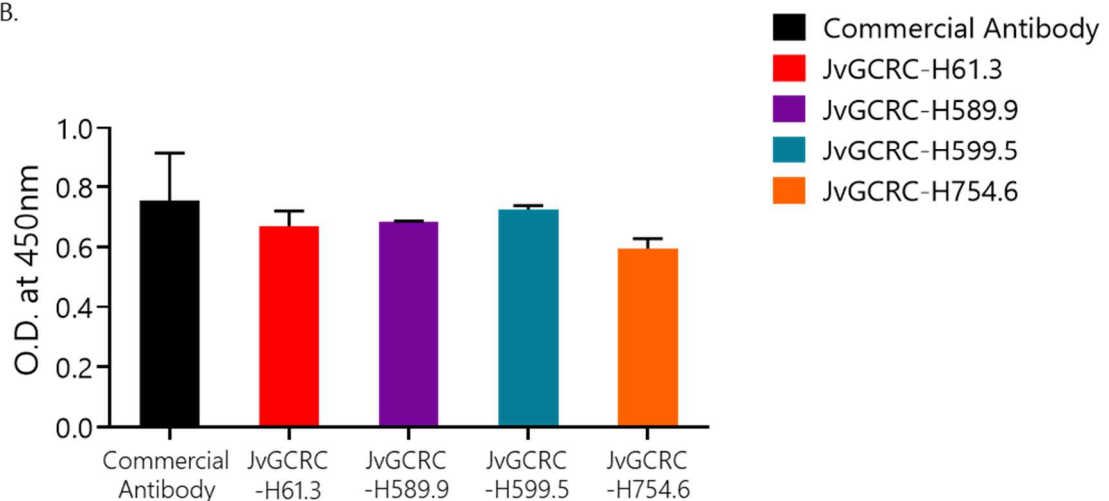


Figure 4.19 – Validation of purified antibodies against human EPCR in ELISA. (A.) Titration of antibodies was performed testing different concentrations of primary antibodies (0.1 – 0.25 – 0.5 – 1 – 3 – 6 µg/mL). (B.) ELISA performed using control (Sigma) and purified antibodies used at a working dilution of 3 µg/mL. Plates in both experiments were coated with full-length EPCR protein diluted at 0.5 µg/mL. All results are presented as mean values of O.D. (optical density) with absorbance at 450 nm.

The purified antibodies produced signals similar to that produced by the commercial antibody (Sigma). Consequently, purified antibodies were used to perform epitope mapping as discussed in the next section.

4.3.2.5 Mapping of epitope recognised by purified mAbs on the target antigen

To identify the epitope recognised by each purified antibody, an epitope mapping using a library of overlapping peptides analysed with ELISA was performed as described in section

4.2.2.3.7. Peptides were generated by GeneScript based on the sequence of the antigen used to generate our antibodies (aa 18-210, relative to the extracellular domain of EPCR). In order to unequivocally identify the epitope, signals obtained from each set must come from the same portion of sequence. Then, comparing the sequence relative to the peptides recognised by the antibody in each set, it is possible to restrict the epitope sequence to few amino acids.

Figure 4.20 shows the results relative to the mAb purchased from Sigma. The antibody bound to the full-length protein, which was used as a positive control. Moreover, a signal with similar intensity was detected from one peptide in each set. Peptide TNTT**IQLQPLQEPESWART** was recognised in set-1 and overlaps with the peptide **IQLQPLQEPESWART** recognised in set-2, highlighted in green are the amino acids shared by both sequences. Such data provide the first evidence of positive correlation between signals. However, in order to narrow down the amino acids involved in the binding, it is important to take into consideration also flanking peptides that still overlap with the peptide bound by the antibody, but yet are not recognised by it. In this case, the recognised sequence is preceded by the peptide LEGPDTNTT**IQLQP** and followed by the peptide **SWARTQSGLQSYLLQ**, highlighted in red are the amino acids shared with the target peptide. Combining these data, it is possible to find what are the amino acids that form the epitope for this antibody: **IQLQPLQEPESWART**. Thus, data suggest that the epitope for Sigma antibody is **LQEPE**. Interestingly enough, the manufacturer of the monoclonal antibody used as a control for this analysis did not release any record regarding the epitope mapped by its product on the antigen, thus it was not possible to cross reference our results, which, on the other side, look decisive. The antibody was generated against the full-length EPCR recombinant protein with GST tag.

The same approach was applied to determine the sequence that constitutes the epitope for the four purified antibodies. Unfortunately, results obtained are not clear-cut in this case.

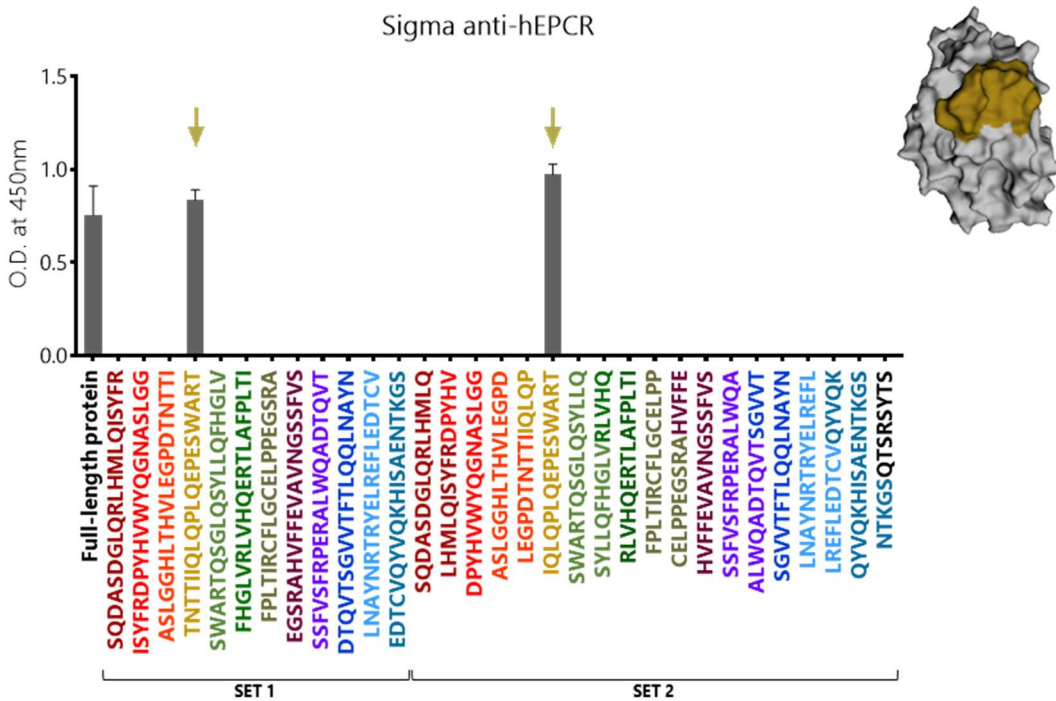


Figure 4.20 – Epitope mapping of Sigma anti-EPCR mAb. Epitope mapping was performed using overlapping peptides representing the extracellular domain of the hEPCR protein. Binding to the target peptides was assessed by ELISA for commercial mAbs from Sigma. Results are presented as mean values of optical density (O.D.) with absorbance at 450 nm. Arrows indicate peptides that match across both set 1 and set 2 of peptides, color-coded for easier interpretation of data. A 3D image of the structure of the protein shows the localisation of the protein. Images were realised using EzMol 2.1 online software.

Figure 4.21 refers to the purified mAb JvGCRC-H61.3, which produces significant signal binding to the control. The antibody binds peptides in both sets, although with a decreased intensity of the signal. The peptide targeted in set-1 is **ASLGGHHLTHVLEGPDTNTTI**, which pairs with the two peptides targeted in set-2, namely **ASLGGHHLTHVLEGPDPD** and **LEGPDTNTTIIQLQP**. Again, considering the flanking peptides it is possible to narrow down the amino acids required for the binding of the antibody. The recognised sequence is preceded by the peptide DPYHVWYQGN**ASLG**G and followed by the peptide **IQLQP**LQEPESWART, highlighted in red are the amino acids shared with the target peptide. Removing the amino acids that do not participate in the binding from the target peptide it is possible to identify the potential target sequence as follows: **ASLGGHHLTHVLEGPDTNTTIIQLQP**, suggesting that the ultimate epitope is the sequence **HLTHVLEGPDTNTTI**. Nevertheless, the presence of unspecific signal relative to the last peptide in set-1 poses a degree of uncertainty on the process of epitope identification.

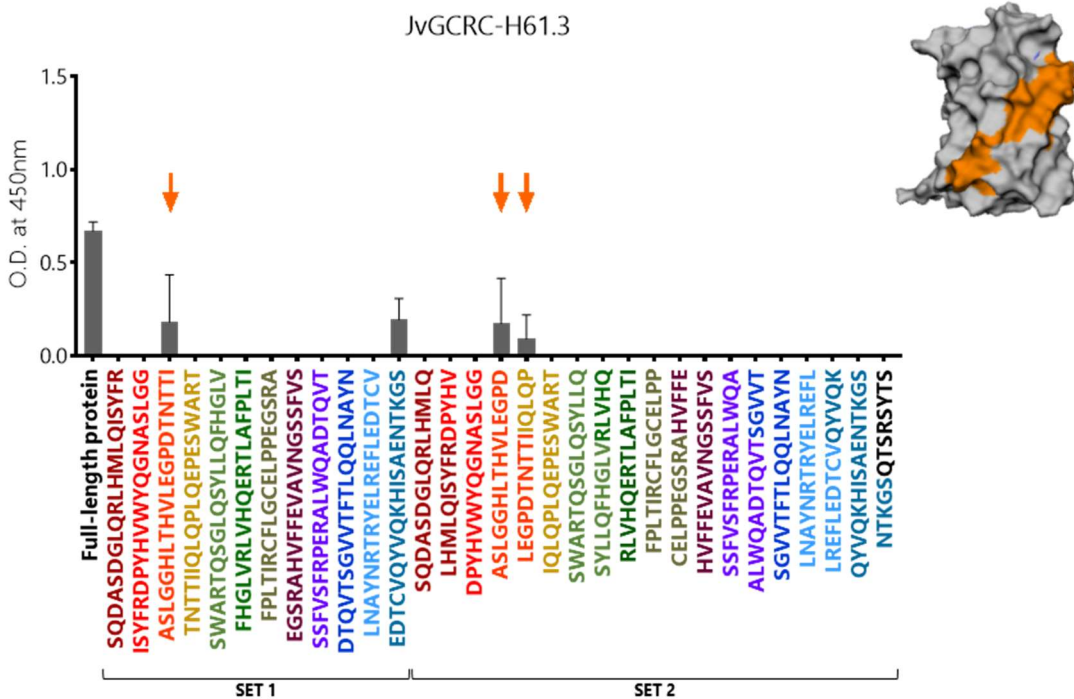


Figure 4.21 – Epitope mapping of JvGCRC-H61.3 anti-EPCR mAb. Epitope mapping was performed using overlapping peptides representing the extracellular domain of the hEPCR protein. Binding to the target peptides was assessed by ELISA for purified mAbs JvGCRC-H61.3. Results are presented as mean values of optical density (O. D.) with absorbance at 450 nm. Arrows indicate peptides that match across both set 1 and set 2 of peptides, color-coded for easier interpretation of data. A 3D image of the structure of the protein shows the localisation of the peptide recognised. Images were realised using EzMol 2.1 online software.

Figure 4.22 refers to the purified antibody JvGCRC-H589.9. This antibody also binds well to the full protein. Non-specific binding to two different peptides, one from each set, was observed. Two potential binding sites were highlighted that map distant from each other on the native structure of EPCR. The first potential binding site is determined by low binding to peptide **SWARTQSGLQSYLLQFHGLV** from set-1, which matches with peptide **SYLLQFHGLVRLVHQ** from set-2. Flanking peptides are **SWARTQSGLQSYLLQ** and **RLVHQERTLAFLPTI**, which narrows down the potential amino acid sequence recognised to **SYLLQFHGLV**. A second potential binding site was identified matching the sequences of two peptides, **SSFVSFRPERALWQADTQVT** and **DTQVTSGVVTFTLQQLNAYN**, from set-1 and peptide **ALWQADTQVTSGVVT** from set-2. Considering the flanking peptides **SSFVSFRPERALWQA** and **SGVVTFTLQQLNAYN**, it is possible to inference the potential target sequence as **ALWQADTQVTSGVVT**.

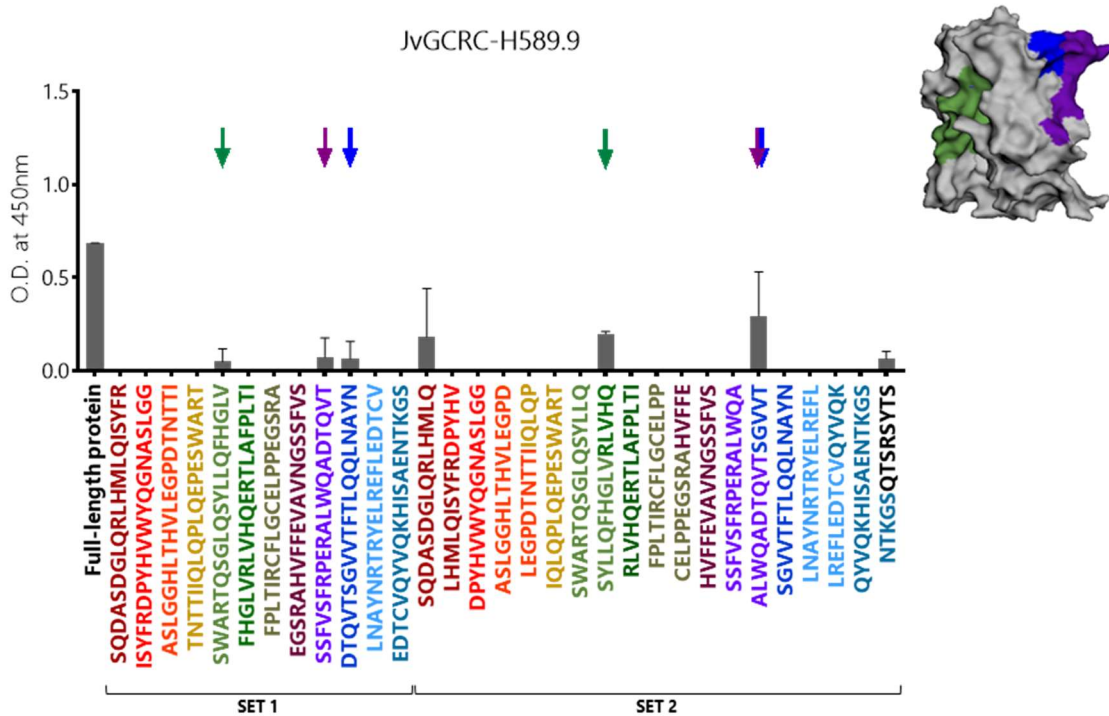


Figure 4.22 – Epitope mapping of JvGCRC-H589.9 anti-EPCR mAb. Epitope mapping was performed using overlapping peptides representing the extracellular domain of the hEPCR protein. Binding to the target peptides was assessed by ELISA for purified mAbs JvGCRC-H589.9. Results are presented as mean values of optical density (O. D.) with absorbance at 450 nm. Arrows indicate peptides that match across both set 1 and set 2 of peptides, color-coded for easier interpretation of data. A 3D image of the structure of the protein shows the localisation of the peptides recognised. Images were realised using EzMol 2.1 online software.

Concerning the purified antibody JvGCRC-H599.5, it was not possible to identify any potential epitope sequence. Interestingly, the antibody was able to bind to the full-length protein, but the three signals obtained from the wells containing the peptides could not be matched with each other (Figure 4.23), suggesting that no specific binding occurred, thus not allowing for interpretation.

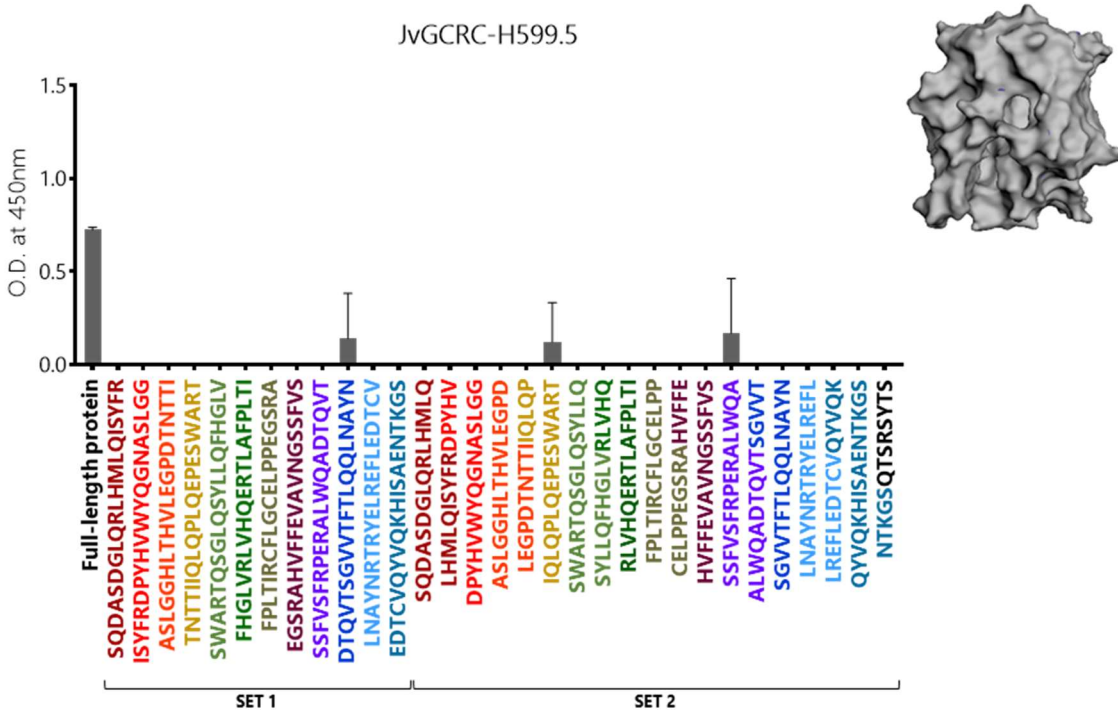


Figure 4.23 – Epitope mapping of JvGCRC-H599.5 anti-EPCR mAb. Epitope mapping was performed using overlapping peptides representing the extracellular domain of the hEPCR protein. Binding to the target peptides was assessed by ELISA for purified mAbs JvGCRC-H599.5. Results are presented as mean values of optical density (O. D.) with absorbance at 450 nm. Arrows indicate peptides that match across both set 1 and set 2 of peptides, color-coded for easier interpretation of data. A 3D image of the structure of the protein shows that no identification was possible. Images were realised using EzMol 2.1 online software.

JvGCRC-H754.6 antibody also presented two different potential binding sites, distant on the conformational structure of EPCR Figure 4.24. A strong signal, similar to the one obtained with the full-length protein, was produced by the binding of the antibody to the peptide EDTCV**QYVQKHISAENTKGS** in set-1, which matches with signals obtained with peptides **QYVQKHISAENTKGS** and **NTKGSQTTSYTS** from set two. This case is an interesting one as it refers to the final peptides in which the whole sequence was split. Indeed, since the last 8 amino-acid-long sequence **QTSRSYTS** in the last peptide of set-2 are not represented in the last peptide of set-1, nothing can be deduced about their involvement in the binding with the antibody. Nevertheless, the preceding peptide **LREFLEDTV****QYVQK** in set-2 adds useful information, identifying the binding region in the sequence **QYVQKHISAENTKGS**. The second signal detected from a peptide in set-1 refers to the sequence **EGSRAHVFEEAVNGSSFVS**. Despite the very low intensity, such peptide can be matched with the two peptides **CELPPEGSRAHVFFE** and **HVFFEAVNGSSFVS** recognised in set-2. In this case, there is no need to crosscheck with flanking peptides since the target sequence **EGSRAHVFEEAVNGSSFVS** fully overlaps with the peptide bound by the antibody in set-1.

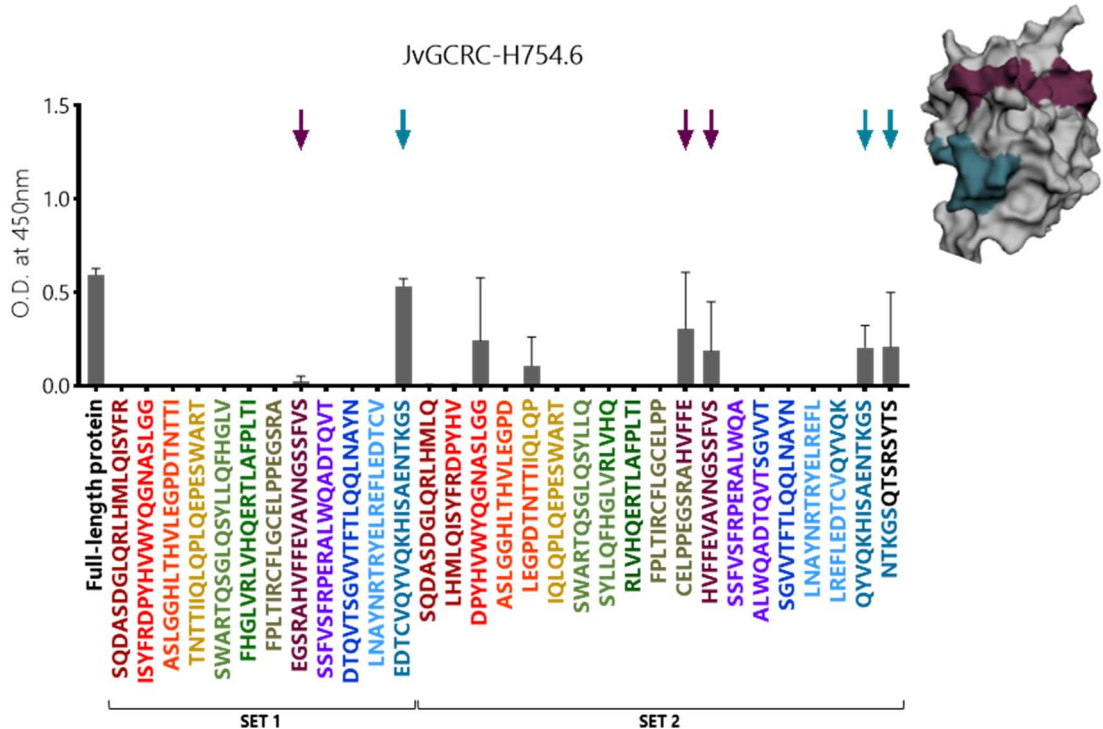


Figure 4.24 – Epitope mapping of JvGCRC-H754.6 anti-EPCR mAb. Epitope mapping was performed using overlapping peptides representing the extracellular domain of the hEPCR protein. Binding to the target peptides was assessed by ELISA for purified mAbs JvGCRC-H754.6. Results are presented as mean values of optical density (O. D.) with absorbance at 450 nm. Arrows indicate peptides that match across both set 1 and set 2 of peptides, color-coded for easier interpretation of data. A 3D image of the structure of the protein shows the localisation of the peptides recognised. Images were realised using EzMol 2.1 online software.

4.4 Discussion

Data presented in the previous chapters suggested EPCR could be targeted in aggressive PCa therapy. Therefore, this study intended to generate a monoclonal antibody which could be used in various immunotherapy treatment strategies such as CAR T cells, NK cell mediated killing and for delivering specific cytotoxic drug cargos to EPCR expressing tumour cells. Secondly, the generated antibody could be used for screening EPCR expression in prostate cancer (PCa) and other cancer settings as a prognostic marker for assessing disease severity.

Before proceeding to the generation of new antibodies, information on existing antibodies against EPCR was collected. For this reason, comprehensive research was conducted to find the availability of antibodies against the human EPCR using web-based resources such as CiteAb and Antibodypedia, although most of the times such research is made difficult by the absence of a standardised classification for antibodies. The research was performed using "EPCR" and its synonyms "PROCR" and "CD201" as keywords on the databases. Querying Antibodypedia, 144 commercially available mAbs targeting human EPCR were found, of which 90 are murine and three are human - the relative list of reagents can be found at the following link: <https://www.antibodypedia.com/gene/11183/PROCR>. The Citeab platform provides a list of references for each antibody that matches the search. Thus, it was used to search for studies in which anti-human EPCR mouse antibodies were employed, in order to identify the relative mechanisms of action exerted (<https://www.citeab.com/antibodies/search?q=epcr>). The results indicated that mouse mAbs anti-EPCR have already been used before in blocking experiments *in vitro* on CRC cells, *in vivo* on MDA-MB-231 breast cancer cells inoculated in SCID mice (Schaffner et al. 2013). Moreover, there are in literature examples of blocking anti-EPCR mouse mAbs that have been generated for studies but that do not appear on the market (Zoltan, Alexander et al. 1997, Nayak et al. 2009). Blocking mAbs against EPCR in the past two decades were extensively produced to study the biologic function in the coagulation pathway of the interaction of EPCR with its ligand protein C. However, to date there are no reports available regarding the use of anti-EPCR mAbs for targeted cancer therapy, which exposes a potential niche in the field for the development of a new therapeutic tool.

To produce anti-human EPCR mouse mAbs for this study, hybridomas were generated in collaboration with the team of Prof. Hans-Martin Jäck at the University of Erlangen

(Germany). Although over the years new strategies have been developed to increase the efficiency of the hybridoma technology, it still presents significant hurdles at each step that make it an extremely time-consuming and resource-demanding process. In the present project, attentive approaches were used in order to guarantee the performance of the best protocol, tailored on the specific needs. Two mice were immunised using the human EPCR recombinant protein, rather than whole cells overexpressing EPCR, in order to reduce the generation of non-specific antibodies-producing hybridomas. Cell fusion was performed using the most efficient electrofusion method. A two-step screening approach based on ELISA and FCM analysis of CSNs was used to select the hybridomas producing IgG molecules specific for the human EPCR. Monoclonality and stability of the antibodies were ensured cloning the hybridomas by limiting dilutions. Overall, 1,300 hybridomas were screened. 572 hybridomas were producing IgGs, of which only 19 were specific for human EPCR. Six stable hybridomas that retained the ability to produce antibodies were then subcloned and sequenced, determining an efficiency of generation of 0.5%.

Selected hybridomas were sequenced to obtain essential information for potential mAbs engineering, function optimisation, database banking, and patent application. Hybridoma sequencing confirmed the subclass of the four mAbs being IgG1, which is the most suitable IgG subclass for therapeutic strategies that rely on the antibody's effector function. Indeed, due to the sequence of the hinge region, IgG1 represents a more stable and flexible molecule compared to the other IgG subclasses, which is of great importance during the connection of effector cells and target. Moreover, the IgG1 molecules have a longer *in vivo* half-life, can permeate through vasculature, and exert Fc-mediated biological effects, such as ADCC, CDC and ADCP (An 2010; Parray, Shukla et al. 2020). Sequencing also provided information regarding the Fabs regions of the light constant (LC) chains of the antibodies. Apart from clones 74.2, all the antibodies bear a class κ-LC, which reflects the fact that hybridoma cells produce mostly IgG formed by heavy chains assembled with κ-LC (Babrak, McGarvey et al. 2017). Antibodies containing κ-LC present an elbow angle, defined as the angle formed at the joint of the variable domains (VL and VH) and the constant domains (CL and CH1), smaller (less than 180°) and prone to higher flexibility in solution compared to λ-LC bearing antibodies (Stanfield, Zemla et al. 2006). It has been reported that the assembly of heavy chains with κ-LC increases the efficiency of antibody secretion (Montaño, Morrison 2002). For these reasons hybridomas producing κ-LC molecules were preferred over λ-LC producers. Furthermore, one of the aims of this project was to patent the best

performing antibody generated, which means that complete data sets are preferred so to provide a more exhaustive description of the antibody. Since it was not possible to identify the entire sequence of the heavy chain of clone 1222.15, it also was not considered for the following steps of antibody characterisation. Eventually, four clones were selected and purified: 61.3, 589.9, 599.5, 754.6.

The relevance of generating new mAbs lies in the advantage of their use to design therapeutic strategies as well as their application as reagents for molecular assays. The validation process provides the experimental documentation supporting an antibody suitability for the intended use or uses. Nowadays, validation represents a very critical aspect of antibody generation that shall not be overlooked as the use of poorly characterised and validated mAbs in research can contribute to lack of reproducibility of pre-clinical studies with a consequent dramatic waste of investment (Weller 2018). Many challenges to the characterisation of mAbs stem from the complexity and high cost of the process itself, which many laboratories cannot afford. In this project, efforts were made to ensure the most extensive characterisation of the mAbs purified possible with the resources available.

Purified antibodies – renamed as JvGCRC-H61.3, JvGCRC-H589.9, JvGCRC-H599.5 and JvGCRC-H754.6 – were tested for several applications, such as Western blot, FCM, immunofluorescence, and ELISA, performing well in all of them as summarised in Table 4.15. From the results obtained during the validation process of the purified mAbs it was possible to confirm that the four antibodies can recognise EPCR in its native conformation. Indeed, the purified antibodies produced clear signals during FCM and immunofluorescence analysis on EPCR-expressing DU145 cells. Working concentration was determined for each mAb and dedicated protocols optimised (see section 4.2.2.3).

Table 4.15 – Summary of the suitability of purified mAbs for different applications.

Clone	Application			
	WB	ELISA	IF	FCM
JvGCRC-H61.3	✓	✓	✓	✓
JvGCRC-H589.9	✓	✓	✓	✓
JvGCRC-H599.5	✓	✓	✓	✓
JvGCRC-H754.6	✓	✓	✓	✓

To reinforce the novelty of the antibodies generated during this study, mapping of the respective epitopes was performed. Depending on whether the epitope is linear (consisting of sequential amino acids in the primary structure) rather than conformational (the amino acids that contribute to the binding being spaced from each other in the protein primary sequence but close in its native structure), it is not always easy and straightforward to identify the exact epitope recognised by an antibody. Several approaches are available for epitope mapping, such as biophysical methods, binding analysis, and mutagenesis. The gold standard method is X-ray Co-Crystallography in which Fab fragment is obtained from the antibody and then complexed with the antigen. Crystal structure of the complex is then obtained following X-ray crystallography. Although this technique provides a very accurate identification of the single amino acids contributing to the interaction between antibody and target protein, it requires a high level of expertise and it is highly expensive. Moreover, is not always possible to obtain diffraction quality crystals, making this the limiting step (Abbott, Damschroder et al. 2014). Yeast display also is commonly used to map conformational epitopes. Peptides of a random mutagenesis library are expressed by yeast cells and mAbs screened based on their selective binding. Compared to the X-ray crystallography the yeast display technique is faster, less expensive while still providing a reasonable degree of accuracy. Nevertheless, because some residues in the epitope contribute more strongly to the interaction with the antibody, they can impair the accuracy of the technique. In addition, mutation can produce alteration in the native protein conformation. Epitope mapping using ELISA with a library of overlapping peptides represents a more accessible approach and, although it ideally suits linear epitopes identification, can be used on antigens with a simple conformation, such as EPCR. However, a drawback of this technique is the low resolution of the epitope sequence. Thus, results provide information about the peptide in which the epitope is localised, without adding further information about nor individual amino acid involved in the interaction or its strength. The results presented in this chapter suggest that epitopes recognised by each antibody are localised in different regions of the protein, except for clone JvGCRC-H599.5, for which it was not possible to identify the epitope localisation on EPCR.

Many factors can affect peptide-based epitope identification. Firstly, the antibody might recognise a conformational rather than linear epitope, thus more than one peptide can be recognised by the antibody during the assay, like in the case of clone JvGCRC-H589.9. Conversely, it can occur that the sequence recognised by the antibody is disrupted during the generation of the peptides and not represented in the library, thus preventing the

antibody's binding. This could explain the impossibility to obtain information about the epitope recognised by clone JvGCRC-H599.5. Antibody binding is also regulated by the glycosylation of the antigen and native EPCR presents 4 N-glycosylations. While N-glycosylations can be maintained in the recombinant protein when produced in human cells, they are absent in peptides and this can affect the antibody's recognition of the target.

The identification of the sequence relative to the epitope recognised by each antibody provides information to predict whether they exert biological functions. Blocking antibodies compete with the natural ligand for the binding to the epitope on the antigen. Previous studies identified the protein C binding amino acids on EPCR as *Arg-81, Leu-82, Val-83, Glu-86, Arg-87, Phe-146, Tyr-154, Thr-157, Arg-158, and Glu-160* (Liaw et al. 2001). Thus, comparison of the position of the residues involved in the binding between EPCR and its ligand protein C to the residues representing the potential epitopes for each mAb helps predicting whether antibodies can exert a blocking function. Table 4.16 summarises the relative amino acid positions contributing to the binding of both protein C and tested antibodies to EPCR. Epitopes recognised by Sigma, JvGCRC-H61.3 and JvGCRC-H754.6 antibodies do not share amino acids recognised also by protein C. Conversely, four amino acids forming the epitope recognised by JvGCRC-H589.9 antibody are also part of protein C binding site on EPCR, which suggests that JvGCRC-H589.9 can potentially have a blocking action. Nothing can be assumed about clone JvGCRC-H599.5, of which no epitope indication is available.

Table 4.16 – Epitope mapping and ligand binding residues comparison. The table below shows the relative positions of the residues required for the binding with protein C and the residues identified as potential epitopes recognised by commercial and purified mAbs against human EPCR.

Ligand	Position of amino acids bound on EPCR
Protein C	81-83; 86-87; 146; 154; 157-158; 160
Antibody	Position of amino acids bound on EPCR
Commercial (Sigma)	73-77
JvGCRC-H61.3	53-67
JvGCRC-H589.9	88-97; 148-162
JvGCRC-H599.5	N/A
JvGCRC-H754.6	188-202

The ability of the purified antibodies to act as blocking agents or not was not investigated *in vitro*. Indeed, *in vitro* competitive assays incubating DU145 cells with protein C, the natural ligand of EPCR, would have been an interesting strategy to assess the potential competition of the purified mAbs for the binding to EPCR.

This chapter provided a complete report of the techniques used to produce new mAbs against the human EPCR with the hybridoma technique. Data collected herein pose the experimental support for further evaluation of the newly generated mAbs ability to mediate ADCC, both *in vitro* and *in vivo*. In the following chapter, potential use of anti-human EPCR mAbs as targeting agents for treatment of invasive PCa is being investigated.

5. Anti-EPCR mAb Subtype Switching and Testing Its Therapeutic Utility Using Targeting Experiments

5.1 Introduction

As previously mentioned in chapter 1, therapeutic IgGs can drive cytotoxicity by engaging the complement system and/or immune effector cells with their Fc region. During complement-dependent cytotoxicity (CDC), mAbs lead cell lysis through deposition of serum complement proteins on opsonised target-cells. On the other hand, ADCC is mediated by cytotoxic NK cells, $\gamma\delta$ T cells monocytes, and macrophages expressing specific Fc receptors that trigger cytotoxic activity upon recognition of the mAbs-antigen complex on target cells (Table 5.1).

Table 5.1 – Effector cells and activating Fc γ Receptors Involved in ADCC. Effector cells and relative receptors for IgG Fc expressed. Partially adapted from (Gómez Román, Murray et al. 2014).

Predominant Fc γ Receptors	Effectors	Interacting IgG (by affinity)
Fc γ RI (CD64)	Monocytes/macrophages	IgG1=IgG3>IgG4
Fc γ RIIa (CD32)	Monocytes/macrophages	IgG1>IgG3>IgG2>IgG4
Fc γ RIIIa (CD16)	NK cells $\gamma\delta$ T cells (subset)	IgG3>>IgG1>>IgG4>>IgG2

The affinity of mAbs for the relative receptors, and thus the potency of the reaction triggered, depends on several factors. Different IgG subtypes can show different affinity for different Fc γ receptors. Binding of the antibody to its cognate antigen induces conformational modifications in the Fc region that enhance the subsequent interaction of the antibody with the Fc receptors on the effector cells. Moreover, antibody-receptor binding strength is affected by the glycosylation degree of the immunoglobulin Fc region. Indeed, the reduced fucosylation of the Fc region of IgG1 has been demonstrated to increase the affinity for the Fc γ RIIIa, thus eliciting a stronger ADCC. NK cells and $\gamma\delta$ T cells are the sole immune cells in which Fc γ RIIIa is expressed in absence of an inhibitory Fc receptor (Pereira, Chan et al. 2018).

Binding of mAbs to the Fc γ RIIIa (CD16) can activate NK cells or other myeloid cells thus triggering the secretion of proinflammatory cytokines (such as IFN γ and TNF- α) and chemokines (such as MIP1 α/β and RANTES) and the release of cytolytic granules containing granzyme B and perforin (although ADCC also involves other killing pathways such as FAS-ligand and oxidative burst pathways). NK cells represent highly useful immune effectors in cell-targeted therapies due to the readiness of their response. Indeed, Fc γ RIIIa activation is enough to trigger resting NK cells without the need of co-stimulatory signals (Felices et al. 2016). NK cell tolerance to self is mediated by the binding of the inhibitory killer cell Ig-like receptors (KIR: CD158) to the HLA (human leukocyte antigen). For these reasons, Fc γ RIIIa is regarded to as the main receptor involved in triggering ADCC *in vitro* and *in vivo*. The specific response to antibody-based therapy in cancer patients also depends on the relative NK cell repertoire, each expressing different combinations of receptors. Indeed, individual NK cell subpopulations shown opposite response to therapeutic mAbs, with the CD56 $^{\text{dim}}$ CD16 $^{+}$ NK cells able to develop ADCC response, in contrast to CD56 $^{\text{bright}}$ NK cells that do not elicit ADCC due to low/no CD16 expression (Muntasell, Cabo et al. 2017).

ADCC has been widely exploited as a therapeutic approach by using targeting mAbs against several tumours. Cetuximab to treat metastatic colorectal cancer (García-Foncillas, Díaz-Rubio 2010), trastuzumab for HER2-positive breast cancer (Petricevic, Laengle et al. 2013), rituximab for B-cell non-Hodgkin lymphoma (NHL) (Weiner 2010) are all examples of ADCC-mediating mAbs used in the clinic. Interestingly, a significant discrepancy exists between effective concentrations of mAbs required *in vitro* and *in vivo*. While typical treatment of cancer patients requires weekly doses to maintain an effective concentration of at least 10 $\mu\text{g}/\text{mL}$ in the serum, to elicit an adequate response *in vitro* mAb concentrations by several orders of magnitude lower are enough (Natsume, Niwa et al. 2009). Efficacy of mAbs to elicit ADCC *in vivo* has also been demonstrated to be impaired by the presence of endogenous IgG in the serum that saturate Fc γ RIIIa on NK cells, thus requiring higher concentrations of mAbs in order to obtain a therapeutic effect (Preithner, Elm et al. 2006).

Development of anticancer drugs is a long and challenging process. Once the preliminary *in silico* and *in vitro* studies have been conducted to support the suitability in living systems of a potential new therapy under development, the following step consists in proving the concept *in vivo*. Data generated about the efficacy of a drug in preclinical studies are expected to be as predictive as possible of their efficacy once translated in the clinic. For

this reason, the choice of the adequate animal model, based on solid theoretical rationale, plays a fundamental role in the decision-making process towards the promotion or rejection of a specific drug for its use in patients. A good model for preclinical investigations has to be able to reproduce the relevant features of the human disease, be easy to manage and demonstrate the measurable effects of the treatment under study. At the present, 95% of drugs fail to move from phase 1 of clinical development towards market authorisation (Ireson, Alavijeh et al. 2019).

Humans and mice started to evolutionary diverge 87 million years ago, thus there are many similarities as well as relevant differences in systems, such as the immune and metabolic systems, link both species, which might represent an added challenge to any translational study (Bailey, Christoforidou et al. 2013). Nevertheless, murine models are still at the first line for use in therapeutic development. To date, several preclinical models are available to meet the requirement of each step of the drug selection/validation process. Traditional tumour models, such as the subcutaneous cell-line implantation in mice are very useful in the discovery stage as they are easy to manage. Such simple models can be either defined as cell line-derived xenograft (CDX) or syngeneic, depending on whether the cells used to generate tumours originate from a different species from the recipient or from the same species, respectively. On the other hand, complex models provide a higher predictive indication about the clinical efficacy of a drug, although their application and management come with more challenges. Patient-derived xenograft (PDX) models refer to tumour implants resected from patients, usually implanted in immunosuppressed hosts, such as NOD/SCID (non-obese diabetic/severe combined immunodeficiency) mice. However, the lack of a human immune system in such models poses a relevant limit. For this reason, humanised PDX models are arousing more and more interest. The implantation of human T cells, B cells, NK cells and monocytes in rodents that have been engineered to have a 'humanised' immune system, in lieu of their original immune system, renders these better models to recapitulate the complex interaction between the immune system and tumours (Fisher, Kamperschroer et al. 2012). A further refinement in the reproduction of human disease development is provided by the genetically engineered mouse models (GEMMs), in which the presence of key human drivers leads to the spontaneous development of tumours in immunocompetent mice (Van Dyke, Jacks 2002). Such models allow for controlling of either the temporal and spatial expression of oncogenes or silencing of tumour suppressors. Moreover, GEMMs provide an opportunity to allow the interplay between the tumour and

its microenvironment to occur. However, GEM models require complex set-ups and long times for tumour developments thus leading to considerable investments.

The use of immunocompromised mice as the recipients of human-derived tumours is necessary as it prevents immune rejection. However, such models critically preclude the possibility to investigate the potential efficacy of therapies that function as modulators of the immune system. Thus CB17/SCID mice were used for the final part of this project due to the partial impairment of their immune system, which provides this specific mouse strain with normal NK cells, macrophages, and granulocytes. Preclinical validation of the selected target, namely the human EPCR, was addressed using a simple mouse model in which to translate the investigations previously conducted *in vitro* on prostate cancer (PCa) cell lines. To do so, DU145 human androgen-independent prostate xenografts were generated in CB17/SCID mice and consequently mAbs against the human-EPCR were administered and the effects of such therapy on tumour growth and metastases to distal sites formation kinetics investigated.

The aim of this chapter is to test the principle of targeting the human EPCR expressed on PCa cells using mAbs to block tumour growth and metastases by triggering the cytotoxic activity of the host's immune system effector cells.

5.2 Materials and Methods

5.2.1 Materials

5.2.1.1 Reagents

CELL CULTURE MEDIA	PROVIDER
EMEM	SLS (Lonza)
RPMI 1640	SLS (Lonza)
Opti-MEM	Gibco
CULTURE MEDIA SUPPLEMENTS	PROVIDER
2-mercaptoethanol	Gibco
Foetal calf serum (FCS)	Fisher (GE Healthcare)
L-Glutamine	SLS (Lonza)
Sodium Pyruvate	SLS (Lonza)
Puromycin	Sigma
Zeocin	Invitrogen
OTHER CELL CULTURE REAGENTS	PROVIDER
Dimethyl sulfoxide (DMSO)	Insight Biotechnology
Dulbecco's phosphate buffered saline (DPBS)	SLS (Lonza)
Trypan Blue solution (v/v 0.4%)	Sigma
Trypsin/Versene	SLS (Lonza)
CHEMICALS & BIOCHEMICALS	PROVIDER
Double distilled water (ddH ₂ O)	Barnstead, Nanopure Diamond
Nuclease-free water	Ambion
Ethyl alcohol absolute	VWR chemicals
Glycerol	Sigma
Glycine	Sigma
ISOTON II	Beckman Coulter
Ethanol	Fisher Scientific
Hydrochloric acid (HCl)	Fisher Scientific
Sulfuric Acid (H ₂ SO ₄)	Sigma
IMMUNOCHEMICAL REAGENTS	PROVIDER
Alexa Fluor™ 488 conjugated donkey anti-rat IgG	Invitrogen
Alexa Fluor™ 488 conjugated goat anti-mouse IgG	Invitrogen
Anti-Mouse IgG HRP-linked Ab	Cell Signalling Technology
Mouse anti-human EPCR (clone ab56689)	Abcam
Mouse anti-human EPCR (clone M2)	Sigma
Rat anti-mouse EPCR (clone RCR-252)	Novus Biologicals
REAGENT KITS	PROVIDER
Mouse Fc _y RIV ADCC Complete Bioassay	Promega
Mouse Fc _y RIV ADCC Core Bioassay	Promega
FcR Blocking Reagent	Miltenyi Biotec

LIVE/DEAD™ Fixable Violet Dead Cell Reagent	Thermo Fisher Scientific
TMB Substrate Set	Biolegend

OTHERS	PROVIDER
CB17/SCID mice	Charles River
DU145 human prostate cancer cell line	ATCC
LNCaP human prostate cancer cell line	ATCC
PC3 human prostate cancer cell line	ATCC
EPCR Protein, Human, Recombinant (His Tag)	Sino Biological
pBudCE4.1/Luc2	JvGCRC
RediJect D-Luciferin Bioluminescent Substrate	PerkinElmer

5.2.1.2 Equipment

LABORATORY PLASTICS, GLASSWARE AND SHARPS	PROVIDER
Cell culture flasks (T25, T75, T175)	Sarstedt, UK
Conical flasks (50 mL, 100 mL)	Pyrex
Eppendorf tubes (0.5 mL, 1.5 mL, 2 mL)	Sarstedt, UK
12x75 mm polystyrene flow cytometry tubes	Tyco healthcare group
Falcon tubes (50 mL, 15 mL)	Sarstedt, UK
Filter tips (0.5-10 µL, 2-20 µL, 20-200 µL, 200-1000 µL)	Greiner bio-one/ Sarstedt
Flat-bottom culture dishes (6, 24, 96-well)	Sarstedt, UK
Micropipette tips (0.5-10 µL, 20-200 µL, 200-1000 µL)	Sarstedt, UK
Pipettes (5mL, 10mL, 25mL)	Sarstedt, UK
Screw-top tubes (15mL, 50mL)	Sarstedt
Serological pipettes	Sarstedt
Syringes (10 mL, 20 mL)	Becton Dickenson
Universal tubes (20 mL)	Greiner

LABORATORY EQUIPMENT	PROVIDER
4°C refrigerators	Lec
-20°C freezers	Lec
-80°C freezers	Revco/ Sanyo
IVIS Lumina III system	PerkinElmer
Cell culture incubator	Sanyo
Centrifuges	Sanyo, Eppendorf
Class II safety cabinets	Walker
Flow cytometer	Beckman Coulter
Haemocytometers	SLS
Light microscope	Nikon/Olympus
Microcentrifuge	MSE
NanoDrop™ 8000 Spectrophotometer	Thermo scientific
pH meters	Metler Toledo
Pipettes and multichannel pipettes	Gilson, Star Labs, Eppendorf
Ultrapure water dispenser	Barnstead
Vortex	Scientific industries

SOFTWARE	PROVIDER
IVIS Image Analysis Software	PerkinElmer
GraphPad Prism 8	Graph Pad software

5.2.1.3 Cell line growth media

DU145 COMPLETE MEDIUM	CONCENTRATIONS
EMEM	-
FCS	10% v/v
L-glutamine	1 %

DU145-Luc2 COMPLETE MEDIUM	CONCENTRATIONS
EMEM	-
FCS	10% v/v
L-glutamine	1 %
Zeocin	50 µg/mL

PC3 COMPLETE MEDIUM	CONCENTRATIONS
F-12K	-
FCS	10% v/v

LnCAP COMPLETE MEDIUM	CONCENTRATIONS
RPMI 1640	-
FCS	10%
L-glutamine	1 %
Glucose 45%	0.4 %
HEPES	1 %
Na Pyruvate	1 %

5.2.1.4 Buffers and gels

ELISA COATING BUFFER	CONCENTRATIONS
Na ₂ CO ₃	15 mM
NaHCO ₃	35 mM
Buffer was prepared in ddH ₂ O and pH adjusted to 9.6	

ELISA WASHING BUFFER	CONCENTRATIONS
DPBS	1X
Tween-20	0.05% v/v
Buffer was prepared in ddH ₂ O	

ELISA BLOCKING BUFFER	CONCENTRATIONS
DPBS	1X
FCS	2% w/v
Buffer was prepared in ddH ₂ O	

ADCC ASSAY BUFFER	CONCENTRATIONS
RPMI 1640	--
Low IgG	4% v/v

5.2.2 Methods

5.2.2.1 Routine cell culture

DU145, PC3, and LNCaP cell lines were purchased from American Type Culture Collection (ATCC). DU145-Luc2 cells were generated transfecting DU145 cells with the pBudCE4.1/Luc2 Luciferase Reporter Gene. All cell lines were cultured in their dedicated media. The DU145 and DU145-Luc2 cell lines were cultured in Eagle's Minimum Essential Medium (EMEM) with 1% w/v L-Glutamine. In order to maintain selective pressure on DU145-Luc2 cells, the dedicated medium was supplemented with 50 µg/mL zeocin. PC3 cell line was cultured in Kaighn's Modification of Ham's F-12 Medium (F-12K); LNCaP cell line was cultured in RPMI 1640 Medium with 1% w/v L-Glutamine, 0.4% w/v Glucose, 1% v/v HEPES, and 1% w/v Sodium Pyruvate. As a supplementary agent, 10% v/v foetal calf serum (FCS) was added to all media according to ATCC culture methods. Each cell line was cultured at 37°C in the incubator containing 5% v/v CO₂ and humidified air. Cells were routinely passaged at 70-80% confluence. During passaging, cells were washed twice with Dulbecco's Phosphate Saline (DPBS) and detached by incubating with 0.25% w/v Trypsin- 0.53 mM EDTA solution for 5-15 min at 37°C. Equal amounts of cell-specific medium were added immediately upon cell detachment and cells were then centrifuged at 260 g for 5 min. Cell counting was carried out, by re-suspending harvested cell pellet in 1-3 mL of cell-dedicated medium and re-suspending cell solution in Trypan blue (1:10 dilution in PBS). The haemocytometer was used to count the total number of living cells and excluded the number of dead cells (blue stained) from the count. The cell pellet was re-suspended in fresh medium and cells re-cultured in culture flasks by passaging. Stocks of each cell line was prepared at approximately 1x10⁶ cells in 1 mL FCS + 10% v/v DMSO (freezing medium) and stored at -80°C. As required, cells were thawed, gently re-suspended in 10 mL cell-dedicated medium and centrifuged at 150 g for 5 min. Cell pellets were then again gently re-suspended in fresh batch of cell-dedicated medium and plated in a suitable dish. Medium changes ensured removal of DMSO from frozen cells sample and increased the viability of thawed samples.

5.2.2.2 Anti-human EPCR mAbs subtype switch

Subtype switch of the newly generated mAbs against human EPCR was performed entirely at Absolute Antibody (Oxford, UK). Variable domain sequences from JvGCRC-H61.3, JvGCRC-H589.9, JvGCRC-H754.6 and JvGCRC-H599.5 (mouse IgG1) antibodies were identified upon sequencing of the relative hybridomas (described in Chapter 4 of this thesis) and then subcloned into an Absolute Antibody cloning and expression vector for the mouse IgG2b subtype of immunoglobulin heavy and light chains. HEK 293 cells were transiently transfected with heavy and light chain expression vectors and cultured in order to obtain 1 mg of purified antibody for each clone. Antibody purification was performed using affinity chromatography.

The mouse IgG2b mAbs obtained were used for all the experiments presented in the present chapter.

5.2.2.3 ADCC assay

Mouse IgG2b anti-Human EPCR mAbs were used in a dedicated ADCC bioluminescent cell-based assay from Promega (Figure 5.1).

IgG2b antibodies mediate ADCC in mice through the activation of mFc γ RIV receptors on effector cells. Effectors cells used in the specific bioassay are genetically engineered Jurkat T cells that express both mFc γ RIV receptors and a luciferase reporter driven by an NFAT-response element (NFAT-RE). Once the antibodies bind the antigen on the target cells and their Fc domain is bound by the effector cell through the mFc γ RIV receptors the activation of the NFAT pathway triggers the luciferase activity. Subsequently, the intensity of the bioluminescent signal produced is directly proportional to the activation of the cytolytic pathway in the effector cells.

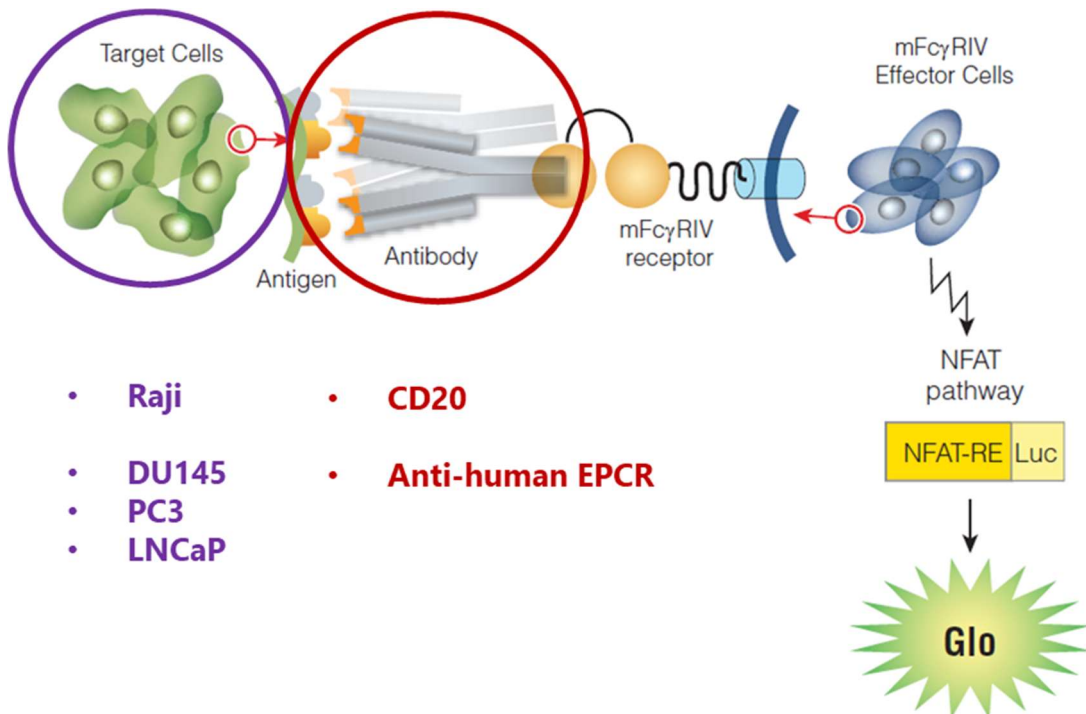


Figure 5.1 – Representation of the mFc_γRIV ADCC Reporter Bioassay. The ADCC reporter bioassay allows the assessment of the ability of mAbs to mediate *in vitro* cell cytotoxicity. Binding of the mAbs to both the target cell expressing the antigen and the mFc_γRIV on the surface of genetically engineered Effector Cells results in receptor clustering, intracellular signalling and NFAT-RE-mediated luciferase activity. The kit provides CD20-expressing Raji cells and anti-CD20 antibody as a positive control for the assay. (This image is reproduced by kind permission of Promega UK)

5.2.2.3.1 Reagents and cells preparation

All the reagents necessary for this assay were included in the dedicated Mouse Fc_γRIV ADCC Bioassay, included control target cells and anti-CD20 antibody. Test cells and test antibody used are listed in Table 5.2.

Table 5.2 – Target cells and antibodies tested in the ADCC bioassay. For the specific dilutions used refer to Figure 5.2.

Control Cells	Density	Control Antibody	Starting Dilution
Raji	Provided in thaw-to-use format	Anti-CD20	30 µg/mL
Target Cells	Density	Test Antibodies	Starting Dilution
DU145	2x10 ⁴ cells/well	Anti-human EPCR IgG2b:	30 µg/mL
PC3	2x10 ⁴ cells/well	• JvCGCC-H61.3 • JvCGCC-H589.9 • JvCGCC-H599.5 • JvCGCC-H754.6	30 µg/mL
LNCaP	2x10 ⁴ cells/well		30 µg/mL
Diluent: assay buffer			

Assay buffer (96% RPMI 1640/4% Low IgG) Serum was prepared adding 1.5 mL of Low IgG Serum to 36 mL of RPMI 1640 medium.

For this assay, DU145, PC3 and LNCaP cell lines were used and the protocol provided by the manufacturer applied. On the day before the start of the assay, cells were harvested and counted, according to the protocol described in section 5.2.2.1. Cells were then resuspended at a density of 2×10^4 cells/well in 100 μl /well of dedicated medium, for a final Effector:Target cell (E:T) ratio of 3.75:1. For each cell line, the 60 inner wells of two white 96-well flat-bottom assay plates were used and allowed to adhere overnight at 37°C in a humidified atmosphere with 5% CO₂. On the day of the assay, target non-adherent cells (Raji – provided with the kit as positive control) were thawed and 500 μl of cell suspension transferred to a 15 mL conical tube containing 9.5 mL of prewarmed assay buffer. 25 μl of such prepared cell suspension was transferred to each of the 10 inner wells of 3 rows of a white 96-well flat-bottom assay plate.

MFcyRIV Effector Cells were thawed after the addition of antibodies serial dilutions to the test plates. 650 μl of cell suspension was transferred to a 15 mL conical tube containing 3.6 mL of prewarmed assay buffer. The cell density is 7.5×10^4 cells/well for a 96-well plate.

Anti-CD20 was used as positive control antibody for the assay, while JvGCRC-H61.3, JvGCRC-H589.9, JvGCRC-H754.6 and JvGCRC-H599.5 antibodies were tested. On the day of the assay, five-fold serial dilutions were prepared using a 96-well plate, starting from 125 μl of 3X the highest concentration for each antibody. For each antibody, 100 μl of assay buffer were transferred to nine wells, then 25 μl of the antibody starting 3X dilution (Dilu 1 = initial dilution = 30 $\mu\text{g}/\text{mL}$) was transferred to the first well with assay buffer (Figure 5.2). Equivalent five-fold serial dilutions were repeated across the remaining wells except for the last.

Bio-Glo Luciferase Assay Buffer was thawed and equilibrated to ambient temperature, protected from light and then mixed with the Bio-Glo™ Luciferase Assay Substrate.

	Dilu 1	Dilu 2	Dilu 3	Dilu 4	Dilu 5	Dilu 6	Dilu 7	Dilu 8	Dilu 9	No Ab
	125 µl	100 µl								

25 µl									
-------	-------	-------	-------	-------	-------	-------	-------	-------	--

Figure 5.2 – Antibody serial dilutions. Serial dilutions prepared for each antibody used in the ADCC bioassay.

5.2.2.3.2 Assay procedure and data analysis

95 µl of culture medium were carefully removed from each well with adherent cells and 25µl of assay buffer add. 25 µl of the appropriate antibody dilution was added to the pre-plated target cells. 25 µl of the mFcγRIV Effector Cells suspension was added to each test well. Plates were then incubated for 6 hours at 37°C in a humidified atmosphere with 5% CO₂. After incubation, plates were equilibrated to room temperature for 15 min. 75µl of Bio-Glo Reagent was added to the test wells of the assay plates. Plates were incubated 30 min at room temperature and then luminescence was measured with 500 ms integration time and automatic attenuation with Infinite M200 Pro TECAN (Tecan Group Ltd, Männedorf, Switzerland).

Fold induction was calculated based on relative light unit (RLU) measured as follows:

$$\text{Fold induction} = \frac{\text{RLU (induced)}}{\text{RLU (no antibody control)}}$$

Data were expressed as RLU versus Log₁₀ [antibody] and fold induction versus Log₁₀ [antibody]. Results were fitted to a 4PL curve, and the half maximal effective concentration (EC50) of antibody response determined using GraphPad Prism software.

5.2.2.4 Administration of anti-human EPCR antibodies to CB17/SCID mice

In vivo studies were conducted on CB17/SCID (severe combined immunodeficient) albino mice purchased from Charles River. Although like SCID mice they still show severe combined immunodeficiency affecting both B and T lymphocytes, CB17/SCID strain mice have normal NK cells, macrophages, and granulocytes. Animals were maintained for the duration of the experiment at Nottingham Trent University pathogen free animal facility in accordance with the Home Office Codes of Practice for the housing and care of animals. These experiments were undertaken with Home Office Approval (Project Licence Number: PB26CF602).

5.2.2.4.1 *In vivo* antibody administration protocol

CB17/SCID mice were immunised with intravenous injection of 5 µg of each of the 4 monoclonal antibodies under test (3 mice/group, 1 group/mAb) and bled every twice a week after injection. Presence of antibodies in the sera was tested by enzyme-linked immunosorbent assay (ELISA) using the sera isolated from the blood (less than 50 µL for the first 3 time points). Data collected were plotted as absorbance (415 nm) absolute values against the days after injection. As a reference, mAbs were tested together with the sera on each assay. Details of the experiment given in Table 5.3

Table 5.3 – Antibody persistence in mouse serum, study design. The table illustrates the setting used for the study to investigate the rate of antibody clearance from the mice circulation. Antibodies were administered by intravenous injection on day1 (D1). Blood samples were taken at different time points, from one mouse in each group in order to reduce the stress to the animals. (M: mouse; D: day)

Group Number	No. of Animals	Anti-hEPCR IgG2b	Blood Sampling	Animal Culled
1	3	Inject 100 µL containing 5 µg of JvGCRC-H61.3 by intravenous injection	M1 -D2	M1 - D11
			M2 - D4	M2 - D15
			M3 - D8	M3 - D18
2	3	Inject 100 µL containing 5 µg of JvGCRC-H589.9 by intravenous injection	M4 – D2	M4 - D11
			M5 - D4	M5 - D15
			M6 – D8	M6 - D18
3	3	Inject 100 µL containing 5 µg of JvGCRC-H599.5 by intravenous injection	M7 - D2	M7 - D11
			M8 – D4	M8 - D15
			M9 – D8	M9 - D18
4	3	Inject 100 µL containing 5 µg of JvGCRC-H754.6 by intravenous injection	M10 -D2	M10 - D11
			M11 – D4	M11 - D15
			M12 – D8	M12 - D18

5.2.2.4.2 Test for presence of mouse anti-EPCR mAbs in serum with Enzyme-Linked Immunosorbent Assay (ELISA)

Indirect ELISA was used to investigate the presence of antibodies against human EPCR in sera isolated from the mice immunised (assay principle has been previously described in section 4.2.2.2). Blood samples were collected from mice at different time points as described in Table 5.3. Samples were allowed to clot for 30 min at room temperature, and then centrifuged at 2,000 g for 10 min at 4°C in order to separate serum. The supernatants were transferred in a fresh Eppendorf tube and used for the assay. Average yield of serum was 30-40 µL/mouse.

Mid-protein absorption 96-wells plates were coated with 50 µL/well of human EPCR recombinant protein in coating buffer with a dilution of 0.5 µg/mL at 4°C overnight. On the day of the assay, plates were washed with washing buffer three times and blocked with 150-200 µL/well of blocking buffer for 30 min at RT. Buffer was discarded and wells probed with 50 µL/well of sera isolated from mice and diluted with 1:2 ratio. Plates were incubated for 1 hour at RT, after which wells were washed with washing buffer three times. 50 µL/well of secondary anti-mouse IgG-HRP antibody in blocking buffer (Table 5.4) was added to each well and the plate incubated 1 hour at RT, after which wells were washed with washing buffer three times. 100 µL of 3,3',5,5'-Tetramethylbenzidine (TMB) substrate were transferred to each well and let react at RT. As soon as the colour change was occurring, the reaction was stopped adding 50 µL/well of 2N sulphuric acid. The absorbance was measured at 450 nm using a TECAN ULTRA spectrophotometer.

Table 5.4 – Secondary antibody used for ELISA analysis. The table reports the details and dilution of the antibodies used.

Coating	Working Dilution	Reference number	Reconstitution buffer
Human EPCR recombinant protein (Sino Biological)	0.5 µg/mL	13320-H08H	ddH ₂ O
Primary pAb	Working Dilution		
Serum from mice	1:2		
Secondary pAb	Working Dilution	Reference number	Clone
Anti-Mouse IgG HRP-linked	1:3000	7076	Polyclonal
Diluent: blocking buffer			

5.2.2.5 Generation of DU145-Luc2 cells expressing Luciferase Reporter Gene

5.2.2.5.1 Target cell line antibiotic kill curve

DU145 cells were cells cultured in 1 mL of cell-dedicated medium in 24-well culture plates were incubated overnight at 37°C in the incubator containing 5% v/v CO₂ and humidified air and grown to 50% confluence. After incubation, the medium was replaced with fresh medium containing varying concentrations of zeocin antibiotic as well as without antibiotic as a negative control. Each concentration was maintained in duplicates as indicated in the 24-well plate format (Figure 5.3) and the medium with antibiotic replaced every 48 hours. Cells were cultured for 14 days, and then cell viability in each well was determined by cell counter (Invitrogen™ Countess™ II Automated Cell Counter). The concentration of antibiotic that completely blocks the growth of cells for both lines was found at 50 µg/mL.

	1	2	3	4	5	6
A	0 µg/mL	0 µg/mL	10 µg/mL	10 µg/mL	20 µg/mL	20 µg/mL
B	30 µg/mL	30 µg/mL	40 µg/mL	40 µg/mL	50 µg/mL	50 µg/mL
C	60 µg/mL	60 µg/mL	70 µg/mL	70 µg/mL	80 µg/mL	80 µg/mL
D	90 µg/mL	90 µg/mL	100 µg/mL	100 µg/mL	110 µg/mL	110 µg/mL

Figure 5.3 – 24 well plate map used for selection of antibiotic optimal concentration. Representation of 24-well plate setup for zeocin titration for determining working selection concentration.

5.2.2.5.2 Competent bacteria transformation for plasmid amplification

XL1-B super-competent bacteria was used for transformation and plasmid amplification were gently thawed on ice. 100 µL of cells were added to a pre-chilled round bottom tube for each clone to be transformed. pBudCE4.1/Luc2 (Figure 5.4) was generated in JvGCRC facilities by Dr. Divya Nagarajan and aliquots at 5 µg/µL kindly gifted. Luc2 DNA was ligated into pBudCE4.1 vectors (previously digested by *Sac I* and *Hind III* restriction enzymes) using T4 ligase. Plasmid was diluted at 20 ng/µL, and 5 µL was transferred to each of the reaction tubes collecting 5 µg of plasmid mix. Each transformation reaction was gently mixed without pipetting by swirling and incubated on ice for 30 min. The transformation reaction was then heat shocked at 42°C for 45 sec before being placed in ice for 2 min. 250 µL of RT LB Broth were added to each reaction. Each transformation reaction was shaken horizontally at 200 rpm, 37°C for 1 hour. 200 µL of each transformation reaction was spread on pre-warmed LB-agar selective plates containing 50 µg/mL ampicillin, and incubated overnight at 37°C. Single colonies were picked from stab culture, plated in LB-agar selective plates containing

50 µg/mL ampicillin, and incubated overnight at 37°C. After incubation, single colonies for each plasmid were then inoculated in 50 mL LB-broth containing 50 µg/mL ampicillin and cultured overnight at 37°C with shaking. Cell cultures with visible cloudy bacterial growth were used for plasmid isolation using QIAGEN QIAfilter Plasmid Midi according manufacturer protocol. Isolated plasmids quantified using Nanodrop 8000 Spectrophotometer and stored in TE buffer at -20°C.

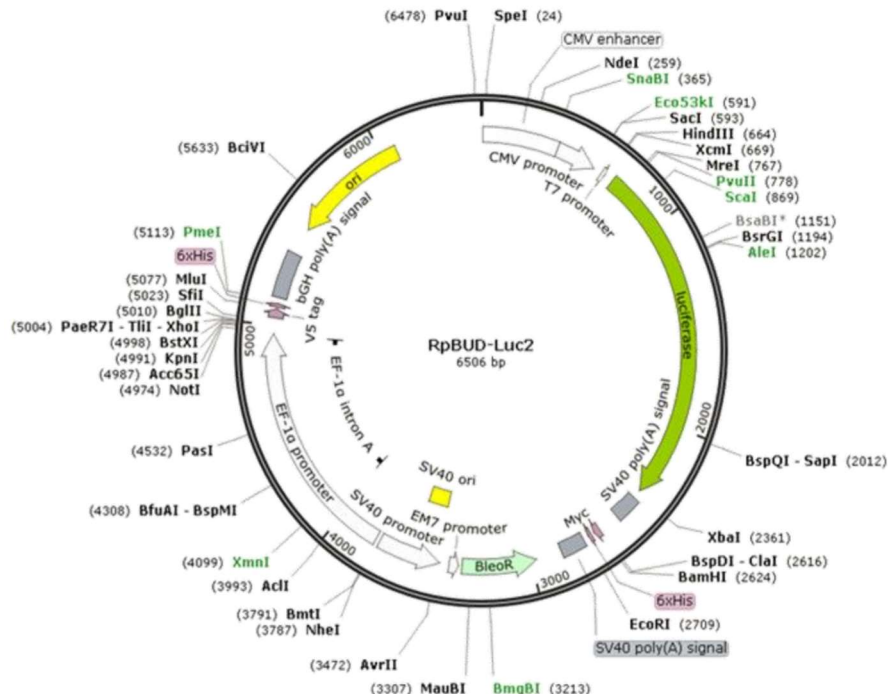


Figure 5.4 – Vector map of pBudCE4.1/Luc2 plasmid. The plasmid was generated in JvGCRC facilities by Dr. Divya Nagarajan and kindly gifted for the purpose of this project.

5.2.2.5.3 Transfection of DU145 cells with Luciferase Reporter Gene

Lipofectamine 3000 was used to transfect cells as per manufacturer's instructions. Briefly, DU145 cell line was plated to reach 60-70% confluence in 6-well plates. Upon reaching confluence, Lipofectamine 3000 Reagent (5.6 µl/well) was diluted in Opti-MEM medium (125 µl /well) and mixed well. Simultaneously, master mix of DNA was prepared by diluting pBudCE4.1/Luc2 plasmid DNA (2.5 µg DNA/well) in OptiMEM medium (125 µl/well), then P3000 Reagent (2 µL/µg of DNA) was added and mixed well. Both solutions were incubated for 5 min at RT. Following incubation, DNA and lipofectamine mixtures were combined and gently mixed and incubated for 20 min at RT to allow the formation of DNA-lipofectamine complexes. The required volume of mixtures was added onto cells and gently swirled around for uniform spreading. Cells were then incubated at 37°C in the incubator containing 5% v/v CO₂ and humidified air for 8 hours. After incubation, culture medium was replaced with 1

mL of fresh culture medium containing zeocin (50 µg/mL). Transfected cells were allowed to reach confluence to obtain cells for luciferase expression assessment.

5.2.2.5.4 Assessment of Luciferase expression in DU145-Luc2 cells

DU145 wt and DU145-Luc2 cells were harvested and counted as described in section 5.2.2.1. Cells dilutions were prepared as described in Table 5.5. For each density, cells were resuspended in 200 µl of dedicated medium in round bottom black 96-multiwell plates. 1 µl ReadyJet D-Luciferin (final concentration 150 µg/mL) was added to each well. Plate was sent for real-time bioluminescence imaging with the *In Vivo* Imaging System (IVIS).

Table 5.5 – Cell dilutions for Luciferase activity assay. The table represents the number of cells needed for each well of a 96-well plate.

DU145 wt (row-column)	DU145-Luc2 (row-column)	Cell density
A-1	A-2	1×10^5
B-1	B-2	5×10^4
C-1	C-2	2.5×10^4
D-1	D-2	12.5×10^3
E-1	E-2	6.25×10^3
F-1	F-2	3.12×10^3
G-1	G-2	0

5.2.2.5.5 Assessment of human EPCR expression in DU145-Luc2 cells with flow cytometry

In order to confirm that the human EPCR protein was expressed on the cell surface of the newly established DU145-Luc2 cell line, FCM analysis was performed. Cells were grown, harvested, and counted as described in section 5.2.2.1. 1×10^6 DU145 cells were aliquoted to each 12x75 mm polycarbonate flow cytometry tubes. 1 µL of LIVE/DEAD™ Fixable Violet Dead Cell Reagent was mixed with 1 mL of DPBS and added to each tube with cells (apart from the unstained control) and incubated at RT for 30 min. Cells were washed with 1 mL of DPBS and centrifuged at 400 g for 5 min. Supernatants were removed by gently flicking the tube and pellets were resuspended by gentle tapping. 5 µL of FcR Blocking reagent was mixed with 45 µL of PBS added to each tube and incubated at RT for 10 min. 50 µL primary antibody was prepared in DPBS as described in Table 5.6, taking into consideration that the final volume per tube is 100 µL thus adjusting antibody dilution accordingly, and added to each test tube except for the unstained and control tubes, and incubated at RT for 30 min.

Table 5.6 – Primary and secondary monoclonal antibodies used for flow cytometry. Antibodies and their dilutions used during the antibody titration and the target recognition specificity assays.

Primary mAb	Working Dilution	Reference number	Clone	Supplier
Rat anti-human EPCR	10 µg/mL	NB600-963	RCR-252	Novus Biological
Secondary pAb	Working Dilution	Reference number	Clone	Supplier
Alexa Fluor™ 488 conjugated Donkey anti-rat IgG	1:500	A21208	Polyclonal	Invitrogen
Diluent: DPBS				

After incubation, cells were washed with 2 mL of PBS and centrifuged at 400 g for 5 min. Supernatants were removed from each sample and pellets were resuspended by gentle tapping. 100 µL of secondary antibody diluted in PBS was added to all but the ‘unstained’ tube, and samples incubated at RT for 30 min in the dark. After incubation, cells were washed with 2 mL of DPBS and centrifuged at 400 g for 5 min. Supernatants were removed from each sample and pellets were resuspended by gentle tapping in 300 µL of ISOTON II™ flow cytometry sheath fluid. Data were acquired using a 10-color/3-laser Beckman Coulter Gallios™ flow cytometer and analysed using Kaluza™ v1.3 data acquisition and analysis software (Beckman Coulter).

5.2.2.6 DU145-Luc2 tumour growth in CB17/SCID mouse model

A preliminary study was conducted to establish the growth rate of DU145-Luc2-generated tumours in CB17/SCID mice. Six mice were implanted with 1×10^6 DU145-Luc2 into the right hand-side flank of each CB17/SCID mouse by subcutaneous injection to generate tumours (Table 5.7).

Table 5.7 – DU145-Luc2 tumour growth in CB17/SCID mouse model dose group panel. The table summarises the experimental setting used for the *in vivo* tumour growth study.

Group Number	No. of Animals	Tumour Implant
1	6	Inject 1×10^6 DU145-Luc2 cells in 100 µL DPBS/mouse into the right hand-side flank by subcutaneous injection

The tumours were monitored twice weekly by callipers and by *in vivo* imaging until termination of the study. Tumour size (TS) was calculated as the mean diameter using the

formula: $TS = (L \times W)/2$, where L and W are the perpendicular diameters measured. For each imaging session, the D-luciferin was administered *intra* peritoneal (0.15 mg/g mice, dissolved in DPBS) and anaesthesia induction begun 10-15 min afterwards. All mice were anaesthetised with an appropriate concentration of isoflurane and imaged using the Perkin Elmer IVIS Lumina III system. On each occasion, bioluminescence imaging was performed. Tumours were let grow up to the size of 1.2 cm, which represented the natural study endpoint. *Post-mortem* and *ex vivo* imaging was performed on all animals culled as per scheduled termination.

5.2.2.7 Tumour growth and antibody administration in CB17/SCID mouse model

Each CB17/SCID mouse was implanted with 2×10^6 DU145-Luc2 by subcutaneous injection into the right hand-side flank to generate tumours. Three groups, each by 10 CB17/SCID mice were randomly formed (Table 5.8).

Table 5.8 – Tumour growth and antibody administration in CB17/SCID mouse model dose groups panel.
The table summarises the experimental setting used for the *in vivo* generation of DU145-Luc2-derived xenografts in CB17/SCID mice.

Group Number	No. of Animals	Tumour Implant	Mice immunisation with mAbs (starting on palpable tumours 2-4mm in diameter)
1 Control	10	Inject 2×10^6 DU145-Luc2 cells in 100 µL DPBS/mouse into the right hand-side flank by subcutaneous injection	<ul style="list-style-type: none"> Administer 100 µL of DPBS/mouse by intravenous injection Once a week 3 times
2 JvGCRC-H61.3	10	Inject 2×10^6 DU145-Luc2 cells in 100 µL DPBS/mouse into the right hand-side flank by subcutaneous injection	<ul style="list-style-type: none"> Administer 5 µg antibody in 100 µL of DPBS/mouse by intravenous injection Once a week 3 times
3 JvGCRC-H599.5	10	Inject 2×10^6 DU145-Luc2 cells in 100 µL DPBS/mouse into the right hand-side flank by subcutaneous injection	<ul style="list-style-type: none"> Administer 5 µg antibody in 100 µL of DPBS/mouse by intravenous injection Once a week 3 times

Tumours were measured regularly twice a week with calliper in order to establish the start of the therapy with anti-human EPCR mAbs. Once the tumours reached a palpable size of a 2-4mm, mAbs were administered via intra-venous injection weekly for 3 weeks, for a total duration of 21 days after palpable tumour development, as described in Table 5.9. A blood sample was taken from the mice to assess the presence of the mAbs being administered (Table 5.9). The tumours were monitored twice weekly by callipers and by *in vivo* imaging

until termination of the study. For each imaging session, the D-luciferin was administered *intra* peritoneal (0.15 mg/g mice, dissolved in DPBS) and anaesthesia induction begun 10–15 min afterwards. All mice were anaesthetised with an appropriate concentration of isoflurane and imaged using the Perkin Elmer IVIS Lumina III system. On each occasion, bioluminescence imaging was performed. Tumours were let grow up to the size of 1.2 cm, which represented the natural study endpoint. *Post-mortem* and *ex vivo* imaging were performed on all animals culled as per scheduled termination. Tumours were taken into tubes containing RPMI 1640 medium and weighted.

Table 5.9 – Mice immunisation with anti-EPCR mAbs dose groups panel. The table summarises the schedule followed for the administration of anti-human EPCR mAbs for targeting of DU145-Luc2-derived tumours.

Group Number	No. of Animals	Mice immunisation with mAbs (starting on palpable tumours 2-4mm in diameter)	Blood Sampling	Animal Culled
1 Control	10	D0 boost no. 1	M1-M2 D1	M1 to M10 D21
			M3-M4 D4	
		D7 boost no. 2	M5-M6 D8	
			M7-M8 D11	
			M9-M10 D15	
		D14 boost no. 3	M1-M2 D18	
2 JvGCRC-H61.3	10	D0 boost no. 1	M11-M12 D1	M11 to M20 D21
			M13-M14 D4	
		D7 boost no. 2	M15-M16 D8	
			M17-M18 D11	
			M19-M20 D15	
		D14 boost no. 3	M11-M12 D18	
3 JvGCRC-H599.5	10	D0 boost no. 1	M21-M22 D1	M21 to M30 D21
			M23-M24 D4	
		D7 boost no. 2	M25-M26 D8	
			M27-M28 D11	
			M29-M30 D15	
		D14 boost no. 3	M21-M22 D18	

5.3 Results

5.3.1 Antibody subtype switch from IgG1 to IgG2b

In order to test the ability of the newly generated anti-human EPCR antibodies to activate effector cells in *in vitro* and *in vivo* murine models, the immunoglobulin subtype was engineered (Table 5.10). The original IgG1 subtype is not able to activate murine NK cells as strongly as its affinity for Fc γ RIV receptors is lower compared to IgG2b.

Table 5.10 – Antibody subtype switch.

Clone	Original subtype	Final subtype
JvGCRC - H61.3	Mouse IgG1	Mouse IgG2b
JvGCRC – H589.9	Mouse IgG1	Mouse IgG2b
JvGCRC – H599.5	Mouse IgG1	Mouse IgG2b
JvGCRC – H754.6	Mouse IgG1	Mouse IgG2b

5.3.2 Application of generated mAbs for *in vitro* tumour targeting: ADCC

The assessment of the ability of the mAbs to induce effector function *in vitro* constituted a fundamental factor for both antibody validation and pre-clinical experiments development. The rationale behind the choice of an ADCC-reporter gene assay kit was the need to reduce the variables that are naturally part of the conventional PBMC-based ADCC assays, thus obtaining more accurate and precise results.

Figure 5.5 shows the results obtained testing the four anti-human EPCR mAbs clones on DU145, PC3 and LNCaP PCa cell lines. Anti-CD20 was used in combination with CD20-expressing Raji cells as a positive control. The results are summarised in Table 5.10.

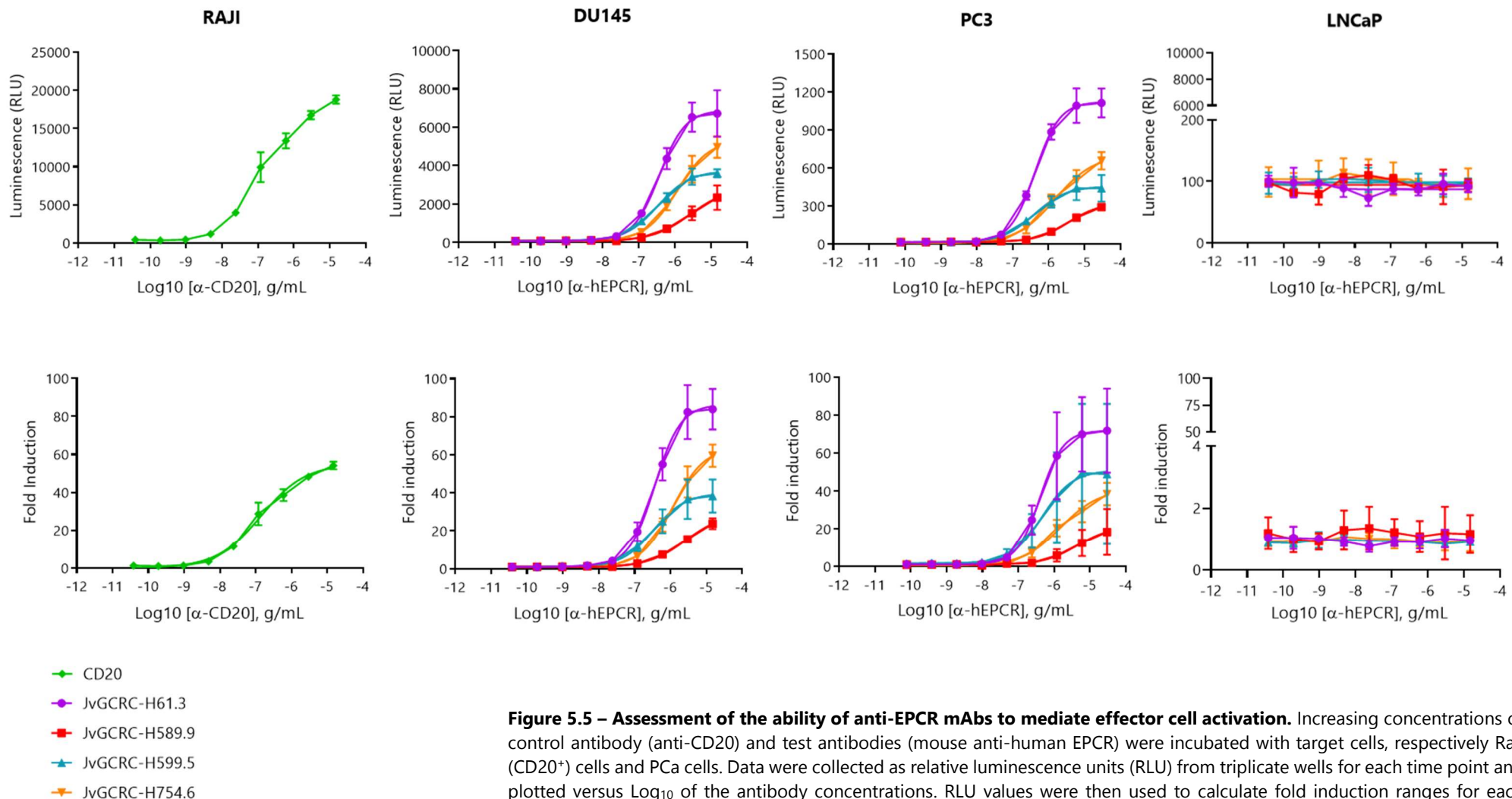


Figure 5.5 – Assessment of the ability of anti-EPCR mAbs to mediate effector cell activation. Increasing concentrations of control antibody (anti-CD20) and test antibodies (mouse anti-human EPCR) were incubated with target cells, respectively Raji (CD20⁺) cells and PCa cells. Data were collected as relative luminescence units (RLU) from triplicate wells for each time point and plotted versus Log₁₀ of the antibody concentrations. RLU values were then used to calculate fold induction ranges for each antibody versus Log₁₀ of the relative concentrations. Eventually fold induction curves were fitted to a 4PL curve using GraphPad Prism and EC₅₀ for each antibody determined.

Table 5.11 – Half maximal effective concentration (EC₅₀) and maximum fold induction.

Antibody	EC ₅₀ (µg/mL)			Maximum Fold Induction			
	Raji (CD20 ⁺)			Raji (CD20 ⁺)			
Anti-CD20	0.5099			53.85			
Antibody	EC ₅₀ (µg/mL)			Maximum Fold Induction			
	DU145	PC3	LNCaP	DU145	PC3	LNCaP	
JvGCRC-H61.3	0.3648	0.402	N/A	86.43	71.94	N/A	
JvGCRC-H589.9	2.71	4.347	N/A	29.39	21.30	N/A	
JvGCRC-H599.5	0.3357	0.4577	N/A	39.83	51.02	N/A	
JvGCRC-H754.6	1.159	1.51	N/A	64.12	41.00	N/A	

Half maximal effective concentration (EC₅₀) and maximum fold induction were measured based on the luminescent signal resulted from the experiments conducted. The EC₅₀ refers to the concentration of the antibody needed to induce a response that is halfway between the baseline and the maximum effect registered. Furthermore, the maximum fold induction value describes the intensity of the effect generated, in this case the activation of effector cells, which is determined as the ration between the luminescence emitted at the highest concentration of the antibody and the signal obtained without antibody.

All the antibodies tested showed to be working in DU145 and PC3 cells. No activity was detected when incubated with LNCaP cells as showed by the absence on luminescence detected (Figure 5.4). As the activation of the NFAT pathway also depends on the density of the antigen on the target cell surface (Patel, Guo et al. 2010), this can provide a reasonable explanation of the failure of the mAbs in inducing effector activity when tested on LNCaP cells. Indeed, as showed in chapter 2, the expression of EPCR on the cell surface of LNCaP cells is limited to a small subpopulation, which might not be enough to activate effector cells in this assay.

The EC₅₀ values calculated for the four mAbs based on the results obtained in DU145 and PC3 cells provide an indication on the relative amount of antibody needed to induce the effector function. As a reference, EC₅₀ of anti-CD20, which is used as a positive control having a strong activating potential, is 0.5099 µg/mL. Clones JvGCRC-H61.3 and JvGCRC-H599.5

also showed a significantly low EC₅₀ in both DU145 and PC3 cells, less than 0.4 µg/mL and 0.5 µg/mL respectively (Table 5.11). Conversely, clones JvGCRC-H589.9 and JvGCRC-H754.6 presented EC₅₀ values higher than 1 µg/mL and 2 µg/mL, respectively. Maximum fold-induction values are also consistent across the two cell lines for each antibody, with a good performance for all the clones except JvGCRC-H588.9, which scored a lower than 30 fold-induction whereas all the other clones, included the anti-CD20 control, registered higher than 40 folds-induction values.

These results presented herein provide a substantial background for the development of the most suitable strategy for testing the antibodies in *in vivo* tumour targeting experiments. So far, the two overall best performing antibodies, based on their relative EC₅₀ and maximum fold change values, are clones JvGCRC-H61.3 and JvGCRC-H599.5. Such information is to be integrated with the clearance rate of the antibodies in the appropriate mouse model, as described in the following section.

5.3.3 Antibody persistence *in vivo* in CB17/SCID mouse model

The purpose of this study was to assess the duration of the presence of anti-EPCR mAbs in the blood of mice (three mice/group) injected with them as described in section 5.2.2.4.1 and shown in Figure 5.6-A. This study investigated the suitability to move forward into the therapeutic settings of the anti-EPCR IgG2b clones that have been generated.

Due to the variable and low volume of blood and, consequently, of serum that was collected from each mouse, obtaining consistent results throughout the entire study was a difficult task. In the first place, since diluted sera were used to perform ELISA, low but potential positive presence of some of the antibodies could have been masked. As an internal control for the technique itself, pure IgG2b anti-EPCR mAbs were used contextually alongside the sera. Interestingly, as shown in Figure 5.6-B, each clone showed a different affinity for the antigen when tested with ELISA, which might have resulted in the alteration of the signals detected from the relative mAb-containing sera. In order to mitigate the effect of the differential affinity, absorbance values obtained testing sera were normalised against the corresponding pure antibody.

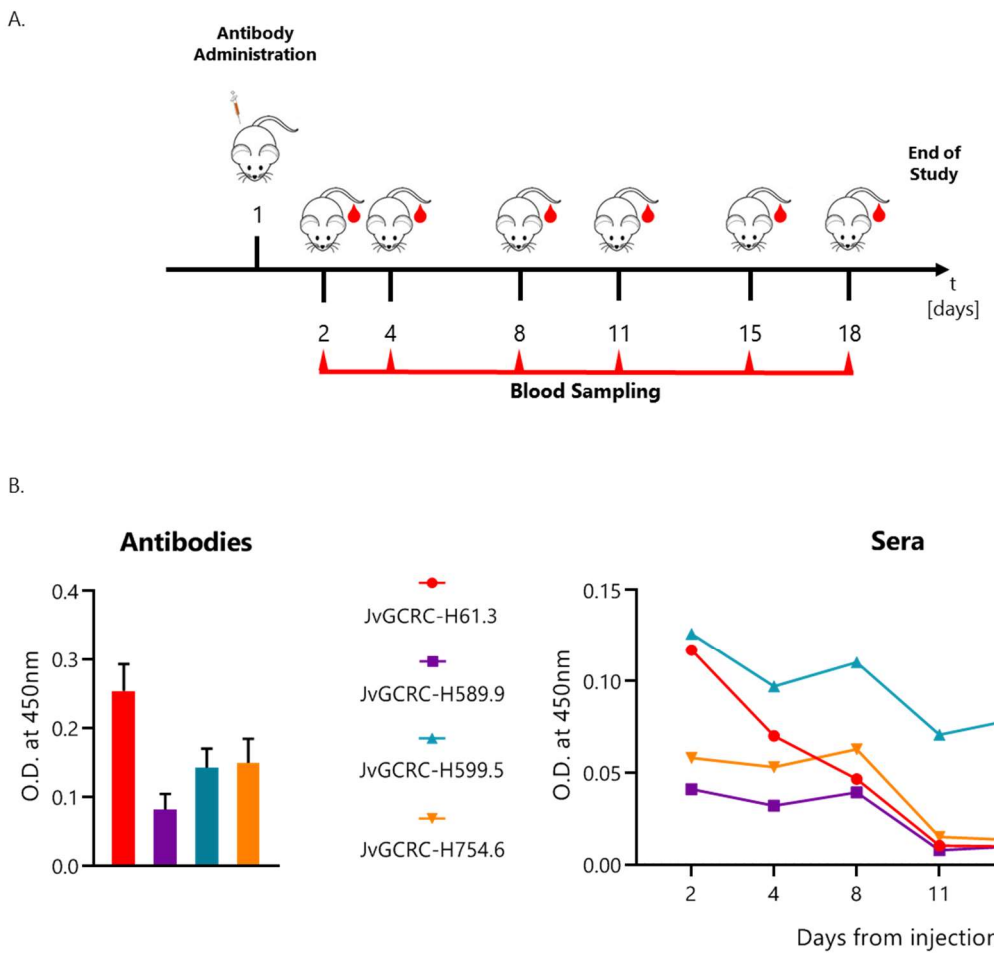


Figure 5.6 – Antibody persistence in serum from mice. CB17/SCID mice (three mice/antibody) were immunised on day 1 with anti-human EPCR IgG2b clones, and presence of antibodies in the sera isolated bleeding mice was assessed regularly from day 2 until day 18 by performing an indirect ELISA (A.). ELISA was performed using antibodies at a working dilution of 3 µg/mL (three wells/antibody) and diluted sera (1:2 – single-well/sample) on plates coated with full-length EPCR protein diluted at 0.5 µg/mL. All results are presented as mean values of O.D. (optical density) with absorbance at 450 nm (B.)

According to the results showed in Figure 5.6-B, the concentration of clones JvGCRC-H61.3 and JvGCRC-H599.5 in sera was the highest on day two after the immunisation. Presence of all the clones dropped drastically after day eight, except for clone JvGCRC-H599.5 that maintained a high titre in the sera up to day 18 after immunisation.

Although the data presented in this section are primarily qualitative rather than quantitative due to technical limitations, they suggest what is the relative clearance rate of the mAbs. Combining such information with the performance of the antibodies described in the previous section, clones JvGCRC-H61.3 and JvGCRC-H599.5 were considered the most suitable for *in vivo* tests.

5.3.3 DU145-Luc2 tumour growth in CB17/SCID mouse model

The first pilot study was designed to investigate tumour growth upon subcutaneous injection of DU145-Luc2 cells in CB17/SCID mouse model.

DU145-Luc2 were generated as described in section 5.2.2.5. In presence of the D-luciferin substrate, the firefly luciferase reporter gene (Luc2) produces luminescence suitable for monitoring tumour growth by *in vivo* live imaging. Figure 5.7-A shows the positive luminescent signal obtained providing the DU145-Luc2 cells with D-luciferin substrate, illustrating that the signal is proportional to the cell density. Moreover, cell surface expression of EPCR in cells was confirmed by flow cytometry analysis (Figure 5.7-B).

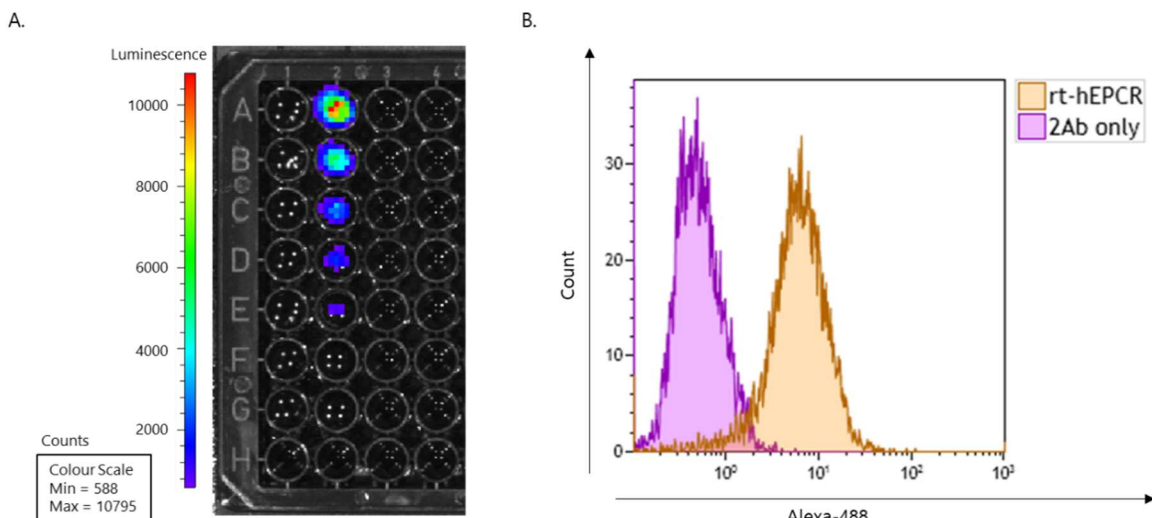


Figure 5.7 – DU145-Luc2 optimisation. DU145-Luc2 cells positively expressed luminescence when incubated with the specific D-luciferin substrate (A.). The population tested positive for human EPCR cell surface expression in flow cytometry analysis (B.).

Such cells were used to test the proof of concept of whether anti-human EPCR mAbs administration could affect DU145-Luc2-derived tumours growth and/or metastases formation. Cells were then injected into six CB17/SCID mice as described in section 5.2.2.6. Tumour growth was assessed regularly both by calliper measurement and *in vivo* imaging until the termination of the study on day 43 (Figure 5.8-A).

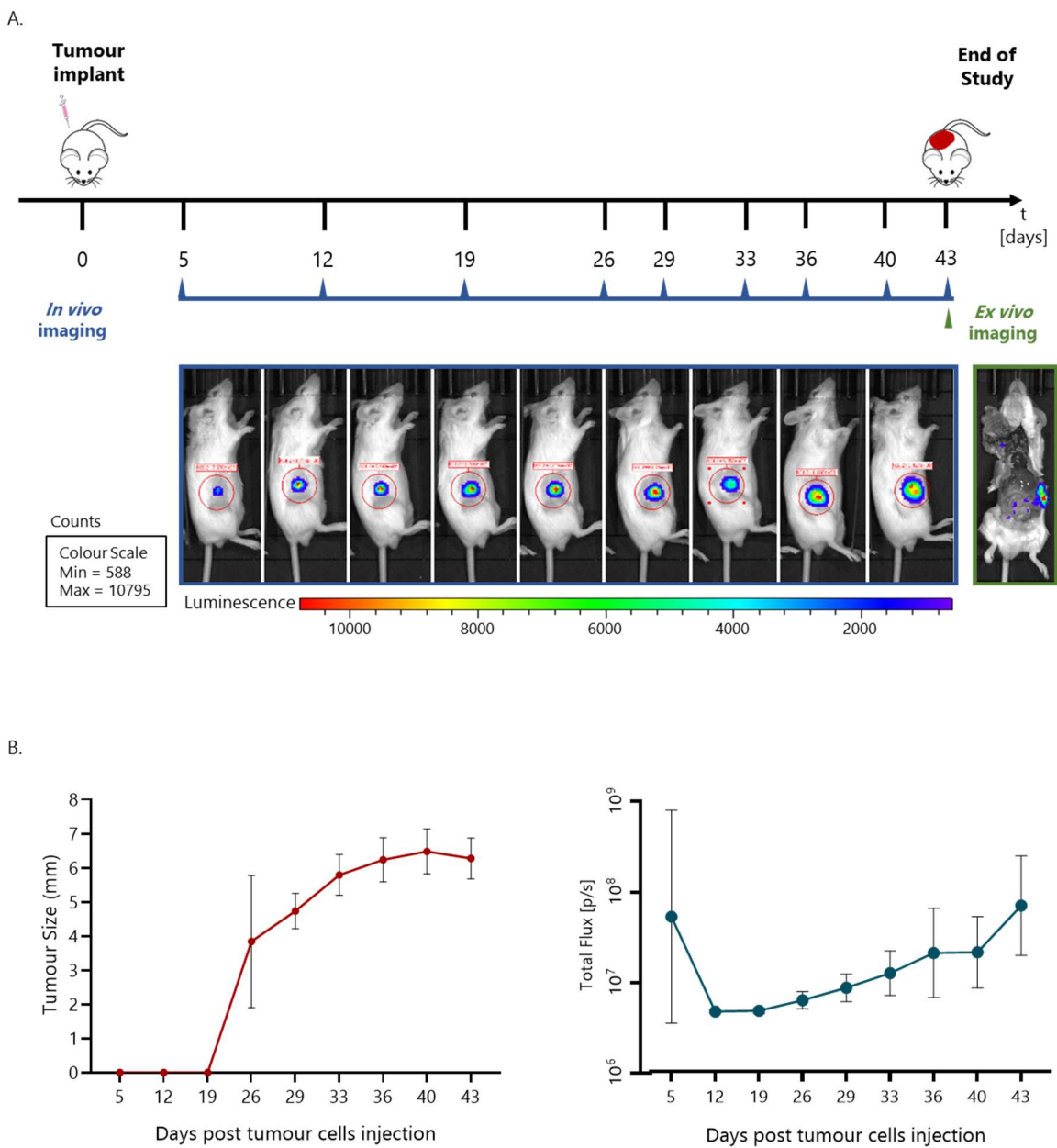


Figure 5.8 – *In vivo* DU145-Luc2-derived tumour growth rate study. Six CB17/SCID mice were injected with DU145-Luc2 cells and tumour growth observed until the size of 1.2 cm was reached on day 43 (A.). Tumours were measured manually with calliper and by live imaging in which signal was expressed as showing the total flux measured (n=6) (B.)

Tumour growth progression is showed in Figure 5.8-B. Although a raised area on the site of injection was noticeable from the first week after the tumour implantation, the effective measurement of tumour size with calliper was possible only starting from day 26. Moreover, mice were imaged and tumour growth observed as a direct proportion of the luminescent signal detected. Data generated by the *in vivo* imaging showed higher variability compared to the manual measurement approach. Manual measurements were used as a reference to identify the starting point for antibody administration during the final *in vivo* experiment. The results showed herein suggest that 1×10^6 cells resulted in a palpable tumour after ~26

days. For this reason, the decision was taken to double the number of cells injected in order to reduce the time needed for the tumours to become measurable.

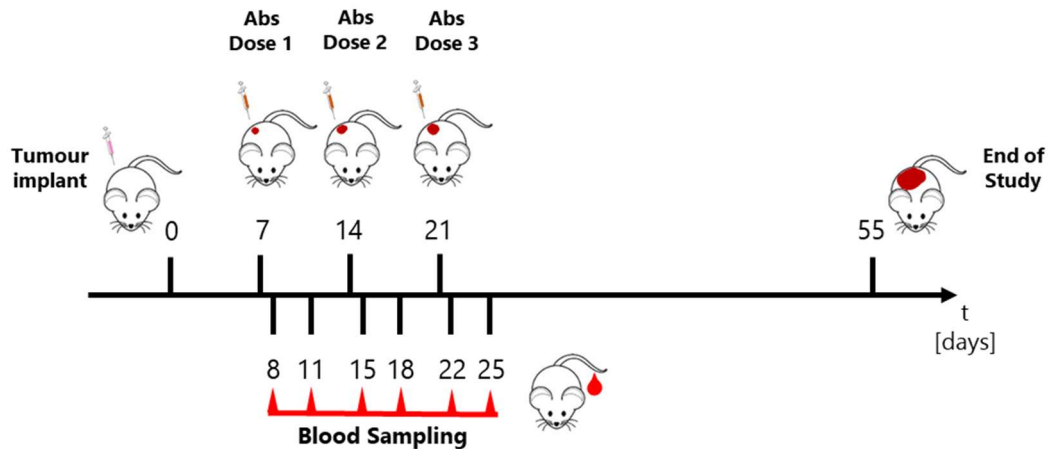
5.3.5 Tumour growth and antibody administration in CB17/SCID mouse model

The purpose of this study is to establish a therapeutic model for PCa investigating the effect of anti-human EPCR mAbs administration on the rates of tumour growth and metastasis formation in CB17/SCID mice. 2×10^6 DU145-Luc2 cells were used to generate tumours in CB17/SCID mice (10 mice/group), and mAbs JvGCRC-61.3 and JvGCRC599.5 administered when palpable tumours reached a size of 2-4mm, as described in section 5.2.2.7, on day 5 in the specific case. MAbs dosing was repeated twice more and weekly and blood samples were taken twice between each dose to assess the presence of the antibodies in the serum (Figure 5.9-A). ELISA analysis of sera isolated from blood confirmed that a free fraction of mAbs was still circulating in the mice in the week following each dose, whereas sera obtained from mice in the control group did not show any reactivity during the assay (Figure 5.9-B). Such results confirmed that the antibody coverage was effective for the duration of 21 days from the first dosing.

Tumour growth was monitored regularly until the endpoint of 1.2 cm size was reached on day 54 (Figure 5.10-A). Tumour size was measured manually by calliper and bioluminescence detected during live imaging of mice after D-luciferin substrate administration (Figure 5.10-B). Based on the results plotted in Figure 5.10-C, no significant difference was observed in tumour growth kinetic in mice treated with JvGCRC-61.3 and JvGCRC599.5 antibodies compared to the control group treated with DPBS alone. The same trend was confirmed by both manual and live imaging measurements.

Tumour weight was analysed at the end of the study showing no significant difference between the three groups, probably due to the high variation in tumour growth across all the animals (Figure 5.11).

A.



B.

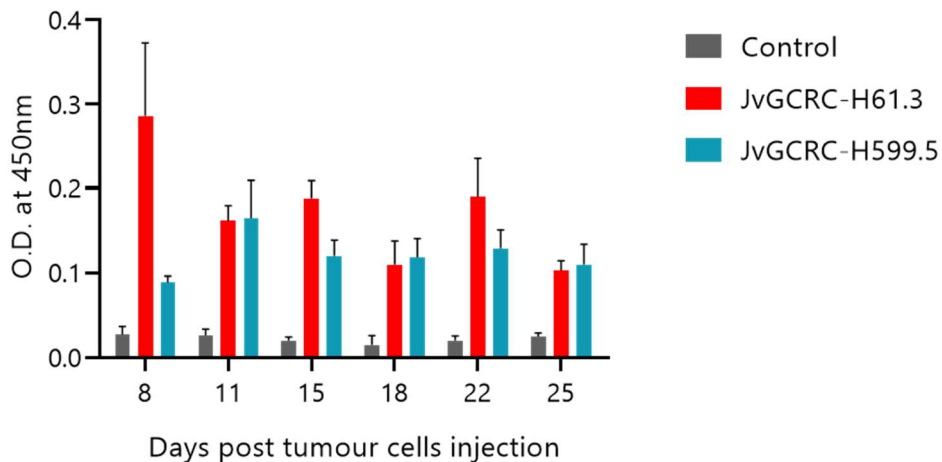


Figure 5.9 – Antibody persistence in sera from mice. Mice in control group were administered with DPBS only, whereas mice in each treated group received a weekly dose of 5 µg of antibody for three weeks. Each group was formed by ten mice. Timeline of antibody administration and blood sample schedule is shown (A.). Differential antibody persistence in immunised mice groups vs control group was assessed performing ELISA on serum samples from mice at each time point (B.).

Furthermore, metastasis formation was investigated during *ex vivo* imaging of mice. Again, no significant difference was reported between the treated and control groups (Figure 5.11). Interestingly, the number of metastases-bearing mice was extremely low (one mouse out of ten) in control group and group treated with JvGCRC599.5 antibody, and absent in group treated with JvGCRC61.3 antibody, suggesting that the DU145-Luc2 cells did not provide a good model for the study of metastases.

Figure 5.10 – *In vivo* assessment of the effects of the treatment with JvGCRC61.3 and JvGCRC599.5 mAbs against human EPCR on tumour growth. 2×10^6 DU145-Luc2 cells were injected in CB17/SCID mice and derived tumours were measured manually and digitally by live imaging (A.). Images of three representative tumour-bearing CB17/SCID mice from control and treated groups showing bioluminescence in DU145-Luc2-derived tumours obtained at different time points of the experiment (B.). Tumour growth kinetic was measured manually and digitally with live imaging and reported as mm and bioluminescence signal, respectively. No significant difference was observed ($n=10$ per group) (C.).

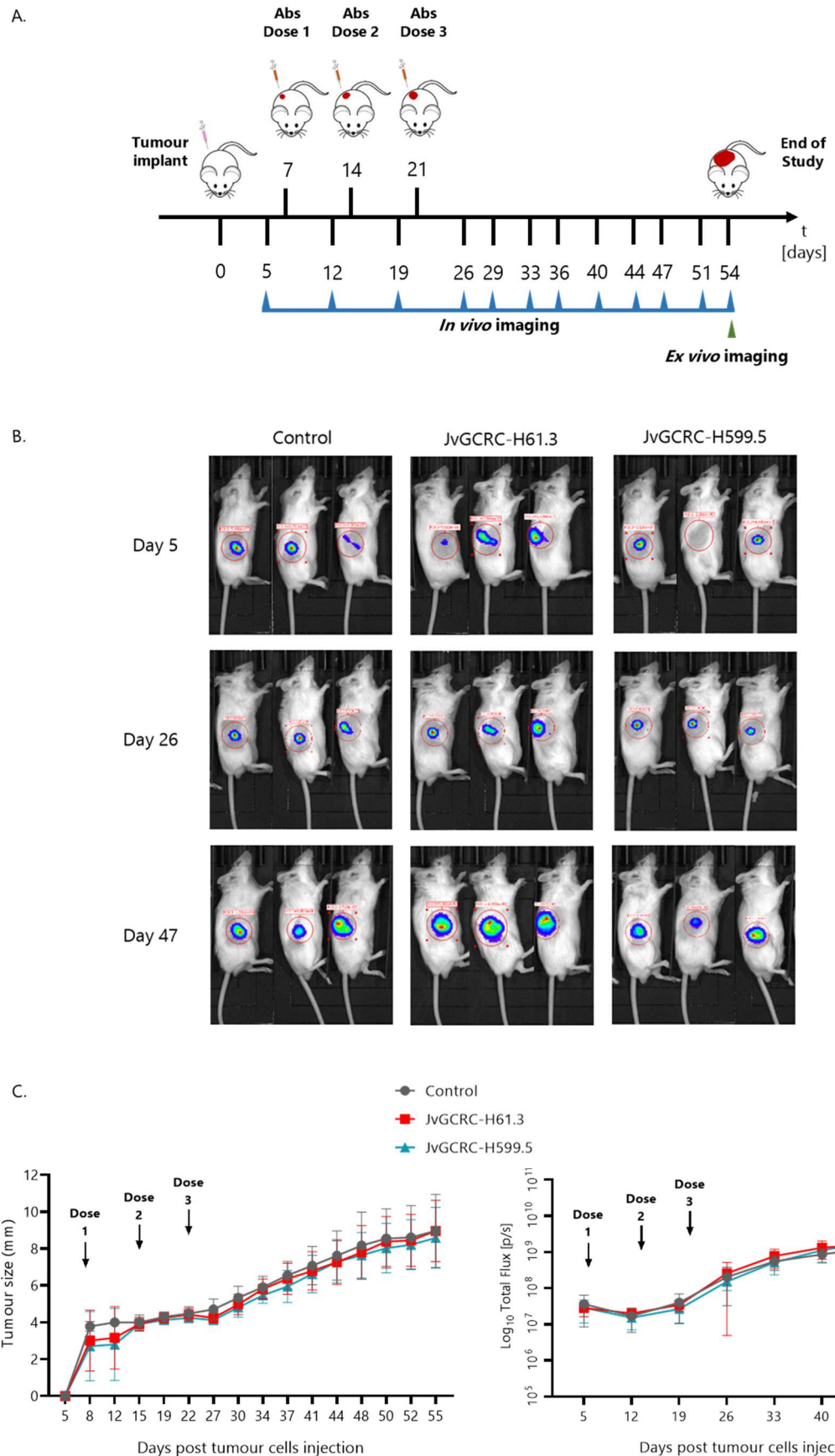
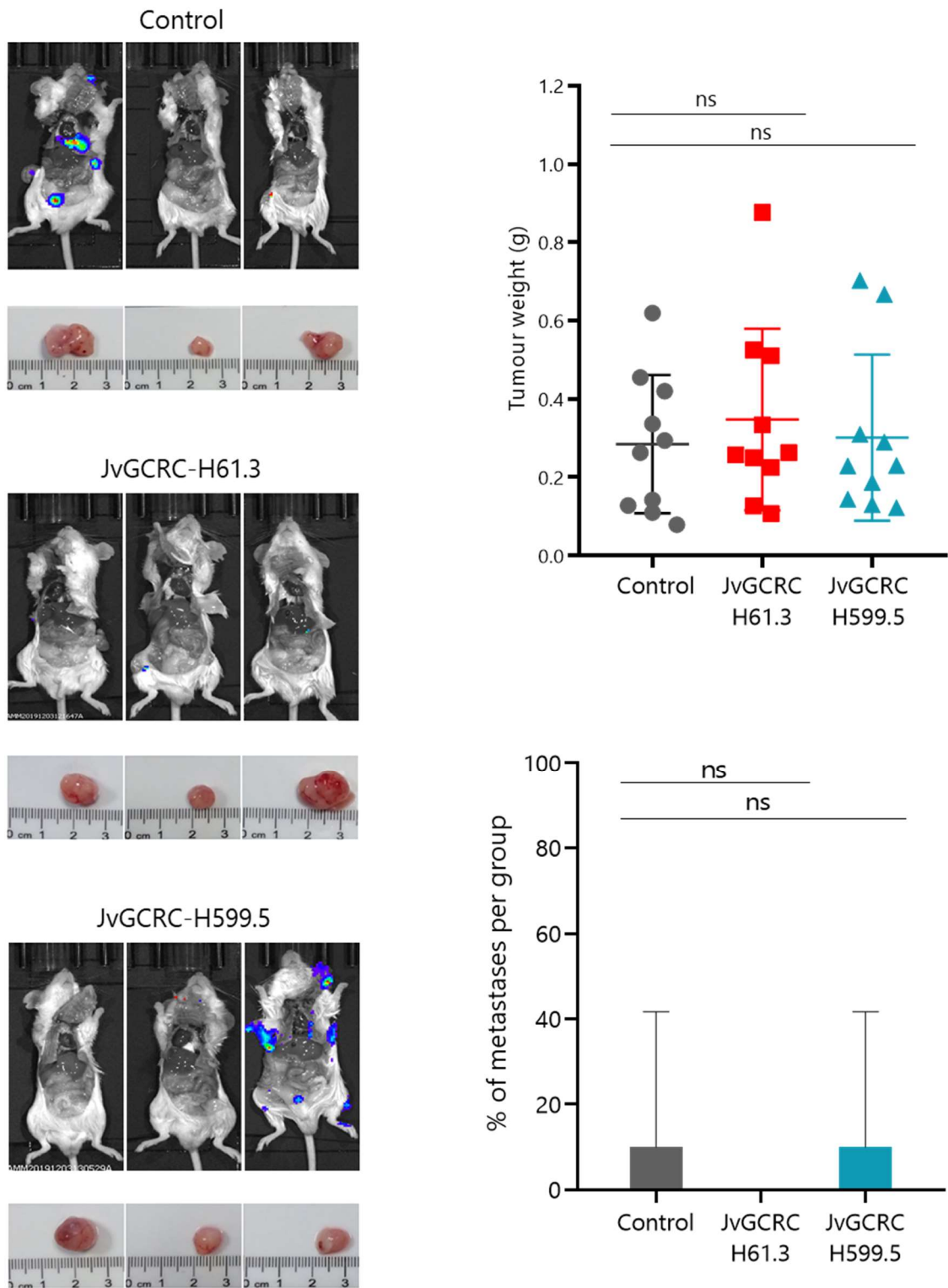


Figure 5.11 – Ex vivo assessment of the effects of the treatment with JvGCRC61.3 and JvGCRC599.5 mAbs against human EPCR on tumour growth. Post-mortem analysis of tumour weight and metastases formation was performed on all the CB17/SCID mice at the end of the study. Images of three representative mice from control and treated groups showing the presence/absence of metastases and micrographs of the relative tumours (left panel). Graphs of tumour weight and percentage of metastases per group are shown in the panel on the right (top and bottom, respectively). No significant difference was observed in both tumour weight and metastases incidence ($n=10$ per group).



5.3.6 Anti-human EPCR JvGCRC-H61.3 mAbs patenting and commercialisation

Based on the overall performance of the four mAbs tested in the present and previous chapter, clone JvGCRC-H61.3 was selected for patenting and commercialisation. The patent application was successfully filed in February 2019 (application no. 1901640.1).

Following the patent filing, the antibody was commercialised by the company 2bscientific.

The product can be found at the following address:

<https://www.2bscientific.com/Products/Aurum/AU-001-002/Mouse-IgG2b-anti-human-EPCRCD201>

5.4 Discussion

In the last 30 years, mAbs-based personalised treatment has become a paramount approach for several blood and solid cancers in the clinic (Scott, Allison et al. 2012). As described in chapter 1, mAbs can exert several mechanisms of action and many mAb-based therapies rely on the ability of mAbs to elicit lysis of tumour cells by exploiting effector cells of the immune system. The previous chapters provided the background for the use of mAbs generated against the human EPCR in developing a targeted therapy for invasive PCa. Based on these results, four clones of the generated mAbs were selected for further assessment of their potential to elicit ADCC in invasive PCa cells both *in vitro* and *in vivo* for drug development.

Firstly, an *in vitro* ADCC assay was performed. Originally, ADCC activity *in vitro* was assessed using isotope-release assays, commonly based on ^{51}Cr . Upon incubation with mAbs and effector cells and if lysis in antigen-expressing target cells occurred, a radioactive signal was detected due to the release of the radiolabel. Thus, such radioactive signal provided a direct quantification of cell lysis as a consequence of the cytotoxic activity of the effector cells. However, such assays rely on the use of PBMCs freshly isolated from donors, which present an intrinsic high variability of cell population and preparation. Nowadays a new approach to *in vitro* ADCC assessment is being used and effector cells-based assays are becoming available. The bioluminescent reporter assay used in this project measures the degree of activation of effector cells following incubation with test mAbs and target cells rather than the consequent cell lysis. ADCC in mice is predominantly mediated by Fc γ RIV, which is the Fc receptor most closely related to the human Fc γ RIIIa (Nimmerjahn, Ravetch 2006). Fc γ RIV-mediated signalling induces dephosphorylation of cytoplasmic NFAT (nuclear factor of activated T cells) that then translocates to the nucleus leading to the expression of ADCC-related genes (Surowy, Cheng et al. 2012). This assay uses Jurkat effector cells, an immortalized line of human T lymphocyte cells, in which an NFAT-response element (NFAT-RE) drives the expression of the luciferase reporter. The use of a standardised assay to assess the ability to mediate ADCC of mAbs provides the advantage to reduce the significant variability of the conventional PBMCs-based assays. Indeed, the degree of the IgG binding to the Fc receptors varies according to their allotypes and affects the therapeutic efficacy of mAbs *in vivo*. Such process has been showed in a study on the anti-CD20 mAb rituximab in which polymorphism of the gene encoding for Fc γ RIIIa correlated with 39% difference in

therapeutic response one year after treatment (Cartron, Dacheux et al. 2002). This chapter presents the results obtained testing the four selected mAbs clones in three PCa cell lines, namely DU145, PC3, and LNCaP, providing an indication about the biological efficacy of each clone. The assay confirmed the ability of the mAbs to activate effector cells, although with different intensities for each clone. Interestingly, none of the clones was able to produce an effect when tested on LNCaP cells. ADCC is triggered upon clustering of the Fc receptors (Stewart et al. 2014), which is facilitated in presence of high expression antigen on the target cell surface, and this could explain the failure of the mAbs in activating the effector cells when tested on LNCaP cells. Indeed, as shown in chapter 2, only a small subpopulation of LNCaP cells expresses EPCR, suggesting that the surface density of the antigen on these cells is not sufficient to trigger the aggregation of Fc γ RIV hence the NFAT-RE activation in Jurkat cells required to produce a bioluminescent signal.

Given the encouraging performance of the mAbs in activating ADCC *in vitro*, the two clones that showed the greatest efficacy in both DU145 and PC3 were selected for *in vivo* testing. Finding the appropriate experimental setting concerning dosing levels and schedules, and endpoint choices of therapeutic agent is not a straightforward process. Moreover, many factors can affect the efficacy of therapeutic agents, the most relevant being their absorption, distribution, metabolism, and excretion (together referred to as ADME) rates once administered in the recipient subject. Interestingly mice can tolerate significantly higher doses of drug compared to humans, and this has an impact on the translatability of the effects registered for a specific therapeutic between different species and is an important factor to consider while designing a study model. Tumour growth in CDX (cell-derived xenograft) models are monitored by calliper measurements and live imaging of fluorescent (based on the jellyfish green fluorescent protein GFP) or, as in this project, luminescent (based on firefly luciferase activity) reactions. However, these optical imaging methods provide low-accuracy tomographic data and are dependent on tissue absorption of the marker proteins that, in turn, can also elicit immune response in immunocompetent mice, with subsequent risk of graft rejection and inhibition of metastasis (Day, Merlino et al. 2015). However, CDX models showed low predictive value for the efficacy of targeted therapeutics in humans, which resulted in only 5-7% of the total drugs tested in such models being approved by the FDA (Day et al. 2015). Indeed, CDX models present important limitations, as they do not reflect the complexity of the original TME, especially when using heterotopic xenografts in which the tumour is maintained in a different anatomical location. As

discussed in chapter 1, the TME is also important in the metastasis establishment process and its absence in CDX models can impair such process thus altering the evaluation of any therapeutic effect on it. Despite all their limits, CDX represent the most used pre-clinical model in drug development studies.

A simple CDX model was adopted to investigate the potential biological effector function of the anti-human EPCR mAbs *in vivo*, quantified by assessing DU145-derived heterotopic xenografts tumour growth rate and metastases formation in CB17/SCID mice. Based on the results obtained with the anti-human EPCR mAbs ADCC *in vitro*, clones JvGCRC-61.3 and JvGCRC-599.5 were selected for this stage of the project. DU145 cells were isolated in 1978 from a human brain metastasis and since then served as main PCa model for *in vitro* and *in vivo* experiments (Stone, Mickey et al. 1978). Although they present a lower metastatic potential compared to PC3 cells, DU145 show higher expression of human EPCR, thus they were used in this project (Wu, Gong et al. 2013). When injected into SCID mice, DU145 cells show a sustained biphasic growth rate with 7-day latency, as well as high metastatic potential with trophy towards organs such as spleen, lung, and liver (Cunningham, You 2015). CB17/SCID mice were selected as animal model due to their partial immune impairment. Indeed, such mouse strain, despite the lack of B cells and T cells that renders it unable to develop an immune response to non-self proteins, still presents macrophages, NK cells and complement activity, which represent a functional innate immune system. Thus, CB17/SCID mice were demonstrated to be a good model to study mAbs potential to trigger ADCC *in vivo* (Flavell, Warnes et al. 2000). As the aim of this final part of the project was to investigate the ability of the mAbs generated against human-EPCR to engage with Fc receptors of effector cells, and since the main immune effectors involved in ADCC are NK cells, CB17/SCID mice represented a suitable model. Furthermore, DU145-derived xenografts in CB17/SCID have already been used in previous study on tumour growth to investigate the effects of treatment with thioxothiazolidinone (Guo, Parise et al. 2009).

Murine EPCR shows 64% similarity of the protein sequence with the human EPCR and is a marker for hematopoietic stem cells in bone marrow (Balazs, Fabian et al. 2006). However, following administration of the mAbs in mice, no side effects were observed throughout the duration of the experiment, which can suggest the absence of an adverse antigen cross-reactivity. Immunisation of DU145-derived xenografts-bearing mice with the designated clones, namely JvGCRC-61.3 and JvGCRC-599.5, did not produce any significant effect on

tumour growth rate nor on the average tumour weight between the control and the treated groups. Moreover, no metastases formation was reported in either control or treated groups, which did not allow for relative analyses.

Unfortunately, this first study was conducted only once, thus leaving unsolved questions that can potentially be addressed in the future. The absence of significant biological effects measured as the variation in tumour growth might be due to a low number of endogenous NK cells. However, as previously mentioned, CB17/SCID mice have already been used successfully to assess ADCC in previous studies on solid tumours (Hu, Li 2010). Specifically, Hu and colleagues observed that the NK activity was impaired in mice with lower percentage of NK cells, suggesting that the adequate response to antibody-based drugs is strictly dependent on the correct effector/target cells ratio. Moreover, high tumour burden has been showed to impair NK activity against tumour cells in mice and patients (Herberman, Djau et al. 1979). This issue could be potentially addressed by infusing functional NK cells stimulated with IL-2 in mice. Moreover, analysis of the presence of NK in the DU145-derived tumours could elucidate if NK cells significantly fail to infiltrate.

Internalisation rate through endocytosis represents an important factor in the pharmacokinetics of mAbs as rapid endocytosis can reduce the amount of drug available for the recognition by effector cells. Such process could represent a limiting factor in efficacy of mAbs in *in vivo* versus *in vitro* settings. Indeed, the ADCC assay procedure allows a prompt and strong interaction between mAbs and effector cells as the latter are provided in excess and soon after the addition of the mAbs to the cells. However, *in vivo* dynamics are complicated by many more factors, such as the ADME, which might affect the availability of antibody to trigger an adequate reaction. Notably, results showed in this chapter suggest that the internalisation rate does not affect ADCC. On the other hand, internalisation might play a role in the absence of effects on the tumour growth upon mAbs administration *in vivo* despite the sustained persistence of the mAbs in the sera, as demonstrated by the results obtained with the ELISA.

Assessment of distant metastases was performed by *ex vivo* imaging based on the expression of the luciferase reporter gene in injected DU154 cells, which did not reveal significant metastasis formation nor in control or in treated mice. Literature reports that only few metastases are generated following subcutaneous implantation of DU145 in SCID mice,

while with orthotopic implantation metastatic spread was reported in 80% of implanted mice (Bastide, Bagnis et al. 2002). Although orthotopic implantation represents a better model for metastatic PCa, it is a more complicated technique with lower tumour take rate compared to subcutaneous injections. Duration of the experiment can also have an impact on metastasis development, although it is not possible to extend the study longer once reached the tumour burden limit set by the law. Another key aspect of the setting of this part of the study is the establishment of DU145-Luc2 cells. Metastases arise from single cells that were able to migrate in secondary sites of the body. In this experiment there is no evidence that all the cells injected were actively expressing luciferase. Thus, it is not possible – without further investigation – to exclude the possibility that metastases formed but were not detected because generated by cells that did not have or had lost luciferase expression.

In the future, further investigation of the pharmacokinetics associated with the clones analysed in this chapter, namely JvGCRC-H61.3 and JvGCRC-H599.5 will provide a greater understanding of the dynamics involved during similar immunisation experiments, allowing for the design of a more suitable model of study. PC3 cells might also represent a valid alternative to DU145 for CDX metastatic model due to their higher metastatic potential in SCID mice (Bastide et al. 2002), although they have a lower EPCR expression compared to DU145. Finally, increasing the concentration of mAbs used at each dose could allow for a stronger availability of the therapeutic in mice.

In conclusion, this study did provide evidence for the biological efficacy of the newly generated mAbs against human EPCR in *in vitro* ADCC. Contrarily, the animal model used to assess the therapeutic efficacy of the two mAb clones did not provide significant evidence for their *in vivo* activity, thus allowing for further research to be conducted.

6. Summary of Discussion

Prostate cancer (PCa) is the most frequent non-cutaneous cancer (33%), and the second most common cancer and the primary cause of death among male population worldwide (Culp, Soerjomataram et al. 2020), although its incidence and mortality rates trends have been seen to decrease in the last years. Its incidence is related to age, environment, diet, family history and ethnicity. Differences in the incidence between countries can be due to the coverage and method of screening. Up to date, in UK there is no standardised screening programme for PCa in the UK and PSA-based PCa screening remains a very controversial method due to its significant level of uncertainty and associated risk in patients. However, other key approaches for PCa screening are currently being used in the clinical practice, such as histopathological analysis of patients' biopsies and live imaging. Conventional treatment for androgen sensitive PCa consists in androgen deprivation therapy in the form of surgical or pharmacological castration. However, hormone-relapsed PCa typically progresses to the metastatic form (mHRPC), which ultimately remains incurable with conventional therapy and is responsible for poor prognosis in patients, for whom immunotherapy might represent the only effective option.

Metastases formation is a multi-step process through which transforming cells from the primary tumour gain the ability to invade surrounding tissues and migrate towards distant sites in the body where they can give rise to secondary tumours (Fares, Fares et al. 2020). Although this represents a highly inefficient process, metastases are accountable for more than 90% of the cancer-associated mortality. The epithelial to mesenchymal transition (EMT) is considered the main cellular program involved in the earliest stages of cancer progression (Pastushenko, Blanpain 2019). Indeed, the acquisition of mesenchymal-like properties enables transforming epithelial cells to (i) lose cell-cell junctions thus detaching from surrounding cells, (ii) degrade the extracellular matrix, (iii) become more motile, (iv) enter the blood stream disseminating in other sites of the body where they can go through the inverse process (MET) giving rise to secondary tumours. Cells going through EMT present a specific pattern of expression of EMT-related markers, most of them being proteins involved in key cellular pathways (i.e. cellular adhesion, cell motility, extracellular matrix remodelling).

To date, immunotherapy represents, on its own or in combination with other conventional therapies, an essential pillar for the treatment of many types of cancer. The concept of exploiting the patient's immune system to target tumour cells has provided a priceless new tool in cancer treatment. The main strategies adopted in immune oncology include whole cell/peptide vaccines, T-cell infusions, dendritic cell infusions (provenge), CARs and monoclonal antibodies, to stimulate the reaction of the host's immune system against cancer cells. Specifically, therapeutic mAb binding to its target can exert many different mechanisms of action. These include antagonism of a soluble ligand or receptor like in checkpoint inhibitor mAbs, blockage of cell–cell interaction, agonism of a receptor, antibody-dependent cellular cytotoxicity (ADCC), antibody-dependent cellular phagocytosis (ADCP), complement-dependent cytotoxicity (CDC), apoptosis, and non-apoptotic programmed cell death. Some mAbs can also exert multiple mechanisms of action on a target (Strohl, Strohl 2012). Many important achievements have been accomplished in the last few decades with the use of immunotherapy in oncology. However, the role of immune checkpoint inhibition in the treatment of PCa is still unclear (Nicholson, Fong 2020), with studies showing a limited efficacy. This leads to an unmet need for new potential immune therapeutic drugs and approaches for the treatment of mHRPC. Several PCa-associated antigens have already been identified, such as prostate-specific membrane antigen (PSMA), prostatic acid phosphatase (PAP), prostate stem cell antigen (PSCA), and therapeutic mAbs generated against them (Khalili, Keshavarz-Fathi et al. 2019). However, such proteins are also expressed in benign prostate epithelial cells. Thus, there is still the need to identify more specific targets and the present project fills in such context, aiming at identifying a novel target expressed by transforming PCa cells that are initiating invasion by undergoing EMT. The target selected herein was EPCR, which involvement in EMT and cancer invasiveness was investigated *in vitro* in PCa cell lines, leading to the validation of EPCR as a potential marker for cells undergoing EMT. Moreover, during this study anti-human EPCR mAbs were generated for their use in targeted cytotoxic immunotherapy.

Drug development is a highly complex and time-consuming process. New potential drugs must pass several steps of selection before they can obtain the pharmaceutical market approval. Before a new drug is approved for the general use, it must go through preclinical and clinical development stages. For this reason, it is important that all the steps of the development are carried out with careful validations. The first key step in drug development is the identification of the target, based on the understanding of its expression in normal

tissues and cancer samples, its physiological role, and the effects of its knockdown in the elected *in vitro* model of study. The following step consists in testing the mechanism of action of the potential drug in cell lines *in vitro* and in animals *in vivo*. The identification of the most suitable model to use in this step is crucial. Only when a potential drug shows convincing results about its efficacy, based on strong and reproducible scientific evidence, it can get into clinical trials. When developing a new mAbs-based immunotherapeutic treatment, it is important to generate mAbs against tumour-specific antigens. Indeed, due to their high antigen specificity, the use of a target broadly expressed in normal tissues can lead to severe and lethal side effects.

As presented in chapter 2, the idea to develop a targeting therapy for mHRPC was conceived following a study conducted by Dr Regad and his team on cPML and its implication in PCa progression (Buczek et al. 2016). To investigate the role of cPML in cancer invasion, an *in vitro* EMT model was developed in DU145 and PC3 cells by generating PML mutants. Mass spectrometry analysis of the DU145 mutants that showed a mesenchymal phenotype after having undergone EMT, provided a pool of proteins that were eligible for being potential markers of invasive cells as well as targets for mAb-based therapy. Eventually the most suitable target was identified in the human EPCR, which met the three criteria of selection by (i) being a cell surface protein (ii) specifically expressed on the invasive cells and (iii) with a limited expression in healthy tissues. EPCR is a cell surface transmembrane protein with an expected molecular weight of ~24/36-46 kDa, depending on its degree of glycosylation. EPCR is mainly expressed in endothelial cells of blood vessels, where it ensures the stability of the endothelial walls. It is a key player in the coagulation pathway, in which it presents the protein C to the thrombin-TM complex for its activation (Stearns-Kurosawa et al. 1996). EPCR is also considered a marker of human hematopoietic stem cells (HSCs) - (Subramaniam et al. 2019) and of multipotent mouse mammary stem cells (MaSCs) - (Wang et al. 2015). Besides its physiological role, EPCR over expression has been reported to correlate with progression in several types of cancer, such as lung (Antón et al. 2012), glioblastoma and leukaemia (Tsuneyoshi et al. 2001), breast (Beaulieu, Church 2007), ovarian (Ducros et al. 2012), and colon (Scheffer et al. 2002). Conversely, EPCR expression has been reported to suppress tumorigenicity in malignant pleural mesothelioma (MPM) (Keshava et al. 2015). The anticoagulant effect of protein C activation through EPCR has been suggested to favour the development of a local coagulation-free environment, thus providing a growth advantage for EPCR-expressing epithelial cancer cells (Scheffer et al. 2002). Endogenous

EPCR cell surface expression was assessed in three PCa cell lines. EPCR was found to be significantly expressed in DU145 and PC3 cells, only a small cell subpopulation of LNCaP showed a detectable level of expression. Interestingly, EPCR expression also correlated with the cell invasion potential that is high in DU145 and PC3 and limited in LNCaP cells. For this reason, DU145 and PC3 cells were selected as *in vitro* models for the purpose of this study.

To validate EPCR as a marker for invasive PCa cells functional studies were performed on DU145 and PC3 PCa cell lines in which EPCR expression was silenced. The relative results are presented in chapter 3. The data reported suggest a correlation between the silencing of EPCR and the expression of EMT markers in both cell lines. Precisely, cells with reduced expression of EPCR showed an overexpression of epithelial factors together with a reduced expression of mesenchymal markers. Such evidence suggests the involvement of EPCR in the EMT process in the PCa cells used as a model for this project. Interestingly, silencing of EPCR also determined a decrease of the cell growth rates as well as the cell migration and invasion potential. Whole transcriptome and proteome analysis confirmed the expression at both RNA and protein levels of genes linked to active EMT. Taken together, the results regarding the functional studies performed upon silencing of EPCR in DU145 and PC3 cells confirmed that EPCR is a good potential target for targeted therapy for aggressive PCa.

When developing antibodies as a research tool it is imperative to assess their specificity. The EuroMAbNet has recently issued a useful step-by-step guide article about selection and validation strategies for antibodies that helped us designing our personal strategy (Roncador, Engel et al. 2016). Such a strategy includes four main steps: (i) target antigen identification, (ii) review of the existing antibodies targeting the same antigen, (iii) antibody validation, (iv) produce data that can support reproducibility for the antibody use. Target identification has been addressed in chapters 2 and 3, where all the data supporting the choice of EPCR as a target for the development of a targeted immunotherapy for aggressive PCa were provided. Chapters 4 and 5 provided the information for antibodies validation. MAbs were thus generated against EPCR using the hybridoma technique in collaboration with Prof. Dr. Hans-Martin Jäck (Department of Medicine - Division of Immunology, University Hospital Erlangen). Eventually, four IgG1 clones were successfully obtained, all showing potentially different epitopes on EPCR. Chapter 4 describes in detail the process of mAbs generation and validation. It is important to make informed decisions when having to select the most efficient antibodies and to do so it is key to set a clear purpose for their use.

Moreover, the anti-EPCR mAbs clones were engineered switching their subclass from IgG1 to IgG2b so to be used in specific murine killing bioassays. Such molecules generated very positive results during the ADCC assay performed to assess their ability to mediate activation of immune effector cells when tested on three different PCa cell lines, namely DU145, PC3, and LNCaP. Interestingly the cell surface expression of EPCR in LNCaP was not enough to trigger the Fc receptor clustering and thus the activation of effector cells *in vitro*. This represent an interesting detail since we know that EPCR is expressed at low levels in normal human tissues, whereas it is overexpressed in invasive prostate cells, thus this could potentially act as a safety checkpoint in activating effector cells *in vivo*.

Although the results obtained *in vitro* were encouraging, the translation of the model *in vivo* did not produce a comparable outcome, suggesting that the system used to test the mAbs efficacy might not be the best suitable for the intended objective. Data presented in chapter 5 show that administration of the anti-EPCR IgG2b molecules in CB17/SCID mice bearing DU145-derived tumours did not elicit antitumour effects. Moreover, it was not possible to assess potential effect of the therapy on metastasis formation as no metastasis was observed in any of the mice, including the ones belonging to the control group. Such results suggest that amendment in the protocol are advisable and the repetition of the *in vivo* experiments is needed.

Blocking anti-EPCR mAbs have been shown to attenuate tumour initiation and growth in breast cancer *in vivo* models using CB17/SCID (Schaffner et al. 2013). The use of blocking murine mAbs against EPCR *in vivo* in baboons has been demonstrated to not produce any relevant side effects, indicating that targeting this protein does not produce major side effects in the host. However, it is not clear whether the therapeutic use of specific targeting mAbs with biological effector function would instead produce significant side effects.

In order to produce a comprehensive assessment of EPCR role in cancer progression and overall expression in normal tissues, one possible route for the future work could be further investigation of EPCR expression in TMA of healthy tissues by immunohistochemistry analysis. Moreover, immunohistochemistry analysis of EPCR expression in PCa biopsy specimens could elucidate EPCR relevance as a prognostic marker for invasive PCa.

Sequencing of the mAbs generated during this project was initially planned in order to obtain the required information that could potentially be used to design CARs that would specifically direct the patient's autologous T-cells towards EPCR-expressing tumour cells. However, due to the wide – although with low/medium levels – expression of EPCR in normal tissues and the extreme precision and efficacy that characterises CAR T-cell therapy, this does not represent a safe option for use in patients. Although the focus of the second part of this project was the evaluation of the potential biological effect of mAbs targeting EPCR, other strategies can be investigated in the future, such as their application as blocking activity.

Bibliography

- ABBOTT, W.M., DAMSCHRODER, M.M. And LOWE, D.C., 2014. Current approaches to finemapping of antigen-antibody interactions. *Immunology*, **142**(4), pp. 526-535.
- ACLOQUE, H., ADAMS, M.S., FISHWICK, K., BRONNER-FRASER, M. and NIETO, M.A., 2009b. Epithelial-mesenchymal transitions: the importance of changing cell state in developmentand disease. *The Journal of clinical investigation*, **119**(6), pp. 1438-1449.
- ALBERTS, B., JOHNSON, A. and LEWIS, J., 2002. Cell Junctions. In *Molecular Biology of the Cell*. (Ed. 4). New York: Garland Science.
- AL-MEHDI, A., TOZAWA, K., FISHER, A.B., SHIENTAG, L., LEE, A. and MUSCHEL, R.J., 2000. Intravascular origin of metastasis from the proliferation of endothelium-attached tumorcells: a new model for metastasis. *Nature medicine*, **6**(1), pp. 100-102.
- AN, Z., 2010. Monoclonal antibodies - a proven and rapidly expanding therapeuticmodality for human diseases. *Protein & cell*, **1**(4), pp. 319-330.
- ANCEY, P., CONTAT, C. and MEYLAN, E., 2018. Glucose transporters in cancer – from tumorcells to the tumor microenvironment. *The FEBS Journal*, **285**(16), pp. 2926-2943.
- ANTOHE, M., NEDELCU, R.I., NICHITA, L., POPP, C.G., CIOPLEA, M., BRINZEA, A., HODOROGEA, A., CALINESCU, A., BALABAN, M., ION, D.A., DIACONU, C., BLEOTU, C., PIRICI, D., ZURAC, S.A. and TURCU, G., 2019. Tumor infiltrating lymphocytes: The regulatorof melanoma evolution. *Oncology Letters*, **5**(17), pp. 4155–4161.
- ANTÓN, I., MOLINA, E., LUIS-RAVELO, D., ZANDUETA, C., VALENCIA, K., ORMAZABAL, C., MARTÍNEZ-CANARIAS, S., PERURENA, N., PAJARES, M.J., AGORRETA, J., MONTUENGA, L.M., SEGURA, V., WISTUBA, I.I., DE LAS RIVAS, J., HERMIDA, J. and LECANDA, F., 2012. Receptor of activated protein C promotes metastasis and correlates with clinical outcome in lung adenocarcinoma. *American journal of respiratory and critical care medicine*, **186**(1), pp. 96-105.
- ANTONARAKIS, E.S., PIULATS, J.M., GROSS-GOUPI, M., GOH, J., OJAMAA, K., HOIMES, C.J., VAISHAMPAYAN, U., BERGER, R., SEZER, A., ALANKO, T., DE WIT, R., LI, C., OMLIN, A., PROCOPIO, G., FUKASAWA, S., TABATA, K., PARK, S.H., FEYERABEND, S., DRAKE, C.G., WU, H., QIU, P., KIM, J., POEHLEIN, C. and DE BONO, J.S., 2020. Pembrolizumab for Treatment- Refractory Metastatic Castration-Resistant Prostate Cancer: Multicohort, Open-Label Phasell KEYNOTE-199 Study. *JCO*, **38**(5), pp. 395-405.
- ARLEN, P.M., MOHEBTASH, M., MADAN, R.A. and GULLEY, J.L., 2009. Promising novel immunotherapies and combinations for prostate cancer. *Future oncology (London,England)*, **5**(2), pp. 187-196.
- ARMSTRONG, A.J., MARENKO, M.S., OLTEAN, S., KEMENY, G., BITTING, R.L., TURNBULL, J.D., HEROLD, C.I., MARCOM, P.K., GEORGE, D.J. and GARCIA-BLANCO, M.A., 2011. Circulating tumor cells from patients with advanced prostate and breast cancer display both epithelial and mesenchymal markers. *Molecular cancer research : MCR*, **9**(8), pp. 997-1007.

BABRAK, L., MCGARVEY, J.A., STANKER, L.H. and HNASKO, R., 2017. Identification and verification of hybridoma-derived monoclonal antibody variable region sequences using recombinant DNA technology and mass spectrometry. *Molecular immunology*, **90**, pp. 287-294.

BACH, D.H., PARK, H.J. and LEE, S.K., 2017. The Dual Role of Bone Morphogenetic Proteins in Cancer. *Molecular therapy oncolytics*, **8**, pp. 1-13.

BADALAMENTI, G., FANALE, D., INCORVAIA, L., BARRACO, N., LISTÌ, A., MARAGLIANO, R., VINCENZI, B., CALÒ, V., IOVANNA, J.L., BAZAN, V. and RUSSO, A., 2019. Role of tumor-infiltrating lymphocytes in patients with solid tumors: Can a drop dig a stone? *Cellular immunology*, **343**, 103753.

BAE, K.M., PARKER, N.N., DAI, Y., VIEWEG, J. and SIEMANN, D.W., 2011. E-cadherin plasticity in prostate cancer stem cell invasion. *American journal of cancer research*, **1**(1), pp. 71-84.

BAERISWYL, V. and CHRISTOFORI, G., 2009. The angiogenic switch in carcinogenesis. *Seminars in cancer biology*, **19**(5), pp. 329-337.

BAGHBAN, R., ROSHANGAR, L., JAHANBAN-ESFAHLAN, R., SEIDI, K., EBRAHIMI-KALAN, A., JAYMAND, M., KOLAHIAN, S., JAVAHERI, T. and ZARE, P., 2020. Tumor microenvironment complexity and therapeutic implications at a glance. *Cell Communication and Signaling*, **18**(1), pp. 59.

BAILEY, M., CHRISTOFORIDOU, Z. and LEWIS, M.C., 2013. The evolutionary basis for differences between the immune systems of man, mouse, pig and ruminants. *Veterinary immunology and immunopathology*, **152**(1-2), pp. 13-19.

BALAZS, A.B., FABIAN, A.J., ESMON, C.T. and MULLIGAN, R.C., 2006. Endothelial protein C receptor (CD201) explicitly identifies hematopoietic stem cells in murine bone marrow. *Blood*, **107**(6), pp. 2317-2321.

BALKWILL, F.R., CAPASSO, M. and HAGEMANN, T., 2012. The tumor microenvironment at a glance. *Journal of cell science*, **125**(Pt 23), pp. 5591-5596.

BARATA, P.C. and SARTOR, A.O., 2019. Metastatic castration-sensitive prostate cancer: Abiraterone, docetaxel, or.... *Cancer*, **125**(11), pp. 1777-1788.

BARBATO, L., BOCCHETTI, M., DI BIASE, A. and REGAD, T., 2019. Cancer Stem Cells and Targeting Strategies. *Cells*, **8**(8), pp. 926.

BASTIDE, C., BAGNIS, C., MANNONI, P., HASSOUN, J. and BLADOU, F., 2002. A Nod Scid mouse model to study human prostate cancer. *Prostate cancer and prostatic diseases*, **5**(4), pp. 311-315.

BATLLE, E. and MASSAGUÉ, J., 2019. Transforming Growth Factor- β Signaling in Immunity and Cancer. *Immunity*, **50**(4), pp. 924-940.

BEATTY, G.L. and GLADNEY, W.L., 2015. Immune Escape Mechanisms as a Guide for Cancer Immunotherapy. *Clinical Cancer Research*, **21**(4), pp. 687-692.

BEAULIEU, L.M. and CHURCH, F.C., 2007. Activated protein C promotes breast cancer cell migration through interactions with EPCR and PAR-1. *Experimental cell research*, **313**(4), pp. 677-687.

BECK, B., LAPOUGE, G., RORIVE, S., DROGAT, B., DESAEDELAERE, K., DELAFAILLE, S., DUBOIS, C., SALMON, I., WILLEKENS, K., MARINE, J.C. and BLANPAIN, C., 2015. Different levels of Twist1 regulate skin tumor initiation, stemness, and progression. *Cell stem cell*, **16**(1), pp. 67-79.

BENONISSON, H., ALTINTAŞ, I., SLUIJTER, M., VERPLOEGEN, S., LABRIJN, A.F., SCHUURHUIS, D.H., HOUTKAMP, M.A., VERBEEK, J.S., SCHUURMAN, J. and VAN HALL, T., 2019. CD3-Bispecific Antibody Therapy Turns Solid Tumors into Inflammatory Sites but Does Not Install Protective Memory. *Molecular cancer therapeutics*, **18**(2), pp. 312-322.

BERTHON, P., CUSSENOT, O., HOPWOOD, L., LEDUC, A., and MAITLAND, N., 1995. Functional expression of sv40 in normal human prostatic epithelial and fibroblastic cells - differentiation pattern of nontumorigenic cell-lines. *International journal of oncology*, **6**(2), pp. 333-343.

BEZUHLY, M., CULLEN, R., ESMON, C.T., MORRIS, S.F., WEST, K.A., JOHNSTON, B. and LIWSKI, R.S., 2009. Role of activated protein C and its receptor in inhibition of tumormetastasis. *Blood*, **113**(14), pp. 3371-3374.

BIFFI, G., ONI, T.E., SPIELMAN, B., HAO, Y., ELYADA, E., PARK, Y., PREALL, J. and TUVESON, D.A., 2019. IL1-Induced JAK/STAT Signaling Is Antagonized by TGF β to Shape CAF Heterogeneity in Pancreatic Ductal Adenocarcinoma. *Cancer Discovery*, **9**(2), pp. 282-301.

BLANCHÈRE, M., SAUNIER, E., MESTAYER, C., BROSHUIS, M., and MOWSZOWICZ, I., 2002. Alterations of expression and regulation of transforming growth factor beta in human cancer prostate cell lines. *The Journal of steroid biochemistry and molecular biology*, **82**(4-5), pp. 297-304.

BRABLETZ, S. and BRABLETZ, T., 2010. The ZEB/miR-200 feedback loop--a motor of cellularplasticity in development and cancer? *EMBO reports*, **11**(9), pp. 670-677.

BUCZEK, M.E., MILES, A.K., GREEN, W., JOHNSON, C., BOOCOCK, D.J., POCKLEY, A.G., REES, R.C., HULMAN, G., VAN SCHALKWYK, G., PARKINSON, R., HULMAN, J., POWE, D.G. and REGAD, T., 2016. Cytoplasmic PML promotes TGF- β -associated epithelial-mesenchymal transition and invasion in prostate cancer. *Oncogene*, **35**(26), pp. 3465-3475.

BÜHLER, P., WOLF, P., GIERSCHNER, D., SCHABER, I., KATZENWADEL, A., SCHULTZE-SEEMANN, W., WETTERAUER, U., TACKE, M., SWAMY, M., SCHAMEL, W.W. and ELSÄSSER-BEILE, U., 2008. A bispecific diabody directed against prostate-specific membrane antigen and CD3 induces T-cell mediated lysis of prostate cancer cells. *Cancer immunology, immunotherapy: CII*, **57**(1), pp. 43-52.

BUONAGURO, F.M., PUZANOV, I. and ASCIERTO, P.A., 2020. Anti-IL6R role in treatment of COVID-19-related ARDS. *Journal of translational medicine*, **18**(1), pp. 165-020-02333-9.

BURNET, F.M., 1970. The concept of immunological surveillance. *Progress in experimental tumor research*, **13**, pp. 1-27.

CABEL, L., LOIR, E., GRAVIS, G., LAVAUD, P., MASSARD, C., ALBIGES, L., BACIARELLO, G., LORIOT, Y. and FIZAZI, K., 2017. Long-term complete remission with ipilimumab in metastatic castrate-resistant prostate cancer: case report of two patients. *Journal for Immuno Therapy of Cancer*, **5**(1), pp. 31.

CARACCIO, C., KRISHNA, S., PHILLIPS, D.J. and SCHÜRCH, C.M., 2020. Bispecific Antibodies for Multiple Myeloma: A Review of Targets, Drugs, Clinical Trials, and Future Directions. *Frontiers in immunology*, **11**, pp. 501.

CARMELIET, P. and JAIN, R.K., 2011. Principles and mechanisms of vessel normalization for cancer and other angiogenic diseases. *Nature Reviews Drug Discovery*, **10**(6), pp. 417-427.

CARTRON, G., DACHEUX, L., SALLES, G., SOLAL-CELINEY, P., BARDOS, P., COLOMBAT, P. and WATIER, H., 2002. Therapeutic activity of humanized anti-CD20 monoclonal antibody and polymorphism in IgG Fc receptor Fc_YRIIIa gene. *Blood*, **99**(3), pp. 754-758.

CHALMERS, A.D., WHITLEY, P., ELSUM, I., YATES, L., HUMBERT, P.O. and RICHARDSON, H.E., 2012. The Scribble-Dlg-Lgl polarity module in development and cancer: from flies to man. *Essays in biochemistry*, **53**, pp. 141-168.

CHAMBERS, A.F., GROOM, A.C. and MACDONALD, I.C., 2002. Dissemination and growth of cancer cells in metastatic sites. *Nature reviews Cancer*, **2**(8), pp. 563-572.

CHARMSAZ, S., SCOTT, A.M. and BOYD, A.W., 2017. Targeted therapies in hematological malignancies using therapeutic monoclonal antibodies against Eph family receptors. *Experimental hematology*, **54**, pp. 31-39.

CHAU, C.H., STEEG, P.S. and FIGG, W.D., 2019. Antibody-drug conjugates for cancer. *The Lancet*, **394**(10200), pp. 793-804.

CHEN, D.S. and MELLMAN, I., 2013. Oncology meets immunology: the cancer-immunity cycle. *Immunity*, **39**(1), pp. 1-10.

CHEN, Y., TAN, W. and WANG, C., 2018. Tumor-associated macrophage-derived cytokines enhance cancer stem-like characteristics through epithelial-mesenchymal transition. *Oncotargets and therapy*, **11**, pp. 3817-3826.

CHIRCOP, M. and SPEIDEL, D., 2014. Cellular Stress Responses in Cancer and Cancer Therapy. *Frontiers in Oncology*, **4**, pp. 304.

CHRISTOFORI, G., 2003. Changing neighbours, changing behaviour: cell adhesion molecule-mediated signalling during tumour progression. *The EMBO Journal*, **22**(10), pp. 2318-2323.

CHUNTHAPONG, J., SEFTOR, E.A., KHALKHALI-ELLIS, Z., SEFTOR, R.E., AMIR, S., LUBAROFF, D.M., HEIDGER, P.M., Jr and HENDRIX, M.J., 2004. Dual roles of E-cadherin in prostate cancer invasion. *Journal of cellular biochemistry*, **91**(4), pp. 649-661.

COTTON, R.G.H. and MILSTEIN, C., 1973. Fusion of Two Immunoglobulin-producing Myeloma Cells. *Nature*, **244**(5410), pp. 42-43.

COUZIN-FRANKEL, J., 2013. Cancer Immunotherapy. *Science*, **342**(6165), pp. 1432-1433.

CULP, M.B., SOERJOMATARAM, I., EFSTATHIOU, J.A., BRAY, F. and JEMAL, A., 2020. Recent Global Patterns in Prostate Cancer Incidence and Mortality Rates. *European urology*, **77**(1), pp. 38-52.

CUNNINGHAM, D. and YOU, Z., 2015. In vitro and in vivo model systems used in prostate cancer research. *Journal of biological methods*, **2**(1), pp. e17.

CURTIS, M., KENNY, H.A., ASHCROFT, B., MUKHERJEE, A., JOHNSON, A., ZHANG, Y., HELOU, Y., BATLLE, R., LIU, X., GUTIERREZ, N., GAO, X., YAMADA, S.D., LASTRA, R., MONTAG, A., AHSAN, N., LOCASALE, J.W., SALOMON, A.R., NEBREDA, A.R. and LENGYEL, E., 2019. Fibroblasts Mobilize Tumor Cell Glycogen to Promote Proliferation and Metastasis. *Cell metabolism*, **29**(1), pp. 141-155.e9.

DAMODARAN, S., KYRIAKOPOULOS, C.E. and JARRARD, D.F., 2017. Newly Diagnosed Metastatic Prostate Cancer: Has the Paradigm Changed? *The Urologic clinics of North America*, **44**(4), pp. 611-621.

DASGUPTA, A. and WAHED, A., 2014. *Chapter 13 - Tumor Markers*. San Diego: Elsevier.

DAVID, C.J. AND MASSAGUÉ, J., 2018. Contextual determinants of TGF β action in development, immunity and cancer. *Nature reviews. Molecular cell biology*, **19**(7), pp. 419–435.

DAY, C.P., MERLINO, G. and VAN DYKE, T., 2015. Preclinical mouse cancer models: a maze of opportunities and challenges. *Cell*, **163**(1), pp. 39-53.

DE CLARO, R.A., MCGINN, K., KWITKOWSKI, V., BULLOCK, J., KHANDELWAL, A., HABTEMARIAM, B., OUYANG, Y., SABER, H., LEE, K., KOTI, K., ROTHMANN, M., SHAPIRO, M., BORREGO, F., CLOUSE, K., CHEN, X.H., BROWN, J., AKINSANYA, L., KANE, R., KAMINSKAS, E., FARRELL, A. and PAZDUR, R., 2012. U.S. Food and Drug Administration Approval Summary: Brentuximab Vedotin for the Treatment of Relapsed Hodgkin Lymphoma or Relapsed Systemic Anaplastic Large-Cell Lymphoma. *Clin Cancer Res*, **18**(21), pp. 5845.

DEBERARDINIS, R.J., MANCUSO, A., DAIKHIN, E., NISSIM, I., YUDKOFF, M., WEHRLI, S. and THOMPSON, C.B., 2007. Beyond aerobic glycolysis: transformed cells can engage in glutamine metabolism that exceeds the requirement for protein and nucleotide synthesis. *Proceedings of the National Academy of Sciences of the United States of America*, **104**(49), pp. 19345-19350.

DI BIASE, A., MILES, A.K. and REGAD, T., 2018. Generation of In Vitro Model of Epithelial Mesenchymal Transition (EMT) Via the Expression of a Cytoplasmic Mutant Form of Promyelocytic Leukemia Protein (PML). *Methods in molecular biology (Clifton, N.J.)*, **1692**, pp. 129-138.

DILLEKÅS, H., ROGERS, M.S. and STRAUME, O., 2019. Are 90% of deaths from cancer caused by metastases? *Cancer Medicine*, **8**(12), pp. 5574-5576.

DOGLIONI, G., PARIK, S. and FENDT, S., 2019. Interactions in the (Pre)metastatic NicheSupport Metastasis Formation. *Frontiers in Oncology*, **9**, pp. 219.

DUCROS, E., MIRSHAHİ, S., AZZAZENE, D., CAMILLERI-BROËT, S., MERY, E., AL FARSI, H., ALTHAWADI, H., BESBESS, S., CHIDIAC, J., PUJADE-LAURAIN, E., THERWATH, A., SORIA, J. and MIRSHAHİ, M., 2012. Endothelial protein C receptor expressed by ovarian cancer cells as a possible biomarker of cancer onset. *International journal of oncology*, **41**(2), pp. 433-440.

DUDLEY, A.C., 2012. Tumor endothelial cells. *Cold Spring Harbor perspectives in medicine*, **2**(3), pp. a006536.

DUNN, G.P., OLD, L.J. and SCHREIBER, R.D., 2004. The Three Es of Cancer Immunoediting. *Annual Review of Immunology*, **22**(1), pp. 329-360.

EAGLE, H., 1955. Nutrition needs of mammalian cells in tissue culture. *Science (New York, N.Y.)*, **122**(3168), pp. 501-514.

ERDOGAN, B. and WEBB, D.J., 2017. Cancer-associated fibroblasts modulate growth factorsignaling and extracellular matrix remodeling to regulate tumor metastasis. *Biochemical Society transactions*, **45**(1), pp. 229-236.

ERLER, J.T., BENNEWITH, K.L., COX, T.R., LANG, G., BIRD, D., KOONG, A., LE, Q.T. and GIACCIA, A.J., 2009. Hypoxia-induced lysyl oxidase is a critical mediator of bone marrowcell recruitment to form the premetastatic niche. *Cancer cell*, **15**(1), pp. 35-44.

ESMON, C.T., 2004. Structure and functions of the endothelial cell protein C receptor. *Critical Care Medicine*, **32**(5 Suppl), pp. S298-301.

ESTRELLA, V., CHEN, T., LLOYD, M., WOJTKOWIAK, J., CORNNELL, H.H., IBRAHIM-HASHIM, A., BAILEY, K., BALAGURUNATHAN, Y., ROTHBERG, J.M., SLOANE, B.F., JOHNSON, J., GATENBY, R.A. and GILLIES, R.J., 2013. Acidity generated by the tumor microenvironmentdrives local invasion. *Cancer research*, **73**(5), pp. 1524-1535.

FARES, J., FARES, M.Y., KHACHFE, H.H., SALHAB, H.A. and FARES, Y., 2020. Molecular principles of metastasis: a hallmark of cancer revisited. *Signal Transduction and TargetedTherapy*, **5**(1), pp. 28.

FEHLINGS, M., SIMONI, Y., PENNY, H.L., BECHT, E., LOH, C.Y., GUBIN, M.M., WARD, J.P., WONG, S.C., SCHREIBER, R.D. and NEWELL, E.W., 2017. Checkpoint blockade immunotherapy reshapes the high-dimensional phenotypic heterogeneity of murine intratumoural neoantigen-specific CD8+ T cells. *Nature Communications*, **8**(1), pp. 562.

FELICES, M., LENVIK, T.R., DAVIS, Z.B., MILLER, J.S. and VALLERA, D.A., 2016. Generation of BiKEs and TriKEs to Improve NK Cell-Mediated Targeting of Tumor Cells. *Methods in molecular biology* (Clifton, N.J.), **1441**, pp. 333-346.

FERNANDEZ-GARCIA, E.M., VERA-BADILLO, F.E., PEREZ-VALDERRAMA, B., MATOS-PITA, A.S. and DURAN, I., 2015. Immunotherapy in prostate cancer: review of the currentevidence. *Clinical and Translational Oncology*, **17**(5), pp. 339-357.

FIDLER, I.J., 2003. The pathogenesis of cancer metastasis: the 'seed and soil' hypothesisrevisited. *Nature reviews. Cancer*, **3**(6), pp. 453-458.

FILLIES, T., WERKMEISTER, R., PACKEISEN, J., BRANDT, B., MORIN, P., WEINGART, D., JOOS, U. and BUERGER, H., 2006. Cytokeratin 8/18 expression indicates a poor prognosis in squamous cell carcinomas of the oral cavity. *BMC cancer*, **6**, pp. 10-2407-6-10.

FISHER, T.S., KAMPERSCHROER, C., OLIPHANT, T., LOVE, V.A., LIRA, P.D., DOYONNAS, R., BERGQVIST, S., BAXI, S.M., ROHNER, A., SHEN, A.C., HUANG, C., SOKOLOWSKI, S.A. and SHARP, L.L., 2012. Targeting of 4-1BB by monoclonal antibody PF-05082566 enhances T- cell function and promotes anti-tumor activity. *Cancer immunology, immunotherapy : CII*, **61**(10), pp. 1721-1733.

FIZAZI, K., DRAKE, C.G., BEER, T.M., KWON, E.D., SCHER, H.I., GERRITSEN, W.R., BOSSI, A., DEN EERTWEGH, A.J.M.V., KRAINER, M., HOUEDE, N., SANTOS, R., MAHAMMEDI, H., NG, S., DANIELLI, R., FRANKE, F.A., SUNDAR, S., AGARWAL, N., BERGMAN, A.M., CIULEANU, T.E., KORBENFELD, E., SENGELOV, L., HANSEN, S., MCHENRY, M.B., CHEN, A., LOGOTHECIS, C. and CA184-043, I., 2020. Final Analysis of the Ipilimumab Versus Placebo Following Radiotherapy Phase III Trial in Postdocetaxel Metastatic Castration-resistant Prostate Cancer Identifies an Excess of Long-term Survivors. *European urology*, **78**(6), pp. 822-830.

FLAVELL, D.J., WARNES, S.L., NOSS, A.L. and FLAVELL, S.U., 2000. Anti-CD7 antibody and immunotoxin treatment of human CD7(+)T-cell leukaemia is significantly less effective in NOD/LtSz-scid mice than in CB.17 scid mice. *British journal of cancer*, **83**(12), pp. 1755- 1761.

FLOROS, T. and TARHINI, A.A., 2015. Anticancer Cytokines: Biology and Clinical Effects of Interferon- α 2, Interleukin (IL)-2, IL-15, IL-21, and IL-12. *Seminars in oncology*, **42**(4), pp.539-548.

FOLKMAN, J., 1971. Tumor angiogenesis: therapeutic implications. *The New England journal of medicine*, **285**(21), pp. 1182-1186.

FONTANA, F., RAIMONDI, M., MARZAGALLI, M., SOMMARIVA, M., LIMONTA, P. and GAGLIANO, N., 2019. Epithelial-To-Mesenchymal Transition Markers and CD44 Isoforms Are Differently Expressed in 2D and 3D Cell Cultures of Prostate Cancer Cells. *Cells*, **8**(2),pp. 143.

FORDE, P.M., CHAFT, J.E., SMITH, K.N., ANAGNOSTOU, V., COTTRELL, T.R., HELLMANN, M.D., ZAHURAK, M., YANG, S.C., JONES, D.R., BRODERICK, S., BATTAFARANO, R.J., VELEZ, M.J., REKHTMAN, N., OLAH, Z., NAIDOO, J., MARRONE, K.A., VERDE, F., GUO, H., ZHANG, J., CAUSHI, J.X., CHAN, H.Y., SIDHOM, J., SCHARPF, R.B., WHITE, J., GABRIELSON, E., WANG, H., ROSNER, G.L., RUSCH, V., WOLCHOK, J.D., MERGHOUB, T., TAUBE, J.M., VELCULESCU, V.E., TOPALIAN, S.L., BRAHMER, J.R. and PARDOLL, D.M., 2018. Neoadjuvant PD-1 Blockade in Resectable Lung Cancer. *N Engl J Med*, **378**(21), pp. 1976-1986.

FORTIER, A., ASSELIN, E. and CADRIN, M., 2013. Keratin 8 and 18 loss in epithelial cancer cells increases collective cell migration and cisplatin sensitivity through claudin1 up- regulation. *Journal of Biological Chemistry*, **288**(16), pp. 11555-11571.

FOUAD, Y.A. and AANEI, C., 2017. Revisiting the hallmarks of cancer. *American journal of cancer research*, **7**(5), pp. 1016-1036.

FRIEDL, P. and GILMOUR, D., 2009. Collective cell migration in morphogenesis, regeneration and cancer. *Nature reviews. Molecular cell biology*, **10**(7), pp. 445-457.

FRISCH, S.M. and SCREATON, R.A., 2001. Anoikis mechanisms. *Current opinion in cellbiology*, **13**(5), pp. 555-562.

FUJITA, K. and NONOMURA, N., 2019. Role of Androgen Receptor in Prostate Cancer: A Review. *The world journal of men's health*, **37**(3), pp. 288-295.

FUKUDOME, K. and ESMON, C.T., 1994. Identification, cloning, and regulation of a novel endothelial cell protein C/activated protein C receptor. *Journal of Biological Chemistry*, **269**(42), pp. 26486-26491.

GAJRIA, D. and CHANDRALAPATY, S., 2011. HER2-amplified breast cancer: mechanisms of trastuzumab resistance and novel targeted therapies. *Expert review of anticancer therapy*, **11**(2), pp. 263-275.

GARBER, K., 2018. Driving T-cell immunotherapy to solid tumors. *Nature biotechnology*, **36**(3), pp. 215-219.

GARCÍA-FONCILLAS, J. and DÍAZ-RUBIO, E., 2010. Progress in metastatic colorectal cancer:growing role of cetuximab to optimize clinical outcome. *Clinical & translational oncology: official publication of the Federation of Spanish Oncology Societies and of the National Cancer Institute of Mexico*, **12**(8), pp. 533—542.

GERHARDT, H., GOLDING, M., FRUTTIGER, M., RUHRBERG, C., LUNDKVIST, A., ABRAMSSON, A., JELTSCH, M., MITCHELL, C., ALITALO, K., SHIMA, D. and BETSHOLTZ, C., 2003. VEGF guides angiogenic sprouting utilizing endothelial tip cell filopodia. *The Journal of cell biology*, **161**(6), pp. 1163-1177.

GLEASON, D.F. and MELLINGER, G.T., 1974. Prediction of prognosis for prostatic adenocarcinoma by combined histological grading and clinical staging. *The Journal of urology*, **111**(1), pp. 58-64.

GÓMEZ ROMÁN, V.R., MURRAY, J.C. and WEINER, L.M., 2014. Chapter 1 - Antibody- Dependent Cellular Cytotoxicity (ADCC). In: M.E. ACKERMAN and F. NIMMERJAHN, eds, *Antibody Fc*. Boston: Academic Press, pp. 1-27.

GOOSSENS, S., VANDAMME, N., VAN VLIERBERGHE, P. and BERX, G., 2017. EMT transcription factors in cancer development re-evaluated: Beyond EMT and MET. *Biochimica et biophysica acta. Reviews on cancer*, **1868**(2), pp. 584–591.

GORDON, S.R., MAUTE, R.L., DULKEN, B.W., HUTTER, G., GEORGE, B.M., MCCRACKEN, M.N., GUPTA, R., TSAI, J.M., SINHA, R., COREY, D., RING, A.M., CONNOLLY, A.J. and WEISSMAN, I.L., 2017. PD-1 expression by tumour-associated macrophages inhibits phagocytosis and tumour immunity. *Nature*, **545**(7655), pp. 495-499.

GRAFF, J.N. and CHAMBERLAIN, E.D., 2014. Sipuleucel-T in the treatment of prostate cancer: an evidence-based review of its place in therapy. *Core evidence*, **10**, pp. 1-10.

GRAHAM, K. and UNGER, E., 2018. Overcoming tumor hypoxia as a barrier to radiotherapy, chemotherapy and immunotherapy in cancer treatment. *International journal of nanomedicine*, **13**, pp. 6049-6058.

GREENBURG, G. and HAY, E.D., 1982. Epithelia suspended in collagen gels can lose polarityand express characteristics of migrating mesenchymal cells. *The Journal of cell biology*, **95**(1), pp. 333-339.

GRETEN, F.R. and GRIVENNIKOV, S.I., 2019. Inflammation and Cancer: Triggers, Mechanisms, and Consequences. *Immunity*, **51**(1), pp. 27-41.

GUEDAN, S., CALDERON, H., POSEY, A.D., Jr. and MAUS, M.V., 2019. Engineering and Design of Chimeric Antigen Receptors. *Molecular Therapy - Methods & Clinical Development*, **12**, pp. 145-156.

GULLEY, J.L., BORRE, M., VOGLZANG, N.J., NG, S., AGARWAL, N., PARKER, C.C., POOK, D.W., RATHENBORG, P., FLAIG, T.W., CARLES, J., SAAD, F., SHORE, N.D., CHEN, L., HEERY, C.R., GERRITSEN, W.R., PRIOU, F., LANGKILDE, N.C., NOVIKOV, A. and KANTOFF, P.W., 2019. Phase III Trial of PROSTVAC in Asymptomatic or Minimally Symptomatic Metastatic Castration-Resistant Prostate Cancer. *Journal of clinical oncology : official journal of the American Society of Clinical Oncology*, **37**(13), pp. 1051-1061.

GUO, C., MANJILI, M.H., SUBJECK, J.R., SARKAR, D., FISHER, P.B. and WANG, X., 2013. Therapeutic cancer vaccines: past, present, and future. *Advances in Cancer Research*, **119**, pp. 421-475.

GUO, F.F. and CUI, J.W., 2019. The Role of Tumor-Infiltrating B Cells in Tumor Immunity. *Journal of Oncology*, **2019**, pp. 2592419.

GUO, J., PARISE, R.A., JOSEPH, E., EGORIN, M.J., LAZO, J.S., PROCHOWNIK, E.V. and EISEMAN, J.L., 2009. Efficacy, pharmacokinetics, tissue distribution, and metabolism of the Myc-Max disruptor, 10058-F4 [Z,E]-5-[4-ethylbenzylidene]-2-thioxothiazolidin-4-one, in mice. *Cancer chemotherapy and pharmacology*, **63**(4), pp. 615-625.

GUPTA, G.P. and MASSAGUE, J., 2006. Cancer metastasis: building a framework. *Cell*, **127**(4), pp. 679-695.

HAENSE, N., ATMACA, A., PAULIGK, C., STEINMETZ, K., MARMÉ, F., HAAG, G.M., RIEGER, M., OTTMANN, O.G., RUF, P., LINDHOFER, H. and AL-BATRAN, S.E., 2016. A phase I trial of the trifunctional anti Her2 × anti CD3 antibody ertumaxomab in patients with advanced solidtumors. *BMC cancer*, **16**, pp. 420-016-2449-0.

HAHN, J.M., MCFARLAND, K.L., COMBS, K.A. and SUPP, D.M., 2016. Partial epithelial- mesenchymal transition in keloid scars: regulation of keloid keratinocyte gene expressionby transforming growth factor-beta1. *Burns & trauma*, **4**(1), pp. 30-016-0055-7.

HANAHAN, D. and WEINBERG, R.A., 2000. The hallmarks of cancer. *Cell*, **7**;100(1):57-70.

HANAHAN, D. and WEINBERG, R.A., 2011. Hallmarks of cancer: the next generation. *Cell*, **144**(5), pp. 646-674.

HARNER-FOREMAN, N., VADAKEKOLATHU, J., LAVERSIN, S.A., MATHIEU, M.G., REEDER, S., POCKLEY, A.G., REES, R.C. and BOOCOCK, D.J., 2017. A novel spontaneous model of epithelial-mesenchymal transition (EMT) using a primary prostate cancer derived cell linedemonstrating distinct stem-like characteristics. *Scientific reports*, **7**, pp. 40633.

HARRIS, D.T., HAGER, M.V., SMITH, S.N., CAI, Q., STONE, J.D., KRUGER, P., LEVER, M., DUSHEK, O., SCHMITT, T.M., GREENBERG, P.D. and KRANZ, D.M., 2018. Comparison of T Cell Activities Mediated by Human TCRs and CARs That Use the Same Recognition Domains. *Journal of immunology (Baltimore, Md.: 1950)*, **200**(3), pp. 1088-1100.

HART, I.R. and FIDLER, I.J., 1980. Cancer Invasion and Metastasis. *The Quarterly review ofbiology*, **55**(2), pp. 121-142.

HASSAN, M., WATARI, H., ABUALMAATY, A., OHBA, Y. and SAKURAGI, N., 2014. Apoptosis and Molecular Targeting Therapy in Cancer. *BioMed Research International*, **2014**, pp.150845.

HENG, W., MU, C.Y., CHEN, C., HUANG, J.A. and WANG, Z.Y., 2013. Endothelial cell proteinC receptor (EPCR) is expressed by lung carcinoma and correlated with clinical parameters. *Clinical laboratory*, **59**(3-4), pp. 375-380.

HERBERMAN, R.B., DJEU, J.Y., KAY, H.D., ORTALDO, J.R., RICCARDI, C., BONNARD, G.D., HOLDEN, H.T., FAGNANI, R., SANTONI, A. and PUCCETTI, P., 1979. Natural Killer Cells: Characteristics and Regulation of Activity. *Immunological reviews*, **44**(1), pp. 43-70.

HIGANO, C., BURCH, P., SMALL, E., SCHELLHAMMER, P., LEMON, R., VERJEE, S. and HERSHBERG, R., October 2005. *Immunotherapy (APC8015) for androgen independent prostate cancer (AIPC): final progression and survival data from a second Phase 3 trial. 13th European Cancer Conference. Paris.*, October 2005 October 2005.

HNASKO, R.M. and STANKER, L.H., 2015. Hybridoma Technology. *Methods in molecularbiology (Clifton, N.J.)*, **1318**, pp. 15-28.

HOBBS, G.A., DER, C.J. and ROSSMAN, K.L., 2016. RAS isoforms and mutations in cancer at a glance. *Journal of cell science*, **129**(7), pp. 1287-1292.

HODI, F.S., O'DAY, S.J., MCDERMOTT, D.F., WEBER, R.W., SOSMAN, J.A., HAANEN, J.B., GONZALEZ, R., ROBERT, C., SCHADENDORF, D., HASSEL, J.C., AKERLEY, W., VAN DEN EERTWEGH, ALFONS J.M., LUTZKY, J., LORIGAN, P., VAUBEL, J.M., LINETTE, G.P., HOGG, D., OTTENSMEIER, C.H., LEBBÉ, C., PESCHEL, C., QUIRT, I., CLARK, J.I., WOLCHOK, J.D., WEBER, J.S., TIAN, J., YELLIN, M.J., NICHOL, G.M., HOOS, A. and URBA, W.J., 2010. Improved Survival with Ipilimumab in Patients with Metastatic Melanoma. *N Engl J Med*, **363**(8), pp. 711-723.

HORNING, A.M., WANG, Y., LIN, C.K., LOUIE, A.D., JADHAV, R.R., HUNG, C.N., WANG, C.M., LIN, C.L., KIRMA, N.B., LISS, M.A., KUMAR, A.P., SUN, L., LIU, Z., CHAO, W.T., WANG, Q., JIN, V.X., CHEN, C.L., and HUANG, T. H., 2018. Single-Cell RNA-seq Reveals a Subpopulation of Prostate Cancer Cells with Enhanced Cell-Cycle-Related Transcription and Attenuated Androgen Response. *Cancer research*, **78**(4), pp. F853-864.

HOWE, L.R., WATANABE, O., LEONARD, J. and BROWN, A.M.C., 2003. Twist Is Up-Regulated in Response to Wnt1 and Inhibits Mouse Mammary Cell Differentiation. *Cancer Res*, **63**(8), pp. 1906.

HU, Z. and LI, J., 2010. Natural killer cells are crucial for the efficacy of Icon (factor VII/human IgG1 Fc) immunotherapy in human tongue cancer. *BMC Immunology*, **11**(1), pp. 49.

HUGGINS, C. and HODGES, C.V., 1941. Studies on Prostatic Cancer. I. The Effect of Castration, of Estrogen and of Androgen Injection on Serum Phosphatases in Metastatic Carcinoma of the Prostate. *Cancer research*, **1**(4), pp. 293-297.

HUGOSSON, J., ROOBOL, M.J., MÅNSSON, M., TAMMELA, T.L.J., ZAPPA, M., NELEN, V., KWIATKOWSKI, M., LUJAN, M., CARLSSON, S.V., TALALA, K.M., LILJA, H., DENIS, L.J., RECKER, F., PAEZ, A., PULITI, D., VILLERS, A., REBILLARD, X., KILPELÄINEN, T.P., STENMAN, U.H., GODTMAN, R.A., STINESEN KOLLBERG, K., MOSS, S.M., KUJALA, P., TAARI, K., HUBER, A., VAN DER KWAST, T., HEIJNSDIJK, E.A., BANGMA, C., DE KONING, H.J., SCHRÖDER, F.H., AUVINEN, A. and ERSPC INVESTIGATORS, 2019. A 16-yr Follow-up of the European Randomized study of Screening for Prostate Cancer. *European urology*, **76**(1), pp. 43-51.

ICHIKAWA, K., WATANABE MIYANO, S., MINOSHIMA, Y., MATSUI, J. and FUNAHASHI, Y., 2020. Activated FGF2 signaling pathway in tumor vasculature is essential for acquired resistance to anti-VEGF therapy. *Scientific Reports*, **10**(1), pp. 2939.

INDOVINA, P., MARCELLI, E., CASINI, N., RIZZO, V. and GIORDANO, A., 2013. Emerging roles of RB family: new defense mechanisms against tumor progression. *Journal of cellularphysiology*, **228**(3), pp. 525-535.

INTERNATIONAL AGENCY FOR RESEARCH ON CANCER, 2018-last update, GLOBOCAN 2018 accessed via Global Cancer Observatory. Available: <https://gco.iarc.fr/today/home>[March, 2020].

IRESON, C.R., ALAVIJEH, M.S., PALMER, A.M., FOWLER, E.R. and JONES, H.J., 2019. The role of mouse tumour models in the discovery and development of anticancer drugs. *British journal of cancer*, **121**(2), pp. 101-108.

IWAI, Y., ISHIDA, M., TANAKA, Y., OKAZAKI, T., HONJO, T. and MINATO, N., 2002. Involvement of PD-L1 on tumor cells in the escape from host immune system and tumorimmunotherapy by PD-L1 blockade. *Proceedings of the National Academy of Sciences of the United States of America*, **99**(19), pp. 12293-12297.

IWANO, M., PLIETH, D., DANOFF, T.M., XUE, C., OKADA, H. and NEILSON, E.G., 2002. Evidence that fibroblasts derive from epithelium during tissue fibrosis. *The Journal of clinical investigation*, **110**(3), pp. 341-350.

JAIN, N., NGUYEN, H., CHAMBERS, C. and KANG, J., 2010. Dual function of CTLA-4 in regulatory T cells and conventional T cells to prevent multiorgan autoimmunity. *Proceedings of the National Academy of Sciences of the United States of America*, **107**(4), pp. 1524-1528.

JAIN, R.K., 2005. Normalization of Tumor Vasculature: An Emerging Concept inAntiangiogenic Therapy. *Science*, **307**(5706), pp. 58-62.

JEGGO, P.A. and LÖBRICH, M., 2007. DNA double-strand breaks: their cellular and clinical impact? *Oncogene*, **26**(56), pp. 7717-7719.

JIE, X.X., ZHANG, X.Y. and XU, C.J., 2017. Epithelial-to-mesenchymal transition, circulatingtumor cells and cancer metastasis: Mechanisms and clinical applications. *Oncotarget*, **8**(46), pp. 81558-81571.

JIN, H., YU, Y., ZHANG, T., ZHOU, X., ZHOU, J., JIA, L., WU, Y., ZHOU, B.P. and FENG, Y., 2010. Snail is critical for tumor growth and metastasis of ovarian carcinoma. *Internationaljournal of cancer*, **126**(9), pp. 2102-2111.

JING, X., YANG, F., SHAO, C., WEI, K., XIE, M., SHEN, H. and SHU, Y., 2019. Role of hypoxia in cancer therapy by regulating the tumor microenvironment. *Molecular Cancer*, **18**(1), pp.157.

JOHNSON, G. and WU, T.T., 2000. Kabat database and its applications: 30 years after the first variability plot. *Nucleic acids research*, **28**(1), pp. 214-218.

JOLLY, M.K., MANI, S.A. and LEVINE, H., 2018. Hybrid epithelial/mesenchymal phenotype(s): The 'fittest' for metastasis? *Biochimica et biophysica acta.Reviews on cancer*, **1870**(2), pp. 151-157.

JONES, P.T., DEAR, P.H., FOOTE, J., NEUBERGER, M.S. and WINTER, G., 1986. Replacing the complementarity-determining regions in a human antibody with those from a mouse. *Nature*, **321**(6069), pp. 522-525.

JOUBERT, N., BECK, A., DUMONTET, C., and DENEVAULT-SABOURIN, C., 2020. Antibody-Drug Conjugates: The Last Decade. *Pharmaceuticals (Basel, Switzerland)*, **13**(9), pp. 245.

JOYCE, J.A. and POLLARD, J.W., 2009. Microenvironmental regulation of metastasis. *Nature reviews.Cancer*, **9**(4), pp. 239-252.

JUNE, C.H., RIDDELL, S.R. and SCHUMACHER, T.N., 2015. Adoptive cellular therapy: a race to the finish line. *Science translational medicine*, **7**(280), pp. 280ps7.

KALLURI, R. and WEINBERG, R.A., 2009. The basics of epithelial-mesenchymal transition. *The Journal of clinical investigation*, **119**(6), pp. 1420-1428.

KALLURI, R. and ZEISBERG, M., 2006. Fibroblasts in cancer. *Nature Reviews Cancer*, **6**(5), pp.392-401.

KAMEN, L., MYNENI, S., LANGSDORF, C., KHO, E., ORDONIA, B., THAKURTA, T., ZHENG, K., SONG, A. and CHUNG, S., 2019. A novel method for determining antibody-dependent cellular phagocytosis. *Journal of immunological methods*, **468**, pp. 55-60.

KANTOFF, P.W., HIGANO, C.S., SHORE, N.D., BERGER, E.R., SMALL, E.J., PENSON, D.F., REDFERN, C.H., FERRARI, A.C., DREICER, R., SIMS, R.B., XU, Y., FROHLICH, M.W., SCHELLHAMMER, P.F. and IMPACT STUDY INVESTIGATORS, 2010. Sipuleucel-T immunotherapy for castration-resistant prostate cancer. *The New England journal of medicine*, **363**(5), pp. 411-422.

KARANTZA, V., 2011. Keratins in health and cancer: more than mere epithelial cell markers. *Oncogene*, **30**(2), pp. 127-138.

KATSUNO, Y., LAMOUILLE, S. and DERYNCK, R., 2013. TGF- β signaling and epithelial-mesenchymal transition in cancer progression. *Current opinion in oncology*, **25**(1), pp. 76-84.

KENNEDY, A.D., BEUM, P.V., SOLGA, M.D., DILILLO, D.J., LINDORFER, M.A., HESS, C.E., DENSMORE, J.J., WILLIAMS, M.E. and TAYLOR, R.P., 2004. Rituximab infusion promotes rapid complement depletion and acute CD20 loss in chronic lymphocytic leukemia. *Journal of immunology (Baltimore, Md.: 1950)*, **172**(5), pp. 3280—3288.

KESHAVA, S., SAHOO, S., TUCKER, T.A., IDELL, S., RAO, L.V. and PENDURTHI, U.R., 2013. Endothelial cell protein C receptor opposes mesothelioma growth driven by tissue factor. *Cancer research*, **73**(13), pp. 3963-3973.

KESHAVA, S., RAO, L.V.M. and PENDURTHI, U.R., 2015. Endothelial Cell Protein C Receptor Promotes Apoptosis in Malignant Pleural Mesothelioma Cells. *Blood*, **126**(23), pp. 2241- 2241.

KESSEN BROCK, K., PLAKS, V. and WERB, Z., 2010. Matrix metalloproteinases: regulators of the tumor microenvironment. *Cell*, **141**(1), pp. 52-67.

KHALILI, N., KESHAVARZ-FATHI, M., SHAHKARAMI, S., HIRBOD-MOBARAKEH, A. and REZAEI, N., 2019. Passive-specific immunotherapy with monoclonal antibodies for prostate cancer: A systematic review. *Journal of oncology pharmacy practice: official publication of the International Society of Oncology Pharmacy Practitioners*, **25**(4), pp. 903-917.

KILPELÄINEN, T.P., TAMMELA, T.L.J., ROOBOL, M., HUGOSSON, J., CIATTO, S., NELEN, V., MOSS, S., MÄÄTTÄNEN, L. and AUVINEN, A., 2011. False-positive screening results in the European randomized study of screening for prostate cancer. *European journal of cancer*, **47** 18, 2698-705.

KIM, Y.N., KOO, K.H., SUNG, J.Y., YUN, U.J. and KIM, H., 2012. Anoikis resistance: an essential prerequisite for tumor metastasis. *International journal of cell biology*, **2012**, pp.306879.

KIM, Y.R., YOO, J.K., JEONG, C.W. and CHOI, J.W., 2018. Selective killing of circulating tumor cells prevents metastasis and extends survival. *Journal of Hematology & Oncology*, **11**(1),pp. 114.

KIM, Y., AHN, Y., JUNG, J., LEE, Y., LEE, J. and KANG, J.L., 2019. Programming of macrophages by UV-irradiated apoptotic cancer cells inhibits cancer progression and lung metastasis. *Cellular & Molecular Immunology*, **16**(11), pp. 851-867.

KLEFFEL, S., POSCH, C., BARTHEL, S.R., MUELLER, H., SCHLAPBACH, C., GUENOVA, E., ELCO,C.P., LEE, N., JUNEJA, V.R., ZHAN, Q., LIAN, C.G., THOMI, R., HOETZENECKER, W., COZZIO, A., DUMMER, R., MIHM, M.C., Jr, FLAHERTY, K.T., FRANK, M.H., MURPHY, G.F., SHARPE, A.H., KUPPER, T.S. and SCHATTEN, T., 2015. Melanoma Cell-Intrinsic PD-1 Receptor Functions Promote Tumor Growth. *Cell*, **162**(6), pp. 1242-1256.

KLOSS, C.C., LEE, J., ZHANG, A., CHEN, F., MELENHORST, J.J., LACEY, S.F., MAUS, M.V., FRAIETTA, J.A., ZHAO, Y. and JUNE, C.H., 2018. Dominant-Negative TGF- β Receptor Enhances PSMA-Targeted Human CAR T Cell Proliferation And Augments Prostate Cancer Eradication. *Molecular Therapy*, **26**(7), pp. 1855-1866.

KÖHLER, G. and MILSTEIN, C., 1975. Continuous cultures of fused cells secreting antibody of predefined specificity. *Nature*, **256**(5517), pp. 495-497.

KORTLEVER, R.M., SODIR, N.M., WILSON, C.H., BURKHART, D.L., PELLEGRINET, L., BROWN SWIGART, L., LITTLEWOOD, T.D. and EVAN, G.I., 2017. Myc Cooperates with Ras by Programming Inflammation and Immune Suppression. *Cell*, **171**(6), pp. 1301-1315.e14.

KRIZBAI, I.A., GASPARICS, A., NAGYOSZI, P., FAZAKAS, C., MOLNAR, J., WILHELM, I., BENCS, R., ROSIVALL, L. and SEBE, A., 2015. Endothelial-mesenchymal transition of brain endothelial cells: possible role during metastatic extravasation. *PLoS One*, **10**(3), pp.e0119655.

KUNKEL, H.G., SLATER, R.J. and GOOD, R.A., 1951. Relation between Certain Myeloma Proteins and Normal Gamma Globulin. *Proceedings of the Society for Experimental Biology and Medicine*, **76**(1), pp. 190-193.

KWON, E.D., DRAKE, C.G., SCHER, H.I., FIZAZI, K., BOSSI, A., VAN DEN EERTWEGH, A.J., KRAINER, M., HOUDE, N., SANTOS, R., MAHAMMEDI, H., NG, S., MAIO, M., FRANKE, F.A., SUNDAR, S., AGARWAL, N., BERGMAN, A.M., CIULEANU, T.E., KORBENFELD, E., SENGELØV, L., HANSEN, S., LOGOTHETIS, C., BEER, T.M., MCHENRY, M.B., GAGNIER, P., LIU, D., GERRITSEN, W.R. and CA184-043, I., 2014. Ipilimumab versus placebo after radiotherapy in patients with metastatic castration-resistant prostate cancer that had progressed after docetaxel chemotherapy (CA184-043): a multicentre, randomised, double-blind, phase 3 trial. *The Lancet. Oncology*, **15**(7), pp. 700-712.

KWON, E.D., FOSTER, B.A., HURWITZ, A.A., MADIAS, C., ALLISON, J.P., GREENBERG, N.M. and BURG, M.B., 1999. Elimination of residual metastatic prostate cancer after surgery and adjuvant cytotoxic T lymphocyte-associated antigen 4 (CTLA-4) blockade immunotherapy. *Proceedings of the National Academy of Sciences of the United States of America*, **96**(26), pp. 15074-15079.

LAZEBNIK, Y., 2010. What are the hallmarks of cancer? *Nature Reviews Cancer*, **10**(4), pp. 232-233.

LEE, C. and KANTOFF, P., 2019. Treatment of Metastatic Prostate Cancer in 2018. *JAMA Oncology*, **5**(2), pp. 263-264.

LEE, K.J., CHOW, V., WEISSMAN, A., TULPULE, S., ALDOSS, I. and AKHTARI, M., 2016. Clinical use of blinatumomab for B-cell acute lymphoblastic leukemia in adults. *Therapeutics and clinical risk management*, **12**, pp. 1301-1310.

- LEE, S. and MARGOLIN, K., 2011. Cytokines in cancer immunotherapy. *Cancers*, **3**(4), pp.3856-3893.
- LEE, Y.C., CHENG, C.J., BILEN, M.A., LU, J.F., SATCHER, R.L., YU-LEE, L.Y., GALICK, G.E., MAITY, S.N. and LIN, S.H., 2011. BMP4 promotes prostate tumor growth in bone through osteogenesis. *Cancer research*, **71**(15), pp. 5194-5203.
- LI, C., CHEN, J., HO, Y., HSU, W., WU, L., LAN, H., HSU, D.S., TAI, S., CHANG, Y. and YANG, M., 2019. Snail-induced claudin-11 prompts collective migration for tumour progression. *Nature cell biology*, **21**(2), pp. 251-262.
- LIAO, T.T. and YANG, M.H., 2020. Hybrid Epithelial/Mesenchymal State in Cancer Metastasis: Clinical Significance and Regulatory Mechanisms. *Cells*, **9**(3), pp. 623. doi:10.3390/cells9030623.
- LIAW, P.C., MATHER, T., OGANESEYAN, N., FERRELL, G.L. and ESMON, C.T., 2001. Identification of the protein C/activated protein C binding sites on the endothelial cellprotein C receptor. Implications for a novel mode of ligand recognition by a major histocompatibility complex class 1-type receptor. *The Journal of biological chemistry*, **276**(11), pp. 8364-8370.
- LILIAN, R.T., 2018. Display Technologies for the Selection of Monoclonal Antibodies for Clinical Use. In: MARIANA LOPES DOS, ed, *Antibody Engineering*. Rijeka: IntechOpen, pp.Ch. 3.
- LIU, C.Y., LIN, H.H., TANG, M.J. and WANG, Y.K., 2015. Vimentin contributes to epithelial-mesenchymal transition cancer cell mechanics by mediating cytoskeletal organization and focal adhesion maturation. *Oncotarget*, **6**(18), pp. 15966-15983.
- LIU, J., KAUR, G., ZHAWAR, V. K., ZIMONJIC, D. B., POPESCU, N. C., KANDPAL, R. P., and ATHWAL, R. S., 2009. Role of SV40 integration site at chromosomal interval 1q21.1 in immortalized CRL2504 cells. *Cancer research*, **69**(19), pp. 7819–7825.
- LIU, X., YUN, F., SHI, L., LI, Z.H., LUO, N.R. and JIA, Y.F., 2015. Roles of Signaling Pathways in the Epithelial-Mesenchymal Transition in Cancer. *Asian Pacific journal of cancer prevention : APJCP*, **16**(15), pp. 6201-6206.
- LIU, Z.C., CHEN, X.H., SONG, H.X., WANG, H.S., ZHANG, G., WANG, H., CHEN, D.Y., FANG, R., LIU, H., CAI, S.H. and DU, J., 2014. Snail regulated by PKC/GSK-3beta pathway is crucial forEGF-induced epithelial-mesenchymal transition (EMT) of cancer cells. *Cell and tissue research*, **358**(2), pp. 491-502.
- LOH, C.Y., CHAI, J.Y., TANG, T.F., WONG, W.F., SETHI, G., SHANMUGAM, M.K., CHONG, P.P. and LOOI, C.Y., 2019. The E-Cadherin and N-Cadherin Switch in Epithelial-to-Mesenchymal Transition: Signaling, Therapeutic Implications, and Challenges. *Cells*, **8**(10), pp. 1118.
- LONGO, D.L., 2010. New therapies for castration-resistant prostate cancer. *The New England journal of medicine*, **363**(5), pp. 479-481.
- LUGANO, R., RAMACHANDRAN, M. and DIMBERG, A., 2020. Tumor angiogenesis: causes, consequences, challenges and opportunities. *Cellular and molecular life sciences : CMLS*, **77**(9), pp. 1745-1770.

LUQUE-CABAL, M., GARCÍA-TEIJIDO, P., FERNÁNDEZ-PÉREZ, Y., SÁNCHEZ-LORENZO, L. and PALACIO-VÁZQUEZ, I., 2016. Mechanisms Behind the Resistance to Trastuzumab in HER2-Amplified Breast Cancer and Strategies to Overcome It. *Clinical Medicine Insights Oncology*, **10**(Suppl 1), pp. 21-30.

LV, X., LI, J., ZHANG, C., HU, T., LI, S., HE, S., YAN, H., TAN, Y., LEI, M., WEN, M. and ZUO, J., 2017. The role of hypoxia-inducible factors in tumor angiogenesis and cell metabolism. *Genes & diseases*, **4**(1), pp. 19–24.

MACCARTHY-MORROGH, L. and MARTIN, P., 2020. The hallmarks of cancer are also the hallmarks of wound healing. *Science Signaling*, **13**(648), pp. eaay8690.

MAIA, M.C. and HANSEN, A.R., 2017. A comprehensive review of immunotherapies in prostate cancer. *Critical reviews in oncology/hematology*, **113**, pp. 292-303.

MAMIDI, S., CINCI, M., HASMANN, M., FEHRING, V. and KIRSCHFINK, M., 2013. Lipoplex mediated silencing of membrane regulators (CD46, CD55 and CD59) enhances complement-dependent anti-tumor activity of trastuzumab and pertuzumab. *Molecular Oncology*, **7**(3), pp. 580-594.

MANI, S.A., GUO, W., LIAO, M.J., EATON, E.N., AYYANAN, A., ZHOU, A.Y., BROOKS, M., REINHARD, F., ZHANG, C.C., SHIPITSIN, M., CAMPBELL, L.L., POLYAK, K., BRISKEN, C., YANG, J. and WEINBERG, R.A., 2008. The epithelial-mesenchymal transition generates cells with properties of stem cells. *Cell*, **133**(4), pp. 704-715.

MANJUNATH, N., WU, H., SUBRAMANYA, S. and SHANKAR, P., 2009. Lentiviral delivery of short hairpin RNAs. *Advanced Drug Delivery Reviews*, **61**(9), pp. 732-745.

MANTOVANI, A., ALLAVENA, P., SICA, A. and BALKWILL, F., 2008. Cancer-related inflammation. *Nature*, **454**(7203), pp. 436-444.

MARTIN, R.M., DONOVAN, J.L., TURNER, E.L., METCALFE, C., YOUNG, G.J., WALSH, E.I., LANE, J.A., NOBLE, S., OLIVER, S.E., EVANS, S., STERNE, J.A.C., HOLDING, P., BEN-SHLOMO, Y., BRINDLE, P., WILLIAMS, N.J., HILL, E.M., NG, S.Y., TOOLE, J., TAZEWELL, M.K., HUGHES, L.J., DAVIES, C.F., THORN, J.C., DOWN, E., DAVEY SMITH, G., NEAL, D.E., HAMDY, F.C. for the CAP TRIAL GROUP, 2018. Effect of a Low-Intensity PSA-Based Screening Intervention on Prostate Cancer Mortality: The CAP Randomized Clinical Trial. *JAMA*, **319**(9), pp. 883-895.

MATEO, J., CARREIRA, S., SANDHU, S., MIRANDA, S., MOSSOP, H., PEREZ-LOPEZ, R., NAVA RODRIGUES, D., ROBINSON, D., OMLIN, A., TUNARIU, N., BOYSEN, G., PORTA, N., FLOHR, P., GILLMAN, A., FIGUEIREDO, I., PAULDING, C., SEED, G., JAIN, S., RALPH, C., PROTHEROE, A., HUSSAIN, S., JONES, R., ELLIOTT, T., MCGOVERN, U., BIANCHINI, D., GOODALL, J., ZAFEIRIOU, Z., WILLIAMSON, C.T., FERRALDESCHI, R., RIISNAES, R., EBBS, B., FOWLER, G., RODA, D., YUAN, W., WU, Y.M., CAO, X., BROUH, R., PEMBERTON, H., A'HERN, R., SWAIN, A., KUNJU, L.P., EELES, R., ATTARD, G., LORD, C.J., ASHWORTH, A., RUBIN, M.A., KNUDSEN, K.E., FENG, F.Y., CHINNAIYAN, A.M., HALL, E. and DE BONO, J.S., 2015. DNA-Repair Defects and Olaparib in Metastatic Prostate Cancer. *The New England journal of medicine*, **373**(18), pp. 1697-1708.

MATUSZAK, E.A. and KYPRIANOU, N., 2011. Androgen regulation of epithelial-mesenchymal transition in prostate tumorigenesis. *Expert review of endocrinology & metabolism*, **6**(3), pp. 469–482.

MAUDE, S.L., LAETSCH, T.W., BUECHNER, J., RIVES, S., BOYER, M., BITTENCOURT, H., BADER, P., VERNERIS, M.R., STEFANSKI, H.E., MYERS, G.D., QAYED, M., DE MOERLOOSE, B., HIRAMATSU, H., SCHLIS, K., DAVIS, K.L., MARTIN, P.L., NEMECEK, E.R., YANIK, G.A., PETERS, C., BARUCHEL, A., BOISSEL, N., MECHINAUD, F., BALDUZZI, A., KRUEGER, J., JUNE, C.H., LEVINE, B.L., WOOD, P., TARAN, T., LEUNG, M., MUELLER, K.T., ZHANG, Y., SEN, K., LEBWOHL, D., PULSIPHER, M.A. and GRUPP, S.A., 2018. Tisagenlecleucel in Children and Young Adults with B-Cell Lymphoblastic Leukemia. *N Engl J Med*, **378**(5), pp. 439-448.

MELLMAN, I., COUKOS, G. and DRANOFF, G., 2011. Cancer immunotherapy comes of age. *Nature*, **480**(7378), pp. 480-489.

MELLOR, A.L. and MUNN, D.H., 2008. Creating immune privilege: active local suppression that benefits friends, but protects foes. *Nature Reviews Immunology*, **8**(1), pp. 74-80.

MENSCHIKOWSKI, M., HAGELGANS, A., TIEBEL, O., KLINSMANN, L., EISENHOFER, G. and SIEGERT, G., 2011. Expression and shedding of endothelial protein C receptor in prostate cancer cells. *Cancer Cell International*, **11**(1), pp. 4.

MIAO, L., YANG, L., LI, R., RODRIGUES, D. N., CRESPO, M., HSIEH, J. T., TILLEY, W. D., DE BONO, J., SELTH, L. A., & RAJ, G. V., 2017. Disrupting Androgen Receptor Signaling Induces Snail-Mediated Epithelial-Mesenchymal Plasticity in Prostate Cancer. *Cancer research*, **77**(11), pp. 3101-3112.

MICALIZZI, D.S., MAHESWARAN, S. and HABER, D.A., 2017. A conduit to metastasis: circulating tumor cell biology. *Genes & development*, **31**(18), pp. 1827-1840.

MITRUGNO, A., MORAN, N. and METHAROM, P., 2015. Platelets — Allies of Tumour Cells. The Non-Thrombotic Role of Platelets in Health and Disease. InTech.

MIYOSHI, A., KITAJIMA, Y., SUMI, K., SATO, K., HAGIWARA, A., KOGA, Y. and MIYAZAKI, K., 2004. Snail and SIP1 increase cancer invasion by upregulating MMP family in hepatocellular carcinoma cells. *British journal of cancer*, **90**(6), pp. 1265-1273.

MOHAN RAO, L.V., ESMON, C.T. and PENDURTHI, U.R., 2014. Endothelial cell protein C receptor: a multiliganded and multifunctional receptor. *Blood*, **124**(10), pp. 1553-1562.

MONGROO, P.S. and RUSTGI, A.K., 2010. The role of the miR-200 family in epithelial-mesenchymal transition. *Cancer biology & therapy*, **10**(3), pp. 219-222.

MONTANARI, M., ROSSETTI, S., CAVALIERE, C., D'ANIELLO, C., MALZONE, M.G., VANACORE, D., DI FRANCO, R., LA MANTIA, E., IOVANE, G., PISCITELLI, R., MUSCARIELLO, R., BERRETTA, M., PERDONÀ, S., MUTO, P., BOTTI, G., BIANCHI, A.A.M., VENEZIANI, B.M. and FACCHINI, G., 2017. Epithelial-mesenchymal transition in prostate cancer: an overview. *Oncotarget*, **8**(21), pp. 35376-35389.

MONTAÑO, R.F. and MORRISON, S.L., 2002. Influence of the Isotype of the Light Chain on the Properties of IgG. *The Journal of Immunology*, **168**(1), pp. 224-231.

MONTERAN, L. and EREZ, N., 2019. The Dark Side of Fibroblasts: Cancer-Associated Fibroblasts as Mediators of Immunosuppression in the Tumor Microenvironment. *Frontiers in immunology*, **10**, pp. 1835.

MOREL, A., LIÈVRE, M., THOMAS, C., HINKAL, G., ANSIEAU, S. and PUISIEUX, A., 2008. Generation of Breast Cancer Stem Cells through Epithelial-Mesenchymal Transition. *PLOS ONE*, **3**(8), pp. e2888.

MORRISON, S.L., JOHNSON, M.J., HERZENBERG, L.A. and OI, V.T., 1984. Chimeric human antibody molecules: mouse antigen-binding domains with human constant region domains. *Proceedings of the National Academy of Sciences of the United States of America*, **81**(21), pp. 6851-6855.

MROZIK, K.M., BLASCHUK, O.W., CHEONG, C.M., ZANNETTINO, A.C.W. and VANDYKE, K., 2018. N-cadherin in cancer metastasis, its emerging role in haematological malignancies and potential as a therapeutic target in cancer. *BMC Cancer*, **18**(1), pp. 939.

MUNIR, R., LISEC, J., SWINNEN, J.V. and ZAIDI, N., 2019. Lipid metabolism in cancer cells under metabolic stress. *British journal of cancer*, **120**(12), pp. 1090-1098.

MUNTASELL, A., CABO, M., SERVITJA, S., TUSQUETS, I., MARTÍNEZ-GARCÍA, M., ROVIRA, A., ROJO, F., ALBANEZ, J. and LÓPEZ-BOTET, M., 2017. Interplay between Natural Killer Cells and Anti-HER2 Antibodies: Perspectives for Breast Cancer Immunotherapy. *Frontiers in immunology*, **8**, pp. 1544.

NATSUME, A., NIWA, R. and SATOH, M., 2009. Improving effector functions of antibodies for cancer treatment: Enhancing ADCC and CDC. *Drug design, development and therapy*, **3**, pp. 7-16.

NAYAK, R.C., SEN, P., GHOSH, S., GOPALAKRISHNAN, R., ESMON, C.T., PENDURTHI, U.R. and RAO, L.V.M., 2009. Endothelial cell protein C receptor cellular localization and trafficking: potential functional implications. *Blood*, **114**(9), pp. 1974-1986.

NAYYAR, G., CHU, Y. and CAIRO, M.S., 2019. Overcoming Resistance to Natural Killer Cell-Based Immunotherapies for Solid Tumors. *Frontiers in oncology*, **9**, pp. 51.

NEELAPU, S.S., LOCKE, F.L., BARTLETT, N.L., LEKAKIS, L.J., MIKLOS, D.B., JACOBSON, C.A., BRAUNSCHWEIG, I., OLUWOLE, O.O., SIDDIQI, T., LIN, Y., TIMMERMAN, J.M., STIFF, P.J., FRIEDBERG, J.W., FLINN, I.W., GOY, A., HILL, B.T., SMITH, M.R., DEOL, A., FAROOQ, U., MCSWEENEY, P., MUÑOZ, J., AVIVI, I., CASTRO, J.E., WESTIN, J.R., CHAVEZ, J.C., GHOBADI, A., KOMANDURI, K.V., LEVY, R., JACOBSEN, E.D., WITZIG, T.E., REAGAN, P., BOT, A., ROSSI, J., NAVALE, L., JIANG, Y., AYCOCK, J., ELIAS, M., CHANG, D., WIEZOREK, J. and GO, W.Y., 2017. Axicabtagene Ciloleucel CAR T-Cell Therapy in Refractory Large B-Cell Lymphoma. *NEngl J Med*, **377**(26), pp. 2531-2544.

NELSON, A.L., 2010. Antibody fragments: hope and hype. *mAbs*, **2**(1), pp. 77-83.

NELSON, C.M., KHAN, D., BISSELL, M.J. and RADISKY, D.C., 2008. Change in cell shape is required for matrix metalloproteinase-induced epithelial-mesenchymal transition of mammary epithelial cells. *Journal of cellular biochemistry*, **105**(1), pp. 25-33.

NGUYEN, T. and MÈGE, R.M., 2016. N-Cadherin and Fibroblast Growth Factor Receptors crosstalk in the control of developmental and cancer cell migrations. *European journal of cell biology*, **95**(11), pp. 415-426.

NICHOLSON, L.T. and FONG, L., 2020. Immune Checkpoint Inhibition in Prostate Cancer. *Trends in Cancer*, **6**(3), pp. 174-177.

NIMMERJAHN, F. and RAVETCH, J.V., 2006. Fc gamma receptors: old friends and new family members. *Immunity*, **24**(1), pp. 19-28.

OCHOA, M.C., MINUTE, L., RODRIGUEZ, I., GARASA, S., PEREZ-RUIZ, E., INOGÉS, S., MELERO, I. and BERRAONDO, P., 2017. Antibody-dependent cell cytotoxicity: immunotherapy strategies enhancing effector NK cells. *Immunology and cell biology*, **95**(4), pp. 347-355.

OGANESYAN, V., OGANESYAN, N., TERZYAN, S., QU, D., DAUTER, Z., ESMON, N.L. and ESMON, C.T., 2002. The crystal structure of the endothelial protein C receptor and a boundphospholipid. *The Journal of biological chemistry*, **277**(28), pp. 24851-24854.

OLMEDA, D., MONTES, A., MORENO-BUENO, G., FLORES, J.M., PORTILLO, F. and CANO, A., 2008. Snai1 and Snai2 collaborate on tumor growth and metastasis properties of mouseskin carcinoma cell lines. *Oncogene*, **27**, pp. 4690.

OMASITS, U., AHRENS, C.H., MÜLLER, S. and WOLLSCHEID, B., 2014. Protter: interactive protein feature visualization and integration with experimental proteomic data. *Bioinformatics*, **30**(6), pp. 884-886.

PALUMBO, J.S. and DEGEN, J.L., 2007. Mechanisms linking tumor cell-associatedprocoagulant function to tumor metastasis. *Seminars in thrombosis and hemostasis*, **34**(2), pp. 154–160.

PANG, L., LI, J.F., SU, L., ZANG, M., FAN, Z., YU, B., WU, X., LI, C., YAN, M., ZHU, Z.G. and LIU, B., 2018. ALEX1, a novel tumor suppressor gene, inhibits gastric cancer metastasis via thePAR-1/Rho GTPase signaling pathway. *Journal of gastroenterology*, **53**(1), pp. 71-83.

PAOLI, P., GIANNONI, E. and CHIARUGI, P., 2013. Anoikis molecular pathways and its rolein cancer progression. *Biochimica et biophysica acta*, **1833**(12), pp. 3481-3498.

PARK, S.M., GAUR, A.B., LENGYEL, E. and PETER, M.E., 2008. The miR-200 family determinesthe epithelial phenotype of cancer cells by targeting the E-cadherin repressors ZEB1 and ZEB2. *Genes & development*, **22**(7), pp. 894-907.

PARRAY, H.A., SHUKLA, S., SAMAL, S., SHRIVASTAVA, T., AHMED, S., SHARMA, C. and KUMAR, R., 2020. Hybridoma technology a versatile method for isolation of monoclonal antibodies, its applicability across species, limitations, advancement and future perspectives. *International immunopharmacology*, **85**, pp. 106639.

PASTUSHENKO, I. and BLANPAIN, C., 2019. EMT Transition States during TumorProgression and Metastasis. *Trends in cell biology*, **29**(3), pp. 212-226.

PATEL, D., GUO, X., NG, S., MELCHIOR, M., BALDERES, P., BURTRUM, D., PERSAUD, K., LUNA, X., LUDWIG, D.L. and KANG, X., 2010. IgG isotype, glycosylation, and EGFR expression determine the induction of antibody-dependent cellular cytotoxicity in vitro bycetuximab. *Human antibodies*, **19**(4), pp. 89-99.

PEINADO, H., OLMEDA, D. and CANO, A., 2007. Snail, Zeb and bHLH factors in tumour progression: an alliance against the epithelial phenotype? *Nature Reviews Cancer*, **7**, pp.415.

PELED, J.U., KUANG, F.L., IGLESIAS-USSEL, M., ROA, S., KALIS, S.L., GOODMAN, M.F. and SCHARRF, M.D., 2008. The Biochemistry of Somatic Hypermutation. *Annual Review of Immunology*, **26**(1), pp. 481-511.

PENDURTHI, U.R. and RAO, L.V.M., 2018. Endothelial cell protein C receptor-dependentsignaling. *Current opinion in hematatology*, **25**(3), pp. 219-226.

PEREIRA, N.A., CHAN, K.F., LIN, P.C. and SONG, Z., 2018. The "less-is-more" in therapeuticantibodies: Afucosylated anti-cancer antibodies with enhanced antibody-dependent cellular cytotoxicity. *mAbs*, **10**(5), pp. 693-711.

PERLMUTTER, M.A. and LEPORE, H., 2007. Androgen deprivation therapy in the treatment of advanced prostate cancer. *Reviews in urology*, **9 Suppl 1**, pp. S3-S8.

PERURENA, N., ZANDUETA, C., MARTÁNEZ-CANARIAS, S., MORENO, H., VICENT, S., ALMEIDA, A.S., GURUCEAGA, E., GOMIS, R.R., SANTISTEBAN, M., EGEBLAD, M., HERMIDA, J. and LECANDA, F., 2017. EPCR promotes breast cancer progression by altering SPOCK1/testican 1-mediated 3D growth. *Journal of hematology & oncology*, **10**(1), pp.23-017-0399-x.

PETRICEVIC, B., LAENGLE, J., SINGER, J., SACHET, M., FAZEKAS, J., STEGER, G., BARTSCH, R., JENSEN-JAROLIM, E. and BERGMANN, M., 2013. Trastuzumab mediates antibody-dependent cell-mediated cytotoxicity and phagocytosis to the same extent in both adjuvant and metastatic HER2/neu breast cancer patients. *Journal of translational medicine*, **11**, pp. 307-5876-11-307.

PETRYLAK, D.P., TANGEN, C.M., HUSSAIN, M.H., LARA, P.N., Jr, JONES, J.A., TAPLIN, M.E., BURCH, P.A., BERRY, D., MOINPOUR, C., KOHLI, M., BENSON, M.C., SMALL, E.J., RAGHAVAN, D. and CRAWFORD, E.D., 2004. Docetaxel and estramustine compared with mitoxantrone and prednisone for advanced refractory prostate cancer. *The New England journal of medicine*, **351**(15), pp. 1513-1520.

PIERPONT, T.M., LIMPER, C.B. and RICHARDS, K.L., 2018. Past, Present, and Future of Rituximab—The World's First Oncology Monoclonal Antibody Therapy. *Frontiers in Oncology*, **8**, pp. 163.

PLACEK, B.J., HARRISON, L.N., VILLERS, B.M. and GLOSS, L.M., 2005. The H2A.Z/H2B dimer is unstable compared to the dimer containing the major H2A isoform. *Protein science: a publication of the Protein Society*, **14**(2), pp. 514-522.

PLATEL, V., FAURE, S., CORRE, I. and CLERE, N., 2019. Endothelial-to-Mesenchymal Transition (EndoMT): Roles in Tumorigenesis, Metastatic Extravasation and Therapy Resistance. *Journal of Oncology*, **2019**, pp. 8361945.

PLESCA, I., TUNGER, A., MÜLLER, L., WEHNER, R., LAI, X., GRIMM, M., RUTELLA, S., BACHMANN, M. and SCHMITZ, M., 2020. Characteristics of Tumor-Infiltrating Lymphocytes Prior to and During Immune Checkpoint Inhibitor Therapy. *Frontiers in Immunology*, **11**, pp. 364.

POLAKIS, P., 2012. Wnt signaling in cancer. *Cold Spring Harbor perspectives in biology*, **4**(5), pp. a008052.

PORTER, D.L., HWANG, W.T., FREY, N.V., LACEY, S.F., SHAW, P.A., LOREN, A.W., BAGG, A., MARCUCCI, K.T., SHEN, A., GONZALEZ, V., AMBROSE, D., GRUPP, S.A., CHEW, A., ZHENG, Z., MILONE, M.C., LEVINE, B.L., MELENHORST, J.J. and JUNE, C.H., 2015. Chimeric antigen receptor T cells persist and induce sustained remissions in relapsed refractory chronic lymphocytic leukemia. *Science translational medicine*, **7**(303), pp. 303ra139.

PREITHNER, S., ELM, S., LIPPOLD, S., LOCHER, M., WOLF, A., DA SILVA, A.J., BAEUERLE, P.A. and PRANG, N.S., 2006. High concentrations of therapeutic IgG1 antibodies are needed to compensate for inhibition of antibody-dependent cellular cytotoxicity by excess endogenous immunoglobulin G. *Molecular immunology*, **43**(8), pp. 1183-1193.

PROSTATE CANCER UK, , Cancer Mortality Statistics. Available:
<https://www.cancerresearchuk.org/health-professional/cancer-statistics/mortality#:~:text=There%20are%20around%20165%2C000%20cancer,88%2C900%20cancer%20deaths%20in%202017>. [January, 2020].

PSAILA, B. and LYDEN, D., 2009. The metastatic niche: adapting the foreign soil. *Nature reviews.Cancer*, **9**(4), pp. 285-293.

PYLAYEVA-GUPTA, Y., GRABOCKA, E. and BAR-SAGI, D., 2011. RAS oncogenes: weaving a tumorigenic web. *Nature reviews. Cancer*, **11**(11), pp. 761-774.

QUINN, D.I., SHORE, N.D., EGAWA, S., GERRITSEN, W.R. and FIZAZI, K., 2015. Immunotherapy for castration-resistant prostate cancer: Progress and new paradigms. *Urologic oncology*, **33**(5), pp. 245-260.

QURESHI-BAIG, K., ULLMANN, P., HAAN, S. and LETELLIER, E., 2017. Tumor-Initiating Cells: a critical review of isolation approaches and new challenges in targeting strategies. *Molecular cancer*, **16**(1), pp. 40-017-0602-2.

RADISKY, D.C., LEVY, D.D., LITTLEPAGE, L.E., LIU, H., NELSON, C.M., FATA, J.E., LEAKE, D., GODDEN, E.L., ALBERTSON, D.G., ANGELA NIETO, M., WERB, Z. and BISSELL, M.J., 2005. Rac1b and reactive oxygen species mediate MMP-3-induced EMT and genomic instability. *Nature*, **436**(7047), pp. 123-127.

REID, M.A., SANDERSON, S.M. and LOCASALE, J.W., 2020. 9 - Cancer Metabolism. In *Niederhuber J.E. (Ed. 6)* pp. 127-138.e4.

RIBATTI, D., 2017. The concept of immune surveillance against tumors. The first theories. *Oncotarget*, **8**(4), pp. 7175-7180.

ROGERS, L.M., VEERAMANI, S. and WEINER, G.J., 2014. Complement in monoclonal antibody therapy of cancer. *Immunologic research*, **59**(1-3), pp. 203-210.

ROMANO, E., KUSIO-KOBIALKA, M., FOUKAS, P.G., BAUMGAERTNER, P., MEYER, C., BALLABENI, P., MICHIELIN, O., WEIDE, B., ROMERO, P. and SPEISER, D.E., 2015. Ipilimumab- dependent cell-mediated cytotoxicity of regulatory T cells ex vivo by nonclassical monocytes in melanoma patients. *Proceedings of the National Academy of Sciences of the United States of America*, **112**(19), pp. 6140-6145.

RONCADOR, G., ENGEL, P., MAESTRE, L., ANDERSON, A.P., CORDELL, J.L., CRAGG, M.S., ŠERBEC, V.Č, JONES, M., LISNIC, V.J., KREMER, L., LI, D., KOCH-NOLTE, F., PASCUAL, N., RODRÍGUEZ-BARBOSA, J.I., TORENSMA, R., TURLEY, H., PULFORD, K. and BANHAM, A.H., 2016. The European antibody network's practical guide to finding and validating suitable antibodies for research. *mAbs*, **8**(1), pp. 27-36.

ROSENBERG, S.A. and RESTIFO, N.P., 2015. Adoptive cell transfer as personalized immunotherapy for human cancer. *Science (New York, N.Y.)*, **348**(6230), pp. 62-68.

ROSENBERG, S.A., YANG, J.C., SHERRY, R.M., KAMMULA, U.S., HUGHES, M.S., PHAN, G.Q., CITRIN, D.E., RESTIFO, N.P., ROBBINS, P.F., WUNDERLICH, J.R., MORTON, K.E., LAURENCOT, C.M., STEINBERG, S.M., WHITE, D.E. and DUDLEY, M.E., 2011. Durable Complete Responses in Heavily Pretreated Patients with Metastatic Melanoma Using T-Cell Transfer Immunotherapy. *Clinical Cancer Research*, **17**(13), pp. 4550-4557.

RÖTHLISBERGER, D., HONEGGER, A. and PLÜCKTHUN, A., 2005. Domain interactions in the Fab fragment: a comparative evaluation of the single-chain Fv and Fab format engineered with variable domains of different stability. *Journal of Molecular Biology*, **347**(4), pp. 773-789.

RUNCIE, K., BUDMAN, D.R., JOHN, V. and SEETHARAMU, N., 2018. Bi-specific and tri-specific antibodies- the next big thing in solid tumor therapeutics. *Molecular Medicine*, **24**(1), pp. 50.

RUNCIE, K., BUDMAN, D.R. and SEETHARAMU, N., 2019. Polyspecific antibodies for solidtumors, 2019.

SADELAIN, M., 2017. CD19 CAR T Cells. *Cell*, **171**(7), pp. 1471.

SAIF, J.M., VADAKEKOLATHU, J., RANE, S.S., MCDONALD, D., AHMAD, M., MATHIEU, M.,POCKLEY, A.G., DURRANT, L., METHERINGHAM, R., REES, R.C. and MCARDLE, S.E., 2014. Novel prostate acid phosphatase-based peptide vaccination strategy induces antigen-specific T-cell responses and limits tumour growth in mice. *European journal of immunology*, **44**(4), pp. 994-1004.

SAITO, M., 2018. Involvement of partial EMT in cancer progression. *The Journal of Biochemistry*, **164**(4), pp. 257-264.

SANDOVAL, G.J., GRAHAM, D.B., GMYREK, G.B., AKILESH, H.M., FUJIKAWA, K., SAMMUT, B., BHATTACHARYA, D., SRIVATSAN, S., KIM, A., SHAW, A.S., YANG-IOTT, K., BASSING, C.H., DUNCAVAGE, E., XAVIER, R.J. and SWAT, W., 2013. Novel mechanism of tumor suppression by polarity gene discs large 1 (DLG1) revealed in a murine model of pediatric B-ALL. *Cancer immunology research*, **1**(6), pp. 426-437.

SARKAR, S. and DAS, S., 2016. A Review of Imaging Methods for Prostate Cancer Detection. *Biomedical engineering and computational biology*, **7**(Suppl 1), pp. 1-15.

SATO, M., MURAGAKI, Y., SAIKA, S., ROBERTS, A.B. and OOSHIMA, A., 2003. Targeted disruption of TGF-beta1/Smad3 signaling protects against renal tubulointerstitial fibrosis induced by unilateral ureteral obstruction. *The Journal of clinical investigation*, **112**(10), pp.1486-1494.

SAUNDERS, K.O., 2019. Conceptual Approaches to Modulating Antibody EffectorFunctions and Circulation Half-Life. *Frontiers in Immunology*, **10**, pp. 1296.

SCANLON, C.S., VAN TUBERGEN, E.A., INGLEHART, R.C. and D'SILVA, N.J., 2013. Biomarkers of epithelial-mesenchymal transition in squamous cell carcinoma. *Journal of dentalresearch*, **92**(2), pp. 114-121.

SCHAFFNER, F., YOKOTA, N., CARNEIRO-LOBO, T., KITANO, M., SCHAFFER, M., ANDERSON, G.M., MUELLER, B.M., ESMON, C.T. and RUF, W., 2013. Endothelial Protein C Receptor Function in Murine and Human Breast Cancer Development. *PLOS ONE*, **8**(4), pp. e61071.

SCHAID, D.J., 2004. The complex genetic epidemiology of prostate cancer. *Human molecular genetics*, **13**(suppl_1), pp. R103-R121.

SCHEFFER, G.L., FLENS, M.J., HAGEMAN, S., IZQUIERDO, M.A., SHOEMAKER, R.H. and SCHEPER, R.J., 2002. Expression of the vascular endothelial cell protein C receptor in epithelial tumour cells. *European journal of cancer (Oxford, England : 1990)*, **38**(11), pp.1535-1542.

SCHEPISI, G., CURSANZO, M.C., CASADEI, C., MENNA, C., ALTAVILLA, A., LOLLI, C., CERCHIONE, C., PAGANELLI, G., SANTINI, D., TONINI, G., MARTINELLI, G. and DE GIORGI, U., 2019. CAR-T cell therapy: a potential new strategy against prostate cancer. *Journal for immunotherapy of cancer*, **7**(1), pp. 258-019-0741-7.

SCHEPISI, G., FAROLFI, A., CONTEDUCA, V., MARTIGNANO, F., DE LISI, D., RAVAGLIA, G., ROSSI, L., MENNA, C., BELLIA, S.R., BARONE, D., GUNELLI, R. and DE GIORGIO, U., 2017. Immunotherapy for Prostate Cancer: Where We Are Headed. *International journal of molecular sciences*, **18**(12), pp. 2627.

SCHOENHALS, M., KASSAMBARA, A., DE VOS, J., HOSE, D., MOREAUX, J. and KLEIN, B., 2009. Embryonic stem cell markers expression in cancers. *Biochemical and biophysical research communications*, **383**(2), pp. 157-162.

SCHREIBER, R.D., OLD, L.J. and SMYTH, M.J., 2011. Cancer Immunoediting: Integrating Immunity's Roles in Cancer Suppression and Promotion. *Science*, **331**(6024), pp. 1565-1570.

SCOTT, A.M., ALLISON, J.P. and WOLCHOK, J.D., 2012. Monoclonal antibodies in cancertherapy. *Cancer immunity*, **12**, pp. 14.

SCOTT, L.J., 2018. Enzalutamide: A Review in Castration-Resistant Prostate Cancer. *Drugs*, **78**(18), pp. 1913-1924.

SHARMA, A., CAMPBELL, M., YEE, C., GOSWAMI, S. and SHARMA, P., 2019. 77 - Immunotherapy of Cancer in *Rich, R.R. (ed. 5)* pp. 1033-1048.

SHARMA, P. and ALLISON, J.P., 2015. The future of immune checkpoint therapy. *Science (New York, N.Y.)*, **348**(6230), pp. 56-61.

SHARMA, P., PACHYNISKI, R.K., NARAYAN, V., FLECHON, A., GRAVIS, G., GALSKY, M.D., MAHAMMEDI, H., PATNAIK, A., SUBUDHI, S.K., CIPROTTI, M., DUAN, T., SACI, A., HU, S.K., HAN, G.C. and FIZAZI, K.S., 2019. Initial results from a phase II study of nivolumab (NIVO)plus ipilimumab (IPI) for the treatment of metastatic castration-resistant prostate cancer (mCRPC; CheckMate 650). *Journal of Clinical Oncology*, **37**, pp. 142-142.

SHAY, J.W., 2016. Role of Telomeres and Telomerase in Aging and Cancer. *Cancerdiscovery*, **6**(6), pp. 584-593.

SHEPARD, H.M., PHILLIPS, G.L., D THANOS, C. and FELDMANN, M., 2017. Developments in therapy with monoclonal antibodies and related proteins. *Clinical medicine (London,England)*, **17**(3), pp. 220-232.

SHI, Y., FAN, X., DENG, H., BREZSKI, R.J., RYZYK, M., JORDAN, R.E., STROHL, W.R., ZOU, Q., ZHANG, N. and AN, Z., 2015. Trastuzumab Triggers Phagocytic Killing of High HER2 Cancer Cells In Vitro and In Vivo by Interaction with Fc γ Receptors on Macrophages. *TheJournal of Immunology*, **194**(9), pp. 4379.

SHULMAN, M., WILDE, C.D. and KÖHLER, G., 1978. A better cell line for makinghybridomas secreting specific antibodies. *Nature*, **276**(5685), pp. 269-270.

SIEBZEHN'RUBL, F.A., SILVER, D.J., TUGERTIMUR, B., DELEYROLLE, L.P., SIEBZEHN'RUBL, D., SARKISIAN, M.R., DEVERS, K.G., YACHNIS, A.T., KUPPER, M.D., NEAL, D., NABILSI, N.H., KLADE, M.P., SUSLOV, O., BRABLETZ, S., BRABLETZ, T., REYNOLDS, B.A. and STEINDLER, D.A., 2013. The ZEB1 pathway links glioblastoma initiation, invasion and chemoresistance. *EMBO Molecular Medicine*, **5**(8), pp. 1196-1212.

SILVESTRI, I., TORTORELLA, E., GIANTULLI, S., SCARPA, S. and SCIARRA, A., 2019. Immunotherapy in prostate cancer: recent advances and future directions. *EMJ Urol.*, **7**(1), pp.51-61.

SIMANSHU, D.K., NISSLER, D.V. and MCCORMICK, F., 2017. RAS Proteins and Their Regulators in Human Disease. *Cell*, **170**(1), pp. 17-33.

SMALL, E.J., SCHELLHAMMER, P.F., HIGANO, C.S., REDFERN, C.H., NEMUNAITIS, J.J., VALONE, F.H., VERJEE, S.S., JONES, L.A. and HERSHBERG, R.M., 2006. Placebo-controlled phase III trial of immunologic therapy with sipuleucel-T (APC8015) in patients with metastatic, asymptomatic hormone refractory prostate cancer. *Journal of clinical oncology: official journal of the American Society of Clinical Oncology*, **24**(19), pp. 3089-3094.

SONG, H. and YANG, P., 2010. Construction of shRNA lentiviral vector. *North American journal of medical sciences*, **2**(12), pp. 598-601.

SPEES, J.L., LEE, R.H. and GREGORY, C.A., 2016. Mechanisms of mesenchymal stem/stromal cell function. *Stem Cell Research & Therapy*, **7**(1), pp. 125.

SRIVASTAVA, M. and RAGHAVAN, S.C., 2015. DNA double-strand break repair inhibitors as cancer therapeutics. *Chemistry & biology*, **22**(1), pp. 17-29.

STANFIELD, R.L., ZEMLA, A., WILSON, I.A. and RUPP, B., 2006. Antibody Elbow Angles are Influenced by their Light Chain Class. *Journal of Molecular Biology*, **357**(5), pp. 1566-1574.

STEARN-KUROSAWA, D., KUROSAWA, S., MOLLICA, J.S., FERRELL, G.L. and ESMON, C.T., 1996. The endothelial cell protein C receptor augments protein C activation by the thrombin-thrombomodulin complex. *Proceedings of the National Academy of Sciences of the United States of America*, **93**(19), pp. 10212-10216.

STEINWAND, M., DROSTE, P., FRENZEL, A., HUST, M., DÜBEL, S. and SCHIRRMANN, T., 2014. The influence of antibody fragment format on phage display based affinity maturation of IgG. *mAbs*, **6**(1), pp. 204-218.

STEMMLER, M.P., 2008. Cadherins in development and cancer. *Molecular BioSystems*, **4**(8), pp. 835-850.

STEPHEN PAGET, F.R.C.S., 1889. The distribution of secondary growths in cancer of the breast. *The Lancet*, **133**(3421), pp. 571-573.

STEWART, R., HAMMOND, S.A., OBERST, M. and WILKINSON, R.W., 2014. The role of Fc gamma receptors in the activity of immunomodulatory antibodies for cancer. *Journal for Immuno Therapy of Cancer*, **2**(1), pp. 29.

STONE, K.R., MICKEY, D.D., WUNDERLI, H., MICKEY, G.H. and PAULSON, D.F., 1978. Isolation of a human prostate carcinoma cell line (DU 145). *International journal of cancer*, **21**(3), pp. 274-281.

STRACQUADARIO, G., WANG, X., WALLACE, M.D., GRAWENDA, A.M., ZHANG, P., HEWITT, J., ZERON-MEDINA, J., CASTRO-GINER, F., TOMLINSON, I.P., GODING, C.R., CYGAN, K.J., FAIRBROTHER, W.G., THOMAS, L.F., SÆTROM, P., GEMIGNANI, F., LANDI, S., SCHUSTER-BÖCKLER, B., BELL, D.A. and BOND, G.L., 2016. The importance of p53 pathway genetics in inherited and somatic cancer genomes. *Nature Reviews Cancer*, **16**(4), pp. 251-265.

STRATTON, M.R., CAMPBELL, P.J. and FUTREAL, P.A., 2009. The cancer genome. *Nature*, **458**(7239), pp. 719-724.

STROHL, W.R., 2018. Current progress in innovative engineered antibodies. *Protein & cell*, **9**(1), pp. 86-120.

STROHL, W.R. and STROHL, L.M., 2012. Monoclonal antibody targets and mechanisms of action. *Therapeutic Antibody Engineering*. Woodhead Publishing, pp. 163-595.

STYLIANOU, N., LEHMAN, M.L., WANG, C., FARD, A.T., ROCKSTROH, A., FAZLI, L., JOVANOVIC, L., WARD, M., SADOWSKI, M.C., KASHYAP, A.S., BUTTYAN, R., GLEAVE, M.E., WESTBROOK, T.F., WILLIAMS, E.D., GUNTER, J.H., NELSON, C.C. and HOLLIER, B.G., 2019. A molecular portrait of epithelial-mesenchymal plasticity in prostate cancer associated with clinical outcome. *Oncogene* **38**, pp. 913-934.

SUBRAMANIAM, A., TALKHONCHEH, M.S., MAGNUSSON, M. and LARSSON, J., 2019. Endothelial protein C receptor (EPCR) expression marks human fetal liver hematopoietic stem cells. *Haematologica*, **104**(2), pp. e47-e50.

SUGIMOTO, H., MUNDEL, T.M., KIERAN, M.W. and KALLURI, R., 2006. Identification of fibroblast heterogeneity in the tumor microenvironment. *Cancer Biology & Therapy*, **5**(12), pp. 1640-1646.

SUN, J. and STATHOPOULOS, A., 2018. FGF controls epithelial-mesenchymal transitions during gastrulation by regulating cell division and apicobasal polarity. *Development (Cambridge, England)*, **145**(19), pp. dev161927.

SUNDARAM, J., KESHAVA, S., GOPALAKRISHNAN, R., ESMON, C.T., PENDURTHI, U.R. and RAO, L.V., 2014. Factor VIIa binding to endothelial cell protein C receptor protects vascular barrier integrity in vivo. *Journal of thrombosis and haemostasis : JTH*, **12**(5), pp. 690-700.

SURESH, R., BARAKAT, D.J., BARBERI, T., ZHENG, L., JAFFEE, E., PIENTA, K.J. and FRIEDMAN, A.D., 2020. NF-κB p50-deficient immature myeloid cell (p50-IMC) adoptive transfer slows the growth of murine prostate and pancreatic ductal carcinoma. *Journal for ImmunoTherapy of Cancer*, **8**(1), pp. e000244.

SUROWY, T., CHENG, Z., GARVIN, D., MORAVEC, R., PAGUIO, A., COSBY, N. and FAN, F., 2012. Low Variability ADCC Bioassay. *Genetic Engineering & Biotechnology News*, **32**(7), pp. 28-29.

SUSEK, K.H., KARVOUNI, M., ALICI, E. and LUNDQVIST, A., 2018. The Role of CXC Chemokine Receptors 1-4 on Immune Cells in the Tumor Microenvironment. *Frontiers in immunology*, **9**, pp. 2159.

SUZUKI, M., KATO, C. and KATO, A., 2015. Therapeutic antibodies: their mechanisms of action and the pathological findings they induce in toxicity studies. *Journal of toxicologic pathology*, **28**(3), pp. 133-139.

SYDES, M.R., SPEARS, M.R., MASON, M.D., CLARKE, N.W., DEARNALEY, D.P., DE BONO, J.S., TTARD, G., CHOWDHURY, S., CROSS, W., GILLESSEN, S., MALIK, Z.I., JONES, R., PARKER, C.C., RITCHIE, A.W.S., RUSSELL, J.M., MILLMAN, R., MATHESON, D., AMOS, C., GILSON, C., BIRTLE, A., BROCK, S., CAPALDI, L., CHAKRABORTI, P., CHOUDHURY, A., EVANS, L., FORD, D., GALE, J., GIBBS, S., GILBERT, D.C., HUGHES, R., MCLAREN, D., LESTER, J.F., NIKAPOTA, A., O'SULLIVAN, J., PARIKH, O., PEEDELL, C., PROTHEROE, A., RUDMAN, S.M., SHAFFER, R., SHEEHAN, D., SIMMS, M., SRIHARI, N., STREBEL, R., SUNDAR, S., TOLAN, S., TSANG, D., VARUGHESE, M., WAGSTAFF, J., PARMAR, M.K.B., JAMES, N.D. and STAMPEDE INVESTIGATORS, 2018. Adding abiraterone or docetaxel to long-term hormone therapy for prostate cancer: directly randomised data from the STAMPEDE multi-arm, multi-stage platform protocol. *Annals of oncology: official journal of the European Society for Medical Oncology*, **29**(5), pp. 1235-1248.

TAM, W.L. and WEINBERG, R.A., 2013. The epigenetics of epithelial-mesenchymal plasticity in cancer. *Nature medicine*, **19**, pp. 1438.

TANNOCK, I.F., DE WIT, R., BERRY, W.R., HORTI, J., PLUZANSKA, A., CHI, K.N., OUDARD, S., THÉODORE, C., JAMES, N.D., TURESSON, I., ROSENTHAL, M.A., EISENBERGER, M.A. and TAX 327 INVESTIGATORS, 2004. Docetaxel plus prednisone or mitoxantrone plus prednisone for advanced prostate cancer. *The New England journal of medicine*, **351**(15), pp. 1502- 1512.

TAYLOR, F.B., Jr, PEER, G.T., LOCKHART, M.S., FERRELL, G. and ESMON, C.T., 2001. Endothelial cell protein C receptor plays an important role in protein C activation in vivo. *Blood*, **97**(6), pp. 1685-1688.

THIERY, J.P., ACLOQUE, H., HUANG, R.Y. and NIETO, M.A., 2009. Epithelial-mesenchymal transitions in development and disease. *Cell*, **139**(5), pp. 871-890.

TODD, P.A. and BROGDEN, R.N., 1989. Muromonab CD3. A review of its pharmacology and therapeutic potential. *Drugs*, **37**(6), pp. 871-899.

TOKAREW, N., OGONEK, J., ENDRES, S., VON BERGWELT-BAILDON, M. and KOBOLD, S., 2019. Teaching an old dog new tricks: next-generation CAR T cells. *British journal of cancer*, **120**(1), pp. 26-37.

TOLKACH, Y. and KRISTIANSEN, G., 2018. The Heterogeneity of Prostate Cancer: A Practical Approach. *Pathobiology : journal of immunopathology, molecular and cellular biology*, **85**(1-2), pp. 108-116.

TOPALIAN, S.L., WEINER, G.J. and PARDOLL, D.M., 2011. Cancer immunotherapy comes of age. *Journal of clinical oncology: official journal of the American Society of Clinical Oncology*, **29**(36), pp. 4828-4836.

TOPP, M.S., GÖKBUGET, N., STEIN, A.S., ZUGMAIER, G., O'BRIEN, S., BARGOU, R.C., DOMBRET, H., FIELDING, A.K., HEFFNER, L., LARSON, R.A., NEUMANN, S., FOÀ, R., LITZOW, M., RIBERA, J., RAMBALDI, A., SCHILLER, G., BRÜGGEMANN, M., HORST, H.A., HOLLAND, C., JIA, C., MANIAR, T., HUBER, B., NAGORSEN, D., FORMAN, S.J. and KANTARJIAN, H.M., 2015. Safety and activity of blinatumomab for adult patients with relapsed or refractory B-precursor acute lymphoblastic leukaemia: a multicentre, single-arm, phase 2 study. *The Lancet.Oncology*, **16**(1), pp. 57-66.

TOWNSEND, C.L., LAFFY, J.M.J., WU, Y.B., SILVA O'HARE, J., MARTIN, V., KIPLING, D., FRATERNALI, F. and DUNN-WALTERS, D., 2016. Significant Differences in Physicochemical Properties of Human Immunoglobulin Kappa and Lambda CDR3 Regions. *Frontiers in Immunology*, **7**, pp. 388.

TRAN JANCO, J.M., LAMICHHANE, P., KARYAMPUDI, L. and KNUTSON, K.L., 2015. Tumor-Infiltrating Dendritic Cells in Cancer Pathogenesis. *The Journal of Immunology*, **194**(7), pp.2985.

TSUNEYOSHI, N., FUKUDOME, K., HORIGUCHI, S., YE, X., MATSUZAKI, M., TOI, M., SUZUKI, K. and KIMOTO, M., 2001. Expression and anticoagulant function of the endothelial cell protein C receptor (EPCR) in cancer cell lines. *Thrombosis and haemostasis*, **85**(2), pp. 356-361.

VADAKEKOLATHU, J., AMANDA, K.M., DAVID, J.B. and MCARDLE, S.E., 2014. Identification of tumor antigens for clinical evaluation; Tumor Immunology and Immunotherapy. Oxford University Press.

VALASTYAN, S. and WEINBERG, R.A., 2011. Tumor metastasis: molecular insights and evolving paradigms. *Cell*, **147**(2), pp. 275-292.

VAN DYKE, T. and JACKS, T., 2002. Cancer modeling in the modern era: progress and challenges. *Cell*, **108**(2), pp. 135-144.

VAN LEENDERS, GEERT J. L. H., AALDERS, T.W., HULSBERGEN-VAN DE KAA, CHRISTINA A., RUITER, D.J. and SCHALKEN, J.A., 2001. Expression of basal cell keratins in human prostatecancer metastases and cell lines. *The Journal of pathology*, **195**(5), pp. 563-570.

VAN ROOIJ, N., VAN BUUREN, M.M., PHILIPS, D., VELDS, A., TOEBES, M., HEEMSKERK, B., VAN DIJK, L.J., BEHJATI, S., HILKMANN, H., EL ATMIOUI, D., NIEUWLAND, M., STRATTON,M.R., KERKHOVEN, R.M., KESMIR, C., HAANEN, J.B., KVISTBORG, P. and SCHUMACHER, T.N., 2013. Tumor exome analysis reveals neoantigen-specific T-cell reactivity in an ipilimumab-responsive melanoma. *Journal of clinical oncology: official journal of the American Society of Clinical Oncology*, **31**(32), pp. e439-42.

VANKEMMELBEKE, M. and DURRANT, L., 2016. Third-generation antibody drug conjugates for cancer therapy – a balancing act. *Therapeutic Delivery*, **7**(3), pp. 141-144.

VUORILUOTO, K., HAUGEN, H., KIVILUOTO, S., MPINDI, J., NEVO, J., GJERDRUM, C., TIRON, C., LORENS, J.B. and IVASKA, J., 2011. Vimentin regulates EMT induction by Slug and oncogenic H-Ras and migration by governing Axl expression in breast cancer. *Oncogene*, **30**(12), pp. 1436-1448.

WALUNAS, T.L., LENSCHOW, D.J., BAKKER, C.Y., LINSLEY, P.S., FREEMAN, G.J., GREEN, J.M., THOMPSON, C.B. and BLUESTONE, J.A., 1994. CTLA-4 can function as a negative regulatorof T cell activation. *Immunity*, **1**(5), pp. 405-413.

WANG, D., CAI, C., DONG, X., YU, Q.C., ZHANG, X., YANG, L. and ZENG, Y.A., 2015. Identification of multipotent mammary stem cells by protein C receptor expression. *Nature*, **517**(7532), pp. 81-84.

WANG, G., ZHAO, D., SPRING, D.J. and DEPINHO, R.A., 2018. Genetics and biology ofprostate cancer. *Genes & development*, **32**(17-18), pp. 1105-1140.

WANG, Q., TANG, Y., WANG, T., YANG, H.L., WANG, X., MA, H. and ZHANG, P., 2018. EPCR promotes MGC803 human gastric cancer cell tumor angiogenesis in vitro through activating ERK1/2 and AKT in a PAR1-dependent manner. *Oncology letters*, **16**(2), pp.1565-1570.

WANG, Q., YANG, H., ZHUO, Q., XU, Y. and ZHANG, P., 2018. Knockdown of EPCR inhibits the proliferation and migration of human gastric cancer cells via the ERK1/2 pathway in a PAR-1-dependent manner. *Oncology reports*, **39**(4), pp. 1843-1852.

WANG, W., ZHANG, X., PENG, J., LI, X., WANG, A., BIE, Y., SHI, L., LIN, M. and ZHANG, X., 2018. Survival Mechanisms and Influence Factors of Circulating Tumor Cells. *BioMedResearch International*, **2018**, pp. 6304701.

WANG, W., WANG, L., MIZOKAMI, A., SHI, J., ZOU, C., DAI, J., KELLER, E.T., LU, Y. and ZHANG, J., 2017. Down-regulation of E-cadherin enhances prostate cancer chemoresistance via Notch signaling. *Chinese Journal of Cancer*, **36**(1), pp. 35.

WANG, Y., LIU, J., YING, X., LIN, P.C. and ZHOU, B.P., 2016. Twist-mediated epithelial- mesenchymal transition promotes breast tumor cell invasion via inhibition of hippo pathway. *Scientific Reports*, **6**, pp. 24606.

WARBURG, O., WIND, F. and NEGELEIN, E., 1927. The metabolism of tumors in the body. *The Journal of general physiology*, **8**(6), pp. 519-530.

WEBER, J.S., GIBNEY, G., SULLIVAN, R.J., SOSMAN, J.A., SLINGLUFF, C.L., Jr, LAWRENCE, D.P., LOGAN, T.F., SCHUCHTER, L.M., NAIR, S., FECHER, L., BUCHBINDER, E.I., BERGHORN, E., RUISI, M., KONG, G., JIANG, J., HORAK, C. and HODI, F.S., 2016. Sequential administration of nivolumab and ipilimumab with a planned switch in patients with advanced melanoma (CheckMate 064): an open-label, randomised, phase 2 trial. *The Lancet.Oncology*, **17**(7), pp. 943-955.

WEI, S.C., DUFFY, C.R. and ALLISON, J.P., 2018. Fundamental mechanisms of immunecheckpoint blockade therapy. *Cancer Discovery*, **8**(9), pp. 1069-1086.

WEINER, G.J., 2010. Rituximab: mechanism of action. *Seminars in hematatology*, **47**(2), pp.115-123.

WEISKOPF, K. and WEISSMAN, I.L., 2015. Macrophages are critical effectors of antibody therapies for cancer. *mAbs*, **7**(2), pp. 303-310.

WELLER, M.G., 2018. Ten Basic Rules of Antibody Validation. *Anal Chem Insights*, **13**, pp. 1177390118757462.

WELLNER, U., SCHUBERT, J., BURK, U.C., SCHMALHOFER, O., ZHU, F., SONNTAG, A., WALDVOGEL, B., VANNIER, C., DARLING, D., HAUSEN, A.Z., BRUNTON, V.G., MORTON, J., SANSOM, O., SCHÜLER, J., STEMMLER, M.P., HERZBERGER, C., HOPT, U., KECK, T., BRABLETZ, S. and BRABLETZ, T., 2009. The EMT-activator ZEB1 promotes tumorigenicity by repressing stemness-inhibiting microRNAs. *Nature cell biology*, **11**(12), pp. 1487-1495.

WERB, Z. and LU, P., 2015. The role of stroma in tumor development. *Cancer journal(Sudbury, Mass.)*, **21**(4), pp. 250-253.

WEYEMI, U., REDON, C.E., CHOUDHURI, R., AZIZ, T., MAEDA, D., BOUFRAQECH, M., PAREKH, P.R., SETHI, T.K., KASOJI, M., ABRAMS, N., MERCHANT, A., RAJAPAKSE, V.N. and BONNER, W.M., 2016. The histone variant H2A.X is a regulator of the epithelial- mesenchymal transition. *Nature Communications*, **7**(1), pp. 10711.

WHITEMAN, E.L., LIU, C.J., FEARON, E.R. and MARGOLIS, B., 2008. The transcription factors snail represses Crumbs3 expression and disrupts apico-basal polarity complexes. *Oncogene*, **27**(27), pp. 3875-3879.

WILSON, J.M. and PARKER, C., 2016. The safety and efficacy of radium-223 dichloride for the treatment of advanced prostate cancer. *Expert Review of Anticancer Therapy*, **16**(9), pp. 911-918.

WITSCH, E., SELA, M. and YARDEN, Y., 2010. Roles for growth factors in cancer progression. *Physiology (Bethesda, Md.)*, **25**(2), pp. 85-101.

WOLCHOK, J.D., KLUGER, H., CALLAHAN, M.K., POSTOW, M.A., RIZVI, N.A., LESOKHIN, A.M., SEGAL, N.H., ARIYAN, C.E., GORDON, R.A., REED, K., BURKE, M.M., CALDWELL, A., KRONENBERG, S.A., AGUNWAMBA, B.U., ZHANG, X., LOWY, I., INZUNZA, H.D., FEELY, W., HORAK, C.E., HONG, Q., KORMAN, A.J., WIGGINTON, J.M., GUPTA, A. and SZNOL, M., 2013. Nivolumab plus ipilimumab in advanced melanoma. *The New England journal of medicine*, **369**(2), pp. 122-133.

WU, C.T., CHANG, Y.H., LIN, W.Y., CHEN, W.C. and CHEN, M. F., 2015. TGF Beta1 Expression Correlates with Survival and Tumor Aggressiveness of Prostate Cancer. *Annals of surgical oncology*, **22** Suppl 3, pp. 1587-1593.

WU, X., GONG, S., ROY-BURMAN, P., LEE, P. and CULIG, Z., 2013. Current mouse and cellmodels in prostate cancer research. *Endocrine-Related Cancer*, **20**(4), pp. R155-R170.

WU, Y., DENG, J., RYCHAOU, P.G., QIU, S., EVERS, B.M. and ZHOU, B.P., 2009. Stabilization of snail by NF-kappaB is required for inflammation-induced cell migration and invasion. *Cancer cell*, **15**(5), pp. 416-428.

WYLIE, B., MACRI, C., MINTERN, J.D. and WAITHMAN, J., 2019. Dendritic Cells and Cancer: From Biology to Therapeutic Intervention. *Cancers*, **11**(4), pp. 521.

XIE, G., DONG, H., LIANG, Y., HAM, J.D., RIZWAN, R. and CHEN, J., 2020. CAR-NK cells: A promising cellular immunotherapy for cancer. *EBioMedicine*, **59**.

XU, J., QU, D., ESMON, N.L. and ESMON, C.T., 2000. Metalloproteolytic release of endothelial cell protein C receptor. *The Journal of biological chemistry*, **275**(8), pp. 6038-6044.

YANG, J., MANI, S.A., DONAHER, J.L., RAMASWAMY, S., ITZYKSON, R.A., COME, C., SAVAGNER, P., GITELMAN, I., RICHARDSON, A. and WEINBERG, R.A., 2004. Twist, a master regulator of morphogenesis, plays an essential role in tumor metastasis. *Cell*, **117**(7), pp. 927-939.

YANG, M.H., HSU, D.S., WANG, H.W., WANG, H.J., LAN, H.Y., YANG, W.H., HUANG, C.H., KAO, S.Y., TZENG, C.H., TAI, S.K., CHANG, S.Y., LEE, O.K. and WU, K.J., 2010. Bmi1 is essential in Twist1-induced epithelial-mesenchymal transition. *Nature cell biology*, **12**(10), pp. 982-992.

YANG, M., HSU, D.S., WANG, H., WANG, H., LAN, H., YANG, W., HUANG, C., KAO, S., TZENG, C., TAI, S., CHANG, S., LEE, O.K. and WU, K., 2010. Bmi1 is essential in Twist1-induced epithelial-mesenchymal transition. *Nature cell biology*, **12**(10), pp. 982-992.

YAO, D., DAI, C. and PENG, S., 2011. Mechanism of the mesenchymal-epithelial transitionand its relationship with metastatic tumor formation. *Molecular cancer research: MCR*, **9**(12), pp. 1608-1620.

YEE, C., 2014. The use of endogenous T cells for adoptive transfer. *Immunological reviews*, **257**(1), pp. 250-263.

YEKU, O. and SLOVIN, S.F., 2016. Immune Therapy for Prostate Cancer. *Cancer journal(Sudbury, Mass.)*, **22**(5), pp. 334-341.

YOOK, J.I., LI, X.Y., OTA, I., HU, C., KIM, H.S., KIM, N.H., CHA, S.Y., RYU, J.K., CHOI, Y.J., KIM, J., FEARON, E.R. and WEISS, S.J., 2006. A Wnt-Axin2-GSK3beta cascade regulates Snail1activity in breast cancer cells. *Nature cell biology*, **8**(12), pp. 1398-1406.

YOSHIMURA, A. and MUTO, G., 2011. TGF- β function in immune suppression. *Current topics in microbiology and immunology*, **350**, pp. 127-147.

YU, Q. and STAMENKOVIC, I., 2000. Cell surface-localized matrix metalloproteinase-9 proteolytically activates TGF-beta and promotes tumor invasion and angiogenesis. *Genes& development*, **14**(2), pp. 163-176.

YU, W., YANG, L., LI, T. and ZHANG, Y., 2019. Cadherin Signaling in Cancer: Its Functionsand Role as a Therapeutic Target. *Frontiers in Oncology*, **9**, pp. 989.

YUN, C.W. and LEE, S.H., 2018. The Roles of Autophagy in Cancer. *Internationaljournal ofmolecular sciences*, **19**(11), pp. 3466.

ZAROFF, S. and TAN, G., 2019. Hybridoma technology: the preferred method for monoclonal antibody generation for in vivo applications. *BioTechniques*, **67**(3), pp. 90-92.

ZEISBERG, E.M., POTENTA, S., XIE, L., ZEISBERG, M. and KALLURI, R., 2007. Discovery of endothelial to mesenchymal transition as a source for carcinoma-associated fibroblasts. *Cancer research*, **67**(21), pp. 10123-10128.

ZEISBERG, M. and NEILSON, E.G., 2009. Biomarkers for epithelial-mesenchymal transitions. *The Journal of clinical investigation*, **119**(6), pp. 1429-1437.

ZHANG, J., ENDRES, S. and KOBOLD, S., 2019. Enhancing tumor T cell infiltration to enablecancer immunotherapy. *Immunotherapy*, **11**(3), pp. 201-213.

ZHANG, Z., LIU, S., ZHANG, B., QIAO, L., ZHANG, Y. and ZHANG, Y., 2020. T Cell Dysfunction and Exhaustion in Cancer. *Frontiers in Cell and Developmental Biology*, **8**, pp.17.

ZHENG, P.P., LI, J. and KROS, J.M., 2018. Breakthroughs in modern cancer therapy and elusive cardiotoxicity: Critical research-practice gaps, challenges, and insights. *Medicinalresearch reviews*, **38**(1), pp. 325-376.

ZHENG, P., KROS, J.M. and LI, J., 2018. Approved CAR T cell therapies: ice bucket challenges on glaring safety risks and long-term impacts. *Drug discovery today*, **23**(6), pp.1175-1182.

ZHENG, X., CARSTENS, J.L., KIM, J., SCHEIBLE, M., KAYE, J., SUGIMOTO, H., WU, C., LEBLEU, V.S. and KALLURI, R., 2015. Epithelial-to-mesenchymal transition is dispensable for metastasis but induces chemoresistance in pancreatic cancer. *Nature*, **527**(7579), pp. 525-530.

ZHOU, J., TANG, Z., GAO, S., LI, C., FENG, Y. and ZHOU, X., 2020. Tumor-Associated Macrophages: Recent Insights and Therapies. *Frontiers in Oncology*, **10**, pp. 188.

ZHOU, Q., YAN, B., HU, X., LI, X., ZHANG, J. and FANG, J., 2009. Luteolin inhibits invasion of prostate cancer PC3 cells through E-cadherin. *Molecular Cancer Therapeutics*, **8**(6), pp. 1684-1691.

ZHOU, W., XU, G., WANG, Y., XU, Z., LIU, X., XU, X., REN, G. and TIAN, K., 2017. Oxidative stress induced autophagy in cancer associated fibroblast enhances proliferation and metabolism of colorectal cancer cells. *Cell cycle (Georgetown, Tex.)*, **16**(1), pp. 73-81.

ZHU, P., BAEK, S.H., BOURK, E.M., OHGI, K.A., GARCIA-BASSETS, I., SANJO, H., AKIRA, S., KOTOL, P.F., GLASS, C.K., ROSENFELD, M.G. and ROSE, D.W., 2006. Macrophage/Cancer Cell Interactions Mediate Hormone Resistance by a Nuclear Receptor Derepression Pathway. *Cell*, **124**(3), pp. 615-629.

ZITVOGEL, L. and KROEMER, G., 2012. Targeting PD-1/PD-L1 interactions for cancer immunotherapy. *Oncoimmunology*, **1**(8), pp. 1223-1225.

ZOLTAN, L., ALEXANDER, M., TAYLOR FLETCHER B., GARY, F. and ESMON CHARLES T., 1997. Human Protein C Receptor Is Present Primarily on Endothelium of Large BloodVessels. *Circulation*, **96**(10), pp. 3633-3640.